Leakage and Blockage Detection in Pipelines and Pipe Network Systems Using Fluid Transients

By

Xiao-Jian Wang

August 2002

A Thesis Submitted for the Degree of Doctor of Philosophy

School of Civil & Environmental Engineering

The University of Adelaide, SA 5005

Australia

Abstract

Leakage is common problem in pipelines and pipe network systems around the world. To minimize the economic and environmental damage caused by leaks in pipe systems, efficient leak detection methods are necessary. Traditional methods are slow to respond the occurrence of a leak and expensive to operate. One promising alternative to detecting leaks is to use controlled transients (water hammer waves) that travel in a pipe network system at high speeds and pick up a substantial amount of information about the health of the system. The study presented in this thesis is focused on the fundamental understanding and interpretation of the effects of leaks on fluid transients and better uses of fluid transients for leak detection.

The governing equations for transients in a pipeline including a leak have been derived. The leak is included in the governing equations by using a delta function and dimensionless linear governing equations have been obtained. Analytical solutions, which are expressed in terms of a Fourier series, for transients in a pipeline including a leak have been developed for constant and variable boundary conditions. These analytical solutions have provided significant insight into, and better understanding of, pipeline transient problems that are influenced by leaks.

Two new leak detection methods have been developed based on the analytical solutions. A technique using leak-induced damping on fluid transients in a pipeline under constant boundary conditions has been developed. This technique is successful in detecting, locating and quantifying a leak which is 0.1% of the cross-sectional area of the pipeline based on both numerical and experimental tests. Another technique to locate a leak by examining the leak-induced resonant frequency responses has been developed under continuously varying boundary conditions.

The feasibility to detect blockages, another common problem in pipe systems, using fluid transients has also been investigated. An analytical solution for transients in a pipeline including a partial blockage has been developed. A blockage detection technique that

enables the locating and quantification of a blockage in a pipeline has been developed. This technique has been successfully verified based on numerical examples and laboratory experimental tests.

A three-loop laboratory pipe network, for pipe transient study and development of leak and blockage detection techniques, particularly verification of the inverse transient method (ITM), has been constructed at the University of Adelaide as part of this Ph.D. research. Two computer programs, NETTRANS for transient simulation in pipe networks by using the method of characteristics (MOC) and NETFIT for leak detection using the inverse transient method, have been developed. The program NETTRANS has been verified against different transient simulation programs and experimental tests. The inverse transient method for leak detection has been verified for the first time in a laboratory pipe network. The application of the ITM for leak detection is able to indicate presence of a leak; however, it is difficult to locate the leak due to insensitivity of leak for slow transient events.

Statement of Originality

This work contains no material which has been accepted for the award of any other degree or diploma in any university or other tertiary institution and, to the best of my knowledge and belief, contains no material previously published or written by another person, except where due reference has been made in the text.

I give consent to this copy of my thesis, when deposited in the University Library, being available for loan and photocopying.

Signature: Date: 17/02/2003

Xiao-Jian Wang

Acknowledgements

I would like to express my gratitude and thanks to:

- Dr. Martin Lambert and Assoc. Prof. Angus Simpson, my supervisors, for introducing me into the exciting research area of transient pipe flow and their innovative supervision, continuous encouragement and support.
- Prof. Emeritus James Liggett of Cornell University, co-investigator of leak detection project, for his foresight of some of the problems and his positive stimulation and critical insight.
- Dr. John Vítkovský, with whom I worked closely and happily, for his help in the experimental tests, the sharing of some of the database and many valuable discussions.
- Mr. Mark Stephens, Ph.D. student in the pipe transient group, for his help on using NLFIT and help with experimental tests; Mr. Pedro Lee, Ph.D. student in pipe transient group, for his help on experimental tests; Fellow postgraduate students for their friendship and support.
- Laboratory technical staff, Mr. Gregory Atkins, Mr. David Hale and Mr. Ian Cates for their assistance with the experimental tests, and special thanks to Mr Jeffrey Hiorns for his excellent work on the construction of the looped pipe network.
- The Australian government and The University of Adelaide for scholarships, and Australian Research Council for the financial supports on this research and the construction of the pipe network.

Finally I would like to thank my wife Sophia and daughter Cheryl for their love and support, and my parents for their many years encouragement and support.

Table of Contents

List of Figures

List of Tables

Nomenclature

A, A_1, A_2	=	inner pipe cross-sectional area (m^2);
A_L	=	leak area (m^2);
A_S	=	area of side-discharge valve (m^2);
A_n, B_n	=	Fourier coefficients;
A_n', B_n'	=	Fourier coefficients;
A_{nP}, B_{nP}	=	dimensionless amplitude of a transient event;
A_v	=	open area of a valve (m^2);
a	=	wave speed (m/s);
b	=	parameter of leak discharge-head relationship;
b_i	=	parameter of leak discharge-head relationship for the i^{th} leak;
C	=	constant; dimensionless dead end parameter;
$C_0^{(i)}$	=	Fourier coefficient of i^{th} period transient;
$C_m^{(i)}$, $D_m^{(i)}$	=	Fourier coefficients of i^{th} period transient;
C_d	=	orifice discharge coefficient;
$(C_dA_L)_0$	=	equivalent theoretical (lumped) leak size (m^2);
C_k	=	valve parameter;
C_r	=	Courant number;
D, D_1, D_2	=	diameters of pipes (m);
D_L	=	diameter of leak orifice (m);

E	=	a parameter defined as $E = 2e_T R' M\sqrt{H^*_{L0}}$; amplitude of a sinusoidal perturbation (m); objective function (m^2); Young' modulus of elasticity (N/m^2);
E^*	=	dimensionless amplitude of a sinusoidal perturbation = E/H_1;
E_{np}^*	=	amplitude of an oscillation (without measurement position);
E_p^*	=	amplitude of an oscillation (including measurement position);
E_{res}	=	response function of a pipeline;
$E_n^{(1)}$	=	amplitude of nth harmonic component of the first period transient;
$E_n^{(i)}$	=	amplitude of nth harmonic component of the ith period transient;
e	=	pipe roughness (mm); thickness of pipe wall (mm);
e_T	=	linearization error of orifice equation;
F	=	a dimensionless head = H_1/H_S;
F_B	=	blockage-induced force (N);
F_L, F'_L	=	leak parameter; pressure force at leak (N);
F_{Li}	=	leak parameter for the i^{th} leak;
F_{p1}, F_{p2}	=	pressure forces (N);
F_w	=	shear force (N);
f	=	friction factor;
f_s	=	Darcy-Weisbach steady friction factor;
f_u	=	unsteady friction factor;
G	=	blockage resistance parameter;
G_i	=	resistance parameter for the i^{th} blockage;
g	=	gravitational acceleration (m/s^2);
H	=	piezometric head (m);
H_D, H_U	=	downstream and upstream heads (m);

H_e	=	head loss across an elbow (m);
H_0	=	steady state piezometric head (m);
H_1, H_2	=	heads at reservoirs (m);
H_d	=	head at a dead end (m);
H_i	=	the i^{th} calculated transient head; head at node i (m);
H_i^m	=	the i^{th} measured transient head (m);
H_L	=	piezometric head at leak (m);
H_{L0}	=	steady piezometric head at leak (m);
H_{L1}, H_{L2}	=	steady piezometric head at leak 1 and leak 2 (m);
H_s	=	Jouskowsky pressure head rise (m);
H^*	=	dimensionless head $=H/H_1$;
H_0^*	=	dimensionless head $=H_0/H_1$;
H_{L0}^*	=	dimensionless steady head at leak $= H_{L0}/H_1$;
h^*	=	dimensionless head disturbance;
$h_0^*(x^*, t^*)$	=	steady oscillation;
h_p^*	=	envelop of a dimensionless transient event;
J	=	friction resistance term;
J_s	=	quasi-steady friction resistance term;
J_u	=	unsteady friction resistance term;
K_e	=	head loss coefficient across an elbow;
K_B	=	head loss coefficient across a blockage;
K_{ij}	=	head loss coefficient at pipe junction;
K'_{ij}	=	minor loss coefficient at pipe junction;
k_A, k_P	=	parameters in the k_A, k_P unsteady friction model;
L, L_1, L_2	=	length of pipeline (m);

M	=	leak parameter;
m, n	=	component number in a Fourier series;
N_m	=	peaks of a response function;
P_n	=	n^{th} period of a transient;
p, p_1, p_2	=	pressure (N/m^2);
p_d	=	design pressure of pipe (N/m^2);
Q	=	flow rate (m^3/s);
Q_0	=	steady state flow rate (m^3/s);
Q_D, Q_U	=	downstream and upstream discharges (m^3/s);
Q_d	=	flow rate into a dead end during a transient event (m^3/s);
Q_L	=	flow rate through leak (m^3/s);
Q^*	=	dimensionless flow rate $=Q/Q_0$;
Q_0^*	=	dimensionless flow rate $=Q_0/Q_0= 1.0$;
Q_i	=	steady state flow rate at pipe i (m^3/s);
q	=	discharge ratio in a pipe junction;
q^*	=	dimensionless flow rate disturbance;
$R,\ R'$	=	pipeline friction damping factor; linear regression parameter;
R_s	=	steady friction damping factor;
R_u	=	unsteady friction damping factor;
$\overline{R}$	=	overall damping of a transient event;
Re	=	Reynolds number;
R_{nL}, R'_{nL}	=	leak damping factor for n^{th} harmonic (n = 1,2,3,…);
R_{nB}, R'_{nB}	=	blockage damping factor for n^{th} harmonic (n = 1,2,3,…);
R_{n_1L}, R_{n_2L}	=	leak damping factor for harmonics n_1 and n_2;
R_{nLi}	=	i^{th} leak induced damping factor for n^{th} harmonic;

R_{nBi}	=	the i^{th} blockage induced damping factor for n^{th} harmonic;
R_{nL}^{m}	=	multiple-leak damping factor;
$\widehat{R}_{iL}$	=	damping factor caused by N leaks for the i^{th} harmonic;
r_e	=	ratio of an elbow-induced damping over total transient damping;
S	=	sensitivity parameter for transient magnitude in leak detection;
S_1, S_2	=	sensitivity parameter in blockage detection;
S_d	=	dead end parameter;
S_e	=	sensitivity parameter for an elbow;
S_f	=	sensitivity parameter for friction factor;
T	=	natural period of pipeline (s);
T^*	=	dimensionless period of transient = $T/(L/a)$;
Ti	=	i^{th} pressure transducer in the laboratory network (i = 1,2,3..7);
t	=	time (s);
t_0^*	=	dimensionless reference time;
t^*	=	dimensionless time = $t/(L/a)$;
V	=	flow velocity in the pipe (m/s);
V_0	=	steady flow velocity in pipe (m/s);
V_i	=	steady state velocity at pipe i (m/s);
Vi	=	i^{th} control valve in the laboratory network;
V_{in}	=	metered inlet volume (m^3);
V_L	=	leakage volume (m^3);
V_{out}	=	metered outlet volume;
W	=	volume of the pipeline;
W_d	=	volume of a dead end;
x	=	distance along pipeline;

x^*	=	dimensionless distance = x/L;
x_B	=	position of blockage;
x_B^*	=	dimensionless blockage position = x_B/L;
x_{Bi}^*	=	dimensionless position of the i^{th} blockage;
x_d	=	position of an dead end;
x_d^*	=	dimensionless dead end position = x_d/L;
x_e	=	position of an elbow;
x_e^*	=	dimensionless elbow position = x_e/L;
x_L	=	position of leak;
x_L^*	=	dimensionless leak position = x_L/L;
x_{Li}^*	=	dimensionless position of the i^{th} leak;
$\hat{x}_1^*, \hat{x}_2^*$	=	dimensionless leak position in the combined real and imaginary pipeline;
z_L	=	pipe elevation at leak;
z_L^*	=	dimensionless pipe elevation at leak = z_L/H_1;
ΔH	=	head difference;
ΔH_L	=	pressure head at the leak = H_L-z_L;
ΔH_B	=	blockage-induced head loss;
ΔH_L^*	=	dimensionless pressure head at the leak = H_L^*-z_L^*;
ΔH_{L0}^*	=	dimensionless steady-state pressure head at the leak = H_{L0}^*-z_L^*;
ΔP_B	=	pressure difference across a blockage;
ΔR	=	friction damping error;
ΔV	=	line pack or inventory volume (m^3);
Δf	=	error in the Darcy-Weisbach friction factor;

Δx	=	distance interval (m);
δ	=	Dirac delta function;
ε	=	roughness height for pipe wall; a small distance from the leak (m);
ε_L	=	dimensionless leak location error;
ε_S	=	dimensionless leak size error;
$\phi_V, \phi_V^+, \phi_V^-$	=	Kronecker delta function;
λ	=	frequency;
μ	=	Poisson's ratio;
ω	=	dimensionless frequency of a sinusoidal perturbation = $2\pi/T^*$;
ρ	=	density of fluid (kg/m^3);
τ	=	dimensionless opening of a valve;
τ_0	=	shear stress at the wall of the pipe (N/m^2).

Chapter 1

Introduction

As a transportation method, pipelines are becoming increasingly important in many countries. Many new national and international pipelines are being planned and constructed every year. According to the latest international survey conducted by *Pipeline & Gas Journal*, 96,434 km of oil and gas pipelines are in various stages of construction or planned for construction (Tubb 2001). Urbanisation in both developing and developed countries also shows expenditure on water distribution networks increasing at a significant rate. In the U.S. 19,000 km of new water distribution pipelines are installed annually based on data from the American Water Works Association (AWWA) (Smith et al. 2000). With the wide application of pipelines, a variety of pipeline failures ranging from water pipe rupture, gas pipe explosion to oil leakage are reported every year. The failure of a pipeline may be the result of one or several factors including corrosion of the pipe wall, abnormal pressure surges, poor quality of fittings and workmanship, soil movement, traffic loading and ageing of the pipeline (Smith 1986; AWWA 1987). Analysis of the most recently available data from the U.S. Department of Transportation (DOT) indicates that, despite emphasis by regulators and operators, the rate at which pipeline accidents occur showed no significant change over the last 16 years (Hovey and Farmer 1999). Based on an investigation by the Asia Development Bank, the leakage in water distribution networks in the Asia region ranged from 8% in Singapore to 62% in Dhaka, Bangladesh. The average leakage and unaccounted for-water losses are approximately 23% in 23 surveyed developing countries (Rao and Sridharan 1996). In developed countries, the situation is similar. Some North American cities have water losses of approximately 25% (Makar and Chagnon 1999). In many countries

legislation on environmental protection is becoming stricter. For pipeline utilities, pipeline leakage means not only a loss of product, but also large fines if the environment is impacted upon. Therefore, accurate leak detection methods that enable a quick response to pipeline failure are necessary to reduce the loss of valuable materials and to minimise the environmental damage.

Leak detection methods can range from simple line walking and checking visually, to sophisticated model-based techniques. Among these techniques, the methods using fluid transients have shown advantages of quick response. In addition, these methods are easier to apply and more accurate for leak location and size compared to other leak detection techniques based on numerical simulation and simple laboratory tests. However, there is still a gap to apply these methods in real pipe systems. The major objective of this research is to bring these techniques closer to practical application.

The study of fluid transients in a pipe has a history of at least one hundred years. Most of the previous studies investigated transients in relation to severe conditions, for example, a transient induced by a power failure in a pumping system. The focus of these studies was to predict the maximum pressure in a pipe system or to avoid possible cavitation. The main objective was the safety of the pipeline. In this Ph.D. research, the focus is to use fluid transients for leak detection. New methods to generate transients are investigated in this study. Compared to previous transient studies, a transient for leak and blockage detection should have the following characteristics: (a) the magnitude and form of the transient should be controllable for the purpose of leak detection in different situations; (b) the transient should be easy to control and repeatable so a leakage detection manoeuvre can be repeated; and (c) the transient should not jeopardise the safety of a pipeline system, and should have little influence on the normal operation of the pipeline system. .

In addition to leakage, blockages are another problem in pipeline systems. A blockage can be formed by chemical or physical deposition, or formed by a partially closed valve (often left inadvertently in this condition). Existence of a pipeline blockage not only reduces the operation efficiency of a pipeline system, but also sometimes it can cause severe safety problems if the blockage is not identified and repaired in a limited

time. A number of different blockage detection methods have been developed based on different techniques. Like a leak, when a blockage exists in a pipeline or a pipe network, the transients in such a pipeline are changed compared to the no-blockage situation. Therefore, fluid transients in a pipeline or a pipe network system may be used for blockage detection. Although, the main scope of this thesis is on leakage detection, blockage detection is also addressed by investigating the effects of a blockage on a pipeline transient.

Transients in a pipeline system can be expressed by either transient flow rates or transient pressures. Since measurement of transient pressure in pipelines is more accurate (and considerably less expensive) than measurement of flow in practice, transient pressures are used as measured transients both in numerical examples and laboratory studies in this thesis. The fluids in pipelines or in pipe network systems studied in this thesis are water, although the results presented in this study may be applied to other fluids such as oil, liquid natural gas (LNG) and some chemical fluids. The transients used in this study are in such a limited range that no column separation occurs. The transient problems studied are a one-phase problem and no air is involved.

1.1 Objectives and achievements

The objective of the research presented in this thesis is to investigate the possibility and efficiency of fluid transient based methods for leakage and blockage detection in pipeline and pipe network systems, and to improve some previously proposed methods for practical application. To achieve these objectives, the following original work has been conducted in this study

1. Analytical solutions for the transients in a pipeline including a leak or a blockage are developed in order to understand the mechanism of a leak or a blockage on a fluid transient.
2. New leakage and blockage detection techniques based on analytical solutions are developed, and have been tested in a laboratory pipeline.

3. A computer program called NETFIT, which combines a transient solver NETTRANS and a nonlinear regression solver NLFIT, has been developed for leak detection in pipe network systems based on the inverse transient method.
4. A three-loop pipe network has been constructed in the laboratory and is fully operational. The inverse transient method, which has shown promise based on previous numerical simulation and laboratory tests in a single pipeline, has been tested in this experimental network system.

1.2 Structure of this thesis

In this thesis, Chapter 2 contains a review of various leak detection methods used in both single pipelines and pipe networks. The focus of this review is on the hydraulic-based leak detection methods. A simple review of a number of blockage detection techniques is also presented. Chapter 3 deals with the theoretical analysis of fluid transients in a pipeline including a leak. The governing equations for the variation in dimensionless hydraulic grade line are derived. An analytical solution expressed in terms of a Fourier series is developed under constant boundary conditions. The analytical solutions are compared with the numerical results obtained using the method of characteristics (MOC). A new technique for detecting, locating and quantifying leaks in a single pipeline is developed in Chapter 4 based on the analytical solution of Chapter 3 by checking leak-induced damping on a transient event. The leak detection technique is verified using numerical examples and laboratory tests. The possibility to apply this technique into a pipe network is discussed. In Chapter 5, the transients in a pipeline including a leak under variable boundary conditions are studied. Analytical solutions based on Laplace transform and an analytical solution expressed in a Fourier series are obtained. A technique to detect and locate leaks in a single pipeline using resonance involving transients is presented in this chapter. In Chapter 6, behaviour of a pipeline blockage on fluid transients is investigated. The governing equations for a transient in a pipeline including a blockage are derived, and an analytical solution expressed in a Fourier series is developed under constant boundary conditions. A blockage detection technique using blockage-induced transient damping is also developed.

Up to and including Chapter 6, the main focus is on leak and blockage detection techniques in a single pipeline. In Chapter 7, the inverse transient method (ITM), which was developed for leak detection in a water distribution pipe network, is introduced. Three components of the inverse transient method: forward analysis (numerical modelling), experimental measurements and objective function minimisation are discussed. The main focus of Chapter 7 involves issues of forward analysis in a pipe network. These issues include the minor losses in a pipe network, effects of dead ends on a transient event and unsteady friction models. A new computer program called NETFIT, which combines a transient solver NETTRANS and a minimisation solver NLFIT, is introduced in this chapter. This program is developed for leak and blockage detection and pipe roughness calibration in a pipe network system based on the inverse transient technique. A number of gradient-based and global searching minimisation methods are available in this program. In Chapter 8, a newly built three-loop pipe network at Robin Hydraulics Laboratory at Adelaide University is introduced. Various aspects including construction of the apparatus, network calibration, data acquisition and generation of transients are presented. Experimental verification of the inverse transient analysis (ITM) for leak detection based on the three-loop network is presented in this chapter. Finally, conclusions and recommendations of the research presented in this thesis are given in Chapter 9.

Chapter 2

Literature Review on Leakage and Blockage Detection Techniques

2.1 Introduction

Leak detection methods can range from simple line walking and checking visually to sophisticated model-based techniques. Each method has advantages and disadvantages for detecting and locating pipeline leaks effectively. Because leakage in oil and gas pipelines causes much larger financial losses and environmental damage compared with the leakage in water pipelines, most leak detection methods have been developed for oil and gas pipelines. Black (1992) gave a general review of the available pipeline leak detection techniques, classified as observational methods, sensor-based methods, intelligent pigs, single measurement analysis, uncompensated volume balance and model-based leak detection methods. In the review by Furness and Reet (1998), leak detection methods were divided into three groups: simple leak detection systems, pig based monitoring systems and computer-based monitoring systems. Ghafurian et al. (1999) gave a simple introduction to the leak detection techniques developed and installed by Con Edison of New York. The methods discussed in these papers focus on oil and gas pipelines or oil-filled electrical cables. However, concern over water losses in water distribution systems is increasing as the costs of constructing new water storage, energy for pumping, water treatment and distribution have risen over the last 20 years, all of which drive the need for better leak detection methods. The American Water Works Association (AWWA) has recommended that the goal for water losses in a water distribution system should be less than 10% (Liston et al. 1996). While some of the leak detection techniques

invented for oil and gas pipelines can be applied to water distribution systems, most of them are not suitable because of the more complex topology of water distribution networks. During the past decade some new leak detection methods suitable for pipe networks have been formulated. Although few of them have been applied in practice, these techniques are reviewed in this thesis in order to give a comprehensive view of leak detection techniques. Leak detection methods used for pipelines (including pipe networks) can be classified into the following four groups based on the media used for detection:

1. Offline observation and surveillance;
2. Online pig-based methods;
3. Acoustic methods;
4. Hydraulic methods.

The most commonly used leak detection methods are those in the first three groups. These methods are based on regular rather than continuous operation and their main disadvantage lies in the fact that they are slow to respond to leakage and expensive to operate. To monitor a pipeline system continuously, some modelling methods that are based on hydraulic models using system measurements as boundary conditions have been developed. Many of these leak detection techniques are still in a developmental stage. The performance of model-based leak detection techniques is, so far, unsatisfactory for many reasons (Black 1992; Zhang 2001). However, the model-based leak detection methods may represent the future direction of leak detection given improvements in pipeline modelling and system measurement. The U.S. Department of Transportation has adopted API 1130, which specifies computational pipeline monitoring techniques, into 49 CFR (Code for Federal Regulation) Part 195 in order to ensure safe operation of national hazardous liquid pipelines (Scott 1999).

In addition to leaks, blockage development (either completely or partially obstructing the flow of liquid) is another common problem in pipeline and pipe network systems for the chemical, water and energy industries. A blockage can be formed by chemical or physical depositions, or formed by a partially closed valve. Blockages not only decrease the operational efficiency of the pipe systems, but also can cause

serious safety and environmental consequences if the blockage is not identified and corrected. Early detection and accurate location of blockages will enable the operator to take prompt remedial actions that will lower the risk of severe damages significantly. Some methods have been proposed to detect and locate pipeline blockage; however, they are developed far less than the leak detection methods, possibly because blockages cause less significant damage compared to the leaks. No literature citations have been found to classify the blockage detection methods, and the accuracy and efficiency of some of the proposed blockage detection methods have not been verified. Since only a few of blockage detection methods have been developed, a review of the blockage detection methods is given separately in Section 2.6 although many of the blockage detection methods can be related to the leak detection methods.

2.2 Offline observation and surveillance

One of the simplest ways to detect leaks is to patrol the pipeline on a regular basis making a visual check to assess the integrity of the line. Often, people living nearby passively perform unofficial pipeline monitoring and inform the operator of a problem with the pipeline. Tracer gases, using either non-toxic odourants (such as mercaptans) or electrically detectable gases (helium, SF6), can be injected into some gas or chemical pipelines to improve the efficiency of surveillance. The effectiveness of this method strongly depends on the weather conditions and wind direction (Black 1992; Furness and Reet 1998). In addition to use of tracer gases, trained tracking dogs can be used to locate the minute odours from leaked fluids and gases. Some successful cases have been reported, for example three tracking dogs successfully located 150 leaks in a 150km long gas pipeline in 9 days. However, other investigations were disappointing, especially when under emergency conditions (Williams et al. 1983). For some oil and gas pipes, external-sensing systems may be installed along the pipeline to monitor the environment outside of the pipeline. Two of the most common external sensing systems are vapour monitoring and liquid detection cable systems (Schwendeman 1987). These systems normally cannot provide early warning of leakage unless an impervious barrier, which permits the lost materials to accumulate, is placed beneath or above the pipeline.

Some non-destructive techniques are able to detect pipeline defects such as leaks, cracks, and subsurface erosion voids (Bray 1992). Amongst the various non-destructive methods, infrared thermography has proved to be effective especially with the aid of computer analysis of thermal images and application of GPS systems (Williams et al. 1983; Weil et al. 1994). However, the undetermined ambient conditions around the pipeline limit its application of thermography in urban areas for water distribution systems.

2.3 Online pig-based leak detection methods

A pipeline pig is a free moving piston inside the pipeline, sealed against the inside wall using a number of sealing elements. Various pigs are widely used in the oil and gas industry for pipeline commissioning, cleaning, filling, dewaxing, batching and pipeline monitoring (Furness and Reet 1998). Pigs generally need a specially designed apparatus for launching and receiving vessels for recovery. Pigs can be located using fixed signallers along the pipe or an electronic tracking system mounted inside the pig (Pipeline Engineering Inc 2001). Recently, pipeline pigs that carry a wide range of surveillance and monitoring equipment, such as acoustic or ultrasound instruments (Furness and Reet 1998), have been used for monitoring in the oil and gas industry. The pigs are normally used at regular intervals to check the internal conditions of pipelines. By analysing the data transferred from pigs, not only can leaks be located accurately, but also pipe wall corrosion, pits and weld characteristics can be assessed regularly (British Gas 1994).

Although the pig-based leak detection methods are impressive for monitoring the integrity of pipelines, their application is limited to pipes with diameters larger than 200mm. Pig-based methods are unlikely to be applied in water distribution networks where the presence of valves, elbows, pipes with different diameters and pipe flanges limit the pig's movement. Also, even in oil and gas pipelines, the pig-based leak detection methods need to work with other techniques to ensure a quick response to pipeline failure since pig-based monitoring is still a batch rather than a continuous process.

2.4 Acoustic leak detection techniques

A pressured pipeline or a container that is leaking emits an acoustic signal with different frequency ranges that depend on the fluid in the pipe, pressure in the pipe, characteristics of the leak and the conditions around the pipe wall. Acoustic-based leak detection systems have been successfully applied to detect and locate defects in nuclear power plants, petroleum and chemical systems and water distribution systems.

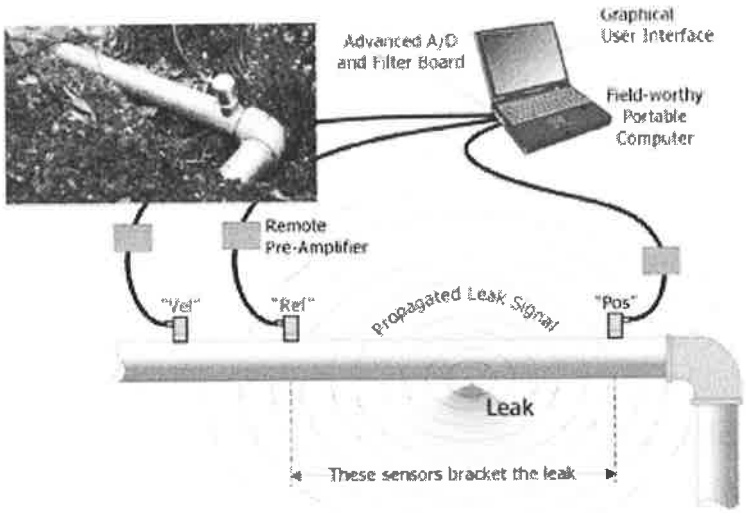

Figure 2.1 - An acoustic leak detection correlator (PALS System from Vista Research Inc.)

The simplest acoustic system is a geophone that is widely used in water distribution systems (Waller 1969; AWWA 1987; Smith et al. 2000). The acoustic signals are measured using a microphone and then processed to help the operators interpret the sounds and locate the leak. The processing includes filtering the unwanted background noise and amplification to increase the signal strength. The geophone (or microphone) can be connected with different attachments to allow use in a variety of situations. The efficiency of the geophone for leak detection depends on the experience and skill of the operator and the level of background noise.

Acoustic leak correlators, which are equipped with microprocessors or portable computers, are used to improve the accuracy of leak location. Figure 2.1 shows a schematic of an acoustic correlator developed by Vista Research Inc. Typically the transducers are placed in contact with the pipe wall at two positions that straddle the location of the suspected leak or break. Then the acoustic signals from both transducers are transferred to a computer for correlation analysis. The correlator is programmed to match the acoustic spectra from the two signals with a suitable time delay. The time delay combined with the acoustic velocity, which can be determined by the pipe size and material information, allows the correlator to calculate the most probable leak location. Acoustic leak detection with correlation is developing rapidly and many sophisticated correlators have been introduced to the market (LOKAL—Fuchs and Riehle 1991; LEAKTEC—Seaford 1994; PALS—Vista Research Inc. 2001). Given favourable conditions, leaks with discharges as small as $0.05m^3$/hour have been located (Fuchs and Riehle 1991). In 1998, most correlators cost more than $US 60,000 (Smith et al. 2000).

The disadvantages of acoustic leak detection techniques are well known (Fuchs and Riehle 1991; Seaford 1994), and factors that affect performance are:

1. Various unwanted interference noise such as that from traffic, wind, water and aircraft;
2. Varying pressure conditions in the pipe, especially varying pipe materials, that change sound propagation conditions from one pipeline section to another;
3. Characteristics of the leak, e.g., a small orifice with high pressure produces clearer and stronger signals that are easier to locate than a large pipe burst surrounded by the water that has escaped or ground water, which produces a weak signal.
4. Multiple leaks tend to give incorrect leak locations;
5. Strong acoustic damping in plastic pipes.

2.5 Hydraulic leak detection methods

Hydraulic leak detection methods use the hydraulic characteristics of fluids in a pressured pipeline to detect, locate and quantify leaks as early as the 1890s

(Joukowsky 1898). Based on the flow conditions of the fluid in the pipeline system, two different levels of leak detection method have been studied: steady state and transient (or unsteady) state. Some methods that were originally applied to steady analysis have been extended to transient analysis. Figure 2.2 describes the hydraulic leak detection methods in relation to the two hydraulic states. Among them, the transient-based mass balance and pressure-flow deviation methods, which are commonly called model-based leak detection methods (Black 1992; Furness and Reet 1998), have been applied in some oil and gas pipelines. The most commonly used methods in water distribution systems are the steady state-based mass balance method, also called a water audit, and the acoustic leak detection method discussed in the previous section.

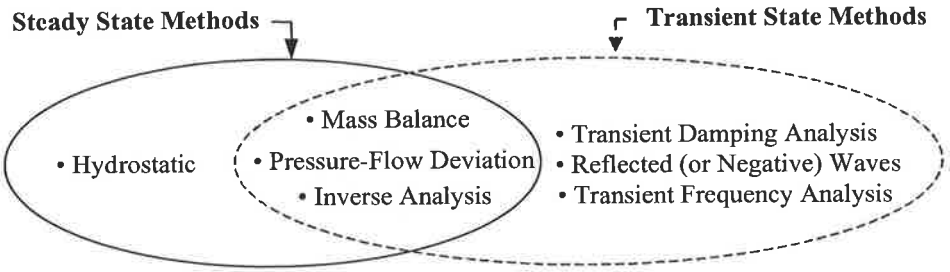

Figure 2.2 Relation of different hydraulic leak detection methods

The various hydraulic leak detection methods presented in Figure 2 are classified based on the different hydraulic effects of the leaks. The presence of leakage in a pipeline results in a pressure decline, the concept behind hydrostatic methods, while the mass balance method is based on mass loss through the leakage. When transient pulses are examined, leaks change the damping, shape and frequency of the transient response. The three transient leak detection methods, namely the transient damping method (developed in this thesis), the reflected wave method and the transient frequency method, analyse changes produced from these three different phenomena. In the pressure-flow deviation method and the inverse transient method the changes in damping, shape and frequency are considered collectively. The magnitude of the leak can be represented by the relative flow rate through the leak with respect to the

flow in the pipeline; however, for some situations the relative leak area with respect to the cross-sectional area of the pipe is more suitable.

2.5.1 Hydrostatic methods

Hydrostatic methods hydraulically examine the pipeline in a static state. To verify the integrity of the pipes, the pipes are sealed and pressurised with water, oil or other fluids. The pressure in pipeline is checked using pre-installed pressure sensors to observe if there is any reduction of pressure that could mean the presence of a leak. Pipe manufacturers or utilities mostly use this method before the pipeline operation (Schwendeman 1987; Hough 1988) together with pipe strength tests. This type of test is easy to conduct, has good accuracy and sensitivity if the change of pressure with temperature is considered. This method is also widely used for leak detection in pressure vessels (Megyesy 1998), in electrical engineering to detect the leaks in high-pressure oil-filled electrical cables (Williams et al. 1983) and in water distribution networks (Paquin et al. 2000). Since the pipeline must be sealed, the hydrostatic leak detection method is difficult to apply to existing pipelines and water distribution networks, which generally are open systems in operation. In addition, this method cannot locate the position of leaks. An approximate leak location can be estimated by checking the flow direction at different sections in the pipeline; however, currently available flowmeters are not sensitive enough to identify the flow rate induced by small leaks. In some cases, the flow rate due to temperature difference in the pipe (or cable) is often as large as the flow rate due to the leaks (Williams et al. 1983).

Typically the hydrostatic method is applied jointly with the mass balance method in which the volume change in relation to a temperature change must be carefully addressed. Vista Research Inc. developed an HT-100 system that was able to test large underground hydrant lines that transport fuel at airports by calculating the expected change in volume due to temperature changes and comparing it to actual measurements (Maresca and Fierro 1996). Vista claims that their HT-100 system can detect leaks as small as 0.004% of pipeline volume in 1½ hours (Vista Research Inc 2001). Location of a leak cannot be detected by these methods.

2.5.2 Mass (or volume) balance methods

Mass (or volume) balance leak detection methods follow the principle that the metered inlet volume, less the metered outlet volume, less the change in the mass inventory (or line pack) due to the compressibility of the fluid and pipe wall should always be zero if the pipeline is not leaking,

$$V_L = V_{in} - V_{out} - \Delta V \tag{2.1}$$

where V_L = leakage volume, V_{in} = metered inlet volume, V_{out} = metered outlet volume and ΔV = line pack or inventory volume. This method and the pressure-flow deviation method (discussed in the next section) are the most commonly used model-based leak detection programs in the oil and gas industry (Griebenow and Mears 1989; Furness and Reet 1998; Zhang 1996). The accuracy of this method mainly depends on the accuracy of the flow meters and the calculation of flow inventory, which can be calculated using the water hammer equations (Liou 1994; Furness and Reet 1998). The detection time will depend on the size of the leak and the flow conditions in the pipeline. Large leak sizes and steady flow require less detection time. Assuming an accurate fluid density is known, the smallest detectable leak has been estimated as 1% of the maximum flow rate during steady state conditions and 4% of the maximum flow rate during strong unsteady state conditions according to Mears (1988).

In water distribution systems, the volume of water flowing into and out of the network may be assessed using a water audit. Typically the mass inventory term ΔV described in Eq. (2.1) is ignored. A water audit is conducted by first dividing the distribution network into sub-districts. If a sub-district can be isolated, such that all inlet and outlet points are metered, or can be accessed for flow measurement, the leakage in a sub-district can be calculated using Eq. (2.1). Because the flows in a distribution network are continually changing, a water audit should be performed over at least a 24-hour period (Smith et al. 2000). Most water distribution networks are difficult to divide into sub-districts, especially for looped networks that are very common in well-designed water distribution systems. Procedures as well as practical measures for water audits of water distribution systems are found in Smith et al. (2000) and AWWA (1987). When using a water audit, not only leakage but also

other unaccounted-for water losses, such as water theft, can be detected. However, the sensitivity of the water audit to leakage is low, and is normally above 10% of total flow rate. A completed water audit normally takes several days depending on the size of the network, and at some cases it may take months.

Mass balance leak detection methods can be used to monitor the integrity of a pipeline system on a real-time basis. The response time to a leak occurrence depends on the size of the leak, complexity of the pipeline system and accuracy of the meters. These methods cannot detect the location of the leak and require its use in combination with other leak detection methods to locate leaks.

2.5.3 Pressure-flow deviation methods

Pressure-flow deviation methods are widely used in model-based leak detection programs in combination with mass balance methods to provide real-time leak detection over a wide range of operating conditions. These methods not only detect leaks but also provide information about the size and location of the leak. The underlying assumption governing this method is that the calculated pressure and flows based on either steady state or transient models should be equal to the measured values if there is no leak in the pipeline. A leak is declared if there are deviations between the two. Because of the quicker detection time, most of the pressure-flow deviation methods applied in the leak detection systems are based on transient models (Billmann and Isermann 1987; Griebenow and Mears 1989; Liou and Tian 1994; Dinis et al. 1999 and Fukushima et al. 2000). Measured values, normally the upstream flow (or pressure) and downstream pressure (or flow) from a SCADA (supervisory control and data acquisition) system, are used as boundary conditions for the transient modelling analysis. The calculated pressure and flows are compared with the measured values at the upstream end, downstream end and at any other location in the pipeline. In reality, the calculated values are rarely equal to the measured values even when there is no leak in the pipeline because of the inaccuracies in measurements and the parameters of the pipeline used in the models, such as density of the fluid, roughness, diameter of the pipe and unsteady friction effects (see Section 4.7 and Section 7.4). Therefore, a tuning process is needed that

is conducted for a pipeline assuming no leaks. Some degree of protection is necessary by setting upper and lower limits on the tuning parameters to reduce the chances of a large leak being masked by the tuning process (Lippitt 1987; Mears 1988).

When a discrepancy between the calculated and measured pressure and flows exceeds a pre-set threshold, a leak alarm is generated. At this point, an application routine is called to determine the size and location of the leak. The size of the leak is estimated from the flow rate discrepancy values. Then the pipeline operation is simulated with the leak assumed at various locations along the pipeline. Calculated pressures and flow rates are compared to the actual measured values, the assumed leak location with the best fit is taken as the estimated position of the leak. The detection time using the pressure-flow deviation method is normally of the order of minutes depending on the size of the leak, accuracy of measurement values and the model used. Based on tests of the Williams Pipelines—a 534.2km, 406.4mm pipeline and a 305.7km, 340.8mm pipeline —a leak flow of 5% of the total flow was determined in a response time of approximately 5 minutes (Mears 1988). Given enough time, the error in the detected leak location was about 16km for a 5% leak flow rate, and 2.4km for 10% leak flow rate. A leak detection system based on the pressure-flow deviation method was installed in the Niigata-Sendai gas pipeline in Japan. Based on site tests, the minimum detectable leak flow rate was about 1.1%. The average detection time was 4 minutes and the average error of the detected leak location was about 6% of the 250km pipeline length (Fukushima et al. 2000).

Based on the assumption of steady state flow conditions, equations for leak location using flow discrepancies at both ends of a pipeline were derived by Furness and Reet (1986) and Baghdadi and Mansy (1988), or more simply by Nigol (1970a, 1970b). Since, in reality, the flow in a pipeline is rarely absolutely steady, a long period measurement is necessary. Therefore, the response time for steady state models is slower, normally of the order of hours.

2.5.4 Inverse analysis methods

Pressure-flow deviation methods are actually a subset of inverse leak detection methods. The reason that these methods are classified in a different group is that inverse methods have been presented for pipeline networks, especially water distribution networks that have much more complex configurations than normal oil and gas pipelines. As a result, inverse methods have many unique characteristics compared to the original pressure-flow deviation methods.

Inverse analyses have been popularly used in groundwater and transport problems. Pudar and Liggett (1992) presented the first application of inverse analysis for leak detection in water distribution systems. Based on a steady state pipe network model, leak flow was modelled assuming an orifice discharging to the atmosphere at the junctions (nodes) of pipes. Minimisation of the deviation between the measured and calculated pressures by a least square regression technique produced solutions for the area and location of the orifice, and thus the leak. Emphases were given on the configurations of the network, which lead to inverse problems that were under-determined, even-determined or over-determined. It was found that calculation of the leak location and size was sensitive to the quantity and quality of the measurement data and the parameters of the pipes. In Mukherjee and Narasimhan (1996), in which a leak at a non-node position was addressed, a similar approach was used and laboratory verification tests were conducted. It was found that for a single leak of 10% of the total flow, two thirds of the cases were successful and for double-leak cases, only one third of cases were successful.

As an improvement to the steady state inverse method, by applying a transient model, Liggett and Chen (1994) developed an inverse transient method (ITM) based on the fact that massive amount of transient measurement data could be provided by modern monitoring systems. Using this approach it was expected that more measurement data could lead to pipe calibration—determination of the friction factors of the pipes--which in turn could lead to better prediction of leaks. This model was examined in a simple network consisting of 11 pipes and 7 nodes using model-generated (based on unsteady flow simulation) measurement data. In addition to the leak information, the inverse transient method can be used for calibration of numerous system parameters

given enough measurement data. Nash and Karney (1999) presented an application of ITM in a series-connected pipeline, where a valve was used for transient generation and again the measurement data were artificially generated by a transient model. To improve the efficiency of the optimisation, which was normally based on a gradient method (Liggett and Chen 1994; Nash and Karney 1999), a genetic algorithm search method was implemented into ITM (Vítkovský et al. 2000)

The inverse transient method has been verified in a straight single pipeline in the Robin Hydraulic Laboratory at the University of Adelaide using *real* measurement data (Vítkovský 2001). Quite surprisingly, the biggest problem confronted during the application was the modelling of the transient in the pipeline. Previously such calculations had been considered as a mature technique. From a pipeline-safety-design point of view, the modelling of pipeline transients is mature since the factor of most interest is the value of the peak pressure head. The present transient models calculate this value reasonably accurately. However, the normal transient models were far from satisfactory when applied in inverse transient method. Compared to the measured transients, the transient models gave less damping and a phase difference, which can result in significant deviations between the measured and calculated data. The main reason for these deviations lies in the unsteady friction (two-dimensional or three-dimensional effects), which are not considered or not correctly considered by most transient models (Wylie and Streeter 1993; Zielke 1968; Vardy and Huang 1991, Brunone et al. 1995). As a result, an improved unsteady friction model, which can accurately simulate a transient event initiated by closing a downstream valve, has been developed (Vítkovský 2001). In applying the improved unsteady friction model, the inverse transient method detected a 0.15% leak of the pipe cross sectional area in terms of both location and size of the leak.

The inverse transient method presents a quick way of monitoring the integrity and for parameter calibration for water distribution systems. With progress in remote communication and computational capabilities, real-time inverse transient analysis is feasible. The real challenge for the application of the inverse transient method is the accurate modelling of transients and boundary conditions in a pipe network. Traditional transient models based on quasi-steady friction always under-predict

transient damping (Wylie and Streeter 1993). Some previous studies on leak detection methods have considered random noise in model-generated data in an attempt to approach real measured data (Liou and Tian 1995; Chen 1995). Although sufficient for a steady state process, systematic errors for a transient process may cause different problems. For example, a slight phase difference between the modelled and measured data (from an error in the assumed wave speed or in the friction model) results in a great difference between measured and computed pressures. Unsteady friction models can partially improve the situation; however, they are still not accurate or practical (such as some 2D models by Eichinger and Lein 1992, Pezzinga 1999) enough to be applied in inverse leak detection successfully. In single oil and gas pipelines, a tuning process normally addresses the differences between measured and modelled values. The possibility of applying a similar procedure to a pipe network, which has more uncertainties, is investigated in this thesis at Chapter 8.

2.5.5 Reflected (or negative) wave methods

When a transient travelling in a pipeline reaches a leak, the transient is partially reflected and partially transmitted. If the reflected wave (normally the first reflected one) can be distinguished from the measured transient, the location of the leak can be determined by multiplying half of the reflection time by the wave speed of the pipeline. The concept of this method is simple and easy to apply with the condition that the initiating time of the transient must be smaller than the reflection time between the leak and measurement location. The size of the leak can be calculated from the decreased magnitude of the reflected transient in comparison to the transient for a no-leak situation (Covas and Ramos 1999; Lee et al. 2000). This method can be used on a regular basis for leak detection. Experimental tests conducted in a 352m long polyethylene pipe with a diameter of 93.8mm showed that a leak of 0.5% of the pipe cross-sectional area could be identified (Brunone 1999). Based on laboratory tests conducted in a single pipeline at the University of Adelaide, a leak of 1mm diameter in a 22mm diameter pipeline was identified successfully (Lee et al. 2000). This method can be used on a real-time basis for monitoring of pipeline rupture. Experimental tests conducted in two PVC pipelines with length of 433m and 1248m

respectively showed that ruptured leaks down to 5% of total pipeline flow could be identified (Silva et al. 1996).

Some pipeline elements, such as elbows, changes in pipe diameters, or partially closed valves also cause transient reflections, which result in a leak induced transient reflection that is not identified in some situations depending on the location of the transient measurement (Furness and Reet 1998). In addition, it is difficult to apply the reflected wave method to pipe networks.

2.5.6 Frequency analysis methods

When a leak exists in a pipeline, the freely damped transients measured in such a pipeline are changed compared to the no-leak situation. To extract the leak information contained in the measured transients, Fourier transforms may be used to transform the time-domain data into the frequency domain. By comparing the dominant frequencies between the no-leak pipeline and leaking pipeline, the leak location can be calculated from the frequencies for limited cases (Jönsson and Larson 1992; Covas and Ramos 1999). The reason for the cases where the method doesn't work is that the changes of transient shape (frequency) not only depends on leakage, but also depends on shape of the transient and the measurement locations (Wang et al. 2002). For example, if a sinusoidal-form transient is used, the presence of a leak in a pipeline will not change the shape of the transient.

Rather than using a freely damped transient, a steady-oscillatory transient (constant amplitude periodic transient) can be generated using a periodic forcing function at a boundary of a pipeline system. Analysis of the response of the pipeline system to different frequency forcing functions determines the leak location and size. For a system with leaks, Mpesha et al. (2001) report that additional resonant pressure peaks characterise the location and size of the leaks as compared to the resonant peaks for the system with no leaks, although recent work at the University of Adelaide has indicated that this approach is invalid (Lee et al. 2002). The application of such a technique is limited by the difficulty in generating a high-frequency forcing function using an oscillating valve. Alternatively, a boundary forcing function can be

achieved by a vibrating membrane attached at an end of a pipe section. The feasibility of this apparatus is currently under investigation at the University of Adelaide (Lee et al. 2002).

2.5.7 Transient damping methods

When a transient propagates in a pipeline, the transient decays due to pipe friction and leaks. By examining the leak-induced damping as compared to the transient damping in the same pipeline without leakage, leaks can be detected. This effect was applied for real-time non-interceptive pipeline integrity monitoring using pseudo-random binary disturbances (Liou 1998). The presence of the leak was detected by the discontinuity of the impulse response at the leak along the pipeline. A sensitivity study based on the method of characteristics showed that the damping of a pipeline impulse depends on size of the leak and the pressure in the pipeline.

More recently, a linear analytical solution for the transient in a pipeline with leaks was derived by Wang et al. (2002). The analytical solution showed that the friction-induced damping of pipeline transient is exactly exponential and that leak-induced damping is approximately exponential. The rate of the leak-induced damping not only depends on the size and location of the leak, but also depends on the pressure in the pipeline, transient measurement position and initial condition of the transient (shape of the transient). Based on the analytical solution, a leak detection technique has been developed as part of this Ph.D. research. This method does not require rigorous determination and modelling of boundary conditions and modelling of the transient behaviour in the pipeline. The technique has been successfully used in detecting, locating and quantifying a 0.2% size leak with respect to the cross-sectional area of a pipeline based on both numerical and laboratory experiments (Wang et al. 2002). Details of this work are given in the Chapter 3 and Chapter 4 of this thesis, and the possibility of applying this method into pipeline networks is investigated.

2.6 Blockage detection methods

This section presents a review of the previously developed blockage detection methods. Compared to leak detection methods, fewer blockage detection methods have been developed. Because many leak detection methods may be applied for blockage detection in pipeline and pipe network systems, some potential methods will be discussed in this section. Similar to leak detection methods, blockage detection methods used for pipelines (including pipe networks) can be classified into the following four groups:

1. Pipe-strain based methods
2. Methods based on chemical properties
3. Online pig and optical fibre camera (OFC) methods
4. Hydraulic methods

Unlike a leak, most blockages do not emit an obvious acoustic signal. A review of the above four types of methods is given in the following sections with an emphasis on hydraulic methods.

2.6.1 Pipe-strain based methods

Because the presence of a blockage does not create any visible change at the vicinity of the pipeline, offline observation and surveillance methods used for leak detection are not applicable for blockage detection. However, since a blockage may cause a local pressure change, a ROV (remotely operated vehicle) based inspection method was presented by Rogers (1995) by measuring the blockage-induced strain change of the pipe wall. Since this method cannot be applied continuously, the response for a blockage occurrence is slow. In addition, the difficulty in distinguishing the blockage-induced strain change from other sources, such as temperature changes, limits the application of this method in a real pipeline.

2.6.2 Methods based on chemical properties

In petroleum and chemical engineering, blockage development is related to the chemical components of the fluid in the pipes. For example, with the increase of some of hydrates in a sub-sea flow line, the possibility of blockage formation increases significantly (Hunt 1996). Therefore, analyzing the fluid properties and ingredients helps in determining the potential development of the blockage (Hunt 1996). Unfortunately, this method cannot provide the location of the blockage, nor can it be applied to water distribution systems.

2.6.3 Online pig and OFC based methods

On-line pig-based methods are the most commonly used method not only for blockage detection, but also for blockage repair and clearance. With the regular application of a pig operation, the development of a blockage can be avoided at an early stage (Pipeline Engineering Inc 2001). However, similar to the leak detection, the pig-based methods cannot be easily applied to a pipe network for blockage detection due to the complexity of the pipe network. An apparatus used in the water distribution pipe network for pipe inspection, which is similar to a pig, is an optical fibre camera (Stephens 2002). By inserting an optical fibre camera into a pipe, the conditions of a pipe wall can be inspected. This technique not only gives the information of blockage, but also the corrosion condition of the inside pipe wall. A major problem for this method is the efficiency since the optical fibre camera can only move a limited distance at moment.

2.6.4 Hydraulic-based methods

Similar to leaks, presence of a blockage also changes the hydraulic characteristics of the fluids in a pipeline system. Therefore, each method developed for leak detection has the potential for blockage detection by examining the changed hydraulic characteristics. Some hydraulic-based blockage detection methods have been presented and will be discussed in the following sections. Some potential blockage detection methods, which have been presented for leak detection, are discussed. The magnitude of a blockage is normally characterised by the ratio ($r_B = C_d A_B/A$) of the

cross-sectional area of a blockage ($C_d A_B$) over the pipe cross-sectional area (A). The value of r_B ranges from 0.0 to 1.0 with 0.0 indicating no blockage and 1.0 a fully closed blockage.

Because a blockage acts to reduce the volume of a pipeline available for flow, theoretically, the presence and magnitude of a blockage can be obtained by checking the reduced total volume of a pipeline (Scott and Yi 1999). The reduction of pipeline volume depends on the length and diameter of the blockage. A fairly long partial blockage is required to get an observable reduction of pipeline volume. In this method, the volume of the pipeline is estimated by the relative expansion of the pipeline volume by a liquid bleeding-off test (Scott and Yi 1999). The performance of this method depends on the blocking agents and the fluids in the pipeline. For example, only aged and hardened solids, such as waxes will be distinguished from oil in a pipeline.

Because the presence of a blockage does not change the mass conservation of the fluid in a pipeline under steady state, the mass (or volume) balance methods widely used for leak detection cannot be used for blockage detection. However, a blockage does influence the momentum balance of the fluid in a pipeline. This momentum imbalance is normally characterised using a head loss of the flow across the blockage. This head loss will influence the steady state pressure distribution along a pipeline (Scott and Satterwhite 1998) and in a pipe network (Jiang et al. 1996). The magnitude of a blockage can be estimated from the measured pressures based on a trial-and error scheme. Because both the blockage and pipe friction cause head loss, accurate friction information of the pipeline is necessary to apply this type of method. Both numerical and laboratory tests showed that locating a blockage was difficult, and the magnitude of the blockage was significantly influenced by the location of the blockage.

Compared to leakage, fewer blockage detection methods have been developed based on transient methods. Adewumi et al. (2000) investigated the possibility of using a reflected transient by a blockage to detect the existence, location and severity of blockages, and the method has shown some promise based on several numerical

examples. The results of the Ph.D. study reported in this thesis shed some light on the unsteady behaviour of a blockage in a pipeline. An analytical solution is derived in Chapter 6 to understand the effects of a blockage on the fluid transients. In addition, the feasibility of applying the inverse transient method (Liggett and Chen 1994) for blockage detection is under investigation at the University of Adelaide (Stephens et al. 2002).

2.7 Summary

For model-based leak detection methods, the extension to transient analysis improves the efficiency of leak detection in simple pipeline systems due to their quick response and real-time application. The application of some other transient-based leak detection methods including transient reflection methods, transient damping and transient frequency analysis in simple pipelines can further improve the response time and accuracy of leak detection and location.

Currently the most commonly used method for leak detection in water distribution systems is the combined application of a water audit and acoustic methods, which are time intensive and inefficient. The transient-based inverse leak detection method has shown promise in integrity monitoring and pipe parameter calibrations in water distribution systems. However, application to the real pipeline networks is very much in its infancy. There is still a gap to apply these "efficient" transient methods in real pipe systems. The research presented in this Ph.D. research will help close this gap.

There has been much less research conducted on blockage detection compared to leak detection technique. A limited application of transient based blockage detection method has shown promise. Transient-based methods, which are successful for leak detection, may be used for blockage detection and are investigated in this research.

Chapter 3

Behaviour of a Leak on Pipeline Transients under Constant Boundary Conditions

3.1 Introduction

Fluid transients, which can be initiated by a pump shutting down, valve movement, change in tank level or pipe vibration, are common phenomena in pipeline systems. The pipe flow and pressure transients can be described by a set of non-linear, hyperbolic equations derived from the conservation of mass and Newton's second law of motion (conversation of linear momentum) (Wylie and Streeter 1993). A closed-form solution for these equations is impossible due to the nonlinearity of the momentum equation. A number of methods have been developed to solve these equations analytically where the nonlinear term is either neglected (Allievi 1925) or linearized (Wood 1937; Rich 1945). These equations can also be solved numerically using the method of characteristics (MOC) and other numerical methods (Chaudhry 1987; Wylie and Streeter 1993) where the nonlinear terms are approximated using different schemes. Predominately, transient pipe flows have been studied using one-dimensional models assuming a uniform velocity profile due to its calculation efficiency. The neglected two-dimensional or three-dimensional friction effects are normally approximated by unsteady-friction models (Zielke 1968; Brunone et al. 1995; Vardy and Hwang 1991) with reasonable success. In this chapter and in the following chapters, transient pipe flow is investigated as a one-dimensional problem. The effects of unsteady friction on fluid transients are investigated in Chapter 4.

When a leak exists in a pipeline, the transients in such a pipeline are changed compared to the no-leak situation. Transient response of a pipeline with a distributed leak was investigated by Wiggert (1968). He found that the transients in a pipeline were greatly affected by the magnitude of distributed lateral flow. To investigate the effects of the demands on the transients in a field pipe network test, McInnis and Karney (1995) used a similar distributed leak model based on the method of characteristics. Predominately, the transients in a pipeline with leaks were studied numerically using the method of characteristics (MOC), in which the leak is considered as a boundary condition based on an orifice equation and flow conservation (Wylie and Streeter 1993). Although, the numerical methods have the advantage of generality on simulating complex network topology and with different boundary conditions, analytical solutions can provide significant insight into the understanding of the effects of a leak on pipeline transients. In this chapter, effects of a leak on pipeline transients are investigated analytically. Some of the results presented in this chapter are included in Wang et al. (2002), in which a leak has a theoretical square-root discharge-head relationship. Leaks with different discharge relationships are also considered in this chapter. Details of the derivation of the governing equations for transients in a pipeline with a leak, which have been presented in Wang et al. (2002), are included here for the completeness of the thesis and for the convenience of the reader. Analytical solutions expressed as a Fourier series under constant boundary conditions are obtained and details of the derivation of the solution are given in Appendix A. The solution for transients in a pipeline having more than one leak is also given. The linearization error on the accuracy of the analytical solution is investigated and the analytical solutions are compared with the numerical results based on the method of characteristics.

3.2 Governing equations

A control volume located between points 1 and 2 in Figure 3.1 is considered for the derivation of the unsteady flow equations (continuity and momentum) with leakage. The pipe is assumed to be horizontal with a leak located at $x = x_L$, as shown in Figure 3.1, where Q_L is the discharge out of the leak.

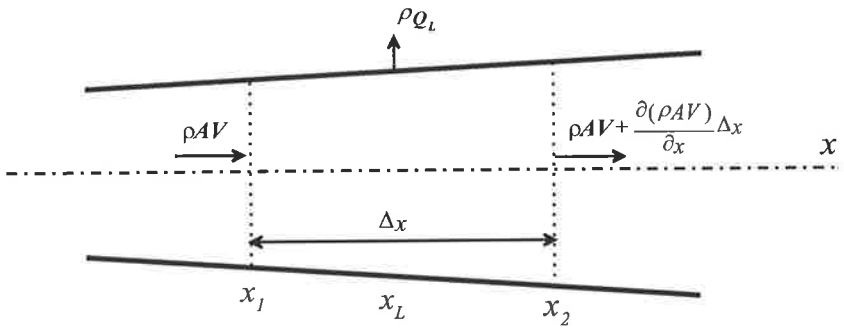

Figure 3.1 A pipe section with a leak

Adapting the non-leak equation of Wylie and Streeter (1993), conservation of mass in the control volume gives

$$\frac{\partial}{\partial t}(\rho A)\Delta x+\frac{\partial}{\partial x}(\rho AV)\Delta x=-\rho Q_L \tag{3.1}$$

where x = distance along the pipeline, t = time, ρ = fluid density, A = cross-sectional area of the pipe, and V = velocity of flow. Dividing Eq. (3.1) throughout by Δx and letting Δx approach zero gives

$$\frac{\partial}{\partial t}(\rho A)+\frac{\partial}{\partial x}(\rho AV)=-\rho Q_L\delta(x-x_L) \tag{3.2}$$

The Dirac delta function is defined as

$$\delta(x-x_L)=\begin{cases}\infty & \text{if} \quad x=x_L \\ 0 & \text{otherwise}\end{cases} \tag{3.3}$$

so that

$$\lim_{\varepsilon\to 0}\int_{x_L-\varepsilon}^{x_L+\varepsilon}\delta(x-x_L)\,dx=1 \tag{3.4}$$

where ε = a small distance on the either side of the leak. Note that $\delta(x\text{-}x_L)$ has dimension of (L^{-1}). Considering the compressibility of the water, the elasticity of the pipe wall and constant pipe-cross section area (A), with some simplifications (Wylie and Streeter 1993), Eq. (3.2) is expressed in the more usual water-hammer-equation form (with the addition of the leak term) of

$$\frac{\partial H}{\partial t}+\frac{Q}{A}\frac{\partial H}{\partial x}+\frac{a^2}{gA}\frac{\partial Q}{\partial x}+\frac{a^2}{gA}Q_L\delta(x-x_L)=0 \tag{3.5}$$

in which H = piezometric head, Q = the flow rate in the pipeline, a = wave speed in the fluid and g = gravitational acceleration.

Conservation of momentum in the control volume with respect to the x-direction gives (Wylie and Streeter 1993)

$$\frac{\partial}{\partial t}(\rho AV)\Delta x+\frac{\partial}{\partial x}(\rho AV^2)\Delta x=\sum F_x \tag{3.6}$$

The forces acting on the control volume as shown in Figure 3.2 are:

1. Pressure forces at section 1 and section 2: $F_{p1}=p_1A_1$, $F_{p2}=p_2A_2$
2. Pressure force on the converging (or diverging) sides: $F_{p12}=0.5(p_1+p_2)(A_1-A_2)$
3. Weight of the fluid: $F_w=\rho gA\Delta x$
4. Shear force: $F_s=\tau_0\pi D(x_2-x_1)$
5. Pressure force at the leak orifice: $F_L=p_LA_L$

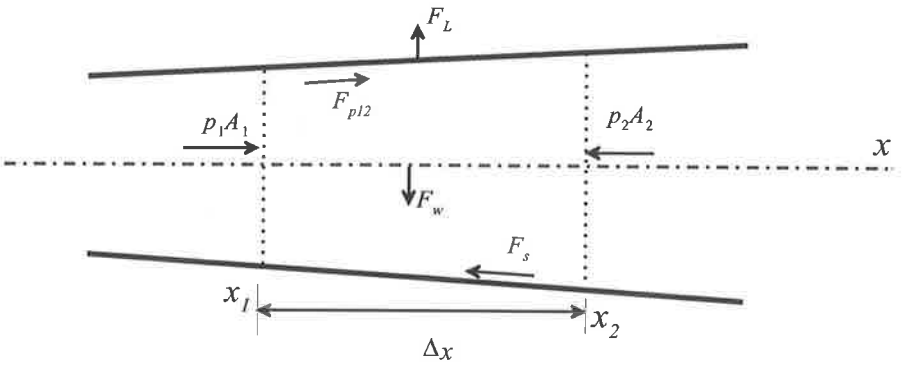

Figure 3.2 Free-body diagram for derivation of the momentum equation

Considering the downstream flow direction as positive, the total x direction force components acting on the control volume can be expressed as

$$\begin{aligned}\sum F &= p_1A_1-p_2A_2-0.5(p_1+p_2)(A_1-A_2)-\tau_0\pi D(x_2-x_1)\\ &=0.5(p_1-p_2)(A_1+A_2)-\tau_0\pi D(x_2-x_1)\end{aligned} \tag{3.7}$$

Note that the weight force and pressure force at the leak orifice do not act in the x-direction and are not considered in the conservation of momentum. Substituting Eq. (3.7) into Eq. (3.6), then dividing by Δx and letting Δx approaching to zero gives

$$\frac{\partial}{\partial t}(\rho AV)+\frac{\partial}{\partial x}(\rho AV^2)+A\frac{\partial p}{\partial x}+\tau_0\pi D=0 \tag{3.8}$$

Applying the Darcy-Weisbach formula for shear stress ($\tau_0 = \rho f V^2/8$) to Eq. (3.8) gives

$$\frac{\partial}{\partial t}(\rho AV)+\frac{\partial}{\partial x}(\rho AV^2)+A\frac{\partial p}{\partial x}+\frac{\rho AfV^2}{2D}=0 \tag{3.9}$$

where f = Darcy-Weisbach friction factor and D = pipe diameter. In Eq. (3.9), the unsteady shear stress is approximated by the steady state shear stress, and the pipe friction during the transient event is described by the steady state Darcy-Weisbach friction factor—a common assumption. However, pipe friction during unsteady events has been shown to be significantly larger than that predicted by the steady state Darcy-Weisbach friction factor. The effects of unsteady friction are dealt with later in Chapter 4.

Expanding the terms in the parentheses in Eq. (3.9) and rearranging gives

$$V[\frac{\partial}{\partial t}(\rho A)+\frac{\partial}{\partial x}(\rho AV)]+\rho A\frac{\partial V}{\partial t}+\rho AV\frac{\partial V}{\partial x}+A\frac{\partial p}{\partial x}+\frac{\rho AfV^2}{2D}=0 \tag{3.10}$$

Substituting continuity equation Eq. (3.2) into (3.10) and dividing the equation by ρA gives

$$\frac{\partial V}{\partial t}+V\frac{\partial V}{\partial x}+\frac{1}{\rho}\frac{\partial p}{\partial x}+\frac{fV^2}{2D}-\frac{QQ_L\delta(x-x_L)}{A^2}=0 \tag{3.11}$$

Eq. (3.11) can be expressed in the more usual water-hammer-equation form (assuming constant pipe area A) of

$$\frac{\partial H}{\partial x}+\frac{1}{gA}\frac{\partial Q}{\partial t}+\frac{Q}{gA^2}\frac{\partial Q}{\partial x}+\frac{fQ^2}{2DgA^2}-\frac{QQ_L\delta(x-x_L)}{gA^2}=0 \tag{3.12}$$

The leak discharge is a function of the pressure in the pipe and the size of the leak and may be expressed by the orifice equation

$$Q_L = C_d A_L (2g\Delta H_L)^b \tag{3.13}$$

where ΔH_L = H_L-z_L = pressure head at the leak (assuming the pressure outside of the pipe is atmospheric), H_L = piezometric head in the pipeline at the leak, z_L = the pipe elevation at the leak, C_d = leak discharge coefficient, A_L = leak area parameter for the discharge-head relationship of a leak. Theoretically, b is equal to 0.5 for a sharp orifice. The value of b may vary with the shape of the orifice and the Reynolds number. In addition, when b is not equal to 0.5, parameter C_d becomes dimensional. For this reason, an equivalent theoretical leak area is used for a non-theoretical leak and more details are

given in Section 3.3(page 36) and Chapter 4. The results presented in Wang et al. (2002) were based on theoretical leaks of $b = 0.5$.

The following dimensionless quantities are used to non-dimensionalize Eqs. (3.5), (3.12) and (3.13):

$$H^* = \frac{H}{H_1},\ t^* = \frac{t}{L/a},\ x^* = \frac{x}{L},\ Q^* = \frac{Q}{Q_0},\ \text{and}\ \delta(x^* - x_L^*) = \delta(x - x_L)L \tag{3.14}$$

in which H_1 = a reference pressure head (e.g., the head at a tank), L= the pipe length and Q_0 = a reference flow rate. Substituting Eq. (3.13) into Eqs. (3.5) and (3.12), and applying the dimensionless quantities in Eq. (3.14) to Eqs. (3.5), and (3.12) gives

$$\frac{\partial H^*}{\partial t^*} + \frac{V_0}{a}\frac{Q^*\partial H^*}{\partial x^*} + \frac{aQ_0}{gAH_1}\frac{\partial Q^*}{\partial x^*} + \frac{aQ_0}{gAH_1}\frac{C_d A_L}{Q_0}(2gH_1)^b(\Delta H_L^*)^b\delta(x^* - x_L^*) = 0 \tag{3.15}$$

$$\frac{gAH_1}{Q_0 a}\frac{\partial H^*}{\partial x^*} + \frac{\partial Q^*}{\partial t^*} + \frac{V_0}{a}Q^*\frac{\partial Q^*}{\partial x^*} + \frac{fLQ_0}{2DAa}(Q^*)^2 - \frac{V_0}{a}\frac{C_d A_L(2gH_1)^b}{Q_0}Q^*(\Delta H_L^*)^b\delta(x^* - x_L^*) = 0 \tag{3.16}$$

Because V_0/a is small for pipeline systems that have a sufficiently large wave speed, the second term in Eq. (3.15) and the second and the last terms in Eq. (3.16) can be neglected. The dimensionless equations become

$$\frac{\partial H^*}{\partial t^*} + \frac{1}{F}\frac{\partial Q^*}{\partial x^*} + M(\Delta H_L^*)^b\delta(x^* - x_L^*) = 0 \tag{3.17}$$

$$F\frac{\partial H^*}{\partial x^*} + \frac{\partial Q^*}{\partial t^*} + RQ^{*2} = 0 \tag{3.18}$$

in which

$$R = \frac{fLQ_0}{2aDA},\quad M = \frac{C_d A_L}{A}\frac{2a}{(2gH_1)^{1-b}}\ \text{and}\ F = \frac{H_1}{H_S} \tag{3.19}$$

and where $H_s = \frac{aV_0}{g}$ is the Joukowsky pressure head rise, resulting from an instantaneous reduction of velocity V_0 to zero. The dimensionless quantities R, M and F are used to characterize the leak problem. The parameter R was defined by (Liou 1991) as a pipeline characteristic associated with pipe friction. The parameter M in Eq. (3.19)

is a dimensionless leak quantity. The parameter F is the ratio of the steady state pressure head H_1 to the Joukowsky pressure head rise H_s.

Note that in Eq. (3.14), the pressure head in the pipeline is non-dimensionalized using the water head (H_1) in a tank. Liou (1991) and Wylie (1996) proposed that the water hammer equations can be non-dimensionalized using Joukowsky pressure head rise H_s, and result in a similar form (without the leak).

Expressing H^* and Q^* as a steady-state value plus a small transient quantity gives

$$H^* = H_0^* + h^* \text{ and } Q^* = Q_0^* + q^* \tag{3.20}$$

where h^* = a non-dimensional head disturbance from a non-dimensional steady head H_0^*, and q^* = a flow disturbance from a steady flow Q_0^*. When only linear terms are retained, the square root in Eq. (3.17) may be expressed as

$$\begin{aligned}(\Delta H_L^*)^b &= (H_L^* - z_L{}^*)^b = (H_{L0}^* + h^* - z_L^*)^b = (\Delta H_{L0}^* + h^*)^b \\ &\approx (\Delta H_{L0}^*)^b + \frac{bh^*}{(\Delta H_{L0}^*)^{1-b}}\end{aligned} \tag{3.21}$$

where $\Delta H_L^* = H_L{}^* - z_L{}^*$ = dimensionless pressure head at the leak, $H_L{}^*$ = dimensionless piezometric head in the pipeline at the leak, $z_L{}^* = z_L/H_1$ = the dimensionless elevation at the leak, z_L = elevation at the leak, and $H_{L0}{}^*$ = the dimensionless steady-state piezometric head at the leak. The dimensionless linearization error in Eq. (3.21) is

$$e_T = \frac{(\Delta H_L^*)^b - [(\Delta H_{L0}^*)^b + \dfrac{bh^*}{(\Delta H_{L0}^*)^{1-b}}]}{(\Delta H_L^*)^b} \tag{3.22}$$

Substituting Eqs. (3.20) and (3.21) into Eqs. (3.17) and (3.18) and neglecting the higher order term of q^{*2} in the resistance term yields

$$\frac{\partial h^*}{\partial t^*} + \frac{1}{F}\frac{\partial q^*}{\partial x^*} + M\frac{bh^*}{(\Delta H_{L0}^*)^{1-b}}\delta(x^* - x_L^*) = 0 \tag{3.23}$$

$$F\frac{\partial h^*}{\partial x^*} + \frac{\partial q^*}{\partial t^*} + 2Rq^* = 0 \tag{3.24}$$

Using the operation $\frac{\partial}{\partial t}[\text{Eq.(3.23)}] - \frac{\partial}{\partial x}\left[\frac{\text{Eq.(3.24)}}{F}\right]$ and

$$\frac{1}{F}\frac{\partial q^*}{\partial x^*} = -\frac{\partial h^*}{\partial t^*} - M\frac{bh^*}{(\Delta H_{L0}{}^*)^{1-b}}\delta(x^* - x_L^*) \tag{3.25}$$

from the continuity equation, Eq. (3.23), results in

$$\frac{\partial^2 h^*}{\partial x^{*2}} = \frac{\partial^2 h^*}{\partial t^{*2}} + \left[2R + M\frac{b\delta(x^* - x_L^*)}{(\Delta H_{L0}{}^*)^{1-b}}\right]\frac{\partial h^*}{\partial t^*} + 2RM\frac{bh^*\delta(x^* - x_L^*)}{(\Delta H_{L0}{}^*)^{1-b}} \tag{3.26}$$

Eq. (3.26) can be simplified as

$$\frac{\partial^2 h^*}{\partial x^{*2}} = \frac{\partial^2 h^*}{\partial t^{*2}} + [2R + F_L\delta(x^* - x_L^*)]\frac{\partial h^*}{\partial t^*} + 2RF_L\delta(x^* - x_L^*)h^* \tag{3.27}$$

in which $F_L = \dfrac{Mb}{(\Delta H_{L0}^*)^{1-b}}$ is the leak parameter. Since $\Delta H_{L0}^* = \dfrac{H_{L0} - z_L}{H_1}$, if $z_L = 0$, according to the definition of M in Eq. (3.19) the parameter describing the leak is

$$F_L = \frac{\dfrac{C_d A_L}{A}\dfrac{2ab}{(2gH_1)^{1-b}}}{(\dfrac{H_{L0}}{H_1})^{1-b}} = \frac{C_d A_L}{A}\frac{2ab}{(2gH_{L0})^{1-b}} \tag{3.28}$$

where H_{L0} = the steady-state piezometric head at the leak.

3.3 An analytical solution

Consider a pipeline connecting constant upstream and downstream reservoirs so that the boundary conditions for the dimensionless hydraulic line are

$$\text{B.C.} \quad h^*(0, t^*) = 0 \text{ and } h^*(1, t^*) = 0 \tag{3.29}$$

where the first quantity in the parentheses is the dimensionless distance along the pipeline and the second term is the dimensionless time. Supposing a transient is initiated in the pipeline, the initial conditions are

$$\text{I.C.} \quad h^*(x^*,0) = f(x^*), \text{ and } \frac{\partial h^*(x^*,0)}{\partial t^*} = g(x^*) \tag{3.30}$$

in which $f(x^*)$ and $g(x^*)$ are known piecewise continuous functions in the range of $0 \le x^* \le 1$. The head variation in the pipeline is obtained by solving Eq. (3.27) subject to the boundary and initial conditions described by Eqs. (3.29) and (3.30).

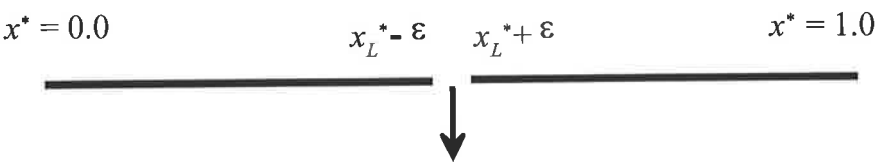

Figure 3.3 A pipeline with a leak

For a pipeline with a leak, the pipeline can be considered as two portions divided by the leak, which is included within a small neighborhood 2ε, as shown in Figure 3.3. By applying a Fourier expansion (details of the derivation are given in Appendix A), the solution to Eq. (3.27) is

$$h^*(x^*,t^*) = \sum_{n=1}^{\infty} \left\{ e^{-(R+R_{nL})t^*} \left[A_n \cos\sqrt{(n\pi)^2 - 4RR_{nL} - (R+R_{nL})^2}\, t^* + B_n \sin\sqrt{(n\pi)^2 - 4RR_{nL} - (R+R_{nL})^2}\, t^* \right] \sin(n\pi x^*) \right\} \tag{3.31}$$

in which $R_{nL} = F_L \sin^2(n\pi x_L^*)$

or
$$R_{nL} = \frac{C_d A_L}{A} \frac{2ba}{(2gH_{L0})^{1-b}} \sin^2(n\pi x_L^*) \qquad (n = 1, 2, 3,\ldots) \tag{3.32}$$

R_{nL} is the leak-induced damping factor for component n, where x_L^* is the dimensionless location of the leak along the pipeline. Since values of R and R_{nL} are normally much smaller than unity, Eq. (3.31) is approximated as

$$h^*(x^*,t^*) = \sum_{n=1}^{\infty} \left\{ e^{-(R+R_{nL})t^*} \left[A_n \cos(n\pi t^*) + B_n \sin(n\pi t^*) \right] \sin(n\pi x^*) \right\} \tag{3.33}$$

The Fourier coefficients, A_n and B_n, are

$$A_n = 2\int_0^1 f(x^*)\sin(n\pi x^*)dx^* \qquad (n = 1, 2, 3,\ldots) \tag{3.34}$$

$$B_n = \frac{2}{n\pi}\int_0^1 g(x^*)\sin(n\pi x^*)dx^* + \frac{(R+R_{nL})A_n}{n\pi} \qquad (n = 1, 2, 3,\ldots) \tag{3.35}$$

Eq. (3.33) shows that a leak in a pipeline causes exponential damping on individual Fourier components. The damping magnitude depends on the leak location (x_L^*), leak parameter F_L and the component number n. Effects of leak location on a fluid transient are combined with component number n through a sine square formula defined in Eq. (3.32). Further information on this formula is presented in Chapter 4 in which a leak

detection method is developed. F_L as defined in Eq. (3.28) is an important parameter to describe the damping effect of a leak on fluid transients and is further discussed here.

The definition of F_L in Eq. (3.28) shows that the magnitude of F_L is proportional to the relative size of the leak (C_dA_L/A). A large area of leak, compared to the cross-sectional area of the pipe, causes greater damping on a fluid transient since a larger size of a leak causes a greater amount of leak discharge. The magnitude of F_L is proportional to the wave speed (a) and is inversely proportional to the square root of the steady pressure at the leak (H_{L0}). This unsteady damping property is different from the steady state where the leak discharge is independent of the wave speed, and is proportional to the pressure at the leak. Therefore, a leak that causes large damping of the fluid transient does not necessarily cause a larger leak discharge. For example, a same size leak causes less damping on transients and more leak discharge in a pipeline with a higher pressure than in a pipeline with a lower pressure.

Another parameter that influences the magnitude of F_L is the coefficient b. If a leak with a non-theoretical discharge-head relationship ($b \neq 0.5$) causes the same leak discharge as a leak with a theoretical discharge relationship ($b = 0.5$), its effect on the transient will be different from the theoretical leak. The ratio of leak parameters is

$$\frac{F_L}{(F_L)_0} = \frac{\dfrac{C_d A_L}{A}\dfrac{2ab}{(2gH_{L0})^{1-b}}}{\dfrac{(C_d A_L)_0}{A}\dfrac{a}{(2gH_{L0})^{0.5}}} = \frac{2bC_d A_L (2gH_{L0})^{0.5}}{(C_d A_L)_0 (2gH_{L0})^{1-b}} \tag{3.36}$$

where $(C_dA_L)_0$ = lumped leak area with the theoretical discharge relationship, and $(F_L)_0$ = leak parameter with the theoretical discharge relationship. Multiplying both the denominator and the numerator by $(C_d A_L H_{L0})^{0.5+b}$ and noticing that $C_d A_L (2gH_{L0})^b = (C_d A_L)_0 (2gH_{L0})^{0.5}$, Eq. (3.36) may be simplified to

$$\frac{F_L}{(F_L)_0} = 2b \tag{3.37}$$

Eq. (3.37) shows that compared to a leak with a theoretical discharge relationship, a leak with a non-theoretical discharge relationship will cause $2b$ times damping of fluid transients although the discharge through these two leaks is the same. Since the value of b for a leak is normally not known unless the leak has been calibrated in advance, the

leaks can be approximated by the theoretical discharge relationship ($b = 0.5$). Given the same value of parameter F_L, an equivalent theoretical leak parameter is

$$(C_d A_L)_0 = C_a (C_d A_L) \tag{3.38}$$

where $C_a = 2b(2gH_{L0})^{b-0.5}$ = leak size adjustment coefficient. Values of C_a for different values of b and H_{L0} are plotted in Figure 3.4.

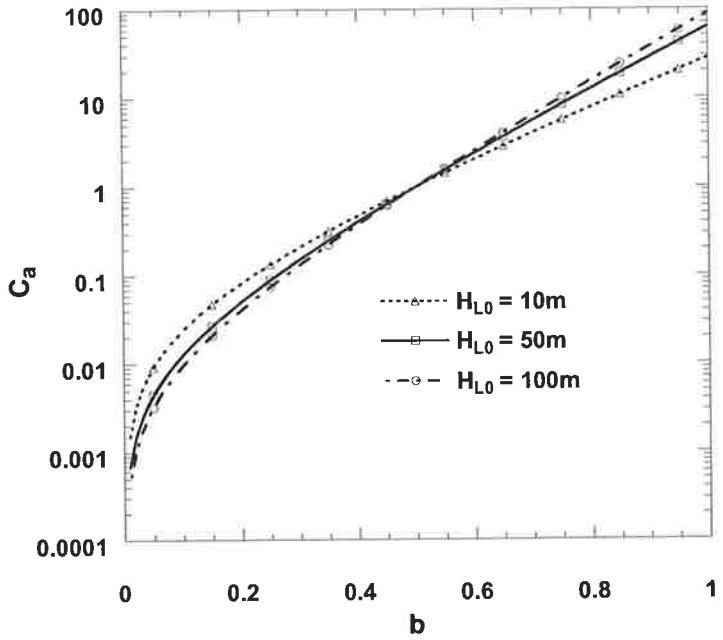

Figure 3.4 Adjustment for the lumped leak area

3.4 Exponential damping

When there is no leak in a pipeline, the analytical solution for a pipeline transient in Eq. (3.33) is expressed as

$$h^*(x^*,t^*) = e^{-Rt^*} \sum_{n=1}^{\infty} \left\{ \left[(A_n \cos(n\pi t^*) + B_n \sin(n\pi t^*) \right] \sin(n\pi x^*) \right\} \tag{3.39}$$

which is exact exponential damping. Therefore, when a transient is initiated in a pipeline, transient measured at any position in the pipeline decays exponentially with the damping rate of R (= $fLQ_0/2aDA$). The shape of the transient is determined by the measurement position x^* and the initial conditions that are characterized by the Fourier parameters A_n and B_n defined in Eqs. (3.34) and (3.35). In contrast, the leak-induced

damping factor, R_{nL} of Eq. (3.32), depends on n and is different for each component; it cannot be removed from the summation sign in Eq. (3.33). Any measured pipeline transient is the summation of a series of exponentially damped harmonic components each with a damping rate of $R + R_{nL}$ (n = 1, 2, 3,...). To investigate the total damping rate of a measured signal, the upper envelope of the transient may be expressed as

$$h_P^*(x^*,t^*) = \sum_{n=1}^{\infty} A_{nP} e^{-(R+R_{nL})t^*} \tag{3.40}$$

in which

$$A_{nP} = \sqrt{A_n^2 + B_n^2}\,\sin(n\pi x^*) \tag{3.41}$$

is the maximum amplitude of an individual component. Since $(R + R_{nl})$<<1.0, for the transient of the first several periods, $(R + R_{nL})t^* < 1.0$. Expanding each exponential function in Eq. (3.40) into a power series and keeping the first two terms, Eq.(3.40) can be expressed as

$$\begin{aligned} h_P(x^*,t^*) &= \sum_{n=1}^{\infty} A_{nP}\left[1-(R+R_{nL})t^* + \ldots\right] \\ &= \sum_{n=1}^{\infty} A_{nP} - \sum_{n=1}^{\infty} A_{nP}(R+R_{nL})t^* + \ldots \\ &= \left(\sum_{n=1}^{\infty} A_{nP}\right)\left[1 - \frac{\sum_{n=1}^{\infty} A_{nP}(R+R_{nL})}{\sum_{n=1}^{\infty} A_{nP}} t^* + \ldots\right] \end{aligned} \tag{3.42}$$

Terms in the bracket can be approximated by an exponential function, thus the overall damping of a measured transient can be approximated as an exponential form

$$h_P^*(x^*,t^*) = \overline{A_P} e^{-\overline{R}t^*} \tag{3.43}$$

in which

$$\overline{A_P} = \sum_{n=1}^{\infty} A_{nP} \quad \text{and} \quad \overline{R} = \frac{\sum_{n=1}^{\infty} A_{nP}(R+R_{nL})}{\sum_{n=1}^{\infty} A_{nP}} \tag{3.44}$$

The damping rate of a measured transient in a pipeline with a leak, $\overline{R}$, is actually the weighted average of $R+R_{nL}$ with weight parameter A_{nP} defined in Eq. (3.41). Firstly, the leak-induced damping for a pipeline transient depends on size and position of the leak, which are included in parameter R_{nL} defined in Eq. (3.32). Since the weighting function A_{nP} is a function of measurement position x^* and the shape of the transient determined by

Fourier parameters, leak-induced damping on a pipeline transient also depends on the measurement position and the initiation of the transient. Therefore, the best way to detect leaks is not by just examining the total damping of a measured pipe transient. Transients initiated in different ways or measured at different locations may give different leak information, and in some cases the transients may not be able to pick up the presence of leaks (Jönsson and Larson 1992; Covas and Ramos 1999). However, since leak-induced damping on any of the individual frequencies defined in Eq. (3.32) is a function of leak size and location only, the leak can be detected by examining the damping of different frequencies. Based on this fact, a new leak detection, location and quantification technique is developed in Chapter 4.

3.5 Multiple leaks

In the preceding sections, only a single leak is considered. However, it is evident there is a linear relationship between the leak and transient solution. For a pipeline with N leaks, an analytical solution can be obtained following the similar procedures as those in Appendix A by dividing the pipeline into $N + 1$ sections. The solution for a transient in a pipeline with more than one leak is similar to that expressed in Eq. (3.33), however, the leak parameter R_{nL} is replaced by

$$R_{nL}^{m} = \sum_{i=1}^{N} R_{nLi} \tag{3.45}$$

where N = number of leaks. For the i^{th} leak, the leak-induced damping factor is defined as

$$R_{nLi} = F_{Li}\sin(n\pi x_{Li}^{*}) = \frac{2(C_d A_L)_i ab_i}{A[2g(H_{L0})_i]^{1-b_i}}\sin^2(n\pi x_{Li}^{*}) \tag{3.46}$$

in which $(C_dA_L)_i$ = lumped leak area of the i^{th} leak, $(H_{L0})_i$ = the steady-state piezometric head at the i^{th} leak, b_i = non-theoretical discharge relationship coefficient of the i^{th} leak and x_{Li}^{*} = dimensionless leak location of the i^{th} leak. The analytical solution for multiple leaks is compared with the numerical results based on MOC in Section 3.7. Procedures for multiple leak detection are developed in Chapter 4.

3.6 Linearization error analysis

In the initial derivation of the governing non-dimensional partial differential equations including a leak, the q^{*2} term was neglected and the orifice equation was linearized in Eq. (3.21) in arriving at the Eqs. (3.23) and (3.24). Reconsidering the equations without linearization gives

$$\frac{\partial h^*}{\partial t^*}+\frac{1}{F}\frac{\partial q^*}{\partial x^*}+M[e_T(\Delta H_{L0}^*)^b+(1+e_T)\frac{bh^*}{(\Delta H_{L0}{}^*)^{1-b}}]\delta(x^*-x_L^*)=0 \tag{3.47}$$

$$F\frac{\partial h^*}{\partial x^*}+\frac{\partial q^*}{\partial t^*}+2RQ_0^*q^*+R(q^*)^2=0 \tag{3.48}$$

Assuming e_T constant and applying the operation $\frac{\partial}{\partial x^*}\left[\frac{\text{Eq.(3.47)}}{F}\right]-\frac{\partial}{\partial t^*}[\text{Eq.(3.48)}]$ gives

$$\frac{\partial^2 h^*}{\partial x^{*2}}=\frac{\partial^2 h^*}{\partial t^{*2}}+F_L^{'}\delta(x^*-x_L^*)\frac{\partial h^*}{\partial t^*}-2R'\frac{1}{F}\frac{\partial q^*}{\partial x^*} \tag{3.49}$$

where $F_L^{'}=F_L(1+e_T)$ and $R'=R(1+q^*)$. Replacing the partial derivative of q^* by applying the continuity equation Eq. (3.23) gives

$$\frac{\partial^2 h^*}{\partial x^{*2}}=\frac{\partial^2 h^*}{\partial t^{*2}}+[2R'+F_L^{'}\delta(x^*-x_L^*)]\frac{\partial h^*}{\partial t^*}+2R'F_L^{'}h^*\delta(x^*-x_L^*)+E\delta(x^*-x_L^*)] \tag{3.50}$$

where $E=2e_TR'M\sqrt{H_{L0}^*}$. Since values of R and R_{nL} are normally much smaller than unity, an approximate solution for Eq. (3.50) is

$$h^*(x^*,t^*)=\sum_{n=1}^{\infty}\left\{e^{-(R'+R_{nL}^{'})t^*}\left[A_n\cos(n\pi t^*)+B_n\sin(n\pi t^*)\right]\sin(n\pi x^*)\right\} \tag{3.51}$$

in which $R_{nL}^{'}=F_L^{'}\sin^2(n\pi x_L^*)=(1+e_T)R_{nL}$. From Eq. (3.51), leak damping is only influenced by the value of e_T, which is the linearization error of the orifice equation, and friction damping is influenced by the value of q^*. The analytical solution given in Eq. (3.33) is accurate when the values of e_T and q^* are small. From the definition of e_T in Eq. (3.22), the absolute values of the linearization error of orifice equation is a function of dimensionless transient magnitude h^*/H_{L0}^* and coefficient b as

$$e_T = \frac{\left|(\Delta H_L^*)^b - [(\Delta H_{L0}^*)^b + \frac{bh^*}{(\Delta H_{L0}^*)^{1-b}}]\right|}{(\Delta H_L^*)^b} \tag{3.52}$$

Variation of e_T with different values of h^* / H_{L0}^* and b is presented in Figure 3.5. To avoid negative pressures in a pipeline, h^* / H_{L0}^* must be less than 1.0. Within this range, the linearization error of orifice equation is less than 6% and thus not significant. Therefore, the influence of the magnitude of the transient on the leak-induced damping is not significant. For $b = 0.5$, the linearization error reaches the maximum.

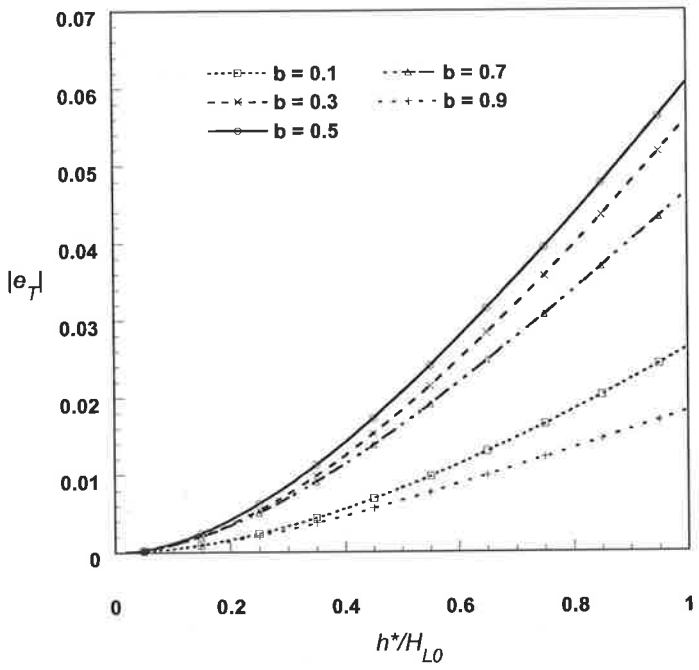

Figure 3.5 Linearization error of the orifice equation

3.7 Comparison with numerical results based on MOC

As a verification of the sensitivity analysis presented in section 3.6, the accuracy of the linear analytical solution is compared with results calculated numerically for the non-linear equations using the method of characteristics (MOC) in which the non-linearity of the friction term is approached by a second-order difference scheme (Chen 1994; Vítkovský 2001). The details of the numerical algorithm are given in Chapter 7.

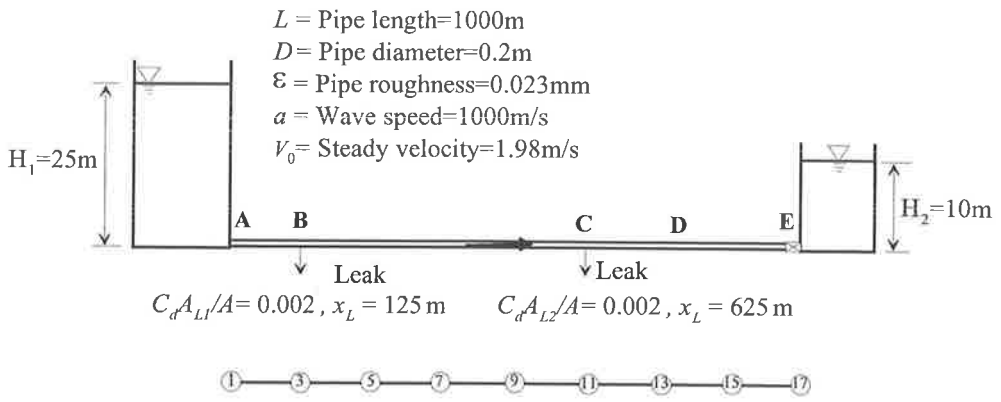

Figure 3.6 A pipeline connecting two constant tanks

A simple horizontal pipeline as shown in Figure 3.6 is used in this section for a comparison of the analytical solution and the numerical results based on the method of the characteristics. The length of the pipeline is L = 1000m, inside diameter is D = 0.2m and the thickness of the pipe wall is e = 8.2mm. The roughness height of the inside pipe wall is ε = 0.023mm. The wave speed of the transient in the pipeline is a = 1000m/s. The pipeline is connected to two tanks with constant water levels, Tank 1 upstream and Tank 2 downstream. Two valves are installed at each end of the pipeline. Two leaks are located 125m downstream from the Tank 1 (Point B) and 625m downstream the Tank 1 (Point C) along the pipeline respectively. The lumped leak areas of the leaks are $(C_dA_L)_B = (C_dA_L)_C = 3.14e^{-5}m^2$, which are 0.1% of the pipe cross sectional area. In the method of characteristics, the pipeline is divided into 16 equal reaches with 17 nodes as shown in Figure 3.6. In this example, the leak is treated as a theoretical orifice (b = 0.5) in both analytical and the numerical solutions.

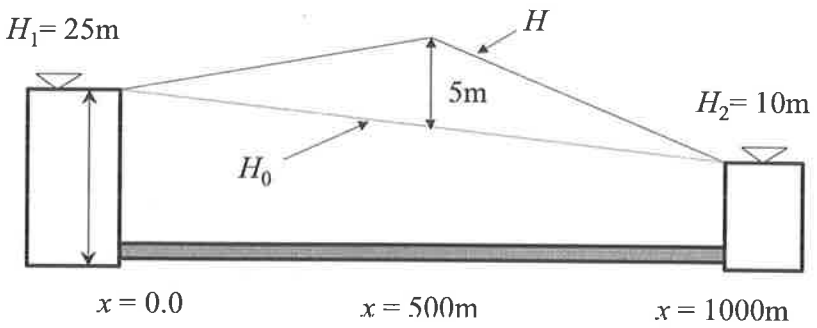

Figure 3.7 Initial transient in the pipeline

Assuming a triangular-form for the initial transient in the pipeline as shown in Figure 3.7, the initial conditions are

$$f^*(x^*) = \begin{cases} 0.40x^* & (0 < x^* \le 0.5, \quad t^* = 0.0) \\ 0.40(1-x^*) & (0.5 < x^* < 1.0, \quad t^* = 0.0) \end{cases} \tag{3.53}$$

$$g^*(x^*) = 0 \qquad (t^* = 0.0) \tag{3.54}$$

These initial conditions can be generated by adjusting the head at Tank 2 while keeping the head at Tank 1 constant (by increasing the water level at the downstream reservoir, H_2, to 15.5m from 10m within 0~1.0s, and reducing to 10m within 1.0~2.0s.) Applying the initial conditions expressed in Eqs. (3.53) and (3.54) with Eqs. (3.34) and (3.35), the Fourier coefficients are

$$A_n = \begin{cases} \dfrac{3.20}{\pi^2}(-1)^{(\frac{n-1}{2})}\dfrac{1}{n^2} & (n = 1,3,5...) \\ 0 & (n = 2,4,6...) \end{cases} \tag{3.55}$$

$$B_n = \begin{cases} \dfrac{A_n R}{n\pi} & (n = 1,3,5...) \\ 0 & (n = 2,4,6...) \end{cases} \tag{3.56}$$

Three different cases are considered for comparison. In case 1, there is no leak in the pipeline system. With the head H_1 = 25m at Tank 1 and H_2 = 10m at Tank 2, and negligible head losses through the fully opened valves at the two ends of the pipeline, the steady flow velocity in the pipeline is V_0 = 1.98 m/s and the friction factor f = 0.015. Based on Eq. (3.19), the friction damping factor is calculated as R = 0.0743. In case 2, the leak at Point B is open, and in case 3, two leaks at both Point B and Point C are open. Since the leaks are small, the flow rate through the each leak is less than 1% of the total flow in the pipeline. The influence of the leak flow on the total pipe flow is negligible, which gives the same friction damping parameters for three cases. The leak parameters used in the analytical solution are calculated as $(F_L)_B$ = 0.047 and $(F_L)_C$ = 0.057 for the leaks at point B and point C by applying Eq. (3.32).

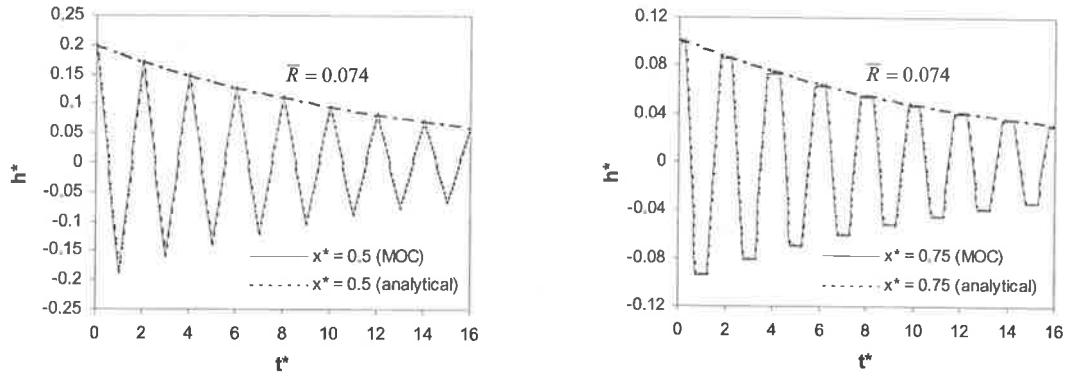

(a) no leak

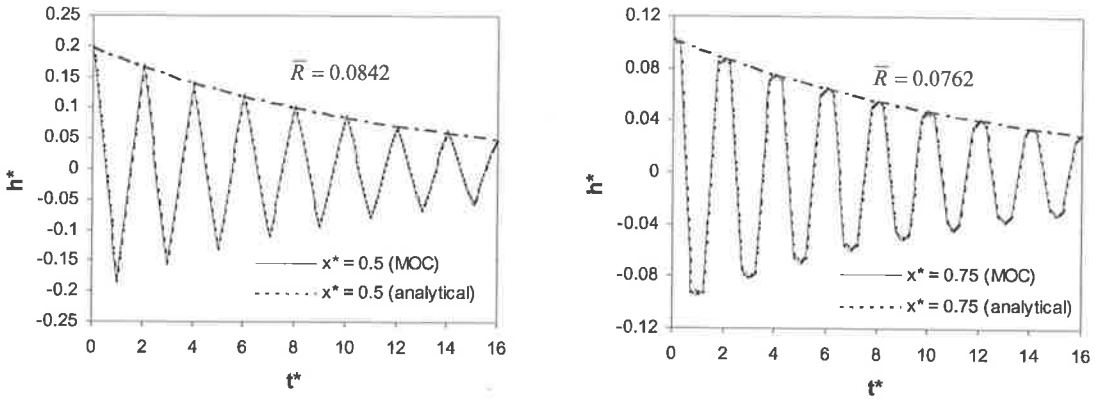

(b) with a leak of C_dA_L/A = 0.1% at x^* =0.125

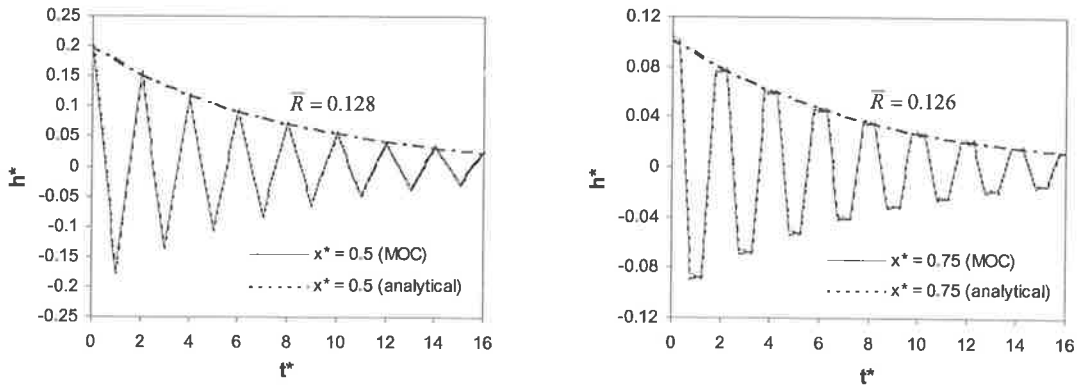

(c) two leaks of $(C_dA_L)_A/A$ = 0.001 at x^* =0.125 and $(C_dA_L)_B/A$ = 0.001 at x^* =0.625

Figure 3.8 Comparison with the MOC solution

Both the linearized analytical solution and the non-linear MOC numerical calculation measured at x^*= 0.5 and x^*= 0.75 are presented in Figure 3.8(a), Figure 3.8(b) and Figure

3.8(c), which are for three different cases. Figure 3.8(a) is a no-leak case, and in Figure 3.8(b) there is a leak of $C_dA_L/A = 0.1\%$ at $x_L^* = 0.125$, while in Figure 3.8(c), there are two leaks at $x^* = 0.125$ and $x^* = 0.625$ with the same size of $C_dA_L/A = 0.001$. In the linearized solution of Eq. (3.33), terms higher than $n > 40$ were neglected. The two solutions are virtually identical for both cases of with and without leaks so that they cannot be distinguished on the plots. Therefore, the non-linear effects of friction and leak on the pipeline transient are negligible if the magnitude of the transient is small.

The transients calculated from MOC are fitted with an exponential function in form of Eq. 3.40, and the fitted results are given in each figure respectively. The regression coefficients of the fitted curves of the exponential damping factors for all three cases are larger than 0.98, confirming the analysis that leak-induced damping for the total transient trace is approximately exponential. When there is no leak (case 1), the total exponential damping coefficient is 0.0742, equal to the frictional damping factor R and independent of the measurement position. When there is a leak in the pipeline (case 2), the damping coefficient is 0.0842 for the transient measured at $x^* = 0.5$ and 0.0762 at $x^* = 0.75$. The damping coefficients calculated using the analytical formula Eq. (3.44) are 0.0845 and 0.0763 respectively, which are close to the results from MOC values. When there are two leaks in the pipeline (case 3), the damping coefficient is 0.128 for the transient measured at $x^* = 0.5$ and 0.126 at $x^* = 0.75$. The corresponding damping coefficients calculated from Eq. (3.44) are 0.129 and 0.127 respectively. Because the condition $(R + R_{nL})t^* < 1.0$ used in the analytical solution Eq. (3.44) is not satisfied in MOC, there is slight difference on the damping coefficients calculated using MOC and analytical solution.

3.8 A leak with a constant discharge relationship

In previous studies of pipe network systems, demands were treated as leaks with constant flow rates (McInnis and Karney 1995). A leak with a constant flow rate means that the parameter $b = 0$ in Eq. (3.13). Substituting $b = 0$ into Eq. (3.32) gives $F_L = 0$ and $R_{nL} = 0.0$, which means the damping of such a leak on the pipeline transient is zero.

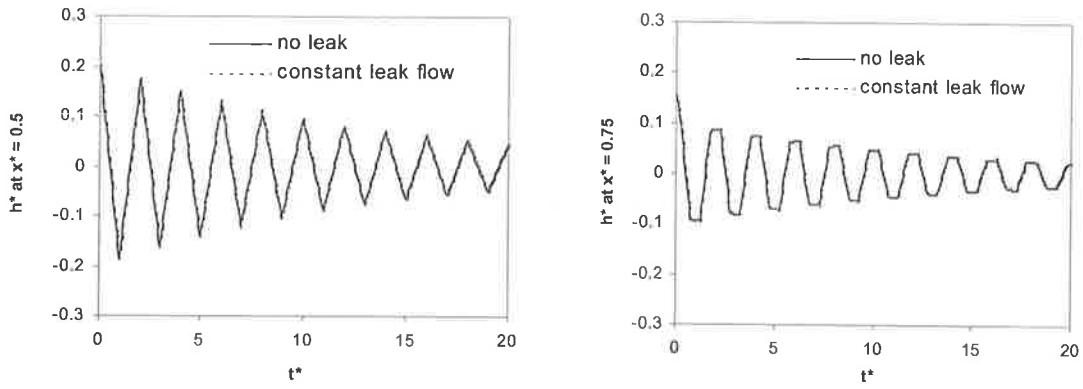

Figure 3.9 Influence of a constant leak flow on pipeline transients

For case 2 used in section 3.7, the leak at point B is replaced with a leak of constant discharge, which is calculated based on steady state as $Q_L = 6.67\times10^{-3}$ m^3/s. The transients are calculated using MOC. Transients measured at two locations $x^* = 0.5$ and $x^* = 0.75$ for two different situations, without a leak and with a constant leak flow at point B are presented in Figure 3.9. Obviously the constant leak flow has little influence on the pipeline transients. Thus constant demands don't either.

From the above analysis, it is very clear that the effects of a leak with a pressure-dependent flow rate and a leak with a constant flow rate on the pipeline transients are significantly different. The former contributes damping on fluid transients, while the latter has no influence. The model of constant leak flow implies that the pressure difference between the pipe inside and outside at the leak is constant. Figure 3.10 plots the inside pressure in the pipeline at the leak. To keep a constant leak flow, the pressure outside the leak must vary as shown in the same figure. In reality, it is impossible that the pressure outside a leak changes in concert to the pressure inside the pipe. Therefore, a constant leak flow doesn't exist in reality and assumption of a constant leak flow is not appropriate. By using such a model, the damping of the transients calculated from a pipeline or a pipe network will be underestimated.

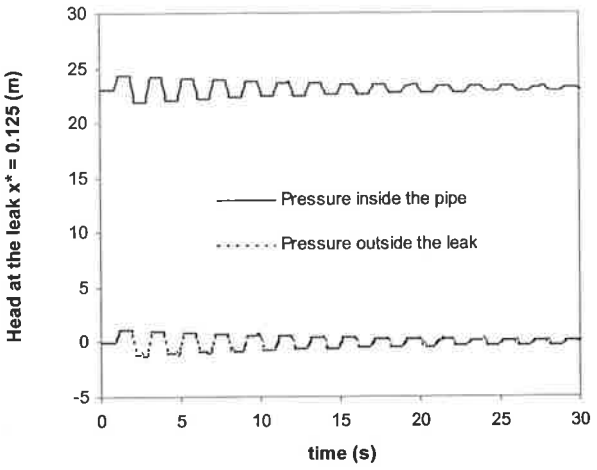

Figure 3.10 The pressures inside and outside the leak under a constant leak flow rate ($C_dA_L/A = 0.001$, $x_L^* = 0.125$)

3.9 Summary

In this chapter, the behaviour of a leak on the pipeline transients is studied. The effect of a leak on unsteady pipe flow is included in the governing equations using a Dirac delta function. By linearizing the friction term and the square-root-form orifice equation, the linear dimensionless governing equations are derived. An analytical solution (Eq. 3.33) expressed in terms of a Fourier series has been developed under constant boundary conditions. Sensitivity analysis shows that linearization generates an insignificant error on the leak-induced damping, while on the other hand, the influence on the friction damping may or may not be significant depending on the magnitude of the fluid transients. By comparison to the numerical solution based on the method of characteristics in which the non-linear effects are included, the analytical solution shows a high degree of accuracy.

The analytical solution indicates that transients in pipelines are damped by both pipe friction and leaks. The steady friction damping is exactly exponential (if R is assumed to be constant), and leak damping is exactly exponential for each of the individual harmonic components. Since the leak-induced damping of an individual component depends on the location and size of the leak, and is independent of the transient itself, the

analytical solution provides a method to detect, locate and quantify a leak, which is investigated in the following chapter. Leak-induced damping of the total transient event is approximately exponential. Since the total damping depends on the form of a transient in addition to the size and location of the leak, leaks cannot be detected effectively by only measuring the total damping of a transient event.

Behaviour of a leak with a constant flow rate is investigated. Although such an assumption is reasonable from a steady state point of view, using such an approach, the damping of the transients calculated from a pipeline or a pipe network will be significantly underestimated.

Chapter 4

Leak Detection Using the Damping of Fluid Transients

4.1 Introduction

The analytical solution developed in Chapter 3 shows that any measured pipeline transient may be represented by the summation of a series of harmonic components that are each exactly exponentially damped with the damping rate of $(R + R_{nL})$ $(n = 1, 2, 3,\ldots)$ (see Section 3.3). Since the friction damping factor R is a function of steady flow conditions, the value of R is known from the pipe roughness and Reynolds number through the Colebrook-White equation or the Moody diagram. The value of friction damping factor R can also be experimentally determined by measuring the damping rate of the transient from a leak-free pipeline. Therefore, for a measured pipeline transient, if the damping rate $(R + R_{nL})$ for an individual harmonic component can be obtained, the leak-induced damping factor R_{nL} can be determined by subtracting R from $(R + R_{nL})$. The outcome is that the leak-induced damping, R_{nL} can be used for leak detection analysis. In this chapter, a technique to detect, locate and quantify a pipeline leak is developed using the leak-induced damping based on the analytical solution developed in Chapter 3. Some of the results presented in this chapter have been presented in Wang et al. (2002). Additional work presented in this chapter includes a sensitivity study of the influence of the friction factor uncertainties on leak detection, multiple leak detection in section 4.6, further experimental verification tests in section 4.8 and the investigation of the possible application of the technique in series pipelines and complex networks in section 4.9.

Chapter 3 showed that leaks with different discharge relationships have different effects on a transient event. Since a leak with a non-theoretical relationship ($b \neq 0.5$) can be expressed by an equivalent theoretical leak ($b = 0.5$), all the leaks studied in this chapter are treated as theoretical leaks if not specifically indicated.

4.2 Fourier series analysis

Assuming that linearization is valid, any measured pipeline transient may be represented by the summation of a series of harmonic components, whose damping values are of interest for leak detection. To investigate the damping of a particular harmonic component, the first step is to decompose a measured transient into its individual components. Theoretically, two types of measurement data, time-domain data and space-domain data, can be used for calculation of the damping coefficient ($R + R_{nL}$) of the harmonic component n. Space-domain data is obtained by measuring the transient pressure head at a number of locations along the pipeline at a single time (in Eq. (3.33) t^* = constant and $0< x^*< 1$). Time-domain data is obtained by measuring the transient pressure history at a single pipeline location (in Eq. (3.33) x^* = constant and $t^*> 0$). Since it is more practical to measure the pressure history at a specific location, the time-domain measurement data have been used in this Ph.D. thesis for calculation of damping rates of individual harmonic components by analyzing the transient period by period using Fourier transforms. This approach is one of the innovative developments of this new leak detection technique presented in this thesis. The feasibility of analyzing pipeline transient period by period is proven in Appendix B. Procedures to obtain the leak-induced damping by analyzing a transient event are as following:

1. Set up a steady flow in the pipeline and then introduce a transient event.
2. Measure the variation of pressure head with time at one or more points along the pipe.
3. Divide the pressure trace into separate periods (Period 1, Period 2, etc. as shown in Figure. B1 of Appendix B) so that each can be analyzed individually.
4. Using a Fourier transformation, such as the Discrete or Fast Fourier Transform (Press et al. 1992), decompose one period of the transient into its separate harmonic components and calculate the amplitude of each component. The amplitude (power) $E_n^{(i)}$ of the n^{th} harmonic for the i^{th} period is expressed as

$$E_n^{(i)} = E_n^{(1)} e^{-(R+R_{nL})(i-1)T^*} \tag{4.1}$$

where $E_n^{(1)} = \dfrac{e^{-(R+R_{nL})(t_0^*+T^*)} - e^{-(R+R_{nL})t_0^*}}{-(R+R_{nL})T^*} \sin(n\pi x^*)\sqrt{A_n^2 + B_n^2}$ = amplitude of n^{th} harmonic component at the first period, t_0^* = dimensionless starting time of the analysis and T^* = dimensionless period defined as $T^* = T/(L/a)$, in which T = natural period of the pipeline. For the reservoir-pipeline-reservoir system (i.e., a pipeline running between two reservoirs) $T^* = 2.0$, and for the reservoir-pipeline-valve system (a pipeline from a reservoir with a valve on the downstream end), $T^* = 4.0$. Details of derivation of Eq. (4.1) are given in Appendix B.

5. Repeat step 4 period by period along the pressure trace.

6. For each harmonic component n, plot the amplitude $E_n^{(i)}$ expressed in Eq. (4.1) versus period in terms of L/a in the Fourier series.

7. Compute the damping coefficient $R + R_{nL}$ from the plotted data using an exponential fitting function in form of Eq. (4.1) where both initial amplitude $E_n^{(1)}$ and the damping coefficient $R + R_{nL}$ can be calculated.

8. Analyze the damping rates of the separate components to determine occurrence, location and magnitude of the leak. Details are presented in the next section.

4.3 Leak detection, location and quantification

Determining the existence, location and size of a leak using damping rates of separate components is now considered in detail.

4.3.1 Detecting the presence of a leak

For a pipeline without a leak, $C_d A_L = 0$ in Eq. (3.33) and hence $R_{nL} = 0$; damping of each component does not depend on the component number, n, and is only dependent on friction damping factor, R. Therefore, given the same steady flow conditions followed by a transient event, presence of a leak is indicated by:

1. the damping rates for some components are larger than the friction-damping factor R, and

2. the damping rates $R + R_{nL}$ of the decomposed harmonic components, determined in step 6 of section 4.2, are significantly different from each other.

Leak-induced damping depends strongly on the position of a leak and on n through a sine squared function in Eq. (3.32). Different components have different responses to a leak. For a leak located in the middle of a pipeline ($x_L^* = 0.5$), components $n = 1$ and 3 have the maximum response whereas the response of component $n = 2$ is zero. Therefore, in practice more than one harmonic component should be used to detect a leak. Figure 4.1 shows the relative response of the first three harmonics ($n = 1$, 2 and 3) to the different leak locations along the pipeline.

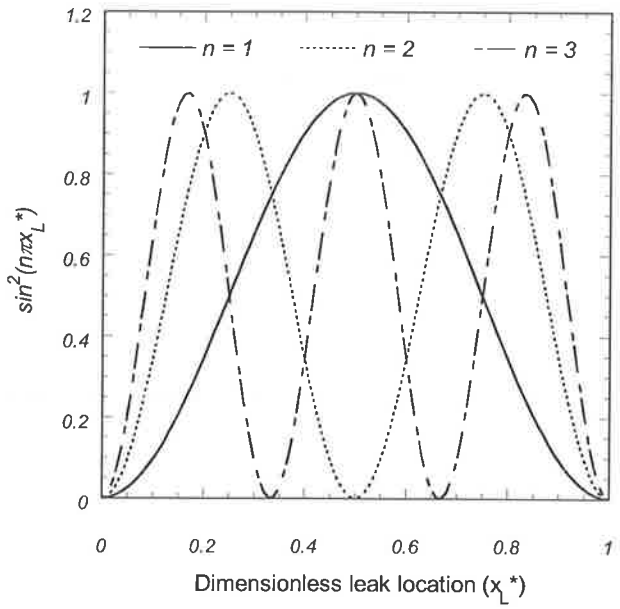

Figure 4.1. Sensitivity of the leak position on the different harmonic components

4.3.2 Location of a leak

Applying a Fourier transform to a measured pipeline transient, the leak location may be calculated from the ratios of the different damping rates of a pair of harmonic components. Consider $n = n_1$ and $n = n_2$, for which leak damping factors are

$$R_{n_1 L} = \frac{2C_d A_L ba}{A(2gH_{L0})^{1-b}} \sin^2(n_1 \pi x_L^*) \text{ and } R_{n_2 L} = \frac{2C_d A_L ba}{A(2gH_{L0})^{1-b}} \sin^2(n_2 \pi x_L^*) \qquad (4.2)$$

The ratio of these two terms is

$$\frac{R_{n_2 L}}{R_{n_1 L}} = \frac{\sin^2(n_2 \pi x_L^*)}{\sin^2(n_1 \pi x_L^*)} \qquad (4.3)$$

which is a function of only leak location x_L^* and not a function of the leak size $C_d A_L$. Eq. (4.3) also shows that value of b for a leak has no influence on locating the leak.

For a measured pipeline transient, the damping rate $R + R_{nL}$ for each harmonic component n can be calculated from its amplitude $E_n^{(i)}$ by analyzing each period. Since the friction damping factor R can be calculated from steady flow conditions, which are normally known, leak-induced damping R_{nL} for any component n is easily obtained by subtraction, giving the ratio of any two leak-induced damping rates as in Eq. (4.3). Solution of Eq. (4.3) for x_L^* yields the leak location. Figure 4.2 shows the theoretical relationship between the damping ratios of harmonic components $n_2 = 2$, $n_1 = 1$ and harmonic components $n_2 = 3$, $n_1 = 1$ with the corresponding leak locations in a pipeline.

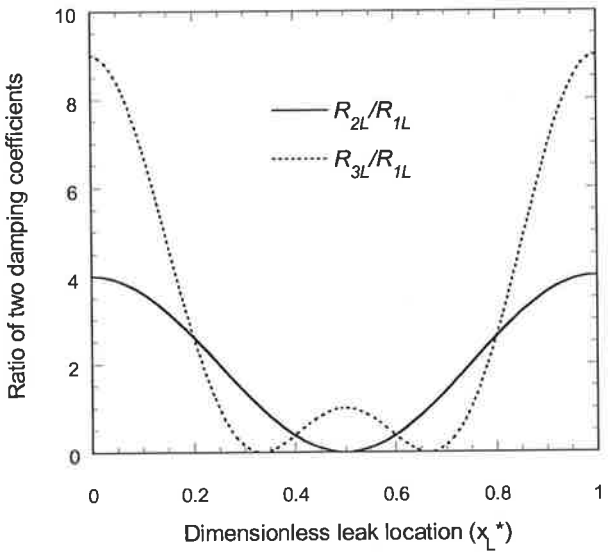

Figure 4.2. Damping ratios of harmonic components

Due to the symmetric nature of the sine-squared function, the relationship between the damping ratio of two harmonic components and leak location is not unique. Two leak locations correspond to one value of the damping ratio R_{2L}/R_{1L} except for $x_L^* = 0.5$. For damping ratios of higher harmonic components, one damping ratio may correspond to a greater number of possible leak locations. For example, a damping ratio of $R_{3L}/R_{1L} < 1.0$ (see Figure 4.2) corresponds to four possible leak locations. Therefore, only harmonic components of $n = 1, 2, 3$ are used for leak detection analysis in this study. The symmetric problem can be solved using different transient events. Two examples of using different transient events are given in Section 4.5, which show that some transient events can give unique leak location.

4.3.3 Size of a leak

Once the position of a leak has been determined, the magnitude of a leak can be easily calculated using (4.2). It is

$$C_d A_L = \frac{R_{nL} A (2gH_{L0})^{1-b}}{2ba \sin^2(n\pi x_L^*)} \qquad (n = 1, 2, 3, \ldots) \tag{4.4}$$

where n is any one of the components. Because the value of b is not known for a leak in advance of leak detection, a value of $b = 0.5$ is used by assuming a theoretical orifice leak. Based on this assumption, a smaller value of leak size is obtained if the actual leak is not a theoretical orifice, in which case it usually has a value of b smaller than 0.5 (details are given in Chapter 3). An example of non-theoretical orifice leak is given in Section 4.8.

Theoretically, the leak magnitude calculated using different components should be the same. Different measurement positions and different forms of transients can be used for added confirmation and to increase accuracy if necessary.

4.4 Sensitivity analysis

From the linearization error analysis in Chapter 3, leak damping is only influenced by the value of e_T, which is the linearization error of the orifice equation. The influence of the linearization on leak detection is investigated in this section. In addition, since leak-induced damping is obtained from total damping of a harmonic component by subtracting the friction damping, the error in calculating friction damping will be transferred to leak-induced damping and, as a result, the outcome of leak detection may be affected. The influence of the error in estimating the friction of pipes on the leak detection is also investigated in this section.

4.4.1 Influence of linearization on leak detection

Noticing that the ratio of any two leak damping coefficients of R'_{nL} (defined in Eq. (3.63)) is independent of parameter e_T, then the location of a leak is not affected by the

error in the linearization of orifice equation. The error of leak size induced by the orifice linearization is defined as

$$\varepsilon_s = \frac{(C_d A_L)_{real} - (C_d A_L)_{apparent}}{(C_d A_L)_{real}} \tag{4.5}$$

Substituting (4.4) into (4.5) gives

$$\varepsilon_s = \frac{R_{nL} - (1+e_T)R_{nL}}{R_{nL}} = -e_T = -\frac{(\Delta H_L^*)^b - [(\Delta H_{L0}^*)^b + \dfrac{bh^*}{(\Delta H_{L0}^*)^{1-b}}]}{(\Delta H_L^*)^b} \tag{4.6}$$

Variation of relative leak size error with parameter of h^* / H_{L0}^* is plotted in Figure 4.3. To avoid negative pressure in a pipeline, h^* / H_{L0}^* must be less than 1.0. Within this range, the errors in the size of a leak caused by the orifice linearization are less than 6% and thus not significant.

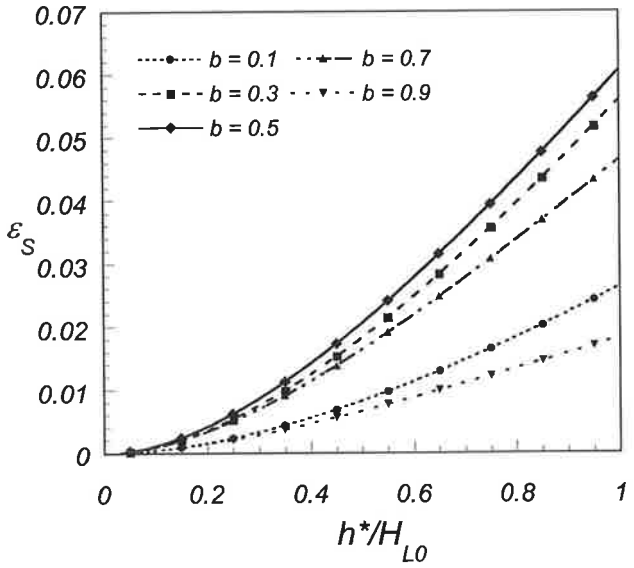

Figure 4.3. Influence of linearization of orifice equation on the leak size

Neglecting the q^{*2} term has no direct influence on location and quantification of a leak, but it does affect friction damping. Because leak damping may be obtained by measuring total damping and subtracting friction damping, linearization may indirectly lead to an experimental error in leak damping. That error shows up in the ratio of the Fourier components and thus influences the calculation of leak location.

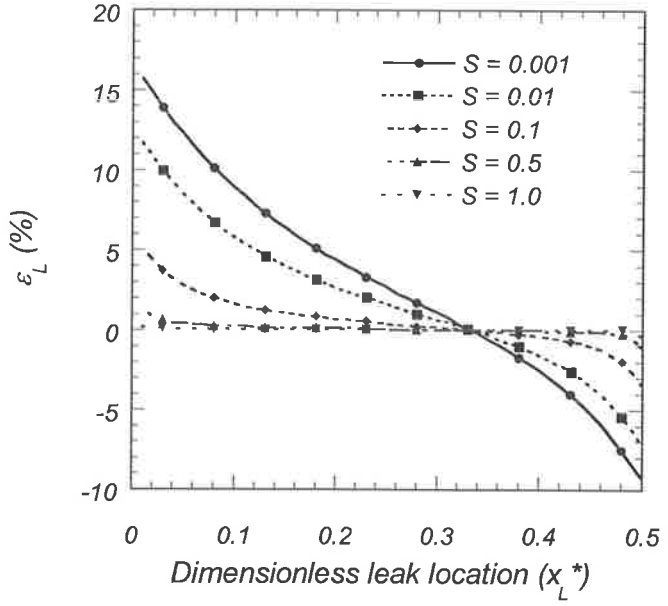

Figure 4.4. Sensitivity of leak location on the sensitivity parameter S

By including the term of q^{*2}, the total damping is $R_{nL} + R(1+q^*)$. If leak damping is obtained by subtracting friction damping R that is calculated from the steady state, the calculated leak damping coefficient is $R_{nL} + Rq^*$, in which R_{nL} is the real leak damping. Then the ratio of leak damping of any two Fourier components is

$$\frac{R_{n_2L} + q^* R}{R_{n_1L} + q^* R} = \frac{\sin^2[n_2\pi(x_L^* + \varepsilon_L)]}{\sin^2[n_1\pi(x_L^* + \varepsilon_L)]} \tag{4.7}$$

in which ε_L = dimensionless distance away from the real leak location. Substituting $\frac{R_{n_2L}}{R_{n_1L}} = \frac{\sin^2(n_2\pi x_L^*)}{\sin^2(n_1\pi x_L^*)}$ into (4.7) and rearranging gives

$$\frac{\dfrac{\sin^2(n_2\pi x_L^*)}{\sin^2(n_1\pi x_L^*)} + S}{1+S} = \frac{\sin^2[n_2\pi(x_L^* + \varepsilon_L)]}{\sin^2[n_1\pi(x_L^* + \varepsilon_L)]} \tag{4.8}$$

where $S = \dfrac{Rq^*}{R_{n_1L}}$.

The leak location error, ε_L, is a function of parameter S and real leak location, x_L^*. Variation of ε_L with parameter S and leak location x_L^* is presented in Figure 4.4 if the first two Fourier components, $n_1 = 1$ and $n_2 = 2$, are used. Due to symmetry, only half of the pipeline is plotted. Figure 4.4 indicates that large values of parameter S cause large

errors in the location of leak, and leaks at different locations have different sensitivities to the parameter S. Leaks close to $x_L^* = 0.33$ are least influenced by error in the friction damping when the first two harmonics are used.

Assuming that pressure at the leak is little influenced by leak location error, leak size error is expressed as

$$\varepsilon_s = \frac{(C_d A_L)_{real} - (C_d A_L)_{apprarent}}{(C_d A_L)_{real}} = 1 - \frac{(1+S)\sin^2(n\pi x_L^*)}{\sin^2[n\pi(x_L^* + \varepsilon_L)]} \tag{4.9}$$

Variation of relative leak size error ε_s with parameter S and leak location x_L^* is presented in Figure 4.5.

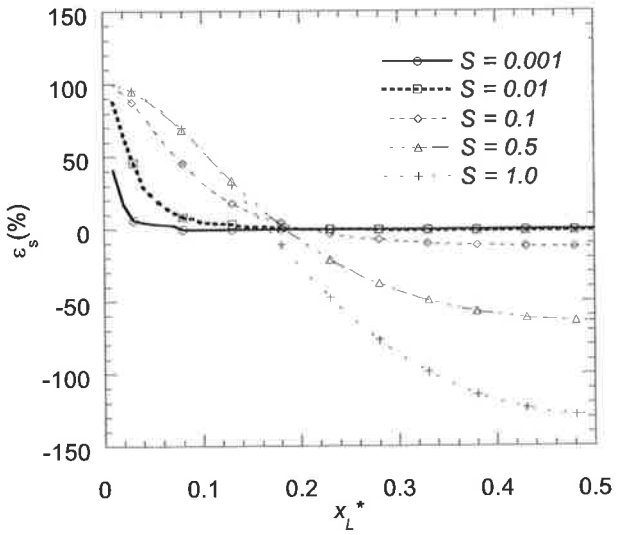

Figure 4.5. Sensitivity of leak size on the sensitivity parameter S

Since leaks close to the ends of the pipeline cause less damping, a small error in the value of leak damping can cause a large error in the calculation of the leak size despite small S. In the application of the proposed leak detection method, small values of parameter S can be achieved using small magnitudes of pipeline transient or small values of friction damping. The latter is achieved using a low steady-state flow rate in the pipeline. Alternatively, friction damping can be obtained from a test in a leak-free pipeline or calculated using a numerical model. An example for such a situation is given in the second numerical application in the following section.

4.4.2 Influence of friction factor uncertainties on leak detection

As mentioned in the above section, because leak damping can be obtained by subtracting friction damping from total damping, any error in calculating the friction damping will be transferred to leak damping and thus this will influence the detection of a leak. In addition to the magnitude of transient, another major factor that may influence the calculation of friction damping is the Darcy-Weisbach friction factor (f) of the pipe. Error in estimating the friction factor can easily be 20% for new pipes in which the roughness is known, and can reach 100% or more for old pipes where the roughness is not known.

By expressing flow rate as a function of friction factor using Bernoulli equation, the definition of R in Eq. (3.19) gives

$$R = \frac{fLQ_0}{2DAa} = \frac{fL\sqrt{\frac{2g\Delta HD}{fL}}}{2Da} = \frac{1}{a}\sqrt{\frac{fLg\Delta H}{2D}} \tag{4.10}$$

By introducing an error Δf in the friction factor f, the friction damping is

$$\begin{aligned} R + \Delta R &= \frac{1}{a}\sqrt{\frac{(f+\Delta f)Lg\Delta H}{2D}} \\ &\approx (\sqrt{f} + \frac{\Delta f}{2\sqrt{f}})\frac{1}{a}\sqrt{\frac{Lg\Delta H}{2D}} \\ &= R + \frac{\Delta f}{2f}R \end{aligned} \tag{4.11}$$

If the friction damping factor in Eq. (4.11) is used to calculate the leak damping, the leak-induced damping on n^{th} component is R_{nL}-ΔR. Therefore, the ratio of two leak-induced damping coefficients for any two components is

$$\frac{R_{n_2L} - \frac{\Delta f}{2f}R}{R_{n_1L} - \frac{\Delta f}{2f}R} = \frac{\sin^2[n_2\pi(x_L^* + \varepsilon_L)]}{\sin^2[n_1\pi(x_L^* + \varepsilon_L)]} \tag{4.12}$$

where ε_L = dimensionless distance away from a real leak location. Substituting $\frac{R_{n_2L}}{R_{n_1L}} = \frac{\sin^2(n_2\pi x_L^*)}{\sin^2(n_1\pi x_L^*)}$ into (4.12) and rearranging gives

$$\frac{\dfrac{\sin^2(n_2\pi x_L^*)}{\sin^2(n_1\pi x_L^*)} - S_f}{1 - S_f} = \frac{\sin^2[n_2\pi(x_L^* + \varepsilon_L)]}{\sin^2[n_1\pi(x_L^* + \varepsilon_L)]} \tag{4.13}$$

where $S_f = \dfrac{R\Delta f}{2R_{n_1 L} f}$ = sensitivity parameter of the friction factor. The leak location error, ε_L, is a function of parameter S_f and real leak location, x_L^*. Similarly, the leak size error caused by the friction factor uncertainties is expressed as

$$\varepsilon_s = \frac{(C_d A_L)_{real} - (C_d A_L)_{apprarent}}{(C_d A_L)_{real}} = 1 - \frac{(1 - S_f)\sin^2(n\pi x_L^*)}{\sin^2[n\pi(x_L^* + \varepsilon_L)]} \tag{4.14}$$

Since Eqs. (4.13) and (4.14) are in the same forms of Eqs. (4.8) and (4.9), variation of ε_L and ε_S with parameter S_f and leak location x_L^* is same as those in Figure 4.4 and Figure 4.5. Because the value of friction factor f is small (0.01~0.04), a small error Δf can generate a large value of S_f compared to parameter S defined in Eq. (4.8), which is a sensitivity parameter of transient magnitude. Therefore, errors in the friction factor may have greater influence on leak detection if the friction damping is calculated based on the definition in Eq. (3.19). For example, in the first example in the next section, if a friction factor f = 0.02, which is 33% larger than the actual value of f = 0.015, is used, the sensitivity parameter is calculated as S_f = 0.49. Applying this value to Figure 4.4 and Figure 4.5 gives the leak location error of 2% and leak size error of 30%, while the error related to the transient magnitude (S = 0.0063) is less than 1% for both leak location and size.

4.5 Numerical examples

The leak detection method discussed above is tested numerically in this section for a pipeline, shown in Figure 4.6, using the results of simulated transients calculated from the method of characteristics (MOC). Two types of problems, a reservoir-pipeline-reservoir system and a reservoir-pipeline-valve system, are considered.

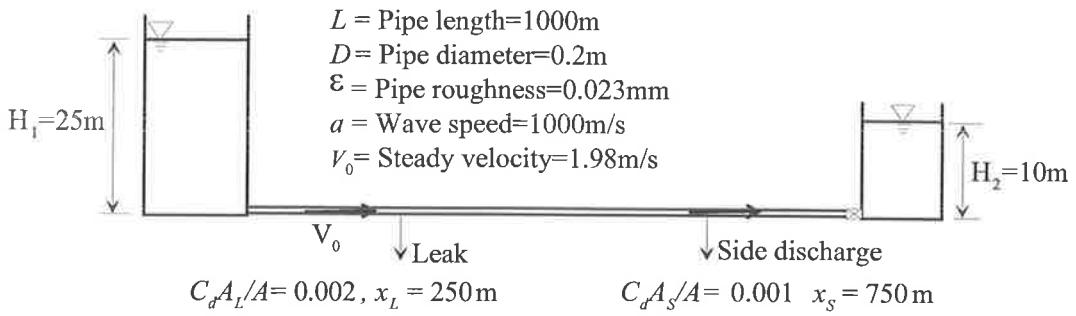

Figure 4.6. A pipeline connected by two reservoirs

4.5.1 Reservoir-pipeline-reservoir system

In this case a transient in the pipeline is initiated by closing a side-discharge valve located 750m ($x^* = 0.75$) away from the upstream reservoir as shown in Figure 4.6, while the valve adjacent to the downstream reservoir is fully open with negligible head loss. The magnitude of the side-discharge valve coefficient is $C_dA_S/A = 0.001$ where A_S = area of the side-discharge valve and C_d = discharge coefficient. Closing time of the side-discharge valve is 0.05s. For the first test (case 1) the leak at $x_L^* = 0.25$ is removed ($C_dA_L/A = 0$) to consider a "non-leak" case, while for case 2 a leak of relative size of $C_dA_L/A = 0.002$ is assumed. The leak is assumed to be a theoretical orifice ($b = 0.5$). The transient head in the pipeline is calculated numerically by a standard method-of-characteristics program using 16 pipe reaches. The calculations are started from steady state. The Darcy-Weisbach friction factor is calculated as $f = 0.015$ using the Swamee-Jain formula (Streeter and Wylie 1983). The steady state friction-damping factor is $R = 0.0742$ with a steady-flow Reynolds number of 3.96×10^5. The sensitivity parameter, S, is calculated as 0.0063. Based on the previous sensitivity analysis, the leak location error, ε_L, and leak size error, ε_s, are both less than 1%.

Figure 4.7 presents the leak detection analysis using the numerically generated measurement transient. Measured pressures at $x^* = 0.75$ are shown in Figure 4.7(a) for cases of no leak (case 1) and with a leak (case 2). The amplitudes for separate components, n, are obtained by applying a discrete Fourier transform algorithm to analyze the measured data in Figure 4.7(a), the results of which are presented in Figure 4.7(b). The transient signals were analyzed period by period with an interval

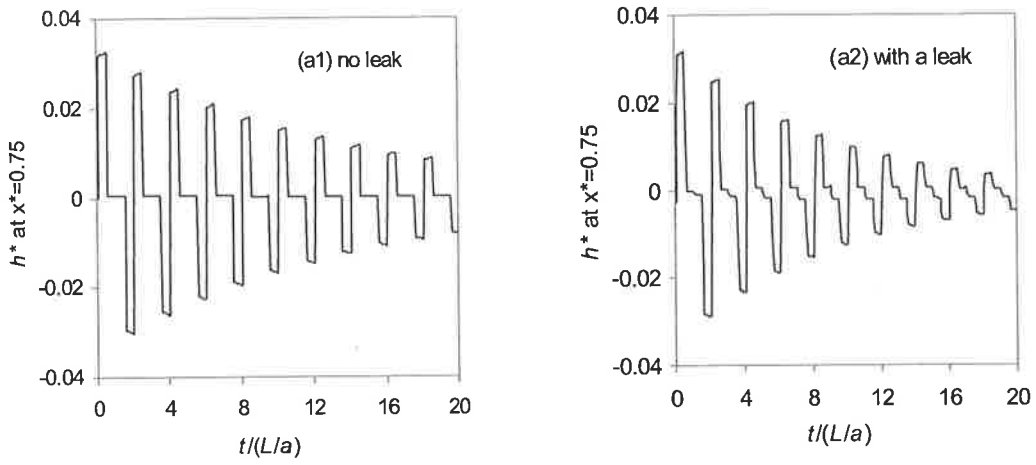

(a). Time history of the measured pipeline transients (MOC)

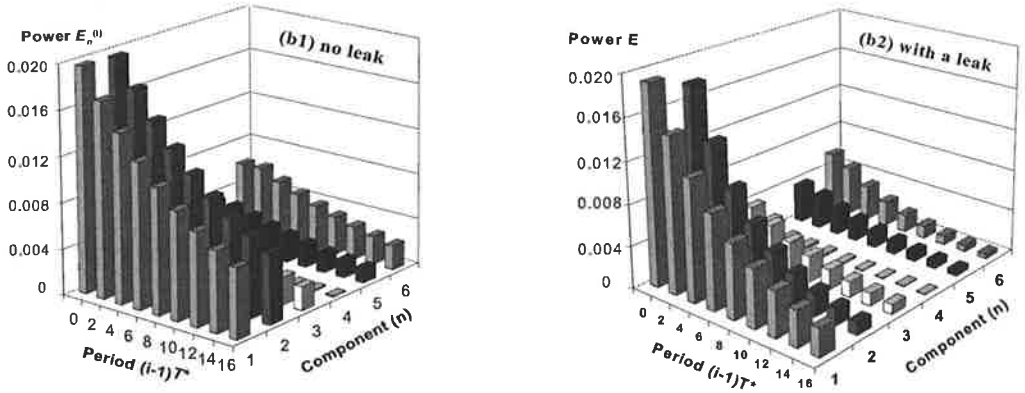

(b) Fourier series analysis of the transients

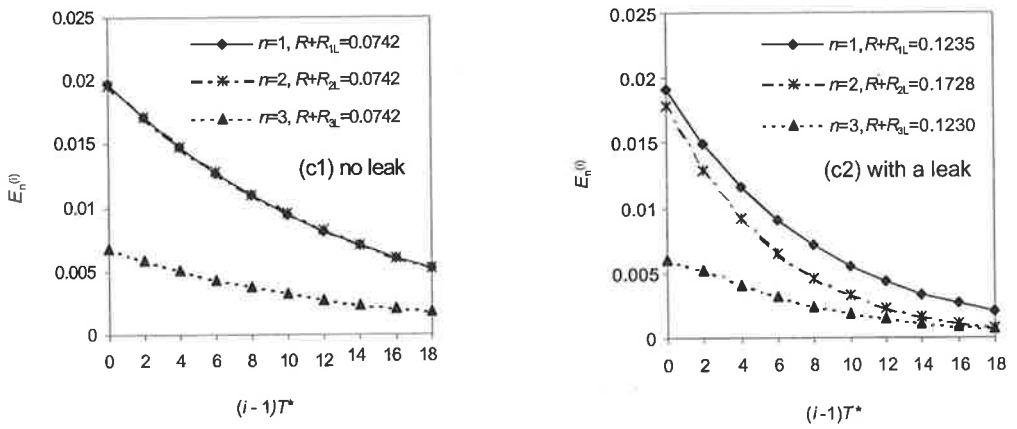

(c) Damping of harmonic components with period

Figure 4.7. Fourier series analysis of the transients measured from a pipeline without a leak (case 1) and with a leak (case 2) of $C_dA_L/A = 0.1\%$ at $x_L^* = 0.25$ ($T^* = 2.0$).

of $t^* = 2.0$. Figure 4.7(c) shows computed amplitudes of the Fourier series of the first three harmonic components plotted against period in terms of L/a. In Figure 4.7(c1)--the no leak case--the damping rate $R + R_{nL}$ for all three harmonic components is determined to be $R = 0.0742$ by fitting an exponential equation Eq. (4.1) to the decaying amplitudes. In Figure 4.7(c2)--in which a leak was present--the damping rates $R + R_{nL}$ are 0.1235, 0.1728, 0.1230 for the first three components. The second value is significantly different from the first and third and all are larger than the friction-damping factor. The leak-induced damping rates R_{nL} for components $n = 1$, 2 and 3 are 0.0493, 0.0986 and 0.0488, which are obtained by subtracting R from $R + R_{nL}$ (see Table 4.1). The ratios of two leak-induced damping rates defined in Eq. (4.3) are $R_{2L}/R_{1L} = 2.00$ and $R_{3L}/R_{1L} = 0.990$. These two ratios in Figure 4.2, correspond to leak locations $x_L^* = 0.25$ and $x_L^* = 0.75$, the former being the real leak location. Applying Eq. (4.4) in which $b = 0.5$, based on either of the calculated leak locations and $R_{1L} = 0.0493$, the calculated leak size is $C_d A_L/A = 0.002$, which is identical to the real magnitude of the leak used to generate the MOC transient data.

Table 4.1 Results of Fourier transform analysis on the transients presented in numerical examples

Examples	Cases	Harmonic Components		
		$n = 1$	$n = 2$	$n = 3$
Reservoir-Pipeline-Reservoir System (Figure 4.7)	Case 1 (no leak) R	0.0742	0.0742	0.0742
	Case 2 (with a leak) $R+R_{nL}$	0.1235	0.1728	0.1230
	Leak damping R_{nL}	0.0493	0.0986	0.0488
Reservoir-Pipeline-Valve System (Figure 4.9)	Case 3 (no leak) R	0.00145	N/A[#]	0.00145
	Case 4 (with a leak) $R+R_{nL}$	0.0153	N/A[#]	0.0788
	Leak damping R_{nL}	0.0138	N/A[#]	0.0773

[#] The even harmonic components are equal to zero for the reservoir-pipeline-valve problem

Table 4.2 Results using transients from the different measurement locations (R = 0.0742)--Case 1

Measurement position	R_{1L}	R_{2L}	R_{3L}	R_{2L}/R_{1L}	R_{3L}/R_{1L}
$x^* = 0.375$	0.0493	0.0976	0.0506	1.980	1.026
$x^* = 0.500$	0.0493	0.0676[#]	0.0494	1.371[#]	1.002
$x^* = 0.625$	0.0494	0.0976	0.0508	1.976	1.028
$x^* = 0.750$	0.0493	0.0986	0.0488	2.000	0.999

[#] Large error since the amplitudes of component $n = 2$ are close to zero.

Following the same procedure, transient damping, measured at different pipeline positions, $x^* = 0.375$, 0.5, and 0.625, was analyzed. Damping rates for separate harmonic components are presented in Table 4.2. The Fourier transform analysis of transients measured at different locations gives almost identical results for the damping rate for each component except for R_{2L} at $x^* = 0.5$, where a large error is introduced since the amplitude of the component $n = 2$ is close to zero.

The results in Table 4.2 for R_{1L} and R_{3L} show that the analysis can be performed for the measurement site located anywhere ($0 < x^* < 1$) along the pipeline. The results of the Fourier series analysis of numerical verifications presented in Figure 4.7 and Figure 4.9 are included in Table 4.1.

4.5.2 Reservoir-pipeline-valve system

A reservoir-pipeline-valve case provides an additional numerical example. For the pipeline of 1000m (between $x^* = 0.0$ and 1.0) in Figure 4.8, a transient is initiated by closing the downstream valve. The initial steady flow in the pipeline is $Q_0 = 2.0$ *L/s*, which can be achieved by a partially opened downstream valve. The Reynolds number of the flow in pipeline is 11,160. The Darcy-Weisbach friction factor is calculated as f = 0.0302 using the Swamee-Jain formula and the friction damping factor $R = 0.0048$. The leak detection method presented earlier in the paper was developed from the general solution presented in (Eq. 3.33) based on boundary conditions of two constant-head reservoirs. Thus, it cannot be directly applied to this particular example; however, it can be applied by adding an imaginary symmetric section (dashed portion) to the original pipeline as shown in Figure 4.8.

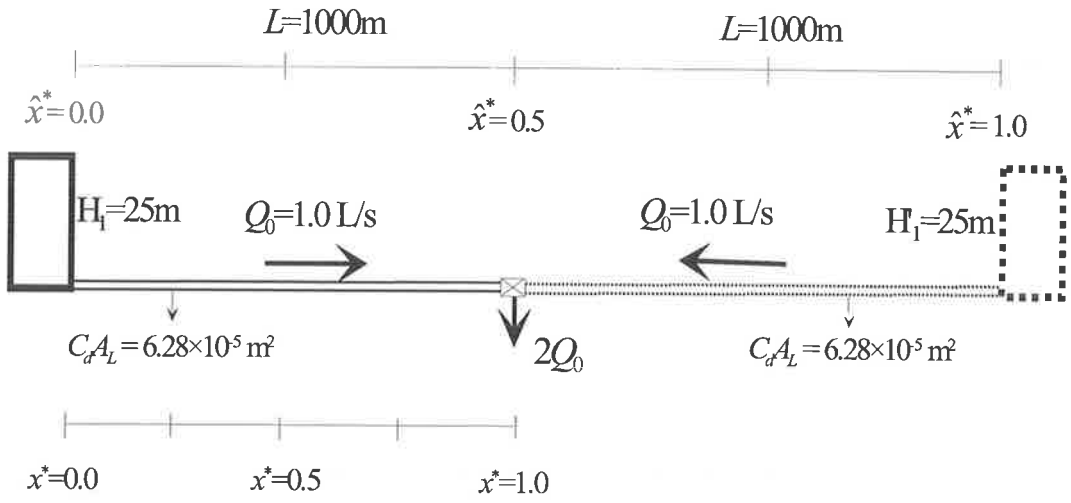

Figure 4.8. A pipeline connecting an upstream reservoir and downstream valve, and the added imaginary symmetric pipeline (D = 0.2m, a = 1000m/s, ε = 0.023mm).

Two cases, referred to as case 3 and case 4, are now considered. In case 3, no leak is present in the pipeline, and in case 4, a leak of C_dA_L/A = 0.002 (b = 0.5) is present at x^* = 0.25. The transient pressures, generated by MOC for the original pipeline, are measured at x^* = 0.75 for the two cases that are presented in Figure 4.9(a). The presence of the leak has very obvious effects on the transient damping and shape. Note that the period of the transients is $4L/a$ for cases 3 and 4, while for cases 1 and 2 the transient period is $2L/a$.

The amplitudes of different harmonic components are given in Figure 4.9(b) for cases 3 and 4 respectively. Amplitudes of all even harmonic components (n = 2, 4, 6,...) are close to zero. Damping of the first two odd harmonics, fitted using Eq. (4.1), are presented in Figure 4.9(c). Due to the large magnitude of q^* (q^* = 1.0) in this case, sensitivity parameter S is calculated as 0.35. Therefore, as stated in the sensitivity analysis, the accuracy of leak detection will be significantly affected if the value used for friction damping is incorrect. As a result, an accurate value of the friction damping would need to be obtained from a test in a leak-free pipeline (see case 3). For case 3, the friction damping rates determined from a leak-free pipeline are R = 0.00153 for harmonic components n = 1 and 3. For case 4, friction plus leak-

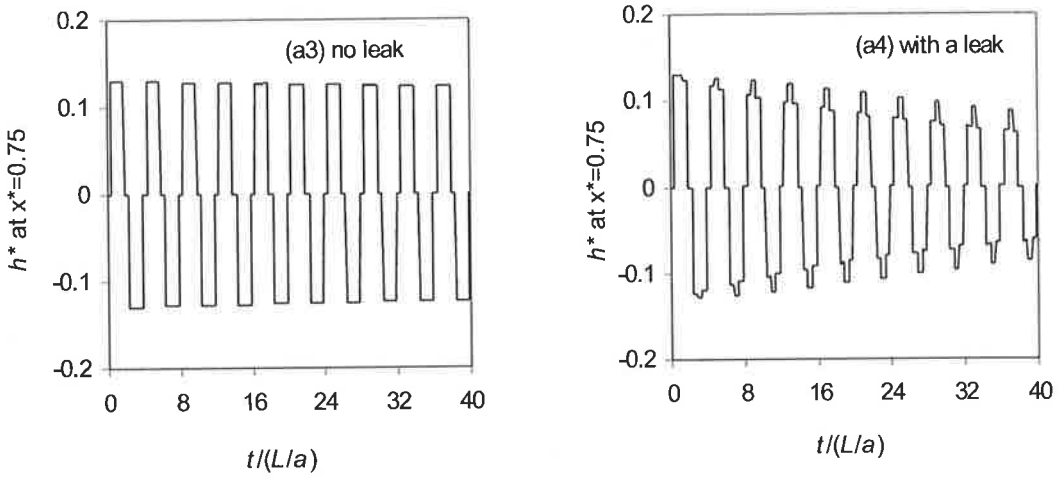

(a) Time history of the measured pipeline transients (MOC)

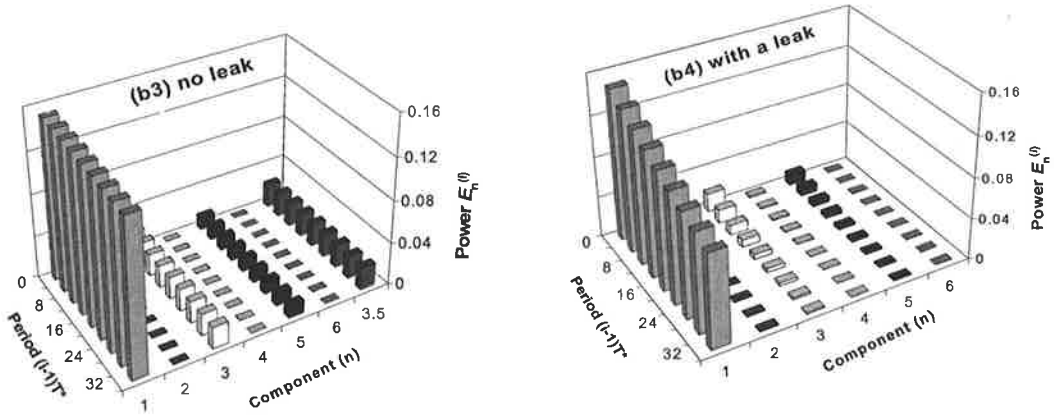

(b) Fourier series analysis of the first period transient ($0< t^* < 4.0$)

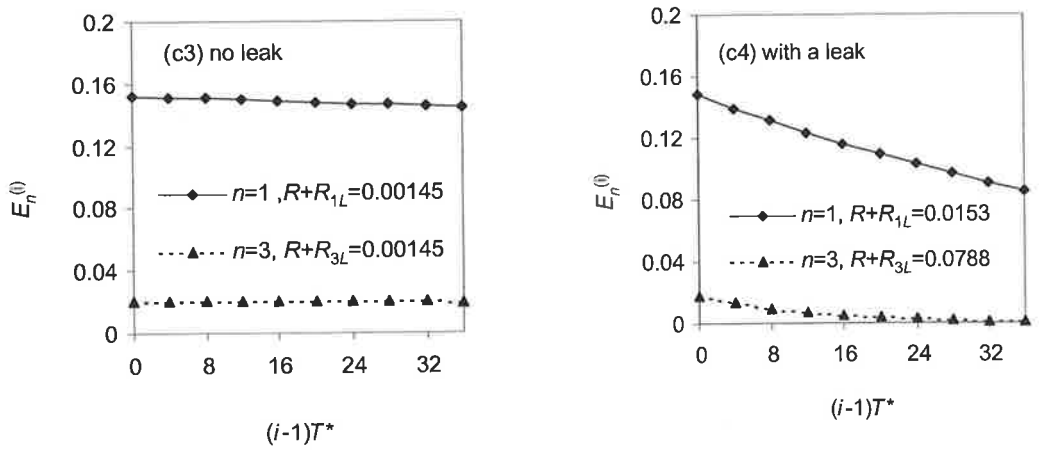

(c) Damping of harmonic components with period (i = 1, 2, 3...)

Figure 4.9 Fourier series analysis of the transients measured from a pipeline without a leak (case 3) and with a leak (case 4) of C_dA_L/A = 0.1% at x_L^* = 0.25 by closing a downstream valve (T^* = 4.0)

induced damping rates for n = 1 and 3 are $R + R_{1L} = 0.0153$ and $R + R_{3L} = 0.0788$. Therefore, leak-induced damping for harmonic components n = 1 and 3 are $R_{1L} = 0.0138$ and $R_{3L} = 0.0773$ (see Table 4.1), and the damping ratio for the first and the third harmonics is $R_{3L}/R_{1L} = 5.60$. The corresponding leak positions are determined using Figure 4.2 as $\hat{x}_1^* = 0.124$ or $\hat{x}_2^* = 0.876$. Applied to the real pipeline, the leak position of $\hat{x}_1^* = 0.124$ becomes $x^* = 0.248$, which is close to the real leak location of $x^* = 0.25$. The other possible leak is located in the imaginary symmetric section. As a result, the location detected using this type of transient system is unique. Applying $R_{1L} = 0.0138$ and $x_L^* = 0.124$ in Eq. (4.4), the magnitude of the leak is calculated as $C_dA_L/A = 0.0020$, which is identical to the actual leak size $C_dA_L/A = 0.002$.

4.6 Multiple leaks

In the previous sections, only a single leak was investigated. The feasibility to locate and quantify multiple leaks using leak-induced transient damping is investigated in this section.

Assuming that the effect of small leaks on a pipeline transient is independent of each other, the general solution for the transient in a pipeline with multiple leaks can be expressed as

$$h^*(x^*,t^*) = \sum_{n=1}^{\infty}\left\{ e^{-(R+\sum_{j=1}^{N} R_{nLj})t^*}\left[A_n \cos(n\pi t^*) + B_n \sin(n\pi t^*)\right]\sin(n\pi x^*)\right\} \qquad (4.15)$$

where $R_{nLj} = \dfrac{aC_d A_{Lj}}{A\sqrt{2gH_{Lj}}}\sin^2(n\pi x_{Lj}^*)$ = the leak damping factor for the leak located at x_{Lj}^*, and A_{Lj} = the leak area (j =1, 2, 3,...N), and N = number of the leaks. There are two unknowns for one leak, the leak location x_{Lj}^* and the leak size C_dA_{Lj}/A. Theoretically, N multiple leaks can be solved using damping rates of $2N$ harmonics as shown in Eq. (4.16). For the i^{th} harmonics

$$\sum_{j=1}^{N}\frac{aC_d A_{Lj}}{A\sqrt{2gH_{Lj}}}\sin^2(\pi x_{Lj}^*) = \hat{R}_{iL} \qquad (i = 1, 2, 3,...2N) \qquad (4.16)$$

where $\hat{R}_{iL}$ = damping caused by N leaks for the i^{th} harmonic. Eq. (4.16) is a set of non-linear, simultaneous equations, and can be solved using a least-squares solver. However, the solutions are not unique due to the symmetrical property of leak damping-as observed for the single leak case. An example of a two-leak case is given here to demonstrate the feasibility to locate multiple leaks.

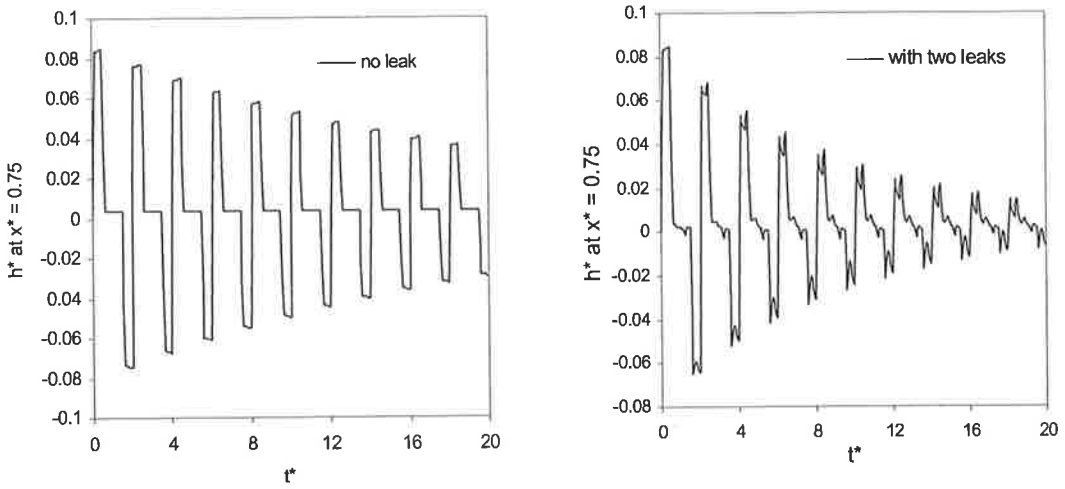

Figure 4.10 Transients from a pipeline with two leaks

For the pipeline (L = 1000m, a = 1000m/s, D = 0.2m, f = 0.015, H_1 = 25m and H_2 = 20m) as shown in Figure 4.6, two leaks are located at x_{L1}^* = 0.1875, x_{L2}^* = 0.375. The sizes of the leaks are C_dA_{L1}/A = 0.2%, C_dA_{L2}/A = 0.1%. The transient was initiated by closing a side discharge of C_dA_S/A=0.002 at x^*= 0.75. The transients measured at x^* = 0.75 are given in Figure 4.10. By analyzing the transient using a Fourier transform, the leak-induced damping rates for harmonics of n = 1, 2, 3, 5 (the amplitude of harmonic n = 4 is close to zero therefore is not used) are R_{1L} = 0.0686, R_{2L} = 0.1012, R_{3L} = 0.0942, R_{5L} = 0.013.

By assuming one leak, applying ratio R_{2L}/R_{1L} = 1.475 gives leak location of x_L^* = 0.292 (or x_L^* = 0.708), and applying R_{3L}/R_{1L} = 1.373 gives leak location of x_L^* = 0.236 (or x_L^* = 0.764). If the assumption of one leak is correct, the leak location obtained from two different damping ratios should be identical, or very close (based on the previous sensitivity analysis, the error of leak location is less than 1% for this case). Since the

detected leak locations based on ratios of $R_{2L}/R_{1L}$and R_{2L}/R_{1L} are almost 19% different, multiple leaks should be considered.

Two leaks are assumed, and four components are needed. Substituting the damping values of these components (n = 1, 2, 3, 5) into Eq. (4.16) gives

$$\begin{aligned}
&\frac{aC_d A_{L1}}{A\sqrt{2gH_{L1}}}\sin^2(\pi x_{L1}^*)+\frac{aC_d A_{L2}}{A\sqrt{2gH_{L2}}}\sin^2(\pi x_{L2}^*)=R_{1L}\\
&\frac{aC_d A_{L1}}{A\sqrt{2gH_{L1}}}\sin^2(2\pi x_{L1}^*)+\frac{aC_d A_{L2}}{A\sqrt{2gH_{L2}}}\sin^2(2\pi x_{L2}^*)=R_{2L}\\
&\frac{aC_d A_{L1}}{A\sqrt{2gH_{L1}}}\sin^2(3\pi x_{L1}^*)+\frac{aC_d A_{L2}}{A\sqrt{2gH_{L2}}}\sin^2(3\pi x_{L2}^*)=R_{3L}\\
&\frac{aC_d A_{L1}}{A\sqrt{2gH_{L1}}}\sin^2(5\pi x_{L1}^*)+\frac{aC_d A_{L2}}{A\sqrt{2gH_{L2}}}\sin^2(5\pi x_{L2}^*)=R_{5L}
\end{aligned} \tag{4.17}$$

Since H_{L1} and H_{L2} are functions of x_{L1}^* and x_{L2}^* respectively, there are four independent unknowns in equation set (4.17), which are A_{L1}, x_{L1}^*, A_{L2} and x_{L2}^*. The equations set (4.17) is solved using a least-square solver by trying different leak locations. For any guesses leak locations x_{L1}^* and x_{L2}^*, corresponding leak sizes A_{L1} and A_{L2} can be calculated. The error for each calculation using guessed x_{L1}^* and x_{L2}^* and calculated leak sizes A_{L1} and A_{L2} is calculated by

$$E=\sum_{j=1}^{4}\left(\frac{aC_d A_{L1}}{A\sqrt{2gH_{L1}}}\sin^2(j\pi x_{L1}^*)+\frac{aC_d A_{L2}}{A\sqrt{2gH_{L2}}}\sin^2(j\pi x_{L2}^*)-R_{jL}\right)^2 \tag{4.18}$$

The correct values of leak size and leak position should gives the smallest error E. In the calculation, when the leak size calculated using least-squares is negative, the leak size is set to zero, which results in a larger error E. The Figure 4.11 gives the calculated error expressed in Eq. (4.18) for the guessed leak locations. Due to the large range of the error associated with different guessed locations, a log scale is applied for better plotting effect.

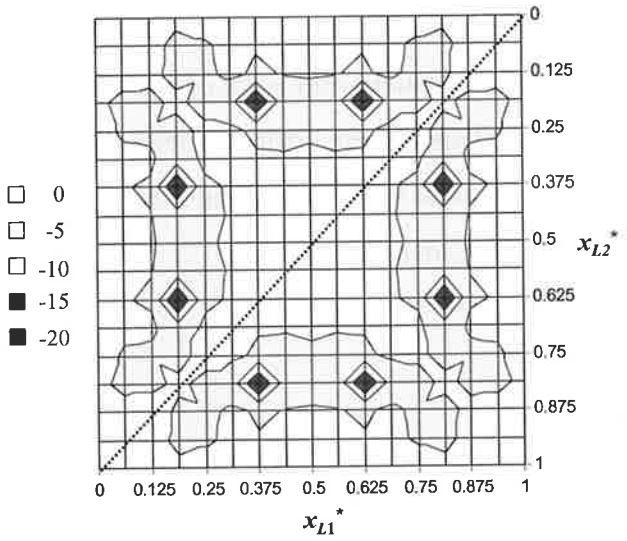

Figure 4.11 Least-square error (ln E) of guessed leak locations

By setting $x_{L1}^* < x_{L2}^*$, Figure 4.12 shows that there are four possible solutions where the least-square error is close to zero. In this case, the value of the least square defined in Eq. (4.18) is $E = 4.16\times10^{-10}$. These possible solutions are

(a) $x_{L1}^* = 0.1875$, $C_dA_{L1}/A = 0.002$ and $x_{L2}^* = 0.375$ $C_dA_{L2}/A = 0.001$.

(b) $x_{L1}^* = 0.1875$, $C_dA_{L1}/A = 0.002$ and $x_{L2}^* = 0.625$ $C_dA_{L2}/A = 0.001$.

(c) $x_{L1}^* = 0.375$, $C_dA_{L1}/A = 0.001$ and $x_{L2}^* = 0.8125$ $C_dA_{L2}/A = 0.002$.

(d) $x_{L1}^* = 0.625$, $C_dA_{L1}/A = 0.001$ and $x_{L2}^* = 0.8125$ $C_dA_{L2}/A = 0.002$.

Solution (a) is the real solution. Although the solution is not unique due to the nonlinear and symmetric property of Eq. (4.16), the possible solutions can be used as a complement for other leak detection methods (e.g. the acoustic leak detection method) and can significantly improve leak detection efficiency.

Because the number of leaks in a pipeline is not known in advance. Procedures to apply the technique presented for multiple leaks are as follows:

1. By applying the ratio of damping rates of the first two components (i.e. R_{2L}/R_{1L}), a leak can be located and quantified.

2. A different ratio of two damping rates is used to confirm the leak location and size obtained in step 1. If there is only one leak in the system, the leak location and size obtained from steps 1 and 2 should be identical, or very close.

3. If the leak location and size obtained from steps 1 and 2 are significantly different, two leaks are considered, and at least four components are needed. By solving the equations sets described in Eq. (4.16), the locations and sizes of two leaks can be obtained. If two-leak assumption is correct, the least square error defined in Eq. (4.18) should be close to zero. Otherwise, more leaks should be assumed and more harmonics are needed for the detection of leaks using damping analysis.

4.7 Unsteady friction

In the derivation of Eq. (3.9), the friction loss was assumed to be represented by a steady-state relationship. For rapidly varying flow, experiments have shown that damping of transients is greater than that predicted by the steady-state Darcy-Weisbach head loss equation. This difference can be addressed using unsteady friction models such as those by Zielke (1968), Brunone et al. (1995), Vardy and Hwang (1991), and Bergant et al. (2001). Applying an unsteady friction model, the total friction factor f may be expressed as

$$f = f_s + f_u \tag{4.19}$$

where f_s represents the quasi-steady contribution to the friction factor and f_u is an additional contribution due to unsteadiness. To account for the unsteady friction damping, the friction-damping factor R in Eq. (3.33) is replaced by

$$R = R_s + R_u \tag{4.20}$$

in which R_s represents damping by steady friction, and R_u represents damping by unsteady friction. In contrast to steady friction damping, R_s, the value of unsteady friction damping, R_u, is not constant, and varies for different Fourier components. For this case, the e^{-Rt^*} term in Eq. (3.33) cannot be taken outside the summation sign. The value of R_u (and hence R) can be determined by experimental tests or by a numerical model that incorporates an appropriate unsteady friction model, e.g. the modified Brunone model (Vitkovský, 2001).

4.8 Experimental verification

Experimental tests were conducted in a single pipeline in the Robin Hydraulics Laboratory at the University of Adelaide. The pipeline is a straight 37.2m copper pipe with internal diameter of 22mm between two pressurized tanks as shown in Figure 4.12. Five pressure transducers (accuracy 0.06% of full range, 0-70 meters) are located at equidistant points along the pipeline and two one-quarter-turn ball valves are installed at both ends for flow control. A side-discharge orifice, used to simulate a leak, is installed at the one-quarter position (point B) with a leak orifice size of 1mm diameter. To initiate a transient, another side-discharge valve was installed at point D. The pipeline is strictly anchored with supports at an interval of 1.0m in the axial direction. As a result, the structural damping in this pipeline is negligible compared to the friction damping. More details of this experimental apparatus are found in Vítkovský (2001).

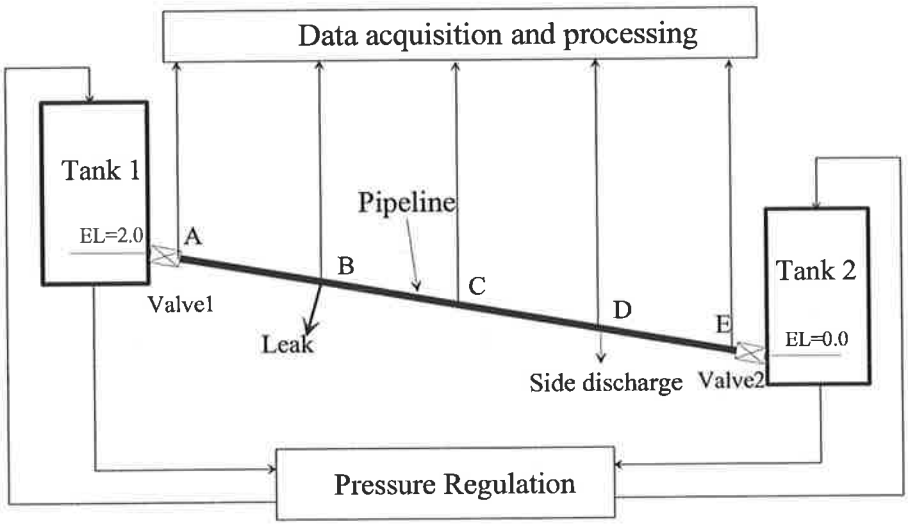

Figure 4.12 Laboratory pipeline

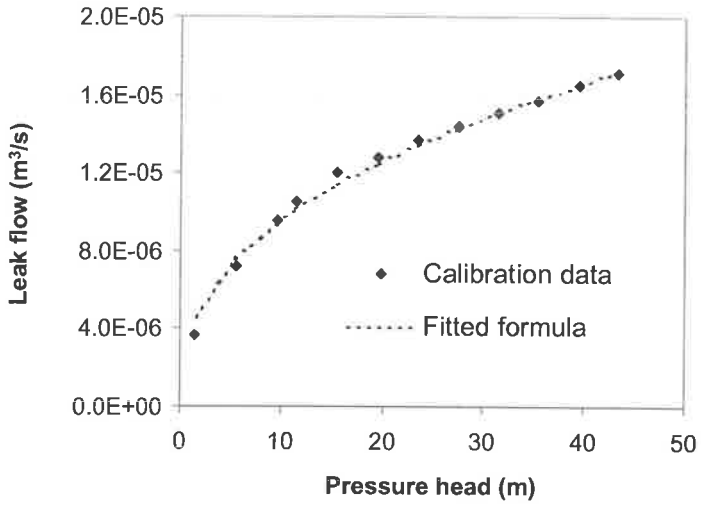

Figure 4.13 Calibration of the leak discharge relationship

In order to switch on and off a leak during the experimental test to simulate cases of with and without a leak, the leak orifice is connected with a small ball valve. A short pipe section is formed outside of the leak and the water is not directly discharged to atmosphere exactly. As a result, a non-theoretical discharge-head relationship was obtained in the calibration of 1mm leak as shown in Figure 4.13 (a formula of $b = 0.5$ gave a larger regression error as shown in Vítkovský (2001)). The orifice equation was fitted to the data using a standard least square fit and the fitted orifice equation is

$$Q_L = 8.0\times10^{-7}(2gH_L)^{0.45} \tag{4.21}$$

Based on the analysis in Chapter 3, the non-theoretical leak described in Eq. (4.16) can be transferred to an equivalent theoretical leak by adjusting the value of C_dA_L. The size of the equivalent theoretical leak is calculated as

$$(C_dA_L)_0 = C_a(C_dA_L) \tag{4.22}$$

where $C_a = 2b(2gH_{L0})^{b-0.5}$ = leak size adjustment coefficient.

4.8.1 Reservoir-pipeline-reservoir system

Two tests were conducted. Test I is a no–leak case and in Test II a 1mm leak is located at point B (Figure 4.12). The flow conditions are as follows: wave speed a = 1,320m/s, head at tank 1 H_1 = 23.6m, head at Tank 2 H_2 = 22.8m. Applying Eqs. (4.21) and (4.22) gives the equivalent theoretical leak parameter $(C_dA_L)_0 = 5.00\times10^{-7}$ m^2. The steady flow

velocity in the pipeline (measured at the downstream tank) is V_0 = 0.567m/s, and the steady friction damping factor is calculated as R_s = 0.0109.

In Test I, the valves at locations A and E and the side-discharge valve at D were opened and steady state was achieved. The side-discharge valve at D was then closed quickly. In Test II, valves at locations A and E, the leak at B and the side-discharge valve at D were open until steady state was obtained. The side-discharge valve at D was then sharply closed. For both tests, the flow rates through the side-discharge valve were about 0.005L/s. Only the measured pressures at point D (x^* = 0.75) for Test I and Test II are used for leak detection analysis and they are plotted in Figure 4.14(a). The sampling frequency of the measurement is 2000Hz. The leak-induced damping of Test II is obvious compared to the transient in Test I that has no leak.

Figure 4.14(b) shows the computed amplitudes of different harmonic components. The amplitude of each component is less in Test II than in Test I, which is an indication of presence of a leak.

Friction damping factors obtained from the no-leak case (Test I) are presented in Figure 4.14(c). Damping factors of the first three harmonic components (n = 1, 2, 3) are R_1 = 0.0244, R_2 = 0.0382, R_3 = 0.0563 (see Table 4.3), all being larger than the steady friction damping factor Rs = 0.0109, calculated using steady state friction. The differences between the measured and the calculated damping values are due to unsteady friction. It accounts for 50%, 71% and 80% of the total of the R value for the first three components. As a result, despite a small value of sensitivity parameter S (S = 0.00036), the friction damping in this case cannot be calculated from the steady state conditions, and must be obtained either from a leak-free measurement or from a numerical analysis using suitable unsteady friction models. As previously indicated, values of unsteady friction damping are different for different Fourier components. In Figure 4.14(c), regression coefficients of the fitted curves of the damping factors are larger than 0.99, experimentally confirming the analysis that damping including unsteady friction damping, for each component is exponential.

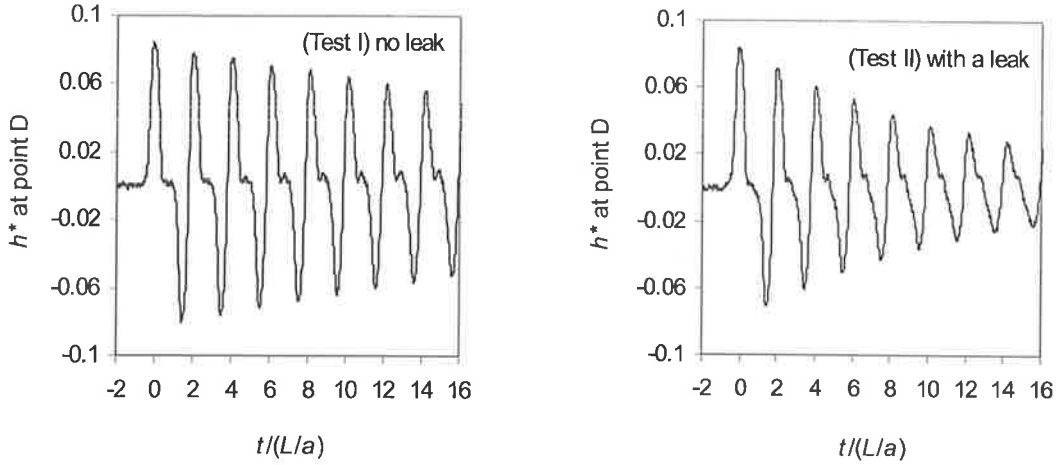

(a) Measured transient from a pipeline

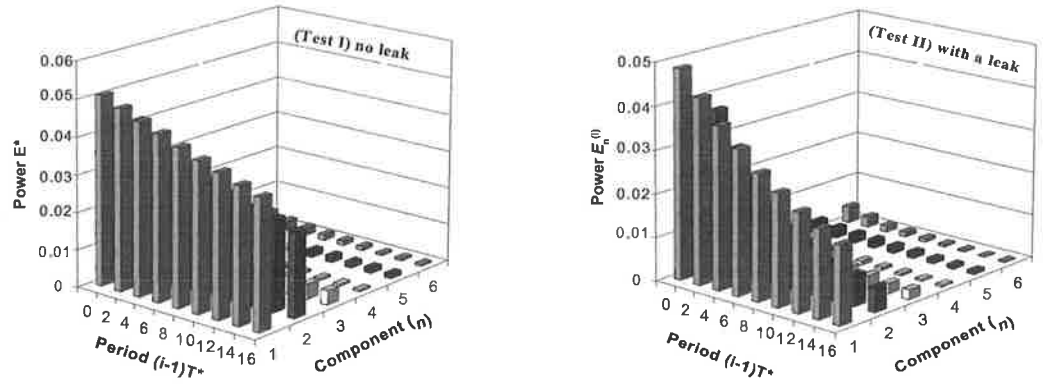

(b) Frequency analysis

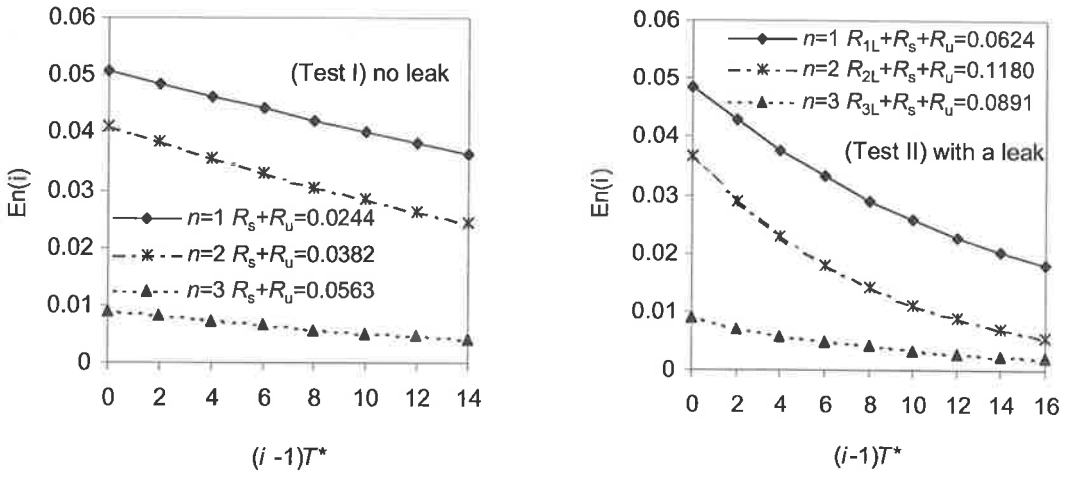

(c) Damping of individual Fourier components

Figure 4.14 Experimental verification leak detection using the transient damping

Table 4.3 Results of Fourier transform analysis on the transients presented in experimental tests

Examples	Tests	Harmonic Components		
		$n = 1$	$n = 2$	$n = 3$
Reservoir-Pipeline-Reservoir System Figure 4.14	Test I (no leak) $R_s + R_u$	0.0244	0.0382	0.0563
	Test II (with a leak) $R_s + R_u + R_{nL}$	0.0624	0.1180	0.0891
	Leak damping R_{nL}	0.0380	0.0798	0.0328
Reservoir-Pipeline-Valve Problem Figure 4.15	Test III (no leak) $R_s + R_u$	0.0374	N/A#	0.0609
	Test IV (with a leak) $R_s + R_u + R_{nL}$	0.217	N/A#	0.0895
	Leak damping R_{nL}	0.1796	N/A#	0.0286

#The even harmonic components are equal to zero for the reservoir-pipeline-valve problem

In Tests I and II, since the steady flow conditions were similar and both the transients were initiated by closing the side-discharge valve at approximately the same speed of closure, steady and unsteady friction effects are similar. Leak-induced damping rates for the first three harmonic components (n = 1, 2, 3), which are calculated by subtracting friction damping from total damping, are R_{1L} = 0.0380, R_{2L} = 0.0798, and R_{3L} = 0.0328 (see Table 4.3). The ratios of damping rates R_{2L} and R_{1L}, and R_{3L} and R_{1L} are $\frac{R_{2L}}{R_{1L}} = 2.10$, and $\frac{R_{3L}}{R_{1L}} = 0.863$. Corresponding leak locations for these damping ratios are x_L^* = 0.242 (or x_L^* = 0.758) and x_L^* = 0.255 (or x_L^* = 0.745) by applying these two ratios in Figure 4.2. Averaging of these results gives the location as x_L^* = 0.249, almost the exact real location of the leak. Using R_{1L} = 0.0380, R_{2L} = 0.0801 and leak location x_L^* = 0.242 and x_L^* = 0.255, the magnitude of the leak is calculated, from Eq. (4.4) using b = 0.5, as $(C_dA_L)_0 = 4.912\times10^{-7}$ and $(C_dA_L)_0 = 4.917\times10^{-7}$ m^2, which are about 1.7% smaller than the real leak size of $(C_dA_L)_0 = 5.00\times10^{-7}$ m^2.

4.8.2 The reservoir-pipeline-valve system

Experimental tests conducted by Vítkovský (2001) from a reservoir-pipeline-valve problem provide additional experimental verification. For the pipeline as shown in

Figure 4.12, the transients were initiated by closing Valve 1 connected to the Tank 1 from a steady state. The pressure heads at two tanks were H_1 = 26.5m, H_2 = 26.6m, and the steady velocity before closing the Valve 1 was V_0 = 0.15m/s giving Reynolds number of **Re** = 3200.

Test III (in comparison to Test I and Test II in the above section) is a no-leak case, in which the leak at point B was not open. In Test IV, the 1mm diameter orifice leak at Point B was open. The transients measured at Point A are plotted in Figure 4.15(a).

Following a similar procedure to that in Section 4.8.1, the transients are decomposed into Fourier components and the damping coefficient of each of the components was analyzed using a fitting function described by Eq. (4.1). In this example, since the amplitudes of the second component (n = 2) are close to zero for both tests, only components of n = 1, and 3 are used for leak detection analysis. In Test III, the damping coefficients, including steady and unsteady friction damping for components of n = 1 and n = 3, are $R_s + R_u$ = 0.0374 and $Rs + Ru$ = 0.0609. In Test IV, the damping coefficients for these two components are $R_s + R_u + R_{1L}$ = 0.217 and $Rs + Ru + R_{3L}$ = 0.0895. The same friction damping is assumed in Test III and Test IV since the transient events were generated similarly in both tests. Therefore, the differences in the damping coefficients between the two tests are caused by the leak. The leak induced damping coefficients for components of n = 1, and 3 are R_{1L} = 0.1796, and R_{3L} = 0.0286 (see Table 4.3). The ratio of two components is R_{3L}/R_{1L} = 0.159. Similar to the second numerical example (Section 4.5.2), the leak location on the artificial pipeline, which includes the real pipeline and an imaginary pipe section, can be calculated by applying R_{3L}/R_{1L} = 0.159 to Figure 4.2. The possible leak locations are $\hat{x}_L^*$ = 0.374 (or $\hat{x}_L^*$ = 0.299, 0.626, and 0.701). In this case, there are four possible leak locations due to use of R_{3L}/R_{1L} (see Figure 4.2). Applied to the real pipeline, the leak position of $\hat{x}_L^*$ = 0.374 becomes x^* = 0.748, which is close to the real leak location of x^* = 0.75. Similarly, the other three possible leak locations

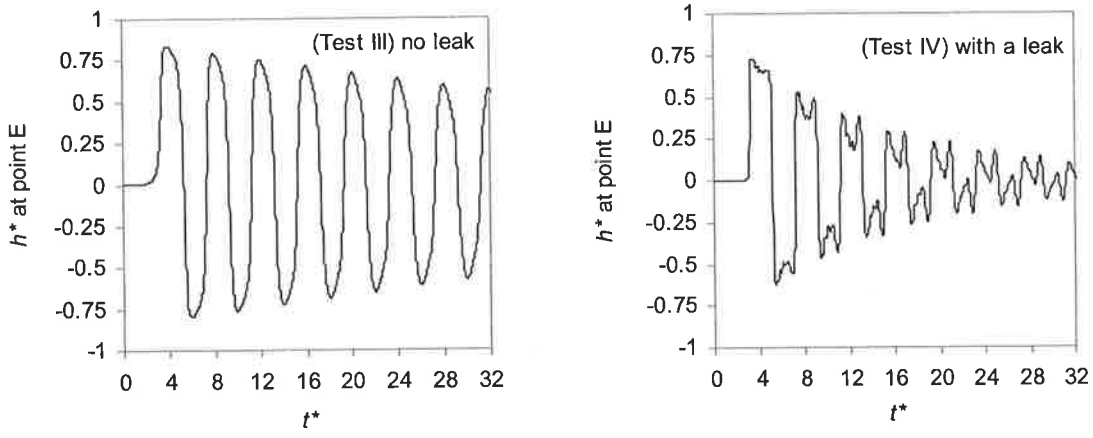

(a) Measured transient from a pipeline

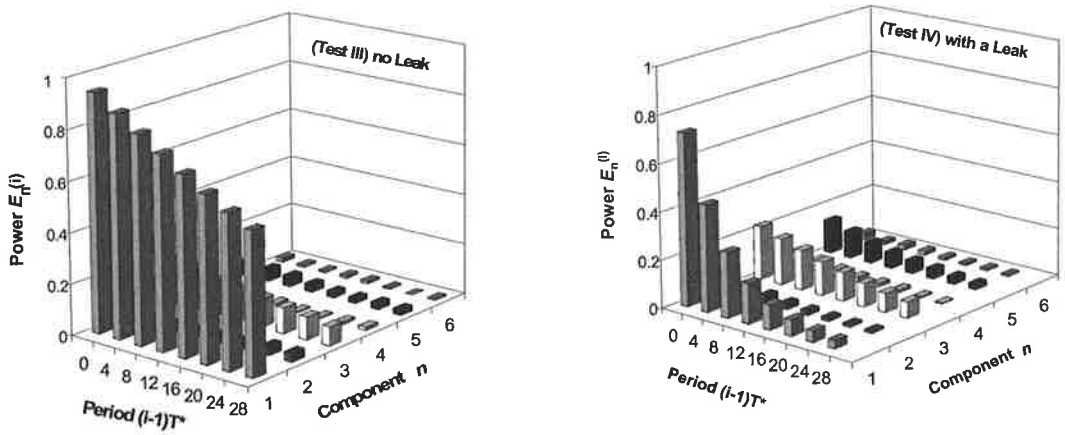

(b) Frequency analysis

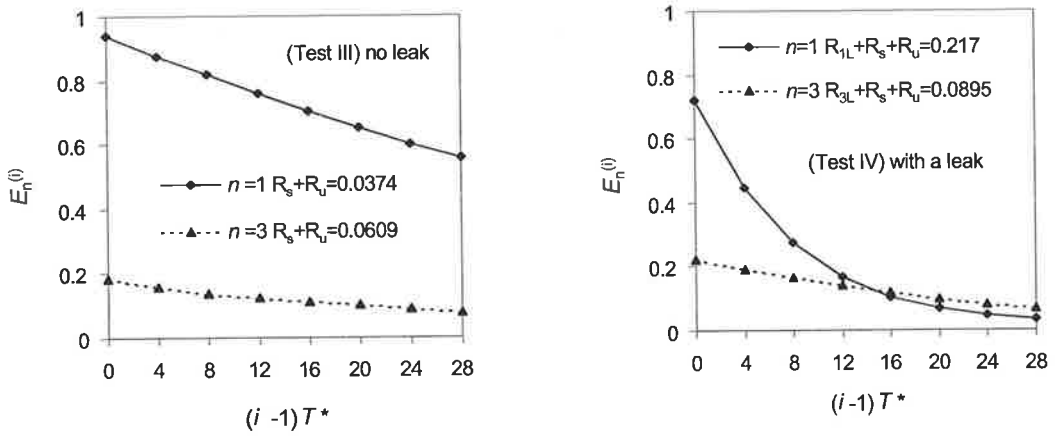

(c) Damping of individual Fourier components

Figure 4.15 Experimental verification of leak detection using the transient damping for on a reservoir-pipeline-valve system

corresponding to $\hat{x}_L^*$ = 0.299, 0.626, and 0.701 are x^* = 0.598, 1.252 and 1.402. The locations x^* = 1.252 and 1.402 are located in the imaginary symmetric section. As a result, there are two possible leak locations detected using this type of transient system. Applying R_{1L} = 0.1796 or R_{3L} = 0.0286, and x_L^* = 0.374 in Eq. (4.4) using b = 0.5, the magnitude of the leak is calculated as $(C_dA_L/A)_0$ = 0.0036 or $(C_dA_L/A)_0$ = 0.0037. Then the detected magnitude of the leak is $(C_dA_L/A)_0$ = 0.00365 which is about 20 % lower than the real value of $(C_dA_L/A)_0$ = 0.005. One reason for this large difference can be explained by the sensitivity analysis in Figure 4.5. When a leak is close to the middle of the pipeline, the influence of a large transient magnitude, which is characterized by sensitivity parameter S, on the leak size becomes non-negligible. In this example, q^* = 1.0, and this gives S = 0.2 from the definition of S in Eq. (4.8). Based on Figure 4.5, the leak size error caused by the transient magnitude (S = 0.2) for the leak at x^* = 0.375 is about 20%.

4.9 Application to a pipeline including series pipes

The possibility to detect leaks in a more complex pipe system using the analytical leak detection technique presented in this chapter has been investigated in this section. A pipeline including two series pipes of different diameters was chosen.

A series pipeline including two different pipe sections is shown in Figure 4.16. The pipeline connects a reservoir at upstream and a valve at the downstream. A leak is located 750m downstream the reservoir. The leak area is $C_dA_L = 6.28\times10^{-5}$ m^2. The valve is partially closed giving steady flow rate of 5.0×10^{-3} m^3/s in the pipeline. When the valve at downstream end is sharply closed, a transient event is initiated in the pipeline. The transients measured at the valve for cases of with and without a leak are given in Figure 4.17. Compared to the transients in a straight single pipeline, the transients from such a series pipeline are more complicated due to reflection and transmission at the pipe junction. Following a similar procedure given in Section 4.2, the transients in Figure 4.17 were decomposed into Fourier series. Some of the Fourier components don't decay in the same manner as those in a single pipeline. Because no explicit analytical solutions are available for the transients in such a pipe system, the transients shown in Figure 4.17

cannot be interpolated as those from a single pipeline. Therefore, the leak detection method presented in this chapter may not be applied in a complex pipe system.

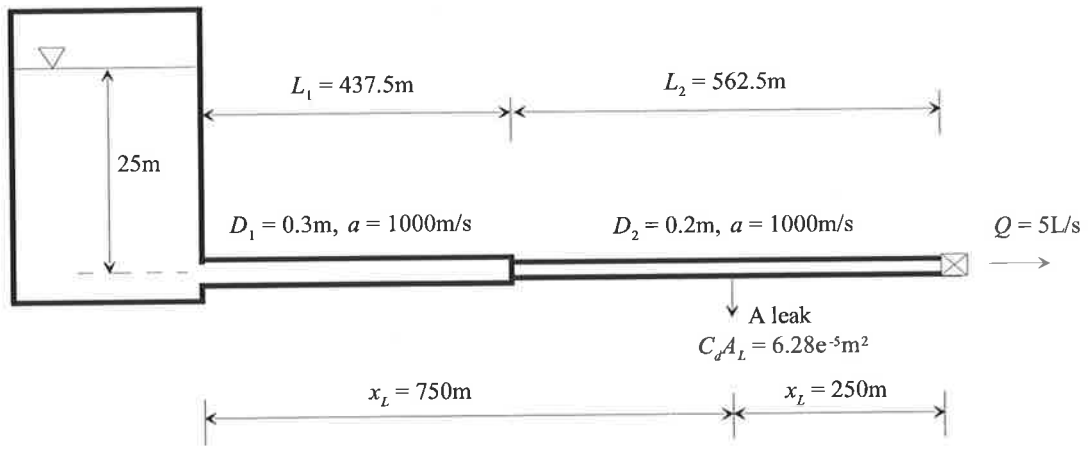

Figure 4.16 A series pipeline

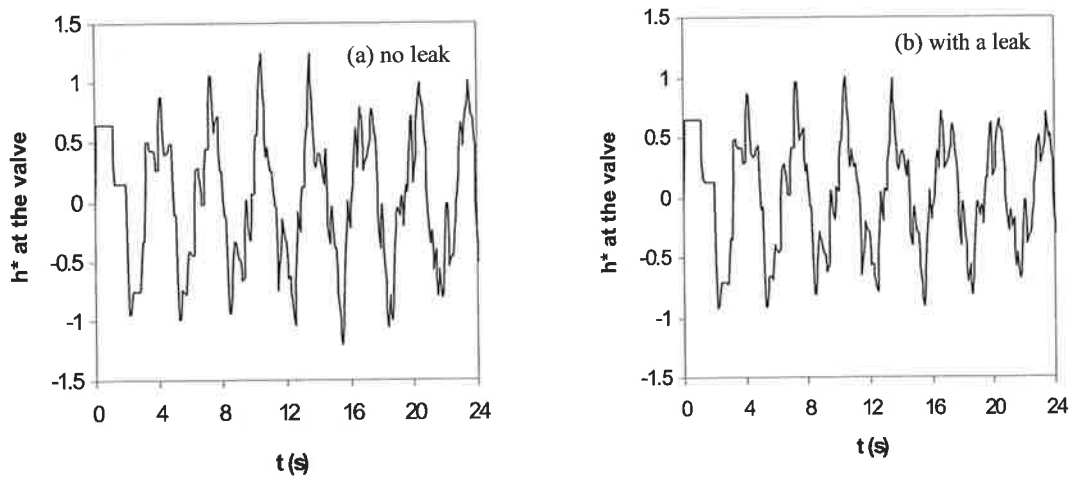

Figure 4.17 Transient from a series pipeline

4.10 Summary

A new technique for leak detection, location and quantification using leak-induced damping on fluid transients based on the analytical solution developed in Chapter 3 has been developed.

Based on the developed leak detection method, the damping rate of an individual Fourier component is useful for finding the magnitude of a leak while the ratio of damping rates between different harmonic components is useful for finding leak location. Leaks of

0.1% of a pipeline's cross-sectional area or smaller can be detected and located based on numerical analysis and experimental results. This method does not require rigorous determination and modelling of boundary conditions and transient behavior in the pipeline. Due to the symmetrical properties of the leak damping, the leak locations obtained using this technique may or may not be unique depending on the leak location itself and the transient event used.

Sensitivity analysis shows that linearization generates an insignificant error in both leak location and quantification. Inaccurate steady-state friction determination (if it is used to find the leak damping by subtraction from total damping), on the other hand, may or may not be significant, depending on the parameters of the pipeline and flow and the location of a leak. Also, if subtraction is used to find leak damping, the added damping caused by unsteady flow may become important. Because larger relative uncertainties in estimating pipe friction, friction factor has a greater influence on the leak detection if the friction damping is obtained from the definition based on the steady state conditions.

Although the leak detection technique presented in this chapter is simple to use and apply, and has some significant advantages for leak detection in pipelines, it does not have the generality of some other methods (e.g., the inverse transient method), and does not seem to be generally applicable to complex systems such as pipe networks. Difficulties in complicated geometries include the complex waveforms created by branches and loops and demands, which may be difficult to distinguish from leaks.

The method presented in this chapter is only valid for leak detection in single pipelines; however, the sensitivity analysis presented in this chapter may provide some guidelines for leak detection in complex pipe network systems. For example, to improve the efficiency of leak detection in a pipe network, the friction damping should be minimized, thus the effects of leaks on fluid transients, on which most of the hydraulic leak detection methods are based, can be more significant. Leak detection in pipe networks is discussed in Chapter 7 and Chapter 8.

Chapter 5

Transients in a Pipeline with a Leak under Variable Boundary Conditions--Coded Transients

5.1 Introduction

The analytical solution given in Section 3.3 is based on known initial conditions for the pipeline transient under constant boundary conditions. The leak detection technique that is developed in Chapter 4 is based on similar boundary conditions. When a variable boundary condition exists, for example a continuous perturbation of the downstream reservoir, both the analytical solution and the leak detection technique cannot be applied. An analytical solution was derived by applying the Laplace transform (Wang et al. 2001) considering a continually changing boundary condition. However, the analytical solution based on the Laplace transform does not provide helpful physical insight into the effects of a leak on a pipeline transient. Alternatively, a sinusoidal input boundary perturbation can be applied and enables an analytical solution expressed in a Fourier series solution to be obtained. For a general perturbation function, it can be decomposed into a series of sinusoidal functions. The response of the pipeline under such a general perturbation function can be obtained by adding the response solution of each sinusoidal function.

In this chapter, an analytical solution under a sinusoidal boundary perturbation is developed in Section 5.2. The analytical solution is compared with the numerical results based on the method of characteristics (MOC) in Section 5.3. The feasibility for leak detection by applying a continuous boundary perturbation is investigated in Section 5.4 and Section 5.5. Finally, in Section 5.6, the implementation methods used to generate the

continually varying perturbation are discussed. A new concept of the *coded transient*--a designed transient--is introduced in this section.

5.2 A Fourier series solution for a sinusoidal boundary

Assuming a constant upstream reservoir and a sinusoidal perturbation at the downstream reservoir as shown in Figure 5.1, the boundary conditions for the problem are

$$h^*(0,t^*) = 0, \text{ and } h^*(1,t^*) = f(t^*) = E^* \sin(\omega\, t^*) \quad (t^* > 0) \tag{5.1}$$

in which $E^* = E/H_1$ = dimensionless amplitude of the perturbation, E = amplitude of the perturbation, and ω = dimensionless angular frequency of the perturbation.

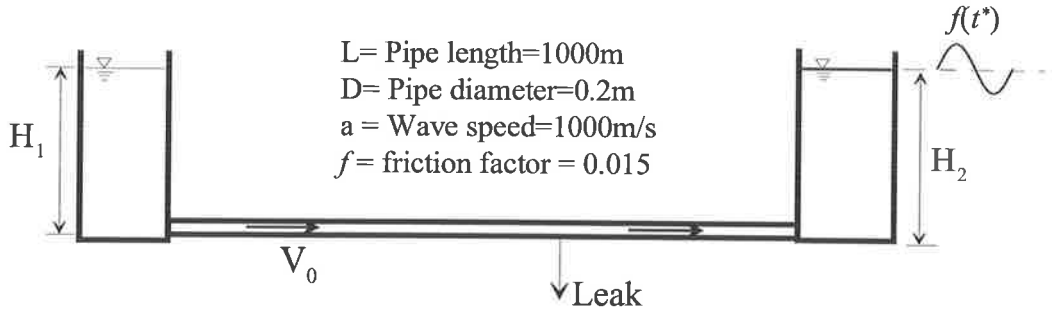

Figure 5.1 A pipeline connected to a constant reservoir and a downstream reservoir with a varying head

Assuming steady state conditions in the pipeline gives the initial condition as

$$h^*(x^*,0) = 0 \text{ and } \frac{\partial h^*(x^*,0)}{\partial t^*} = 0 \tag{5.2}$$

The governing equation for the transient in a pipeline including a leak is derived in Eq. (3.27) as

$$\frac{\partial^2 h^*}{\partial x^{*2}} = \frac{\partial^2 h^*}{\partial t^{*2}} + [2R + F_L \delta(x^* - x_L^*)]\frac{\partial h^*}{\partial t^*} + 2RF_L \delta(x^* - x_L^*)h^* \quad \text{(3.27,repeated)}$$

Eqs. (3.27), (5.1) and (5.2) represent a homogeneous problem with homogeneous initial conditions and inhomogeneous boundary conditions. To obtain homogeneous boundary conditions, let

$$h^*(x^*,t^*) = v(x^*,t^*) + x^* E^* \sin(\omega\, t^*) \tag{5.3}$$

Substituting Eq (5.3) into Eqs. (3.27), (5.1), and (5.2) gives the partial differential equation (P.D.E.), boundary conditions (B.C.) and initial conditions (I.C.) for $v(x^*,t^*)$ as

P.D.E
$$\frac{\partial^2 v^*}{\partial x^{*2}} = \frac{\partial^2 v^*}{\partial t^{*2}} + [2R + F_L\delta(x^* - x_L^*)]\frac{\partial v^*}{\partial t^*} - x^*[2R + F_L\delta(x^* - x_L^*)]E^*\omega\cos(\omega\, t^*) + x^*E^*\omega^2\sin(\omega\, t^*) \tag{5.4}$$

B.C.
$$v^*(0,\ t^*) = 0, \text{ and } v^*(1,\ t^*) = 0 \tag{5.5}$$

I.C.
$$v^*(x^*,\ 0) = 0 \quad \frac{\partial v^*(x^*,\ 0)}{\partial t^*} = x^*E^*\omega \tag{5.6}$$

A solution to Eq. (5.4) subject to the boundary and initial conditions given in Eqs (5.5) and (5.6) is expressed as a Fourier series as (a detailed derivation is given in Appendix C)

$$v(x^*,t^*) = \sum_{n=1}^{\infty} e^{-(R+R_{nL})t^*}[A_n\cos(n\pi t^*) + B_n\sin(n\pi t^*)]\sin(n\pi x^*) + \sum_{n=1}^{\infty}\{A_{np}\cos(\omega\, t^*) + B_{np}\sin(\omega\, t^*)\}\sin(n\pi x^*) \tag{5.7}$$

where $R_{nL} = F_L sin^2(n\pi x_L^*)$ = leak-induced damping coefficient, and the Fourier coefficients in Eq. (5.7) are defined as

$$A_{np} = \frac{a[(n\pi)^2 - \omega^2] - 2b(R + R_{nL})\omega}{[(n\pi)^2 - \omega^2]^2 + [2(R + R_{nL})\omega]^2}, B_{np} = \frac{2a(R + R_{nL})\omega + b[(n\pi)^2 - \omega^2]}{[(n\pi)^2 - \omega^2]^2 + [2(R + R_{nL})\omega]^2} \tag{5.8}$$

$$A_n = -A_{np}, \qquad B_n = \frac{2E^*\omega\cos(n\pi)}{(n\pi)^2} + \frac{(R + R_{nL})A_{np} - \omega B_{np}}{n\pi} \tag{5.9}$$

$$a = \frac{4RE^*\omega\cos(n\pi)}{n\pi} - 2F_L x_L^*\sin(n\pi x_L^*)E^*\omega, \text{ and } b = \frac{-2E^*\omega^2\cos(n\pi)}{n\pi} \tag{5.10}$$

Substituting Eq. (5.7) into Eq. (5.3) gives the general solution of the inhomogeneous boundary condition problem expressed by Eqs. (3.27), (5.1) and (5.2) as

$$h^*(x^*,t^*) = \sum_{n=1}^{\infty} e^{-(R+R_{nL})t^*}[A_n\cos(n\pi t^*) + B_n\sin(n\pi t^*)]\sin(n\pi x^*) + \sum_{n=1}^{\infty}\left[A_{np}\cos(\omega\, t^*) + B_{np}\sin(\omega\, t^*)\right]\sin(n\pi x^*) + x^*E^*\sin(\omega\, t^*) \tag{5.11}$$

A transient induced by a sinusoidal boundary condition is composed of the three parts on the right-hand side of Eq. (5.11). If the boundary perturbation only lasts a short period and then stops, the second and the third parts in Eq. (5.11) become zero and Eq. (5.11) is reduced to Eq. (3.33), which is the damping problem discussed in Chapter 3. On the other hand, if the perturbation lasts long enough, the first part approaches zero, and Eq. (5.11) is simplified to a steady oscillation as

$$h_0^*(x^*,t^*) = \sum_{n=1}^{\infty}\left[A_{np}\cos(\omega\ t^*) + B_{np}\sin(\omega\ t^*)\right]\sin(n\pi x^*) + x^*E^*\sin(\omega\ t^*)$$
$$= \sum_{n=1}^{\infty}\left[A_{np}\cos(\omega\ t^*) + (B_{np}+C_{np})\sin(\omega\ t^*)\right]\sin(n\pi x^*) \qquad (5.12)$$
$$= \sum_{n=1}^{\infty}\left[E_{np}^*\sin(\omega\ t^* + \delta)\right]\sin(n\pi x^*)$$

where $E_{np}^* = \sqrt{A_{np}^2 + (B_{np}+C_{np})^2}$ (5.13)

which is the amplitude of a Fourier component, $\delta = \tan^{-1}(\frac{B_{np}+C_{np}}{A_{np}})$ = the phase angle, and $C_{np} = -\frac{2E\cos(n\pi)}{n\pi}$. Therefore, after a sufficiently long time, the output corresponding to a sinusoidal input is a summation of a series of harmonic oscillations. The frequency of any of the harmonic oscillations is that of the input, and the amplitude of each of the harmonic component is defined by Eq. (5.13).

The value of the amplitude of each component of Eq. (5.13) depends on the amplitude and frequency of the input signal and the parameters of the pipeline and the leak, which may be characterised by parameters R, F_L and x_L^*. Because the amplitude and the frequency of the input signal are known, and the frictional parameter R can be calculated from the steady state conditions, the feasibility to detect the leaks is investigated in the following sections.

5.3 Comparison with numerical solution based on MOC

When deriving the governing Eq. (3.27), q^* was assumed to be small (q^*<<1.0). Under that assumption, a linear governing equation was obtained. The analytical solution expressed in Eq. (5.11) is now compared with the numerical results obtained from the MOC, nonlinear equation. For the pipeline as shown in Figure 5.1 where H_1 = 25m, H_2 = 15 + Esin(ωt)m, and E = 0.25m, two perturbation frequencies, $\omega = 1.0\pi$ and $\omega = 1.5\pi$, are considered. A leak of C_dA_L/A = 0.1% is located at 250m (x_L^* = 0.25) downstream of the upstream reservoir. Based on the steady-state flow conditions, the friction damping parameter is calculated as R = 0.0606 (Eq. 3.19). For the applied perturbations, the

dimensionless amplitude of the transient q^* is less than 0.01. A small transient is needed to keep the linearization error of the analytical solution at a low level.

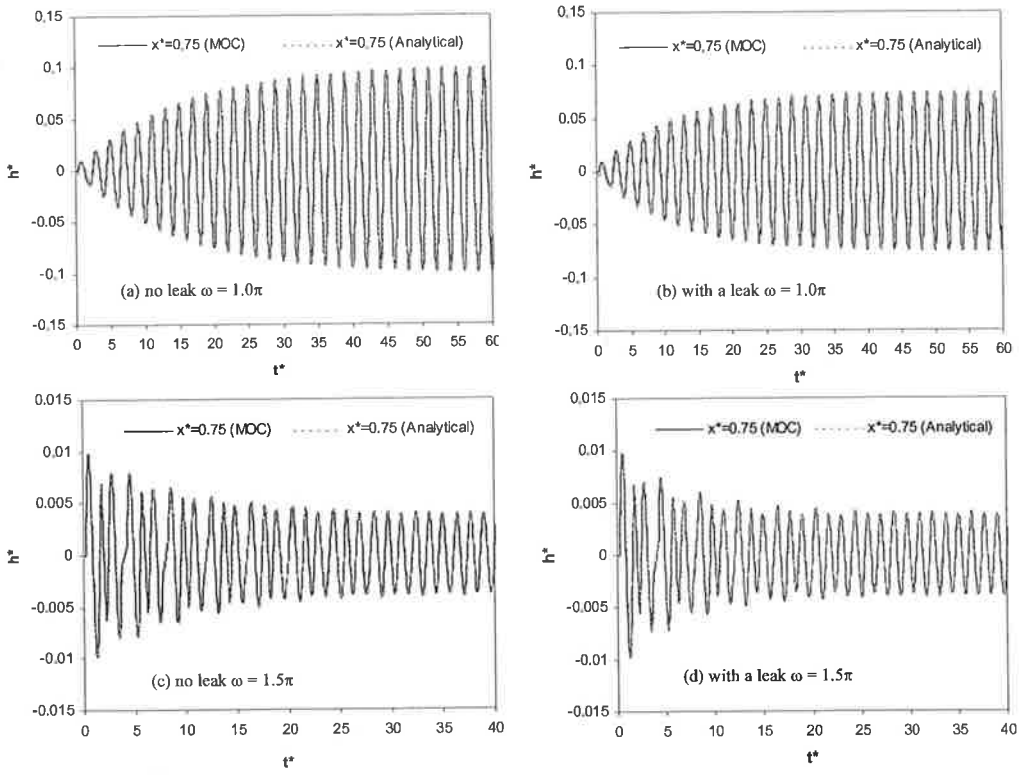

Figure 5.2 Comparison of the analytical solution and the numerical results based on the MOC

The transients measured 750m downstream from the upstream reservoir ($x^* = 0.75$) based on the analytical solution and the MOC are presented in Figure 5.2. For all cases, with and without a leak and two input frequencies, the transients calculated based on the analytical solution of Eq. (5.11) agree very well with the numerical results from the MOC. In the analytical solution, components of $n \leq 20$ are considered. The number of Fourier components that should be considered in the analytical solution depends on the frequency of the input perturbation. More Fourier components should be included for an input perturbation with a high frequency as explained in the following paragraph. When ω is close to 1.0π, the frequency of the boundary perturbation approaches the natural frequency of the pipeline, a resonance condition is created with a significantly larger amplitude than the input signal. For the case without a leak, the transient stops growing and a steady oscillation appears after about 25 periods ($t^* > 50.0$), while when a leak is present, the steady oscillation forms after about 20 periods ($t^* > 40.0$). A steady oscillation is defined here in such a way that the increase of transient amplitudes over 10

periods is less than 0.1%. The presence of the leak reduces the amplitude of the steady oscillation about 40%, but it has no influence on the frequency of the transient. When $\omega = 1.5\pi$, a transient with a fundamental period of $T^* = 1.33$, is observed for both cases of with and without a leak. However, the presence of the leak has little influence on the amplitude of the steady oscillation for non-resonance inputs.

5.4 Effects of a leak on steady oscillation

The above example indicated that a leak has an influence on the amplitude of a steady oscillation and that amplitude is a function of the frequency of the input signals. The amplitude values of the components of $n < 11$ defined in Eq. (5.13) are plotted in Figure 5.3 for the cases given in Figure 5.2. When $\omega = 1.0\pi$, in both cases of with and without a leak, the component of $n = 1$ is dominant, as the amplitudes of other components are negligible. When a linear system is excited with one of the resonant frequencies, the output contains only that frequency with other frequencies being zero. As a result, the summation sign in the response function defined in Eq. (5.12) for a sinusoidal input signal with a resonant frequency can be dropped out and Eq. (5.12) is reduced to one component as

$$h_0^*(x^*,t^*) = \left[E_{np}^* \sin(\omega\, t^* + \delta)\right]\sin(n\pi x^*) \qquad (n\pi = \omega) \tag{5.14}$$

Figure 5.3 shows that when $\omega = 1.0\pi$ the presence of a leak decreases the amplitude of the dominant component $n = 1$ significantly. As a result, the amplitude of the whole transient is decreased by the presence of the leak as shown in Figure 5.2, as is the case where the oscillation is exited with any multiple of a resonant frequency. On the contrary, for the input signal whose frequency is not resonant, the presence of the leak has no obvious influence on the amplitude of the components as can be clearly seen in Figure 5.3(b). In addition, when compared to the cases of resonance, there is no obvious dominant component in the response signal if the dimensionless frequency of the input signal is not resonant. As a result, the response function for a sinusoidal input signal with a non-resonant frequency includes all the components.

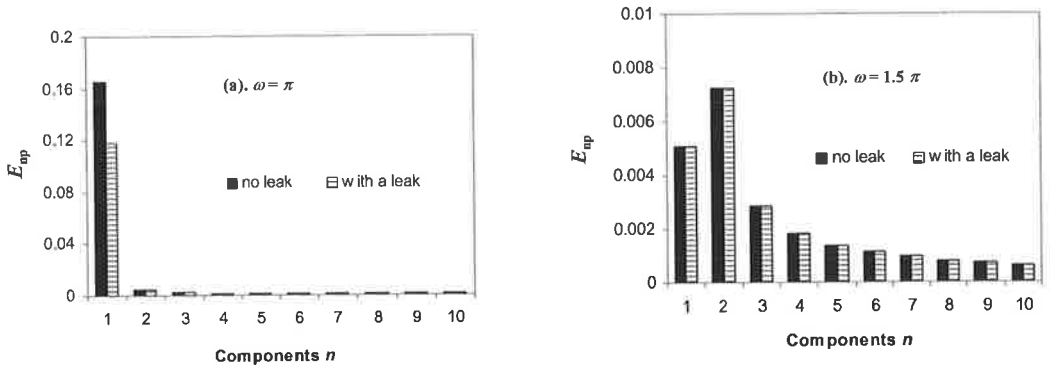

Figure 5.3 Magnitude of the Fourier components

A sensitivity analysis illustrates the above phenomenon. Taking derivatives of the amplitude of the oscillation E_{np}^{*} defined in Eq. (5.13) with respect to leak parameter R_{nL} gives

$$\frac{\partial E_{np}^{*}}{\partial R_{nL}} = -\frac{(A_{np}\dfrac{\partial A_{np}}{\partial R_{nL}} + B_{np}\dfrac{\partial B_{np}}{\partial R_{nL}})}{\sqrt{A_{np}^{2} + (B_{np} + C_{np})^{2}}} \tag{5.15}$$

where

$$\frac{\partial A_{np}}{\partial R_{nL}} = \frac{-8\{[a[(n\pi)^2 - \omega^2] - 2b(R + R_{nL})\omega\}(R + R_{nL})\omega^2}{\{[(n\pi)^2 - \omega^2]^2 + [2(R + R_{nL})\omega]^2\}^2} \frac{-2b\omega}{[(n\pi)^2 - \omega^2]^2 + [2(R + R_{nL})\omega]^2} \tag{5.16}$$

$$\frac{\partial B_{np}}{\partial R_{nL}} = \frac{-8\{[b[(n\pi)^2 - \omega^2] + 2a(R + R_{nL})\omega\}(R + R_{nL})\omega^2}{\{[(n\pi)^2 - \omega^2]^2 + [2(R + R_{nL})\omega]^2\}^2} \frac{2a\omega}{[(n\pi)^2 - \omega^2]^2 + [2(R + R_{nL})\omega]^2} \tag{5.17}$$

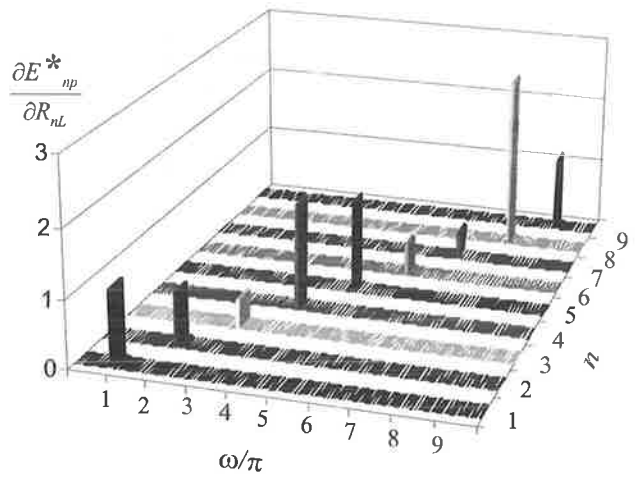

Figure 5.4 Sensitivity of the Fourier components on the leak

Eq. (5.15) is plotted in Figure 5.4 against different values of ω and $n\pi$ (n = 1, 2, 3...). In Figure 5.5, the values of R and R_{nL} are taken from the example in the previous section. Figure 5.4 shows that amplitude of the steady oscillation at $\omega = n\pi$ (n = 1, 2, 3...) is most sensitive to a leak. Substituting $\omega = n\pi$ into Eq. (5.13) gives the resonance amplitude as

$$E_{np} = \frac{E^*}{R + R_{nL}} \sqrt{1 - \left[\frac{2R_{nL}\cos(n\pi) + n\pi F_L x_L^* \sin(n\pi x_L^*)}{n\pi} \right]^2} \approx \frac{E^*}{R + R_{nL}} \qquad (5.18)$$

Since the value of leak parameter R_{nL} is positive, Eq. (5.18) indicates that the presence of a leak in a pipeline decreases the amplitude of the component whose frequency is that of the input signal. Substituting Eq. (5.18) into Eq. (5.14) gives

$$h^*(x^*, t^*) = E_p \sin(\omega\, t^* + \delta) \qquad (n\pi = \omega) \qquad (5.19)$$

where $E_p = \frac{E^*}{R + R_{nL}} \sin(n\pi x^*) =$ amplitude of the steady oscillation. Therefore, the transient in a pipeline under a resonant sinusoidal input signal is a sinusoidal function, and the amplitude of the transient is a function of the amplitude of the input signal E^*, friction damping parameter of the pipeline R, leak damping parameter R_{nL} and measurement location x^*.

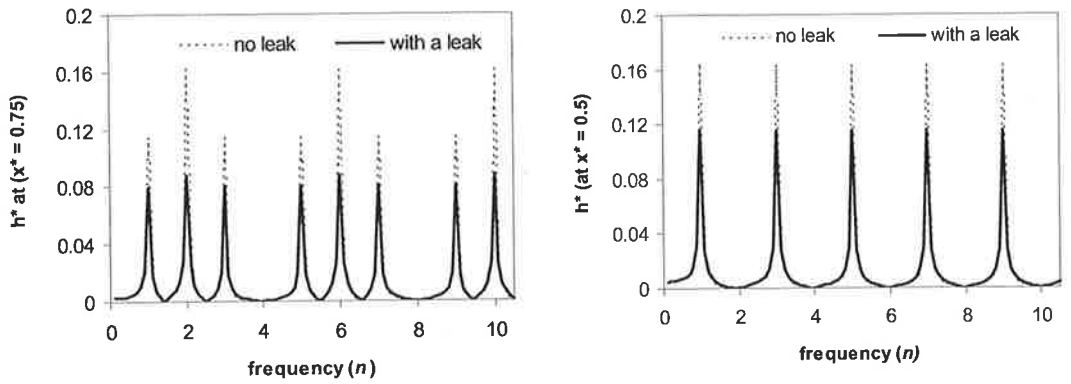

Figure 5.5 Transient response (measured at $x^* = 0.75$ and $x^* = 0.5$) of a leak under different input frequencies

For the example in Section 5.3, the transient responses (from Eq. 5.12) under different input frequencies ($0.0 \sim 10\pi$) are plotted in Figure 5.5. As discussed in the above analysis, Figure 5.5 shows that under a sinusoidal perturbation, the presence of a leak reduces the amplitude of the transient if the input signal is of the resonant frequency of the pipeline. For an input signal that has a non-resonant frequency, the presence of a leak has little influence on the transient. This result is different from those of Mpesha et al (2001) and Mpesha et al. (2002), where presence of a leak caused increased amplitude of the transient at non-resonant input signals, which resulted in additional peaks compared to the no-leak case.

Previous studies (Vítkovský 2001) have found that the transient pressure heads measured from a pipeline cannot be used as boundary conditions in leak detection analysis because under such a boundary condition, the transients measured from the pipeline are very insensitive to the leak. The sensitivity analysis presented in this section gives the reason for those observed phenomena. The above analysis shows that transients from a pipe under a non-resonant boundary condition are almost independent of a leak. This conclusion, on the other hand, shows the potential to detect a leak by applying the resonant frequencies (or by examining the resonant frequencies in a general transient) from a pipeline. Because any pipe section in a pipe network can actually be treated as a single pipe under a variable boundary condition, the results presented in this section may be applicable for transient analysis in pipe networks.

5.5 Leak detection using resonant fluid transients

A leak has a significant influence on transient amplitude when the frequency of the input signal is a multiple of the pipe's natural frequency. The amplitude of the resonant steady oscillation is a function of magnitude of the input signal E^*, friction damping paramcter of the pipeline R, leak damping parameter R_{nL} and measurement location x^*. Since the values of E^*, R, and x^* are known or can be calculated from the flow conditions in the pipeline, the value of a leak damping parameter R_{nL} can be obtained from the amplitude of a steady oscillation defined in Eq. (5.19). The desired parameters are leak location, x_L^*, and size, C_dA_L. Therefore, the leak can be detected and quantified using two values of leak damping parameter, R_{nL}, which can be obtained from two amplitudes of steady oscillations. The technique to detect and quantify a leak based on leak-induced damping coefficients has been discussed in Chapter 4. In this chapter, the focus is on how to obtain the leak-induced damping coefficients (R_{nL}) from the amplitude of the steady oscillation. The following example is used to illustrate the detailed procedures.

For the pipeline shown in Figure 5.1, two frequencies of perturbation signals $\omega=1.0\pi$ and $\omega = 2.0\pi$ are used. The other flow conditions are

Upstream reservoir water level: $H_1 = 25\text{m}$,

Downstream reservoir water level: $H_2 = 15 + 0.25\sin(\omega t)\text{m}$

Leak size: $C_dA_L/A = 0.1\%$ at $x_L^* = 0.25$

Measurement location: $x^* = 0.75$

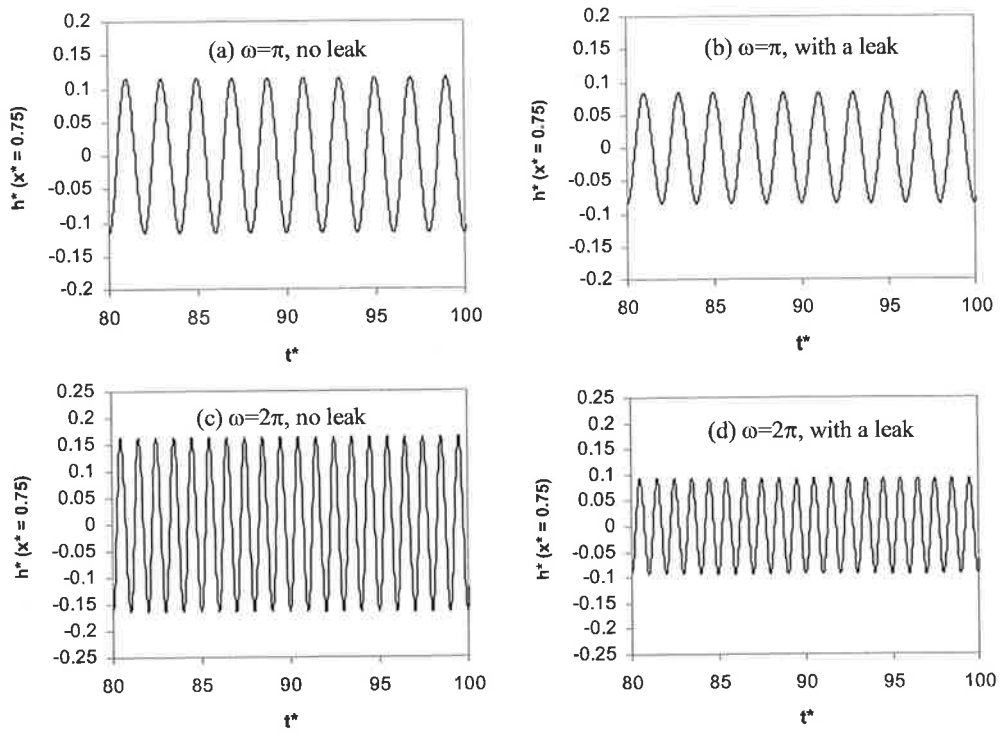

Figure 5.6 Steady transient oscillation calculated from the MOC

The transients calculated using the MOC are plotted in Figure 5.6. A state of steady oscillation forms for all the cases when $t^* > 80$, so only transients in the period of $80 < t^* < 100$ are shown in Figure 5.6 and are used for the leak detection analysis. For both frequencies, the decrease of the amplitudes of the steady oscillation caused by the leak is obvious. For $\omega = 1.0\pi$, the amplitude of the steady oscillation is $E_p = 0.1167$ for no leak case and $E_p = 0.08396$ for the case of with a leak (E_p was defined in Eq. 5.19). Substituting these values into Eq. (5.19) and considering $E^* = 0.01$, $n = 1$ and $x^* = 0.75$ gives $R = 0.0606$ and $R + R_{1L} = 0.0842$. For $\omega = 2.0\pi$, the amplitude of the steady oscillation is $E_p = 0.1651$ for the no-leak case and $E_p = 0.0925$ for the case of with a leak. Substituting these values into Eq. (5.19) and considering $E^* = 0.01$, $n = 2$ and $x^* = 0.75$ gives $R = 0.0606$ and $R + R_{2L} = 0.1081$. For both frequencies, the friction damping parameter calculated from Eq. (5.19) is same as that calculated based on the steady state flow condition, thus verifying the accuracy of the analysis in the previous section. The leak-induced damping coefficients for both frequencies are calculated by subtracting the friction damping from total damping coefficients as $R_{1L} = 0.0236$ and $R_{1L} = 0.0475$. Applying the ratio of $R_{2L}/R_{1L} = 2.01$ to Figure 4.2 and Eq. 4.4 in Chapter 4 gives the leak

location of $x_L^* = 0.25$ (or $x_L^* = 0.75$), and size of the leak of $C_dA_L/A = 0.00099$, which are almost same as the real leak location $x_L^* = 0.25$ and size of $C_dA_L/A = 0.001$.

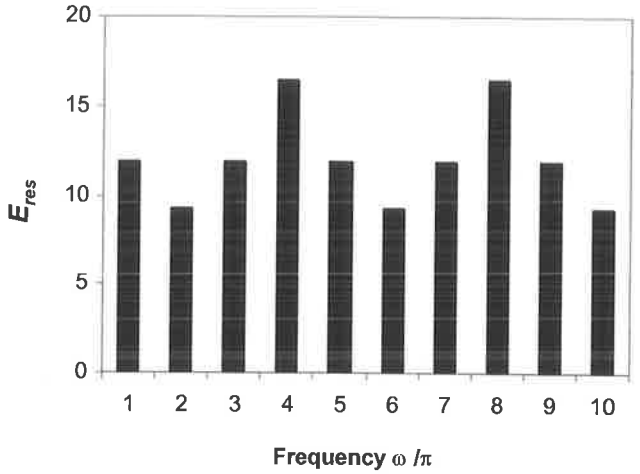

Figure 5.7 Response function of the pipeline with a leak at $x_L^* = 0.25$

In the above example, two amplitudes of steady oscillation, corresponding to two input resonant frequencies, are used to locate and quantify the leak. Notice that the value of the leak-induced damping coefficient $R_{nL} = F_L \sin^2(n\pi x_L^*)$ depends on frequency n and leak location x_L^*. Whenever the value of nx_L^* is equal (or close) to an integer ($N_m = 1, 2, 3,...$), the value of R_{nL} becomes (or is close to) zero. Then based on Eq. (5.19) the amplitude of the steady oscillation will become (or is close to) the maximum value. Therefore, if there is a response map about the amplitude of the steady oscillation corresponding to a series of input resonant frequencies, the leak location can be obtained from the maximum amplitude as $x_L^* = N_m / n$. According to Eq. (5.19), a pipeline response function, which is independent of the measurement position and input signal, can be defined as

$$E_{res} = \frac{E_p}{E^* \sin(n\pi x^*)} = \frac{1}{R + R_{nL}} \tag{5.20}$$

The response function E_{res} for the pipeline as shown in Figure 5.1, where there is a leak at $x_L^* = 0.25$, is given in Figure 5.7. The response function reaches the first ($N_m = 1$) maximum at $n = 4$, which means nx_L^* is equal to (or close to) N_m. Therefore, the leak location can be calculated as $x_L^* = N_m/n = 0.25$. Similarly, the response function reaches the second ($N_m = 2$) maximum value at $n = 8$, which gives the leak location of $x_L^* = N_m/n = 2/8 = 0.25$. In this case, the leak location is exactly calculated from the response function. For some leaks, to obtain the exact location needs a response function of a

higher frequency. However, the leak location still can be approximately calculated from the response function of the lower frequencies. For example, a response function, Eq. (5.20), for a pipeline with a leak at $x_L^* = 0.35$ and friction damping parameter of $R = 0.0606$ is given Figure 5.8. The leak locations calculated from the corresponding maximum responses (N_m) and the frequencies (n) are given in Table 5.1. The seventh maximum response and the frequency $n = 20$ gives the exact leak location $x_L^* = 0.35$ (= 7/20). However, the leak location calculated from the lower frequencies are also close to the real leak location. The average leak location calculated from the frequencies ($n < 20$) is $x_L^* = 0.346$ which is 4 meters away from the real leak location ($x_L^* = 0.350$) in a 1000m long pipeline.

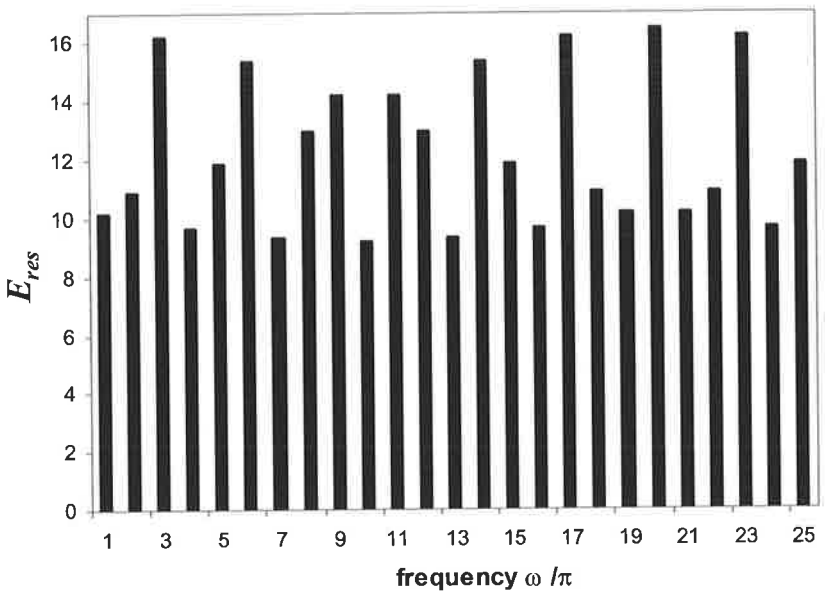

Figure 5.8 Response function of the pipeline with a leak at $x_L^* = 0.35$

Table 5.1 Leak locations calculated from the response function ($x_L^* = 0.35$)

N_m	1	2	3	4	5	6	7	8
n	3	6	9	11	14	17	20	23
x_L^*	0.333	0.333	0.333	0.364	0.357	0.353	0.350	0.348

The first step to obtain the response map for a pipeline is to generate a resonant steady oscillation by injecting a sinusoidal resonant perturbation signal at end of the pipeline. The amplitude of the steady oscillation (E_p) can be measured at any location (x^*) along

the pipeline, and the response function (E_{res}) for this frequency can be calculated from Eq. (5.20). Repeating the above process using different sinusoidal resonant frequencies (ω/π= 1, 2, 3...), the corresponding response functions can be obtained.

Alternatively, a wide-range resonant perturbation signal, which is composed of a series of sinusoidal resonant frequencies, can be used instead of applying different sinusoidal frequencies separately. Because of the linear characteristics of the problem, the wide-range signal can be decomposed into a series sinusoidal signal and be analysed separately. This technique is illustrated in the following example.

For the pipeline as shown in Figure 5.1, the water level at the downstream reservoir varies in a periodic square wave form as shown in Figure 5.9(a) while the water level in the upstream reservoir is constant at H_1 = 25m. The leak is located 375m downstream from the upstream reservoir (x_L^* = 0.375) with the dimensionless leak size of C_dA_L/A = 0.001. The transients at two measurement positions x^* = 0.5 and x^* = 0.75 calculated using the MOC are plotted in Figure 5.10 for both cases of with and without a leak. The transients increase at the beginning and reach a steady oscillation when $t^* > 60$ for the case of without a leak and $t^* > 40$ for the case of with a leak. The presence of the leak also decreases the magnitude of the transients and changes the shape of the transients. The shapes of the transients measured at different locations are different for both cases of with and without a leak. The transients in the period of $70 < t^* < 90$, which are steady oscillations and are used for leak analysis, are given in Figure 5.11.

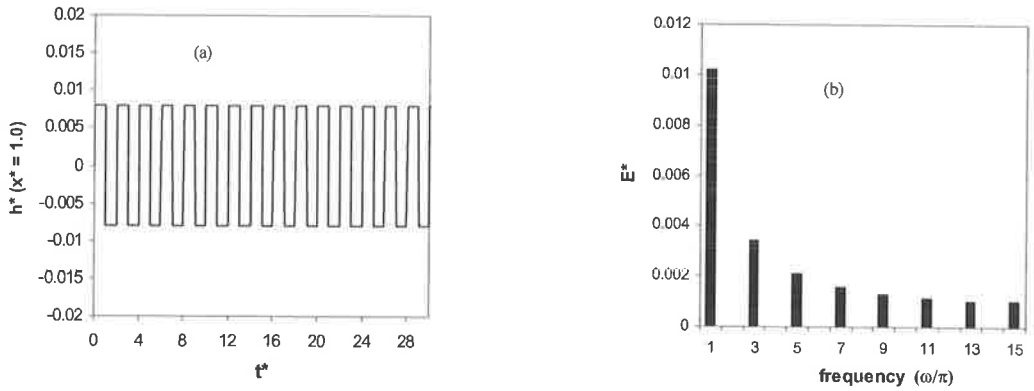

Figure 5.9 A periodic square-wave input signal

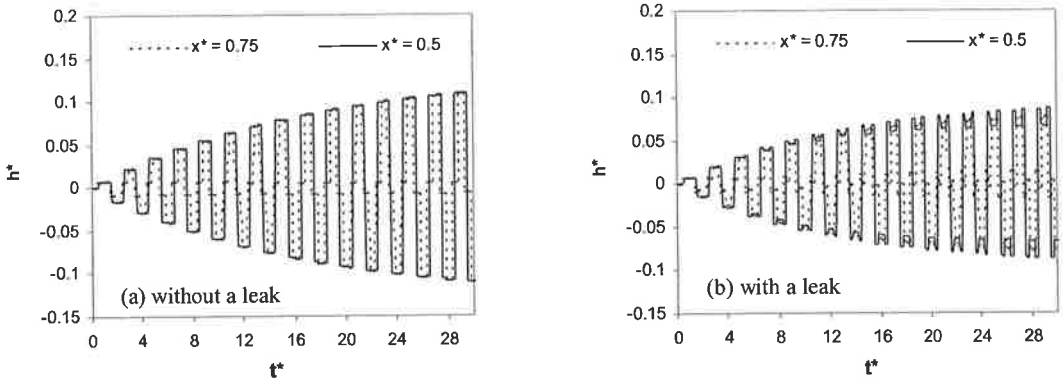

Figure 5.10 Transients obtained from the MOC ($0 < t^* < 30$)

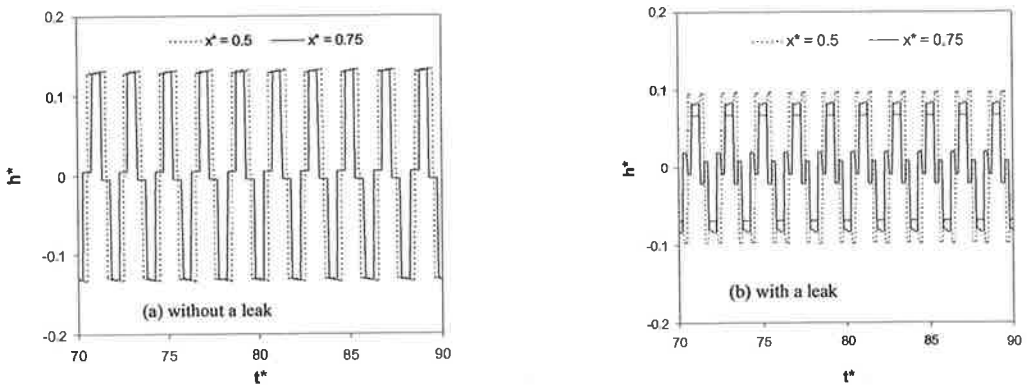

Figure 5.11 Steady transient oscillation obtained from the MOC ($70 < t^* < 90$)

The square wave can be expressed as a series of sinusoidal components

$$f(t^*) = \sum_{n=1}^{\infty} E_n^* \sin(\omega_n t^*) \tag{5.21}$$

The amplitude for each of these sinusoidal components is given in Figure 5.9(b). The amplitudes of the even number of the frequencies (n = 2, 4, 6,...) are zero. The amplitudes of the different frequencies for the transients measured at x^* = 0.5, are given in Figure 5.12(a1) and Figure 5.12(b1). Considering the measurement position x^* = 0.5 and the amplitude of each of the input sinusoidal signal in Figure (5.9b), the response function E_{res} for each frequency can be calculated, and is plotted in Figure 5.12(a2) and

Figure 5.12(b2) for both cases of without and with a leak. When there is no leak, the response functions for all frequencies are same as shown in Figure 5.12(a2). The values of the response function calculated based on the MOC measurement for all frequencies are almost identical the analytical value of $E_{res} = 1/R = 16.50$.

When there is a leak at $x_L^* = 0.375$, the response functions for different frequencies are significantly different as shown in Figure 5.12(b2), indicating the presence of leaks. The leak location can be obtained in two different ways. Noticing the first ($N_m = 1$) and the second ($N_m = 1$) maximum response function occur at frequencies of $n = 3$ and $n = 5$, the corresponding leak locations are $x_L^* = 1/3 = 0.333$ and $x_L^* = 2/5 = 0.40$ which are both reasonable approximations of the real leak location of $x_L^* = 0.375$. Due to the absence of the even frequencies, the frequency $n = 8$, which corresponds to the third ($N_m = 3$) maximum response function and gives exact leak location $x_L^* = 3/8 = 0.375$ is not applicable in this example. By applying this method, the leak location can be estimated from the map of response function without knowing the friction damping parameter R.

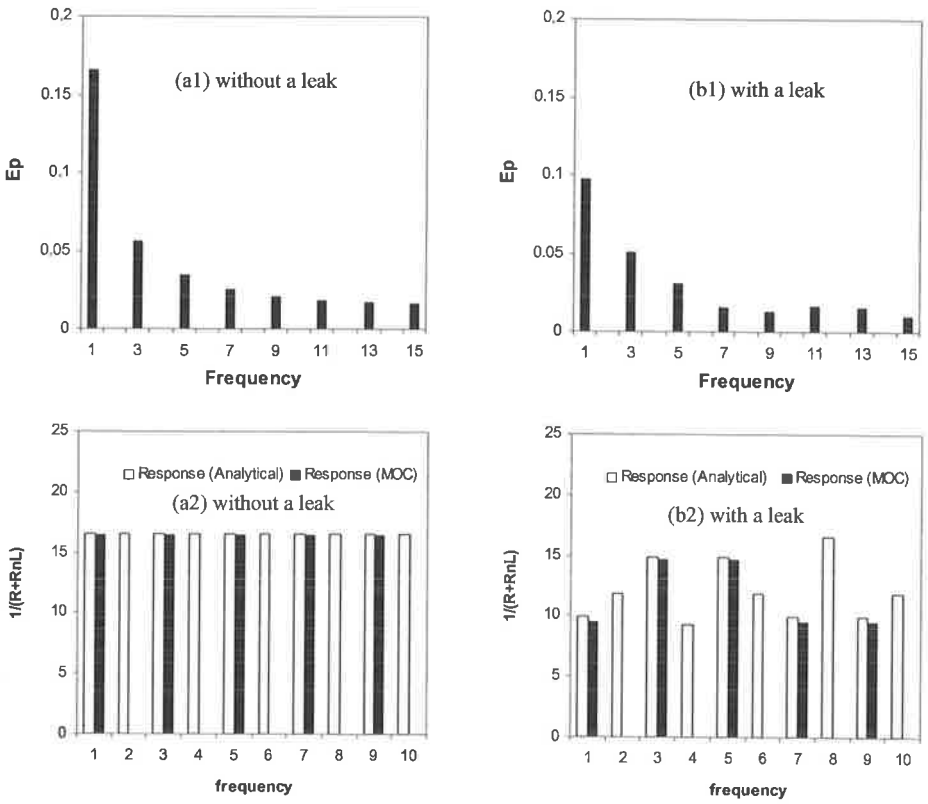

Figure 5.12 Response function of the pipeline

Another method is to use the quantity values of the response functions. Based on Figure 5.12(b2), the response functions for frequencies of $n = 1$ and $n = 3$ are $(E_{res})_1 = 9.50$ and $(E_{res})_3 = 14.60$. Substituting these values to Eq. (5.20) gives the leak-induced damping coefficients of $R_{1L} = 0.0447$ and $R_{3L} = 0.0079$, and ratio of these coefficients is $R_{3L}/R_{1L} = 0.177$. Applying this value to Figure 4.2 in Chapter 4 gives the leak location of $x_L^* = 0.376$ (or $x_L^* = 0.624$), which is very close to the real leak location $x_L^* = 0.375$. The magnitude of the leak can only by estimated from the quantity of the leak-induced damping coefficients. Applying $x_L^* = 0.376$ and $R_{1L} = 0.0447$ to Eq. (4.4) gives the leak size of $C_dA_L/A = 0.00107$, which is also close to the real leak size of $C_dA_L/A = 0.001$.

5.6 Generation of transients--Coded transients

In the previous section, the transients induced by a periodic boundary condition at an end of a pipeline were studied. It has been found that a transient induced by a periodic perturbation whose frequency is a resonant frequency of the pipeline can be used for leak detection. Two techniques are developed to detect, locate and quantify a leak in the pipeline by examining the leak-induced damping on transient amplitude, and leak-induced frequency response. These techniques have been successfully applied in a numerical example, in which a square-wave periodic boundary function for head (H) was assumed and the transients were generated by the method of characteristics (MOC). In this section, the practicability to generate a periodic boundary condition for the purpose of leak detection is discussed.

A transient can be initiated whenever a steady state in a pipeline is disturbed. Such a disturbance may be caused by changes, planned or accidental, in the setting of the control of a man-made system and by changes in the inflow or outflow in a natural system. Theoretically, these changes can be classified as following three types:

1. A change of head at any point along the pipeline, for example a sudden water level increase at a reservoir;
2. A change of flow rate at any pint along the pipeline, for example, closing a downstream valve of a pipeline changes the flow rate at valve to zero; or
3. A change of the relationship between flow and pressure. A typical example is shifting the opening of a valve.

In the previous sections, the transients have been generated by a periodic head (H) function at an end of a pipeline, and based on this boundary condition, the analytical solution was developed. In reality, it is easier to generate a transient by controlling flow rate (Q) or by controlling the opening of a valve than by controlling head (H). For example, a transient can be generated by controlling the movement of a cylinder or opening of a valve at the end of a pipeline. For a pipeline with a variable flow boundary condition at the downstream end and a constant reservoir at the upstream end as shown in Figure 5.13, the analytical solution and leak detection techniques presented in the previous section cannot be applied directly. However, the transient in such a pipeline can be generated by an equivalent pipeline as shown in Figure 5.14. Then the problem of variable flow boundary condition is transferred to a problem of a variable head boundary condition, which has been studied in the previous sections. The amplitude of the equivalent head perturbation is calculated by $E_h = E_q a/g$. The transients calculated using the MOC based on the pipeline in Figure 5.13 (measured at $x^* = 1.0$) and the equivalent pipeline in Figure 5.14 (measured at $\hat{x} = 0.5$) are presented in Figure 5.15 for cases of with and without a leak. Two frequencies $\omega = 0.5\pi$ and $\omega = 1.5\pi$ are considered. The other flow conditions in the pipeline as shown in Figure 5.13 are: $H_1 = 25\text{m}, f = 0.015, Q_0 = 0.05\text{m}^3/\text{s}, E_q = 0.0001\text{m}^3/\text{s}, C_d A_l/A = 0.001, x_L^* = 0.75, \omega^* = 0.5\pi$ and $\omega^* = 1.5\pi$. Then the flow conditions in the equivalent pipeline as shown in Figure 5.14 are $H_1 = 25\text{m}, f = 0.015, Q_0 = 0.05\text{m}^3/\text{s}, E_h = 0.3248\text{m}, C_d A_l/A = 0.001, \hat{x}_L^* = 0.375$, and $(\hat{x}_L^*)_{imaginary} = 0.625, \omega^* = 1.0\pi$ and $\omega^* = 3.0\pi$. The transients generated from two pipelines are almost identical for both cases of with and without a leak under two different frequencies.

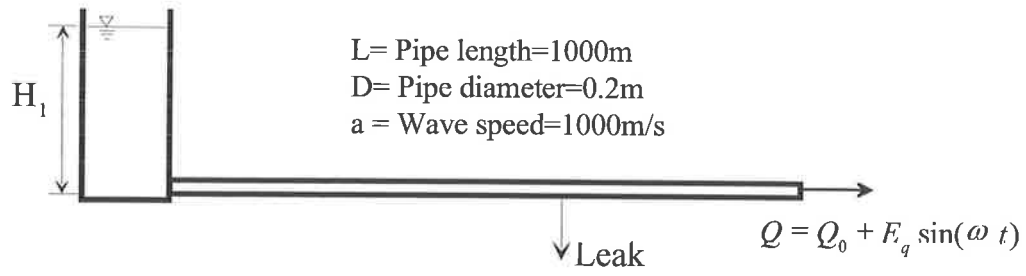

Figure 5.13 A single pipeline with a variable flow boundary condition

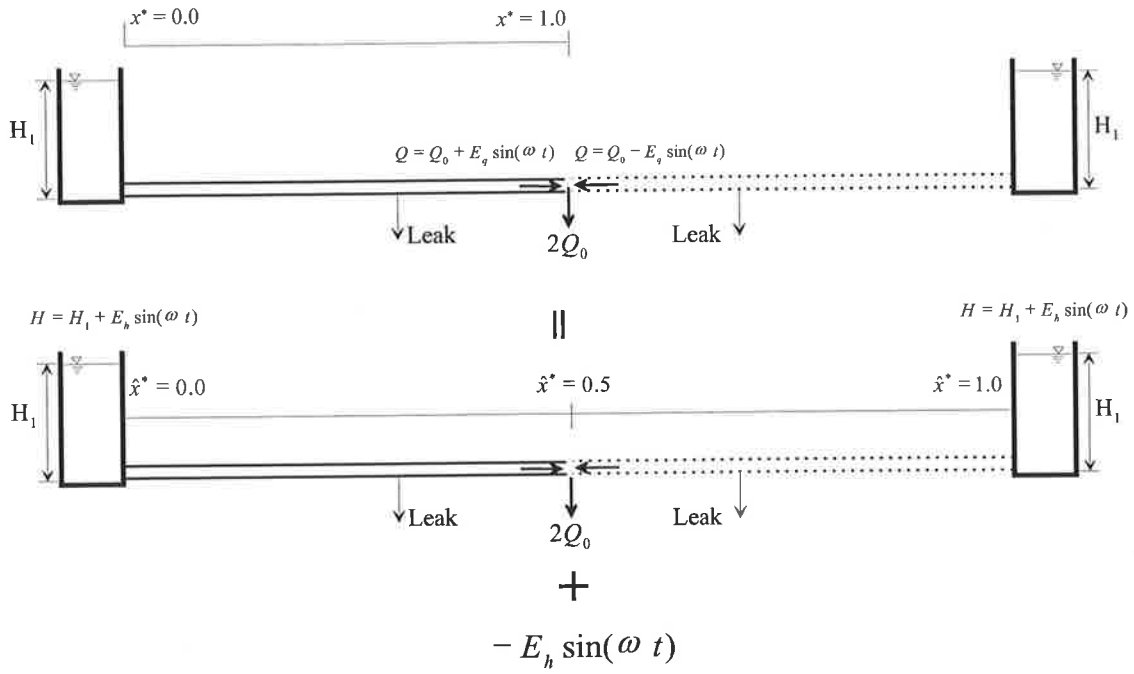

Figure 5.14 A single pipeline with a flow boundary condition and an imaginary pipeline

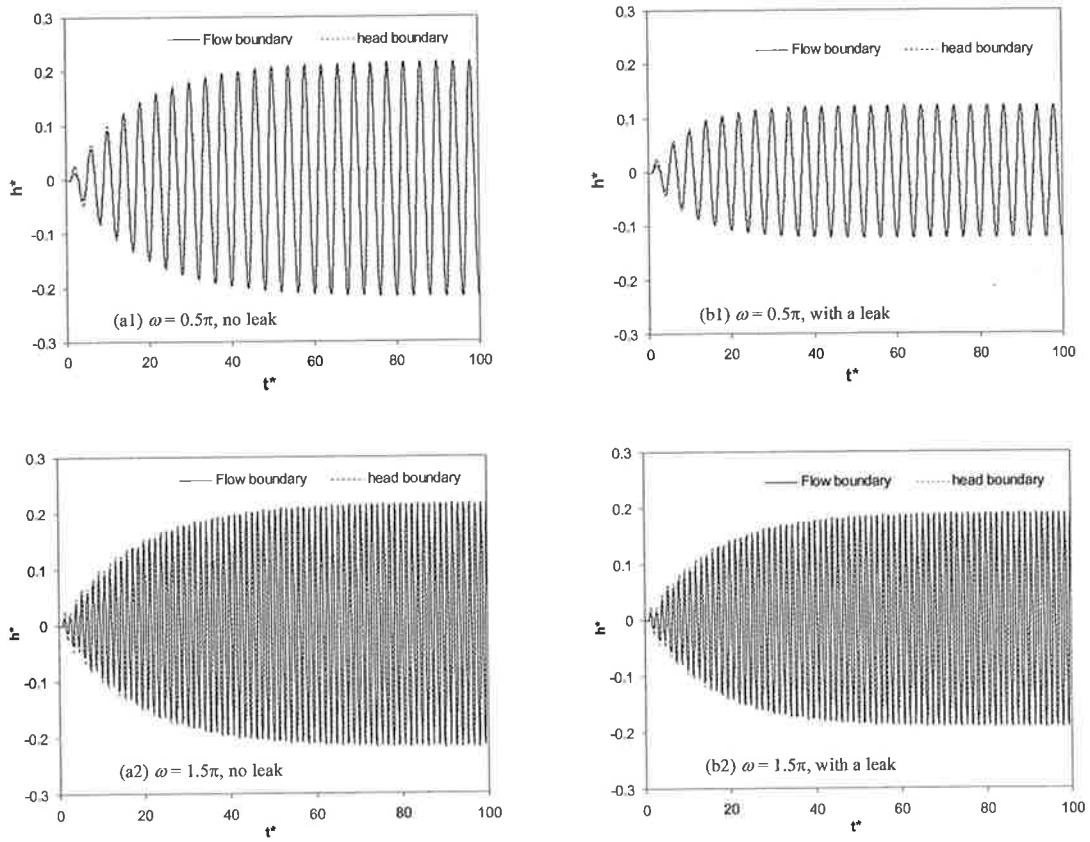

Figure 5.15 Transients calculated using the MOC based on the pipeline in Figure 5.13 (measurement position $x^* = 1.0$) and the equivalent pipeline in Figure 5.14 (measurement position $(\hat{x} = 0.5)$

The leak location and the size can be calculated from the amplitudes of the steady oscillations, firstly based on the equivalent pipeline, and then transferred to the original pipeline. When there is no leak in the pipeline, for both frequencies $\omega^* = 1.0\pi$ (case a1 in Figure 5.15) and $\omega^* = 3.0\pi$ (case a2), the amplitude of the oscillation h^* is measured as E_p = 0.217 (case a1 or a2 in Figure 5.15). Given the measurement position $\hat{x} = 0.5$, and dimensionless amplitude of the input signal $E^* = E_h/H_1 = 0.0130$, the friction damping coefficient is calculated as $R = 0.0599$, which is identical to the theoretical value based on the steady-state condition ($R = Q_0fL/2DA$). When a leak is present, the amplitude of h^* is measured as $E_p = 0.122$ for $\omega^* = 1.0\pi$ (case b1 in Figure 5.15) and $E_p = 0.191$ for $\omega^* = 3.0\pi$ (case b2 in Figure 5.15). Applying these values into Eq. (5.19) gives $R_{1L} = 0.0466$, and $R_{3L} = 0.00806$. Applying the ratio of $R_{3L}/R_{1L} = 0.173$ to Figure 4.2 gives a leak location of $\hat{x}_L^* = 0.375$ (or $\hat{x}_L^* = 0.625$). Transferring back to the pipeline as shown in Figure 5.13 gives unique leak location of $x^* = 0.75$ with another leak location in the imaginary pipeline section. The detected leak location based on the MOC "measurement" is same as the actual leak location $x^* = 0.75$. Applying $\hat{x}_L^* = 0.375$ (not $x^* = 0.75$) and $H_{L0} = 17.5$m in Eq. (4.4) gives the size of the leak as $C_dA_L/A = 0.00101$, which is very close to the real leak size of $C_dA_L/A = 0.001$.

Similarly if a series of frequencies are applied at the end of the pipeline, a response map can be obtained. Applying this response map to the equivalent pipeline gives the transferred leak locations, and the real leak location on the original pipeline can be obtained from the transferred values.

The feasibility of applying a controllable resonant transient, which may be generated using an oscillating cylinder or a membrane--a coded transient, is currently under laboratory investigation at the University of Adelaide (Lee et al. 2002).

5.7 Summary

In this chapter, transients in a pipeline under variable boundary conditions have been studied analytically, and an analytical solution expressed as a Fourier series has been

developed under a sinusoidal boundary condition. By comparison to the numerical solution based on the method of characteristics (MOC) in which the non-linear effects are included, the analytical solution shows a high degree of accuracy for both cases of with and without a leak in a pipeline.

The analytical solution shows that a steady oscillation forms in a pipeline under a continuously varying boundary perturbation, and the formation time and the amplitude of the steady oscillation depends on the pipe friction, the leaks in the pipeline, and input signals. The analytical solution also shows that presence of a leak in a pipeline only influences the amplitude of a resonant transient, and almost has no influence on the amplitude of a non-resonant transient. An analytical relationship between the leak and the resonant amplitude has been obtained. Because the influence of the leak on the resonant amplitude is frequency dependent, and depends on the leak location and size, techniques that are able to detect the presence, location and magnitude, have been developed by examining the magnitudes of resonant amplitudes of different frequencies. These techniques have been applied successfully in several numerical examples.

The insensitivity of a non-resonant transient to a leak in a pipeline indicates that a measured transient cannot be used as a boundary condition in a transient model for leak detection. This conclusion, from another point of view, shows the potential of detecting a leak by applying resonant frequencies (or by examining the resonant frequencies in a general transient) from a pipeline. Because any pipe section in a pipe network can actually be treated as a single pipe under a variable boundary condition, the results presented in this section may be applicable for transient analysis in pipe networks.

Finally, although the analytical solution has been developed based on reservoir-pipeline-reservoir systems, leak detection techniques developed in this chapter can be applied in reservoir-pipeline-valve systems, in which resonant transients are more easily generated.

Chapter 6
Transients in a Pipeline with a Blockage and Blockage Detection

6.1 Introduction

Blockage development is a common problem in pipeline and pipe network systems for chemical, water and energy industries. Blockages not only decrease the operational efficiency of the pipe systems, but also can cause serious safety and environmental consequences if is not identified and removed in a timely manner. Some methods have been proposed to detect and locate pipeline blockages. A ROV (remotely operated vehicle) based inspection method was developed by Rogers (1995) by measuring the blockage-induced strain change of the pipe wall. Since this method cannot be applied continuously, the response for a blockage occurrence is slow. Wu (1994) proposed an acoustic method based on the properties of eigenfrequency shifts of the measured acoustical signals from a pipeline with blockage. Due to the quick decay of the acoustic signals, the measurement interval needs to be less than one hundred meters. In petroleum engineering, blockage development is related to the properties of the fluid in the pipes. Therefore, analyzing the fluid properties and ingredients can indicate the potential development of the blockage (Hunt 1996). Unfortunately, this method cannot provide the location of the blockage. By analyzing the blockage (or leakage)-induced head losses, Jiang et al. (1996) developed a blockage and leakage detection method for a water network of a district heating system. Depending on the measurement locations, only significant leakages and blockages can be detected and located based on his numerical experiments. In the methods developed by Scott and Satterwhite (1998) and Scott and Yi (1999), a blockage was detected and characterized by the mass and momentum (friction loss) balance analysis. These methods could not detect the location of a blockage although the transients were affected by the location of the blockage during

experimental tests. Inspired by the successes based on the leak detection technique using the fluid transients developed in Chapter 3, Chapter 4 and Chapter 5, the feasibility of using fluid transients to detect pipeline blockage is investigated in this chapter.

In this chapter, the governing equations for unsteady flow in a pipeline including a blockage are developed. An analytical solution considering the constant boundary conditions is developed in section 6.3. The analytical solution is compared with numerical solution using the method of characteristics in section 6.4. A new blockage detection method based on the analytical solution is developed in section 6.5, and the accuracy of the proposed blockage detection technique is analyzed by a sensitivity analysis. The proposed method is verified by numerical and experimental methods in section 6.6 and section 6.7.

6.2. Governing Equations

By approaching a pipeline blockage as an orifice, conservation of momentum with respect to the x-direction in a control volume is shown in Figure 6.1 (Wylie and Streeter 1993)

$$\frac{\partial}{\partial t}(\rho AV)\Delta x+\frac{\partial}{\partial x}(\rho AV^2)\Delta x=\sum F_x \tag{6.1}$$

where x = distance along the pipeline, t = time, ρ = fluid density, A = cross-sectional area of the pipe, and V = velocity of flow.

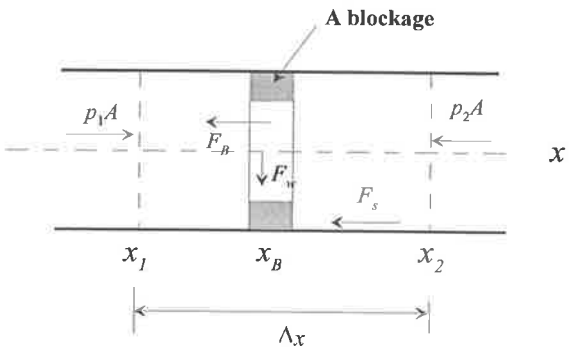

Figure 6.1 Free-body diagram for a pipe section with a blockage

The forces acting on the control volume are:

1. Pressure forces at section 1 and section 2: $F_{p1} = p_1 A$, and $F_{p2} = p_2 A$
2. Shear force: $F_S = \tau_0 \pi D(x_2 - x_1)$
3. Blockage-induced force: $F_B = \Delta P_B A$.

where p_1, p_2 = pressure, g = gravitational acceleration, τ_0 = shear stress, D = pipe diameter, and ΔP_B = pressure difference across the blockage. Considering the downstream flow direction as positive, the total x direction force components acting on the control volume can be expressed as

$$\sum F = p_1 A - p_2 A - \tau_0 \pi D(x_2 - x_1) - \Delta P_B A \tag{6.2}$$

Substituting Eq. (6.2) into Eq. (6.1), then dividing by Δx and letting Δx approach zero gives

$$\frac{\partial}{\partial t}(\rho A V) + \frac{\partial}{\partial x}(\rho A V^2) + A\frac{\partial p}{\partial x} + \tau_0 \pi D - \Delta P_B A \delta(x - x_B) = 0 \tag{6.3}$$

The Dirac delta function is defined as

$$\delta(x - x_B) = \begin{cases} \infty & \text{if} \quad x = x_B \\ 0 & \text{otherwise} \end{cases} \tag{6.4}$$

so that $$\lim_{\varepsilon \to 0} \int_{x_B - \varepsilon}^{x_B + \varepsilon} \delta(x - x_B)\, dx = 1 \tag{6.5}$$

where ε = a small distance on the either side of the blockage. Applying the Darcy-Weisbach friction formula for the wall shear stress ($\tau_0 = \rho f V^2/8$) to Eq. (6.3) gives

$$\frac{\partial}{\partial t}(\rho A V) + \frac{\partial}{\partial x}(\rho A V^2) + A\frac{\partial p}{\partial x} + \frac{\rho A f V^2}{2D} - \Delta P_B A \delta(x - x_B) = 0 \tag{6.6}$$

where f = Darcy-Weisbach friction factor and D = pipe diameter. In Eq. (6.6) it is assumed that the unsteady shear stress can be approximated by the steady state shear stress, and the pipe friction during a transient event is described by the steady state Darcy-Weisbach friction factor--a common assumption. Considering the compressibility

of the water and the elasticity of the pipe wall with some simplifications (Wylie and Streeter 1993), Eq. (6.2) may be expressed in the more usual water-hammer-equation form,

$$\frac{\partial H}{\partial x}+\frac{1}{gA}\frac{\partial Q}{\partial t}+\frac{Q}{gA^2}\frac{\partial Q}{\partial x}+\frac{fQ^2}{2DgA^2}-\Delta H_B\delta(x-x_B)=0 \tag{6.7}$$

in which H = piezometric head, and Q = the flow rate in the pipeline. Similarly, conservation of mass in a pipe section including a blockage is (Wylie and Streeter 1993):

$$\frac{\partial H}{\partial t}+\frac{Q}{A}\frac{\partial H}{\partial x}+\frac{a^2}{gA}\frac{\partial Q}{\partial x}=0 \tag{6.8}$$

where a = wave speed in the fluid. Blockage head loss may be expressed as

$$\Delta H_B=\frac{K_B Q^2}{2gA^2} \tag{6.9}$$

where K_B is the head loss coefficient of the blockage, which can be used as the indicator of the blockage magnitude. If the flow rate is known, the blocked pipe cross-sectional area or diameter of the blockage can be estimated from K_B (Miller, 1983). In Figure 6.1, the length of the blockage is considered as negligible compared to the whole length of the pipeline. Based on such an assumption, the blockage can be approached by a delta function. Although, a pipeline blockage plus the separation and recirculation zone has a finite length, the loss is assumed to be at a point just as it is in standard hydraulic analysis. If the length of a blockage is not negligible compared to the length of the pipeline, then the delta-function approach is not valid, and such a blockage can be considered as a pipe section with a suitable friction factor and cross-sectional area.

The following dimensionless quantities are used to non-dimensionalize Eqs. (6.7), (6.8) and (6.9):

$$H^*=\frac{H}{H_S},\ t^*=\frac{t}{L/a},\ x^*=\frac{x}{L},\ Q^*=\frac{Q}{Q_0},\ \text{and}\ \delta(x^*-x_B^*)=\delta(x-x_B)L \tag{6.10}$$

in which $H_s=\frac{aV_0}{g}$ is the Joukowsky pressure head rise (that results from an instantaneous reduction of velocity V_0 to zero), L = the pipe length, and Q_0 = a reference

flow rate. Substituting Eq. (6.9) into Eq. (6.7) and applying the dimensionless quantities in Eq. (6.10) to Eqs. (6.7), and (6.8) give

$$\frac{\partial H^*}{\partial t^*}+\frac{V_0}{a}\frac{Q^*\partial H^*}{\partial x^*}+\frac{\partial Q^*}{\partial x^*}=0 \tag{6.11}$$

$$\frac{\partial H^*}{\partial x^*}+\frac{\partial Q^*}{\partial t^*}+\frac{V_0}{a}Q^*\frac{\partial Q^*}{\partial x^*}+\frac{fLQ_0}{2DAa}\left(Q^*\right)^2-\frac{V_0}{a}\frac{K_B(Q^*)^2}{2}\delta\left(x^*-x_B^*\right)=0 \tag{6.12}$$

Because V_0/a is normally small, the second term in Eq. (6.11) and the third term in Eq. (6.12) can be neglected. The dimensionless equations become

$$\frac{\partial H^*}{\partial t^*}+\frac{\partial Q^*}{\partial x^*}=0 \tag{6.13}$$

$$\frac{\partial H^*}{\partial x^*}+\frac{\partial Q^*}{\partial t^*}+[R+G\delta(x^*-x_B^*)]Q^{*2}=0 \tag{6.14}$$

in which $R=\frac{fLQ_0}{2DaA}$ = friction resistance parameter, and $G=\frac{K_BQ_0}{2aA}$ = blockage resistance parameter. The dimensionless quantities R, and G are used to characterize the transient problem in a pipeline with a blockage. Noticing that

$$R=\frac{fLQ_0}{2DaA}=\frac{\frac{fL}{D}\frac{Q_0^2}{2gA^2}}{\frac{aQ_0}{gA}}=\frac{H_f}{H_S},\ \text{and}\ G=\frac{K_BQ_0}{2aA}=\frac{K_B\frac{Q_0^2}{2gA^2}}{\frac{aQ_0}{gA}}=\frac{\Delta H_B}{H_s} \tag{6.15}$$

parameter R is the ratio of friction head loss H_f to Joukowsky pressure head rise H_s, and parameter G is the ratio of blockage-induced head loss ΔH_B to Joukowsky pressure head rise H_s.

6.3 An analytical solution with constant boundary conditions

Expressing H^* and Q^* as a steady-state values plus a small transient quantity gives

$$H^*=H_0^*+h^*\ \text{and}\ Q^*=Q_0^*+q^* \tag{6.16}$$

where h^* = a non-dimensional head deviation from a non-dimensional steady head H_0^*, and q^* = a non-dimensional flow deviation from a non-dimensional steady flow Q_0^*. Substituting Eq. (6.16) into Eqs. (6.13) and (6.14) yields H_0 and Q_0 are function of x only

$$\frac{\partial h^*}{\partial t^*} + \frac{\partial q^*}{\partial x^*} = 0 \tag{6.17}$$

$$\frac{\partial h^*}{\partial x^*} + \frac{\partial q^*}{\partial t^*} + [R + G\delta(x^* - x_B^*)](2q^* + q^{*2}) = 0 \tag{6.18}$$

Although a governing equation of h^* is preferred, due to the presence of the delta function in Eq. (6.18) and the difficulty in finding the x-derivative of the delta function, it is not possible to eliminate variable q^*. Applying the operation $\frac{\partial[\text{Eq.}(17)]}{\partial x^*} - \frac{\partial[\text{Eq.}(18)]}{\partial t^*}$ gives the governing equation of q^* as

$$\frac{\partial^2 q^*}{\partial x^{*2}} = \frac{\partial^2 q^*}{\partial t^{*2}} + [2R + 2G\delta(x^* - x_B^*)](1 + q^*)\frac{\partial q^*}{\partial t^*} \tag{6.19}$$

The last term of Eq. (6.19) is non-linear. For a small transient where q^*<<1.0, Eq. (6.19) may be simplified as

$$\frac{\partial^2 q^*}{\partial x^{*2}} = \frac{\partial^2 q^*}{\partial t^{*2}} + [2R + 2G\delta(x^* - x_B^*)]\frac{\partial q^*}{\partial t^*} \tag{6.20}$$

For a pipeline connecting two reservoirs with constant water elevations

$$h^*(0, t^*) = 0 \text{ and } h^*(1, t^*) = 0 \tag{6.21}$$

Substituting Eq. (6.21) into the continuity equation Eq. (6.17) gives flow boundary conditions

$$\frac{\partial q^*(0,t^*)}{\partial x^*} = 0 \quad \text{and} \quad \frac{\partial q^*(1,t^*)}{\partial x^*} = 0 \tag{6.22}$$

If a known transient has been initiated in the pipeline, the initial flow conditions are given as

$$q^*(x^*,0) = f_q(x^*) \text{ and } \frac{\partial q^*(x^*,0)}{\partial t^*} = g_q(x^*) \tag{6.23}$$

By applying a Fourier expansion (similar procedures as those in the Appendix A), the solution to Eq. (6.19) subject to the boundary condition in Eq. (6.22) is

$$q^*(x^*,t^*) = \sum_{n=1}^{\infty}\left\{e^{-(R+R_{nB})t^*}\left[(A'_n\cos(n\pi t^*) + B'_n\sin(n\pi t^*)\right]\cos(n\pi x^*)\right\} \tag{6.24}$$

in which $R_{nB} = 2G\cos^2(n\pi x_B^*)$ = blockage damping parameter for Fourier component n, and x_B^* = dimensionless blockage location along the pipeline. The values of Fourier coefficients in Eq. (6.24) are calculated using the initial conditions as

$$A'_n = 2\int_0^1 f_q(x^*)\cos(n\pi x^*)dx^* \quad (n = 1, 2, 3,.....) \tag{6.25}$$

$$B'_n = \frac{1}{n\pi}\left[\int_0^1 2g_q(x^*)\cos(n\pi x^*)dx^* + A_n(R+R_{nB})\right] \quad (n = 1, 2, 3,.....) \tag{6.26}$$

In reality, it is more accurate and less expensive to measure transient pressure than to measure the transient flow rate in a pipeline due of the low accuracy and slow response of the flow meters. The solution of transient pressure can be obtained by integrating continuity equation Eq. (6.17) with respect to t^* as

$$h^*(x^*,t^*) = \int -\frac{\partial q^*(x^*,t^*)}{\partial x^*}dt^* \tag{6.26a}$$

Substituting Eq. (6.24) into Eq. (6.26a) gives

$$h^*(x^*,t^*) = \sum_{n=1}^{\infty}\left\{e^{-(R+R_{nB})t^*}\left[A_n\cos(n\pi t^*) + B_n\sin(n\pi t^*)\right]\sin(n\pi x^*)\right\} \tag{6.27}$$

where the Fourier coefficients are

$$A_n = -\frac{A'_n(R+R_{nB}) + B'_n n\pi}{(R+R_{nB})^2 + (n\pi)^2}, \text{ and } B_n = \frac{A'_n n\pi - B'_n(R+R_{nB})}{(R+R_{nB})^2 + (n\pi)^2} \tag{6.28}$$

However, more generally the Fourier coefficients A_n and B_n can be determined from the initial pipeline condition of pressure, which can be expressed as

$$h^*(x^*,0) = f_h(x^*) \text{ and } \frac{\partial h^*(x^*,0)}{\partial t^*} = g_h(x^*) \tag{6.29}$$

and

$$A_n = 2\int_0^1 f_h(x^*)\sin(n\pi x^*)dx^* \quad (n = 1, 2, 3,...) \tag{6.30}$$

$$B_n = \frac{2}{n\pi}\int_0^1 g_h(x^*)\sin(n\pi x^*)dx^* + \frac{(R+R_{nB})A_n}{n\pi} \quad (n = 1, 2, 3,...) \tag{6.31}$$

The solution in Eq. (6.27) shows that any measured transient in a pipeline that includes a blockage is the summation of a series of harmonic components that are each exponentially damped with the damping rate of $R + R_{nB}$ (n = 1, 2, 3,...). The friction damping coefficient, $R(= fLQ_0/2aDA)$ of Eq. (6.27), does not contain n, indicating that the Fourier components are damped exponentially by the friction, and that the damping for all components is equal. In fact, e^{-Rt^*} can be taken outside of the summation in Eq. (6.27). In contrast, the blockage-induced damping factor R_{nB} depends on n and is different for each component; it cannot be removed from the summation sign in Eq. (6.27). However for each of individual components, the blockage damping is exactly exponential with the damping rate equal to R_{nB}, which is a function of blockage magnitude and location and is independent of measurement position.

In the above analysis, only a single blockage was considered. Noticing the linear effect of the blockage on the pipeline transient, the solution for the transient in a pipeline with more than one blockage can be expressed as

$$h^*(x^*,t^*) = \sum_{n=1}^{\infty}\left\{e^{-(R+\sum_{i=1}^{N}R_{nBi})t^*}\left[(A_n\cos(n\pi t^*) + B_n\sin(n\pi t^*)\right]\sin(n\pi x^*)\right\} \tag{6.32}$$

where N = number of blockages. For the i^{th} blockage the blockage-induced damping factor is defined as

$$R_{nBi} = 2G_i\cos^2(n\pi x_{Bi}^*) \tag{6.33}$$

in which G_i = blockage resistance parameter for the i^{th} blockage and x_{Bi}^* = dimensionless blockage location of the i^{th} blockage.

6.4 Comparison with numerical results based on MOC

When deriving Eq. (6.20), the nonlinear friction term was neglected. The accuracy of the analytical solution is verified in this section by comparing the analytical solution with results calculated numerically using the method of characteristics (MOC) in which the nonlinear friction term is calculated by a second-order difference scheme (Wylie and Streeter 1993).

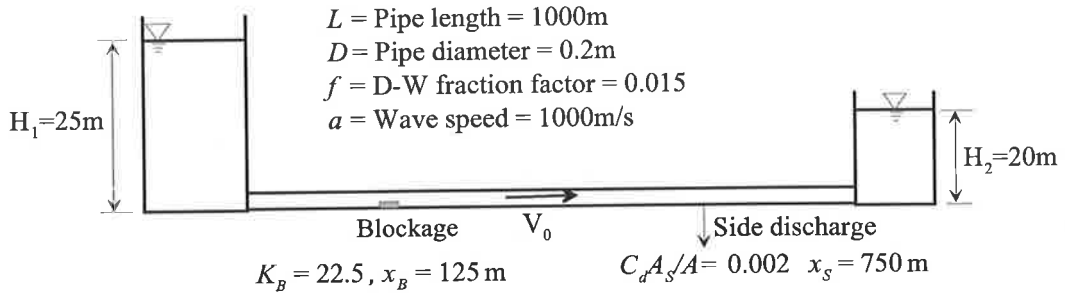

Figure 6.2 A pipeline including a blockage

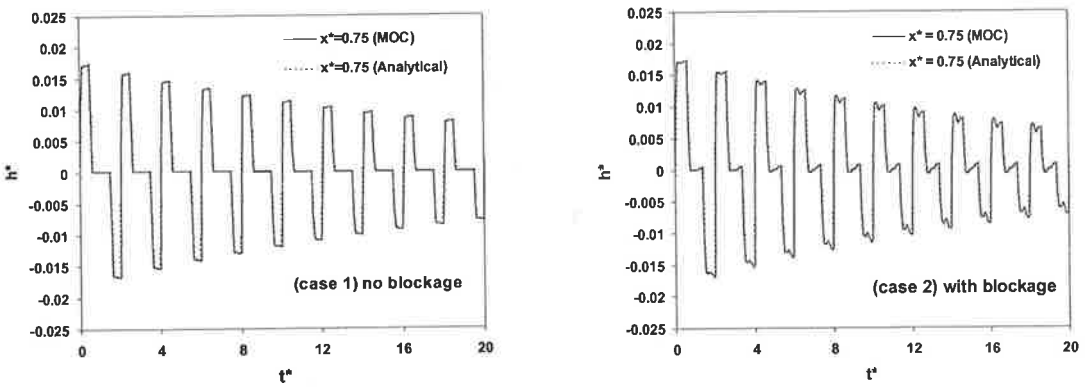

Figure 6.3 Comparison of the analytical solution with the numerical results

For the system configuration in Figure 6.2, two types of tests were conducted. In the first test (case 1) there is no blockage in the pipeline. The steady flow velocity in the pipeline is $V_0 = 1.15$ m/s, which gives the friction parameter $R = 0.0428$. In the second test (case 2), there is a blockage at 125m downstream from the tank 1 ($x_B^* = 0.125$) with magnitude $K_B = 22.5$ giving a blockage with cross-sectional area of about 20% of the pipe cross-sectional area (Miller 1993). In case 2 the steady flow in the pipeline is

reduced to $V_0 = 1.01$ m/s due to the resistance of the blockage and the friction damping parameter is reduced to $R = 0.0379$. The blockage resistance parameter is calculated as $G = 0.011$ based on the definition in Eq. (6.15). A transient event is initiated by closing a side discharge valve installed 750 m away from the upstream tank ($x^* = 0.75$). The magnitude of the side-discharge is $C_d A_S/A = 0.002$ where A_S = area of the side-discharge valve and C_d = discharge coefficient. The closure time of the valve is 0.01s. The initial effect on q^* is less than 0.02.

The transients calculated using the analytical solution of Eq. (6.26) are presented in Figure 6.3 in comparison with the numerical results of the MOC. The Fourier coefficients A_n and B_n in the analytical solution were determined from the numerical calculations. The analytical and numerical results are virtually identical for both cases so that they cannot be distinguished on the plots. Therefore, the non-linear effects of friction term on the pipeline transient are negligible if the magnitude of the transient is small.

6.5 Application to blockage detection

From Eq. (6.27) each of harmonic component is exponentially damped with damping rate $R + R_{nB}$ ($n = 1, 2, 3,\ldots$). The damping coefficient of each of the individual Fourier components can be obtained by decomposing a measured transient history period by period (Wang et al. 2002). By examining the values of the damping coefficients of individual components, the blockage in the pipeline can be detected, located and quantified.

6.5.1 Detection of a blockage

In a pipeline without any blockages, the damping of each Fourier component is independent of the component number, n, and depends only on the friction damping factor, R. Therefore, given steady flow conditions followed by a transient event, presence of a pipeline blockage is indicated by:

(1) The damping rates $R+R_{nB}$ of the decomposed harmonic components are significantly different from each other, and (2) the damping rates for some components are larger than the friction-damping factor R.

Blockage-induced damping depends strongly on the position of the blockage and on n through the cosine squared function $R_{nB} = 2G\cos^2(n\pi x_B^*)$. Different components have different responses to a blockage. For example, for a blockage located in the middle of a pipeline ($x_B^* = 0.5$), even components ($n = 2, 4, 6,\ldots$) have the maximum response whereas the response of the odd component ($n = 1, 3, 5,\ldots$) is zero. Therefore, in practice more than one harmonic component should be used to detect a blockage. Figure 6.4 shows the relative response of the first three harmonics ($n = 1$, 2 and 3) to the different blockage locations along the pipeline.

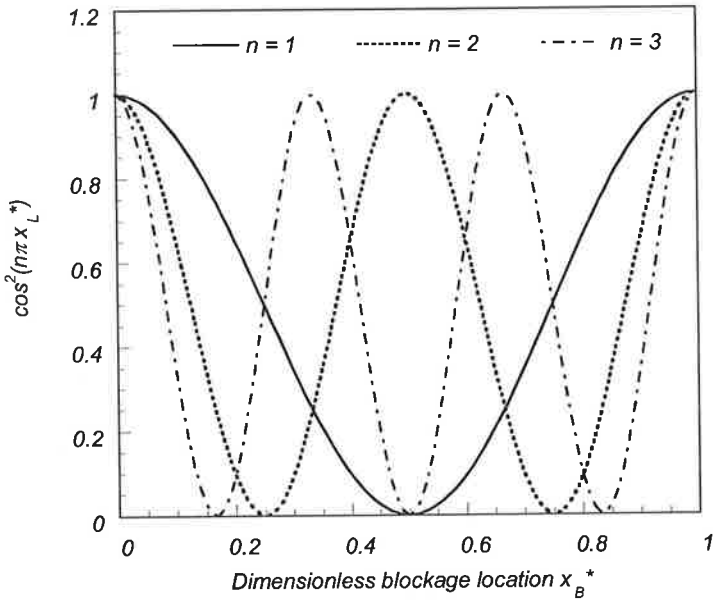

Figure 6.4 Blockage damping on different Fourier components

6.5.2 Blockage location

For each of the Fourier components, the blockage-induced damping is a function of blockage magnitude and location. However, the ratio of any two blockage-induced

damping coefficients defined in Eq. (6.24) is a function of blockage location only, which is expressed as

$$\frac{R_{n_2B}}{R_{n_1B}} = \frac{\cos^2(n_2\pi x_B^*)}{\cos^2(n_1\pi x_B^*)} \tag{6.34}$$

Therefore, the location of the blockage can be determined from the ratio of any two blockage-induced damping coefficients. Since the friction damping factor R can be calculated from the steady flow condition based on estimated pipe friction factor f (influence of error in the friction factor f on the blockage detection is investigated in a sensitivity analysis in Section 6.6.2), the blockage-induced damping for any component R_{nB} is easily obtained by subtraction. Figure 6.5 is a plot of the theoretical relationship between the damping ratios of harmonic components n_2 = 2, n_1 = 1 and harmonic components n_2 = 3, n_1 = 1 with the corresponding blockage locations in a pipeline.

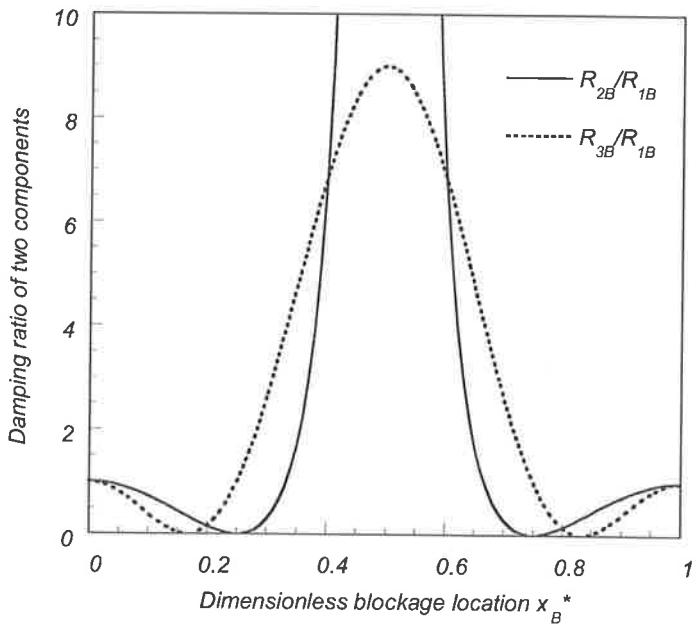

Figure 6.5 Ratio of blockage damping coefficients of two Fourier components

Due to the symmetric character of the cosine squared function, the relationship between the damping ratio of two harmonic components and the blockage location is not unique. Two or up to four blockage locations correspond to one value of the damping ratio R_{2B}/R_{1B} except for x_B^* = 0.5, which is a unique point because the blockage damping R_{1B}

= 0 at $x_B^* = 0.5$. For the damping ratio of higher harmonic components, one damping ratio corresponds to more possible blockage locations; therefore, only harmonic components of $n< 4$ are used for blockage detection analysis in this study.

6.5.3 Magnitude of a blockage

Once the position of the blockage has been determined, the blockage magnitude can be easily calculated using Eq. (6.24). It is

$$G = \frac{R_{nB}}{2\cos^2(n\pi x_B^*)} \quad (n = 1, 2, 3,\ldots) \tag{6.35}$$

where n is any one of the components. Theoretically, the blockage magnitude calculated using different components should be the same. Different measurement positions and different forms of transients can be used for added confirmation and to increase accuracy if necessary.

6.6 Sensitivity analysis

The application of the proposed blockage detection method depends on the accuracy of the values of blockage damping on individual Fourier components. In the derivation of Eq. (6.20), the q^* was assumed small. The influence of the transient magnitude on the blockage-induced damping thus on the blockage detection including location and magnitude is investigated in this section. Since blockage-induced damping is obtained from total damping of a transient component by subtracting the friction damping, the error in calculating friction damping will be transferred to blockage-induced damping and, as a result, the outcome of blockage detection may be affected. An important factor that influences the calculation of friction damping is the determination of the Darcy-Weisbach friction factor (f) of the pipe. The influence of the error in estimating the friction of pipes on the leak detection is also investigated in this section.

6.6.1 Influence of linearization of orifice equation

To investigate the influence of the transient magnitude on the blockage-induced damping, assuming a constant q^* gives the approximate solution of Eq. (6.19), where term of q^* has now been retained as

$$h^*(x^*,t^*)=\sum_{n=1}^{\infty}\left\{e^{-(R'+R'_{nB})t^*}\left[A_n\cos(n\pi t^*)+B_n\sin(n\pi t^*)\right]\sin(n\pi x^*)\right\} \tag{6.36}$$

where $R' = (1+q^*)R$, and $R'_{nB} = (1+q^*)R_{nB}$. The apparent blockage damping for component n is $(R_{nB})_{apparent} = (1+q^*)R_{nB} + q^*R$ in which q^*R is the error introduced from the friction damping. The error in the blockage-induced damping coefficient will lead to the error in the ratio of two coefficients thus will in turn influence the calculation of blockage location and magnitude. Substituting $(R_{nB})_{apparent}$ into Eq. (6.34) and applying $n_1 = 1$ and $n_2 = 2$ gives

$$\frac{\dfrac{\cos^2(2\pi x_B^*)}{\cos^2(\pi x_B^*)}+S_1}{1+S_1}=\frac{\cos^2[2\pi(x_B^*+\varepsilon_L)]}{\cos^2[\pi(x_B^*+\varepsilon_L)]} \tag{6.37}$$

where ε_L = dimensionless distance away from the real blockage location, and $S_1=\dfrac{q^*R}{(1+q^*)R_{1B}}$ = sensitivity parameter influencing the blockage location. Variation of blockage location error ε_L with parameter S_1 and real blockage location x_B^* is shown in Figure 6.6. Blockages at different locations have different sensitivities to the error in the blockage damping. Generally, blockages located close to the pipe ends are the most sensitive to the damping and are more easily detected. Figure 6.6 also indicates that the accuracy of the blockage detection depends on parameter S_1. To increase the accuracy and sensitivity of the proposed method, a smaller value of S_1 should be used. This can be achieved using a smaller magnitude of transient a smaller steady flow rate.

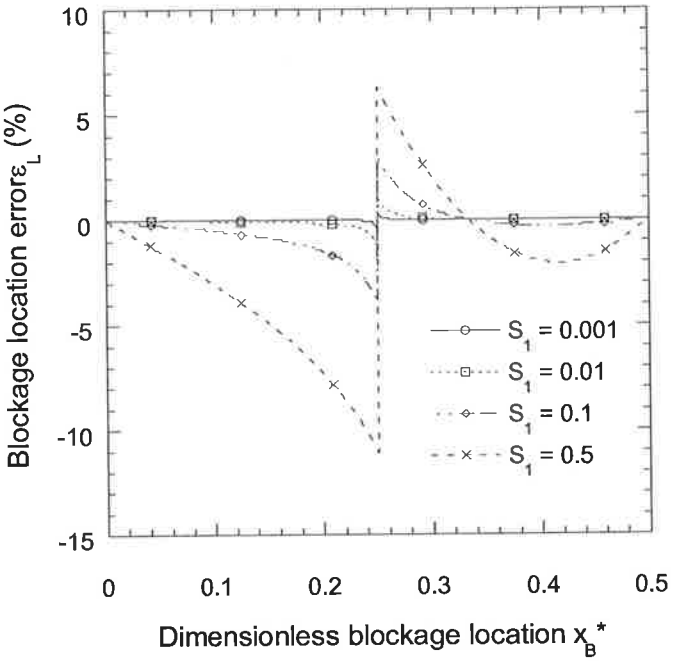

Figure 6.6 Error of blockage location

The error in blockage magnitude induced by the orifice linearization is defined as

$$\varepsilon_s = \frac{G_{real} - G_{apparent}}{G_{real}} \tag{6.38}$$

Substituting Eq. (6.35) into Eq. (6.38) gives

$$\varepsilon_s = \frac{G_{real} - G_{apparent}}{G_{real}} = 1 - \frac{(1+S_2)\cos^2[n\pi(x_B^* + \varepsilon_L)]}{\cos^2(n\pi x_B^*)} \tag{6.39}$$

where $S_2 = q^*(1+\frac{R}{R_{1B}})$ = sensitivity parameter influencing the blockage magnitude.

The magnitude of the blockage is affected by the parameter S_2 and the location of the blockage as shown in Figure 6.7. Smaller values of parameter S_2 tend to cause less error for the blockage magnitudes. Similarly for the parameter S_1, a smaller magnitude of transient or smaller value of friction damping coefficient produces a smaller value of parameter S_2.

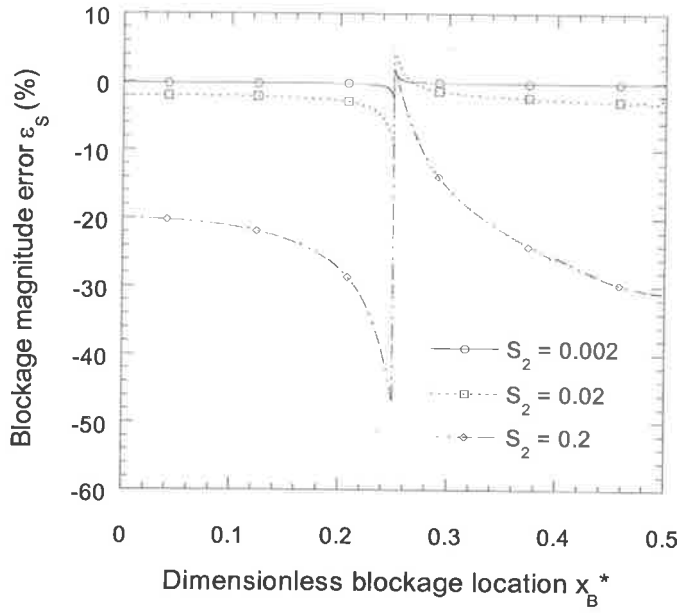

Figure 6.7 Error of blockage magnitude

6.6.2 Influence of pipe friction factor uncertainty

Following a similar process to that presented in Section 4.4.2, if there is an error Δf in estimating the Darcy-Weisbach friction factor (f), the affected friction damping is

$$\begin{aligned} R+\Delta R &= \frac{1}{a}\sqrt{\frac{(f+\Delta f)Lg\Delta H}{2D}} \\ &\approx (\sqrt{f}+\frac{\Delta f}{2\sqrt{f}})\frac{1}{a}\sqrt{\frac{Lg\Delta H}{2D}} \qquad \text{(4.11, repeated)} \\ &= R+\frac{\Delta f}{2f}R \end{aligned}$$

If the affected fraction damping factor in Eq. (4.11) is used to calculate the blockage damping, the blockage-induced damping on n^{th} harmonic component is R_{nB}-ΔR. Therefore, the ratio of two blockage-induced damping coefficients for any two components is

$$\frac{R_{n_2B}-\frac{\Delta f}{2f}R}{R_{n_1B}-\frac{\Delta f}{2f}R}=\frac{\cos^2[n_2\pi(x_L^*+\varepsilon_L)]}{\cos^2[n_1\pi(x_L^*+\varepsilon_L)]} \tag{6.40}$$

where ε_L= dimensionless distance away from a real leak location. Substituting $\frac{R_{n_2B}}{R_{n_1B}}=\frac{\cos^2(n_2\pi x_L^*)}{\cos^2(n_1\pi x_L^*)}$ into (6.40) and rearranging gives

$$\frac{\frac{\cos^2(n_2\pi x_L^*)}{\cos^2(n_1\pi x_L^*)}-S_f}{1-S_f}=\frac{\cos^2[n_2\pi(x_B^*+\varepsilon_L)]}{\cos^2[n_1\pi(x_B^*+\varepsilon_L)]} \tag{6.41}$$

where $S_f=\frac{R\Delta f}{2R_{n_1B}f}$ = sensitivity parameter of the friction factor. The blockage location error, ε_L, is a function of parameter S_f and real blockage location, x_B^*. Similarly, the error in the magnitude of a blockage caused by the friction factor uncertainties is expressed as

$$\varepsilon_s=\frac{(G_B)_{real}-(G_B)_{apprarent}}{(G_B)_{real}}=1-\frac{(1-S_f)\cos^2(n\pi x_B^*)}{\cos^2[n\pi(x_B^*+\varepsilon_L)]} \tag{6.42}$$

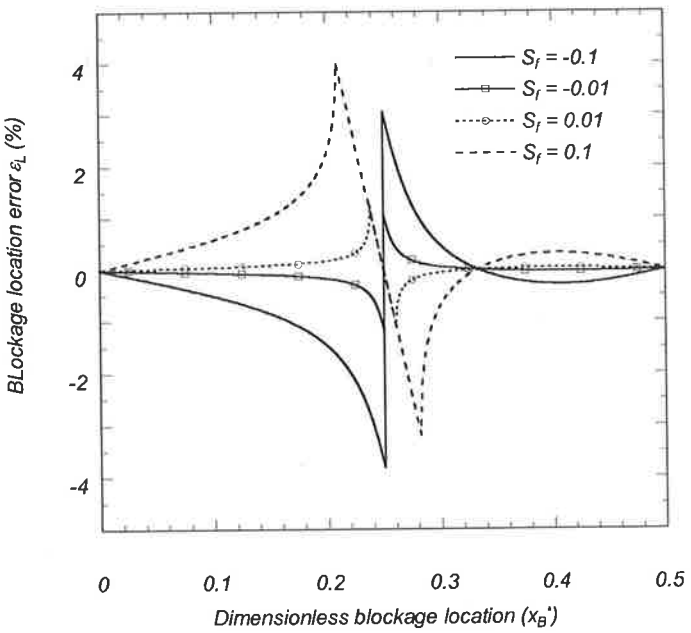

Figure 6.7a Error of blockage location caused by the pipe friction uncertainty

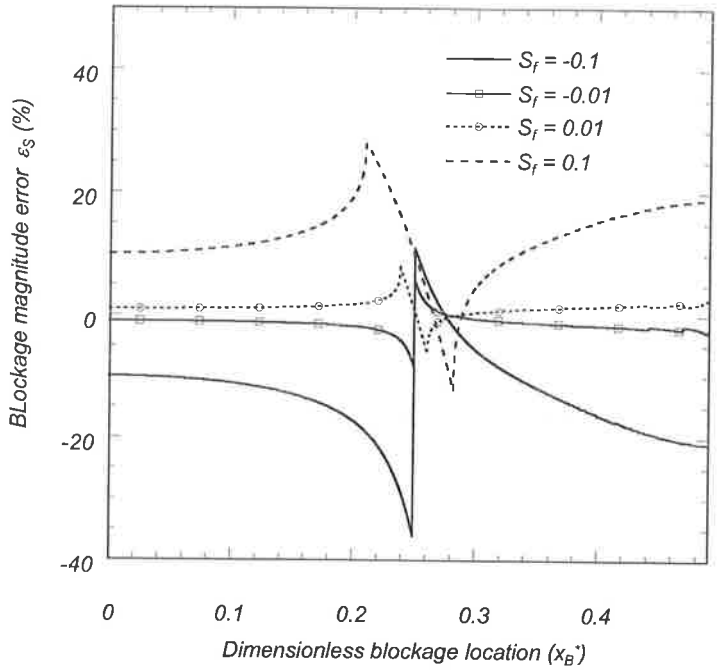

Figure 6.7b Error of blockage magnitude caused by the pipe friction uncertainty

Variations of blockage location error (ε_L) and magnitude error (ε_S) caused by the pipe friction uncertainties are plotted in Figure 6.7a and Figure 6.7b respectively. Errors in both the blockage location and the magnitude increase with the increasing of pipe friction uncertainty parameter S_f. In addition, pipe friction uncertainty has a more significant influence on blockage magnitude (Figure 6.7b) than on blockage location (Figure 6.7a). For a parameter of $S_f = 0.1$, the blockage location may be influenced by 4% while influence on blockage magnitude may be up to 30%.

Like a blockage, a leak in a pipeline causes damping of pipeline transients (Wang et al. 2002). When a leak and a blockage exist at the same time in a pipeline, a method needs to be developed to distinguish these two different types of damping on the transients. According to Eq. (6.15), the blockage parameter G is proportional to the flow in the pipeline. Therefore, a blockage has little influence on the transient damping if the flow in the pipeline is negligibly small. In contrast, leak-induced damping is independent of

the flow in the pipeline (Wang et al. 2002). Therefore, by applying a small steady flow in a pipeline a leak can be detected with little influence from a blockage. Once the characteristics of the leak, including its location and size are known, the blockage detection technique can be applied. The blockage-induced damping can be calculated by subtracting the leak-induced damping. An example of detecting both a leak and a blockage is given in the following section.

6.7 Numerical examples

In this section, two numerical examples are given to illustrate the application of the blockage detection technique proposed in section 6.5. In the first example, there is only a blockage in a pipeline. In the second example, a leak is included.

6.7.1 Problem of a pipeline including a blockage

The numerical example presented in this section is used as an application of the proposed blockage detection method in which the measured transients are generated from the method of characteristics (MOC) as shown in Figure 6.3. In this example, the sensitivity parameters defined in Eqs. (6.37) and (6.39) are $S_1 = 0.03$ and $S_2 = 0.06$, giving an error of the blockage location of 1% and size of 2%. By applying a discrete Fourier transform algorithm to decompose the measured data (Wang et al. 2002), the amplitude for separate components are presented in Figure 6.8(a). The amplitude $E_n^{(i)}$ of the n^{th} harmonic for the i^{th} period may be expressed as

$$E_n^{(i)} = E_n^{(1)} e^{-(R+R_{nB})(i-1)T^*} \tag{6.43}$$

where $E_n^{(1)} = \dfrac{e^{-(R+R_{nB})(t_0^*+T^*)} - e^{-(R+R_{nB})t_0^*}}{-(R+R_{nB})T^*} \sin(n\pi x^*)\sqrt{A_n^2 + B_n^2}$ = the amplitude of the n^{th} harmonic component at the first period, t_0^* = dimensionless starting time of the analysis and T^* = dimensionless period defined as $T^* = T/(L/a) = 2.0$, in which T = period of the transients in a reservoir-pipeline-reservoir system.

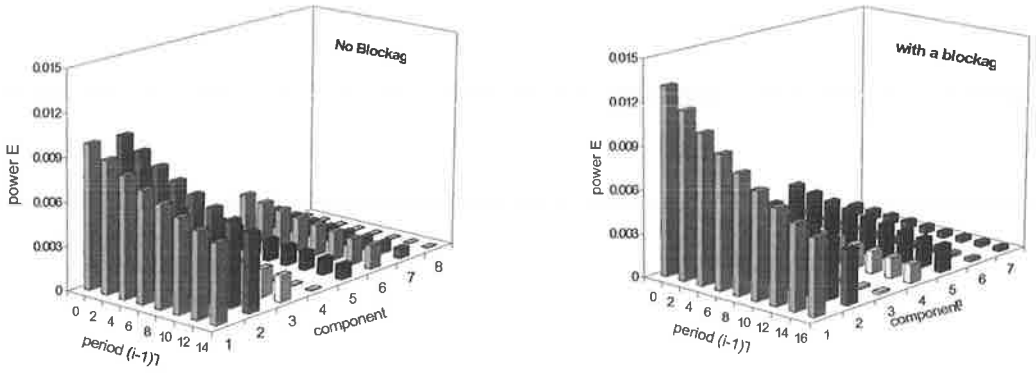

(a) Fourier analysis of the measured transient signal

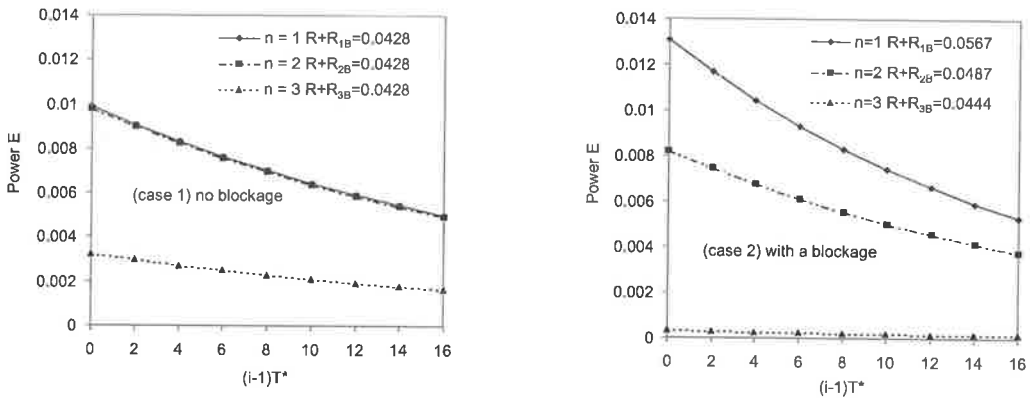

(b) Exponential damping of different Fourier components

Figure 6.8 Numerical example for detecting a blockage using transients

The damping coefficients $R + R_{nB}$ (n = 1, 2, 3) are calculated by applying an exponential fitting function in form of Eq. (6.28) where both initial amplitude $E_n^{(1)}$ and the damping coefficient $R + R_{nB}$ can be calculated. Figure 6.8(b) shows computed amplitudes of the Fourier series of the first three harmonic components plotted against period in terms of L/a. In Figure 6.8(b1)—the no blockage case—the damping rates $R+R_{nB}$ for all three harmonic components are determined as 0.0428 by fitting Eq. (6.40) to the decaying amplitudes, which is equal to the friction-damping factor R of the pipeline. In Figure 6.8(b2)—in which a blockage was present—the damping rates $R+R_{nB}$ are 0.0567, 0.0487, 0.0414 for the first three components. The second value is significantly different from the first and third and all are larger than the friction-damping factor of 0.0428.

According to the steady flow condition, the friction damping parameter is R = 0.0379based on Eq. (6.15). The blockage-induced damping rates R_{nB} for components n = 1, 2 and 3 are 0.0188, 0.0108 and 0.0035, which are obtained by subtracting R from $R+R_{nB}$. The sensitivity parameters defined in Eqs. (6.37) and (6.39) are S_1 = 0.04 and S_2 = 0.06, which are insignificant based on previous sensitivity analyses. The ratios of two blockage-induced damping rates defined in Eq. (6.34) are R_{2B}/R_{1B} = 0.574 and R_{3B}/R_{1B} = 0.186. Using these two ratios in Figure 6.6, the corresponding blockage locations are x_B^* = 0.127 or (x_B^* = 0.3175, x_B^* = 0.683, or x_B^* = 0.873) based on R_{2B}/R_{1B} = 0.574, and x_B^* = 0.123 or (x_B^* = 0.204, x_B^* = 0.796, or x_B^* = 0.877) based on R_{3B}/R_{1B} = 0.186. Two ratios give an approximate same location x_B^* = 0.125, which is the real blockage location. Applying Eq. (6.35) based on the calculated blockage location and R_{1B} = 0.0567, the calculated blockage magnitude G = 0.0115. Applying this value to Eq. (6.15) gives the blockage head loss coefficient of K_B = 22.8, which is close to the real magnitude of the blockage (K_B = 22.5) used to generate the MOC transient data.

In this example, if an error exists in determining the pipe friction factor, say f = 0.014. The sensitivity parameter for pipe friction is calculated as S_f = 0.067. Based on the sensitivity analysis in Section 6.6.2, the influence on blockage location is about 0.5% and on blockage magnitude is about 10%.

6.7.2 Combined leak and blockage detection problem

In the second example, a leak and a blockage are assumed to exist in a pipeline at the same time as shown in Figure 6.9. A blockage with the head loss coefficient of K_B = 22.5 and a leak of C_dA_L/A = 0.001 are located at 125m (x_L^* = 0.125) downstream of the upstream reservoir.

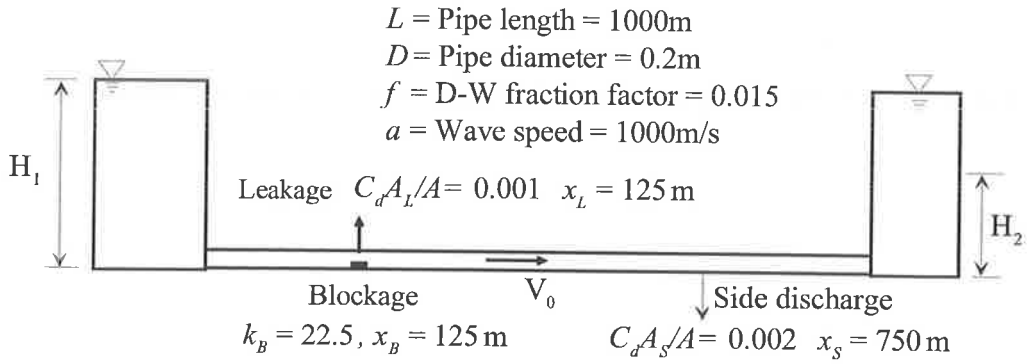

Figure 6.9 A pipeline with a leak and blockage

As discussed in section 6.5.4, to apply the blockage detection technique proposed, leak-induced damping needs to be distinguished from the total damping caused by both the leak and blockage. The first test (Test I) is based on a negligible small pipe flow, which can be achieved by setting the same reservoir heads ($H_1 = H_2 = 25$m) at the upstream and downstream reservoirs. The transients are generated by closing a side-discharge of $C_dA_S/A = 0.002$ located at 750m ($x^* = 0.75$). The transient measured at $x^* = 0.75$ is given in Figure 6.10(a). The transient is decomposed into a Fourier series period by period (Wang et al. 2002) and the damping coefficients of the first two Fourier components are shown in Figure 6.10(b). In this case, despite the relative large dimensionless transient ($q^* = 1.0$), the leak detection sensitivity parameter S ($S = q^*R/R_{1L} = 0.05$) is small due to small value of friction damping with respect to leak damping ($R = 0.00038$, $R_{1L} = 0.0072$). As a result, the errors of leak location and leak magnitude induced by the transient magnitude q^* are under 1% and 10% respectively based on the sensitivity analysis in Section 4.4.1. Since the steady flow in the pipeline is negligible small, the friction and blockage-induced damping is negligible. Therefore, the leak-induced damping for the first two Fourier components are $R_{1L} = 0.0072$ and $R_{2L} = 0.0231$, and the ratio of two damping coefficients is $\frac{R_{2L}}{R_{1L}} = 3.208$. Applying this value to Figure 4.2 gives the leak locations of $x_L^* = 0.138$. Applying these leak locations and $R_{1L} = 0.0072$ to Eq. (4.4) gives the relative sizes of $C_dA_L/A = 0.00091$.

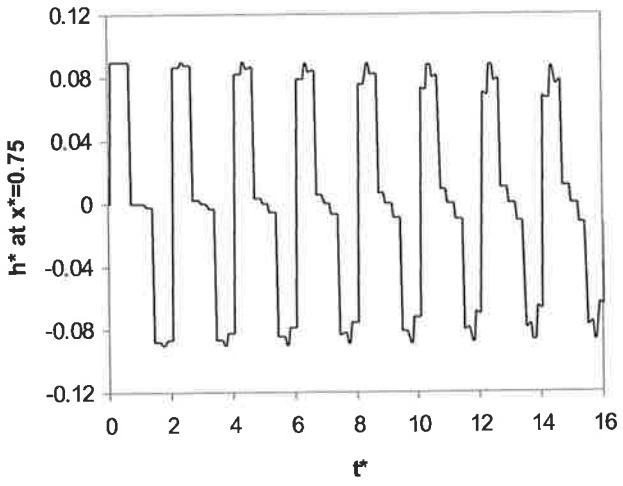

(a) Measured transients

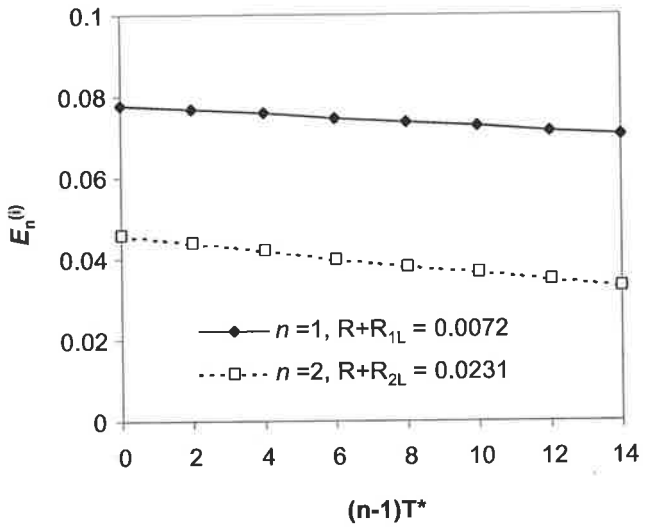

(b) Damping analysis

Figure 6.10 Transient damping caused by the leak in a pipeline including a leak and a blockage (Test I)

Because of the existence of the leak, the steady flow in the pipeline is not exactly zero. Applying an average leak size of $C_dA_l/A = 0.00091$, the steady velocity in the pipeline is calculated as $V_0 = 0.5Q_{L0} = C_d A_L \sqrt{2gH_{L0}} = 0.01$m/s. As a result, the friction damping is not zero, and the damping factor is calculated as $R = \frac{fLV_0}{2Da} = 0.00038$. By considering the friction damping, the upgraded leak damping coefficients of the first two Fourier

components are R_{1L} = 0.00682 and R_{2L} = 0.02272, and the ratio of two damping coefficients is $\frac{R_{2L}}{R_{1L}} = 3.33$. Applying these two values to Figure 4.2 gives a leak location of x_L^* = 0.133. Applying this leak location and R_{1L} = 0.00682 to Eq. (4.4) gives the relative sizes of C_dA_L/A = 0.00095. Repeating the above process, the leak location is calculated as x_L^* = 0.130, and the leak size is C_dA_L/A = 0.00096. The calculated location and the size of the leak are close to the real location (x_L^* = 0.125) and size (C_dA_L/A = 0.001).

There are two options available for blockage detection. One option is to repair the leak first especially if the leak-induced damages may be serious. Then the problem changes to detecting a pipeline blockage as illustrated in the first example. Another option is to run blockage detection technique without eliminating the leak in advance. In such a situation, the leak-induced damping, which may be calculated from the detected location and size, needs to be considered and subtracted from the total damping of measured transients. The detailed process is illustrated below.

In the second test (Test II), the heads in the two reservoirs are set as H_1 = 25m and H_2 = 20m. The steady flow in the pipeline is measured as Q_0 = 0.0317m^3/s. The transient is generated by closing the side discharge at x^* = 0.75. The transient measured at x^* = 0.75 is shown in Figure 6.11(a). Compared to the transient in Figure 10(a), the transient in Figure 6.11(a) experiences greater damping due to the increased steady pipe flow, which leads to the friction and blockage-induced damping becoming significant. Similarly, the transient may be decomposed into a Fourier series period by period (Wang et al. 2002) and the damping coefficients of the first two Fourier components are shown in Figure 6.11(b). The total damping including friction damping, leak-induced damping and blockage-induced damping for the first two Fourier components are $R + R_{1L} + R_{1B}$ = 0.0632 and $R + R_{1L} + R_{1B}$ = 0.0712. Based on Eq. (6.15) and known value for f the friction damping is calculated as R = 0.0379. Based on Eq. (3.32), the leak damping coefficients for the first two components are calculated as R_{1L} = 0.0074, and R_{2L} = 0.0235. Thus, the blockage-induced damping for the first two coefficients are R_{1B} =

0.0179, and R_{2B} = 0.0098, and the ratio of two damping coefficients is $\frac{R_{2B}}{R_{1B}} = 0.547$. Applying this value to Figure 6.5 gives the blockage locations of $x_B^* = 0.131$. Applying $x_B^* = 0.131$ and $R_{1B} = 0.0179$ to Eq. (6.35) and then to Eq. (6.15) gives blockage head loss coefficient of $K_B = 21.1$, which is close to the real valve of $K_B = 22.5$.

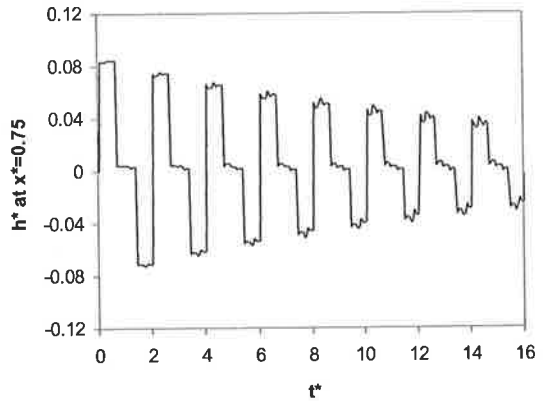

(a) Measured transients

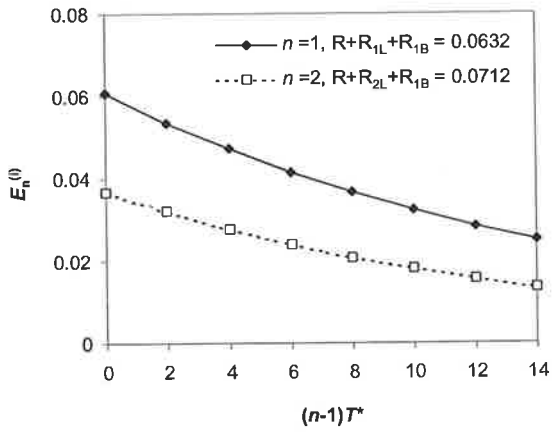

(b) Damping analysis

Figure 6.11 Transient damping caused by friction, the leak and the blockage in a pipeline (Test II)

6.8 Laboratory experimental verification

Experimental tests were conducted in a single pipeline in the Robin Hydraulics Laboratory at the University of Adelaide to verify the practical feasibility of the proposed blockage detection method. The experimental setup is the same as those

described in Figure 4.12, and is shown in Figure 6.12. A blockage is simulated by a partially closed valve (Valve 1) located near the Tank 1.

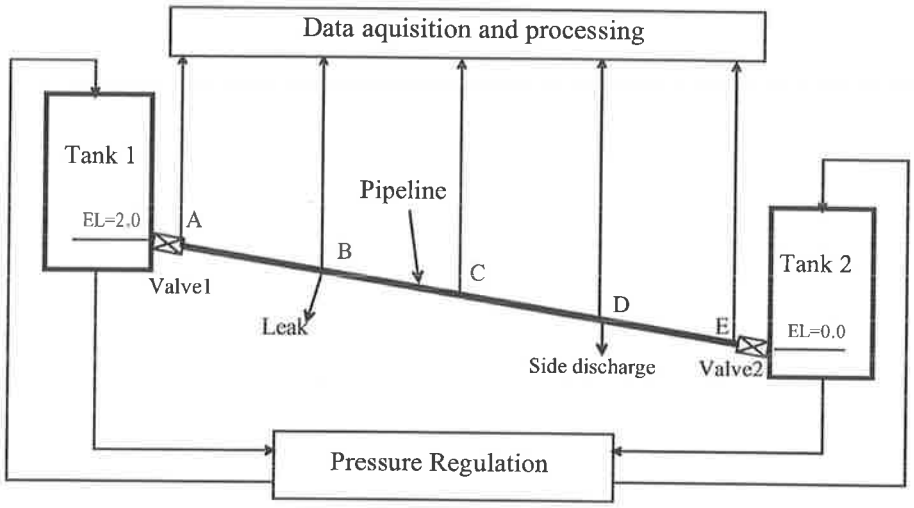

Figure 6.12 Laboratory setup for blockage detection

Two tests were conducted. Test I is a no–blockage case (Valve 1 is fully open) and in Test II, the Valve 1 is partially closed. The flow conditions are as follows:

Length of the pipeline	$L = 37.2$m,
Pipe diameter	$D = 0.022$m,
Thickness of the pipe wall	$e = 1.6$mm,
Wave speed	$a = 1{,}320$m/s,

In both Test I and Test II, the heads at two tanks are set as $H_1 = 27.53$m, and $H_2 = 26.60$m. In Test I, the Valve 1 is fully open, and the steady flow velocity in the pipeline was $V_0 = 0.80$m/s. Given the Reynolds number of **Re** = 15400, the Darcy-Weisbach friction factor is calculated as $f = 0.017$ (smooth pipe) and the steady friction damping factor is calculated as $R = 0.0087$. In Test II, the Valve 1 is partially closed, the steady flow in the pipeline is reduced to $V_0 = 0.36$m/s, and the steady friction damping factor is calculated as $R = 0.0036$. Based on the total head loss and the steady flow in the pipeline, the head loss coefficient of the partially closed Valve 1 is calculated as $K_B = 114.9$.

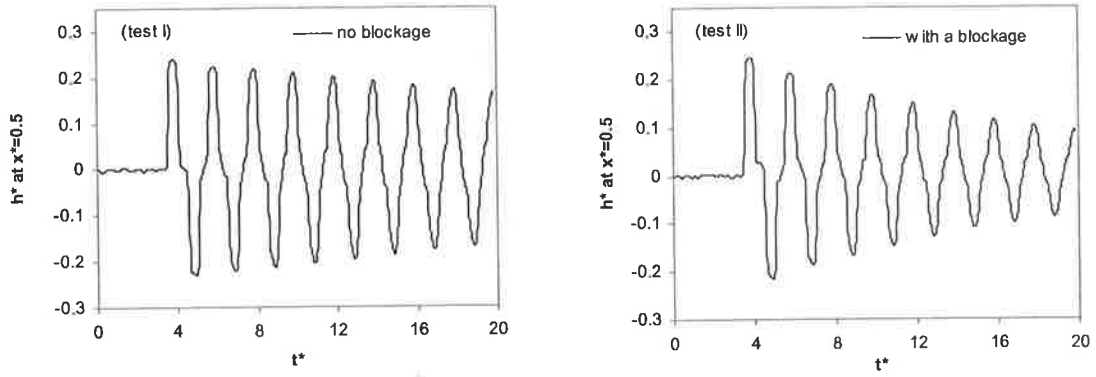

(a) Measured transients

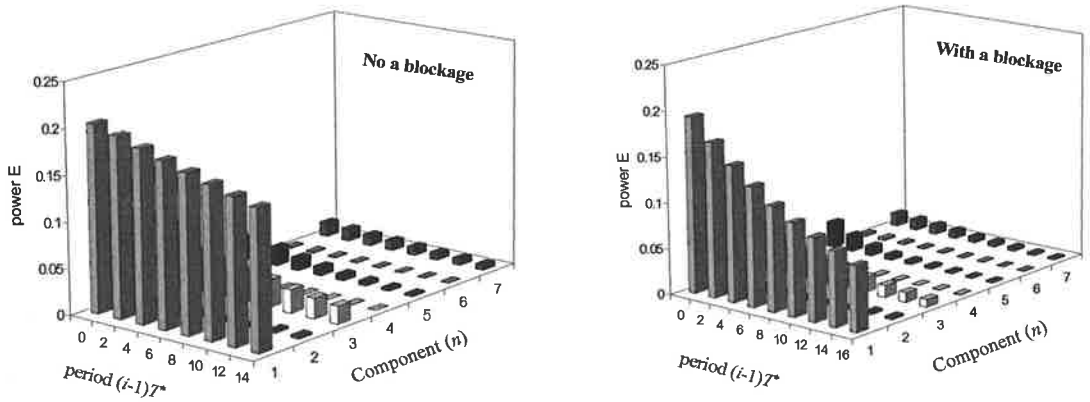

(b) Frequency analysis

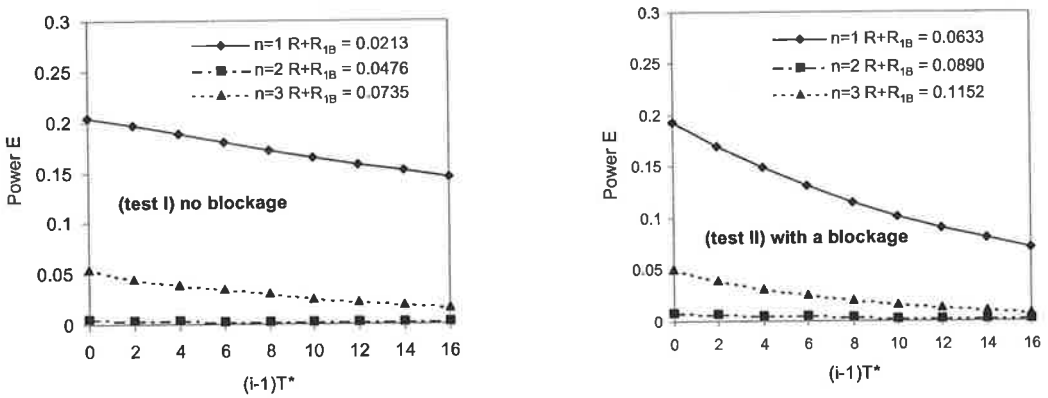

(c) Damping analysis

Figure 6.13 Laboratory experimental verification of blockage detection technique

In Test I, the valves at locations A and E and the side-discharge valve at D are opened and a steady state condition is achieved. The side-discharge solenoid valve at D is then closed quickly. In Test II, the valve 1 at A is partially closed, and the valve at location E is fully open. The side-discharge valve at D is open until steady state conditions are obtained. The side-discharge valve at D is then sharply closed. During the tests, pressures are measured by five pressure transducers at points A, B, C, D, and E. Measured pressures in the middle of the pipeline ($x^* = 0.50$) from both Test I and Test II are plotted in Figure 6.13(a). The blockage-induced damping of Test II is obvious compared to the transient in Test I that has no blockage.

Figure 6.13(b) shows the computed amplitudes of different harmonic components by decomposing the transient signal into a Fourier series period by period. Each component was fitted to an exponential function, and the damping coefficient of each component was calculated.

The damping coefficients of the first three components ($n = 1, 2, 3$) for both Test I and Test II are presented in Figure 6.13(c). For the no-blockage case (Test I), friction damping coefficients of the first three harmonic components are $R_1 = 0.0213$, $R_2 = 0.0476$, $R_3 = 0.0735$, all being larger than the steady friction damping factor $R_s = 0.0087$, calculated using steady state friction. The differences between the measured and the calculated damping values are due to unsteady friction. It accounts for 46%, 76% and 84% of the total for the first three components.

In Test I and Test II, since the transients were initiated by closing the side-discharge valve in the same amount of time, the unsteady friction damping effects are approximately same. Therefore, in Test II the friction damping coefficients for the first three components are $R_1 = 0.0161$, $R_2 = 0.0424$ and $R_3 = 0.0683$. By subtracting the friction damping from the total damping, blockage-induced damping coefficients for the first three components ($n = 1, 2, 3$) are $R_{1B} = 0.0472$, $R_{2B} = 0.0466$, $R_{3B} = 0.0469$. The ratios of damping coefficients R_{2B} and R_{1B}, and R_{3B} and R_{1B} are $\frac{R_{2B}}{R_{1B}} = 0.994$, and

$\frac{R_{3B}}{R_{1B}} = 0.994$. Corresponding blockage locations for these damping ratios are $x_B^* = 0.0$ (or $x_B^* = 1.0$) by applying these two ratios in Figure 6.5. This is same as the real blockage location $x_B^* = 0.0$. Using $R_{1B} = 0.0472$, $R_{2B} = 0.0466$ and leak location $x_B^* = 0.0$, the head loss coefficient for the blockage is calculated, from Eq. (6.35) and then Eq. (15), as $K_B = 188.8$. The value of the head loss coefficient calculated from the transient experiment is about 40% larger than that based on steady-state test of $K_B = 114.9$. The reason for this difference may be due to the assumption of theoretical blockage head loss relationship of Eq. (6.9). A similar explanation is given in Chapter 3. Another possible reason for the discrepancy of the blockage size is the unsteady orifice loss that was not included in this study.

6.9. Summary

The behaviour of a blockage on pipeline transients is studied in this chapter. A general conclusion of this chapter is that transients in a pipeline can be used for blockage detection. A technique for blockage detection, location and quantification has been developed. Numerical and experimental examples have shown that blockage with cross-sectional area of 20% of the pipe cross section can be detected and located.

The governing equations for transients in a pipeline including a blockage have been developed by approaching a blockage as an orifice and using a Dirac delta function. A simplified linear dimensionless governing equation has been derived. An analytical solution expressed in terms of a Fourier series has been developed under constant boundary conditions. By comparison to the numerical solution based on the method of characteristics (MOC) in which the non-linear effects are included, the analytical solution shows a high degree of accuracy.

The analytical solution indicates that transients in pipelines are damped by both friction and blockages. Blockage-induced damping is exactly exponential for each of the individual harmonic components. Compared to leak-induced damping, which is related

to pressure in the pipeline and is independent of flow rate in the pipeline, blockage damping is proportional to flow rate, and does not have a direct relationship with the pressure in the pipeline. Therefore, blockage detection should be conducted at conditions of a considerable flow rate in order to produce best performance. In addition, the relationship between blockage location and blockage damping is a cosine-square function while leak location and leak damping is a sine-square function.

Sensitivity analyses have shown that accuracy of blockage detection using the method presented in this chapter is influenced by transient magnitude, ratio of friction damping over blockage damping and the accuracy of the pipe friction factor. These factors have a more significant influence on blockage magnitude than on the blockage location.

Similarly for the leak detection technique presented in Chapter 4, the blockage detection technique presented in this chapter is simple to use and apply; however, this method may not be applicable in complex systems such as pipe networks. Feasibility of applying the inverse transient method (Liggett and Chen 1994), which will be discussed in Chapter 7 and Chapter 8, for blockage detection in pipe network systems is currently under investigation at the University of Adelaide (Stephens 2002).

Chapter 7

Application of the Inverse Transient Method for Leak Detection in Pipe Networks

7.1 Introduction

In the previous chapters, analytical solutions for transients in single pipelines have been developed under different boundary conditions. Based on these analytical solutions, new leak and blockage detection methods have been developed. However, these methods cannot be applied in complex pipe network systems. In this chapter, the inverse transient method (ITM), which is a more general leak detection technique suitable for leak detection in pipe networks, is investigated. This method was originally developed by Liggett and Chen (1994) for leak detection and pipe roughness calibration in water distribution pipe network systems, and has shown promise based on numerical simulation results on a simple pipe network (Liggett Chen 1994, Chen 1995), and laboratory applications in a straight single pipeline conducted at the University of Adelaide (Vítkovský 2001). As a further step to apply this method for real pipe network systems, verification of this method in a real pipe network is necessary. For this purpose, a three-loop pipe network made of copper pipe with a diameter of 75mm has been constructed in the Department of Civil & Environmental Engineering at the University of Adelaide. Compared to a single pipeline, this pipe network not only has more pipes and nodes, but also has some special features, such as dead ends and minor losses at junctions and bends. The effects of these features on fluid transients, and as a result on the application of ITM on leak detection, are addressed in this chapter. Details of this pipe network and real applications of ITM based on this network are presented in the Chapter 8.

A block diagram for the inverse transient method is shown in Figure 7.1. The inverse transient method works starting from the generation of a transient event in a pipe network system. The transient pressure variations are measured at different locations in the pipe system. At the same time, the transient event is simulated by applying a numerical model with corresponding initial and boundary conditions. In the numerical model, the parameters for the pipe network include pipe length, pipe diameter, roughness and leaks. Since the parameters of the leaks, including the possibility of no leak, are to be determined in the model, these values have to be estimated in advance.

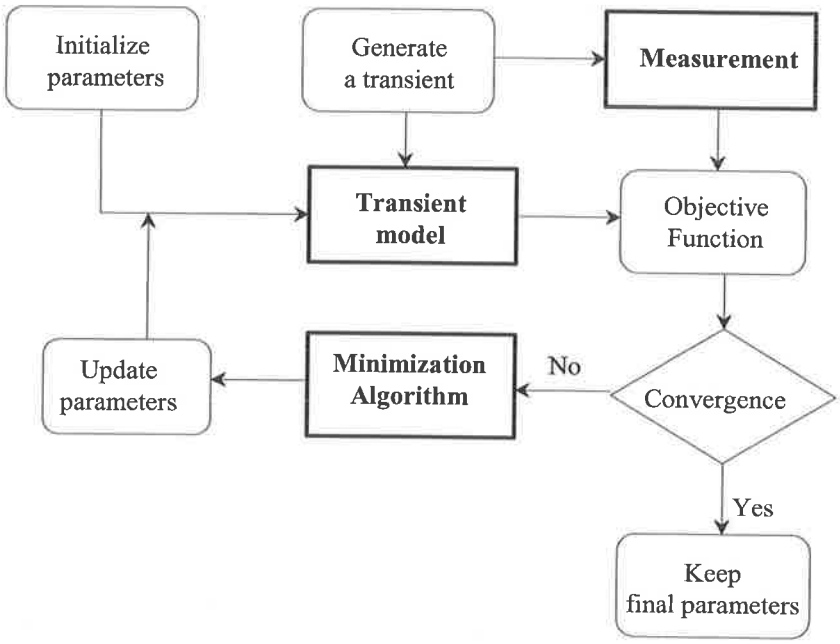

Figure 7.1 Block diagram of the inverse transient method

Based on the initial leak parameters, simulated transients by the numerical model are compared to the corresponding measurements. The match between the simulated and measured transients is quantified by an objective function. If the simulated transients are close to the measurements, the value of the objective function is close to zero. If the transients calculated from the numerical model based on the guessed leak parameters is not close to the measured transients, a large objective function will be obtained. To improve the estimates of parameters, a minimisation scheme of objective function is applied. Based on the improved leak parameters, the numerical model is run again, and

the newly calculated transients are compared to the measurement data. The above process is repeated until the calculated transients are close to the measurements as determined by pre-set accuracy values. At convergence the leak parameters used in the numerical model are assumed to characterize the real leaks.

As shown in Figure 7.1, to apply the inverse transient method, there are three major components: measurement of transients (data acquisition), transient modelling and minimisation. In this chapter, the focus is on transient modelling in pipe networks. More background details of ITM can be found in the theses of Chen (1995) and Vítkovský (2001). Transient measurement and results of applications based on a laboratory pipe network are discussed in the next chapter (Chapter 8). Common problems in simulating transients in pipe networks are discussed in Section 7.2. The governing equations and the method of characteristics, that are the foundation of the transient model used in this study, are introduced in Section 7.3, 7.4 and 7.5. Effects of minor losses and dead ends on transient events are investigated in details at Section 7.6 and 7.7. The minimisation methods to be used in this study are discussed in Section 7.8. Two computer programs, called NETTRANS and NETFIT, developed in this study as part of this Ph.D. research are introduced in Section 7.9.

7.2 Simulation of transients in pipe networks

The study of fluid transients in pipeline and pipe network systems has a history of at least one hundred years (Allievi 1925; Wylie and Streeter 1993). Most of the previous studies investigated the transients for severe conditions, for example, a transient induced by a power failure in a pumping system. The focus of these studies was usually to predict the maximum pressure, normally the first peak, in a pipe system, or minimum pressure to avoid cavitation. The overall objective was the safety of the pipeline. However, to apply a transient event in the inverse transient method requires not only the prediction of the first peak value, but also reliable prediction of entire transient event. Because the inverse transient method is based on the comparison of measured and simulated transients, the simulated transients must be accurate and equal the measurements in phase as well as magnitude in order to achieve proper timing between the measurements and the

simulation. Many factors can influence the accuracy of the prediction of a transient event. These factors (not all) include

1. Skeletonisation of a pipe network system. A pipe network normally consists of large number of pipes with different properties and sizes. Accurate use of the method of characteristics as a numerical method requires that the Courant number (C_r) for each pipe section used in the simulation to be close to unity. By applying a suitable interpolation scheme or wave speed adjustment technique, this requirement can be relaxed to some degree; however, an interpolation scheme introduces numerical errors. Chen (1995) investigated a number of different interpolation schemes and concluded that a third-order time interpolation scheme was the best choice from accuracy and calculation efficiency points of view. During the design of the laboratory pipe network, the length of each pipe section was designed so that Courant number of each of the computational units is equal to one. Therefore, interpolation issues were not required.

2. Simplification of a pipe network. Including all pipe branches within a water distribution system, such as the small pipes to a residence, and some very small dead ends created by closed valves is not practical. In the laboratory network, a short dead end of 300mm long is formed when a valve is closed. The influence of these dead ends on a transient event is investigated in this study.

3. Unsteady friction. Predominately, the transients in the pipe networks are simulated based on a quasi-steady friction model (Darcy-Weisbach). Using steady friction the first cycle of a transient event can be simulated accurately; however, subsequent damping of the transient is under predicted. Although several unsteady friction models have been developed, no efficient and universally applicable model is available for transient simulation in a pipe network system. A general theory for unsteady friction still needs considerably more research and investigation (Brunone et al. 2002). In this study, the existing unsteady models are reviewed, and suitable unsteady friction models for the transient simulation used in ITM for leak detection are chosen considering accuracy and computing efficiency.

4. Minor losses of pipe junctions. In a pipe network system, there are many non-pipe elements including different types of valves, pumps and pump stations, tees, junctions, and air tanks. In the simulation of pipe network systems, the minor losses from junctions and bends are normally neglected. However, these minor losses from junctions can significantly influence the steady state conditions in a pipe network, especially those in which the pipes have large diameter-length ratios (Wood et al. 1993). For these cases, the

pipe friction loss is small compared to the minor losses. The influence of the minor losses from pipe junctions on the unsteady flow in a pipe network system is investigated in this chapter.

7.3 Governing equations

Unsteady equations for the conservation of mass and momentum describe the transient flow in the closed pipes. There are several classical textbooks for the derivation of the governing equations for transient flow in closed pipes (Chaudhry 1986; Wylie and Streeter 1993). A simple description of the governing equations and algorithms used in NETTRANS, a transient simulation program used in this study, is given in this section and the following two sections (Sections 7.4 and 7.5).

Using the Reynolds transport theorem and concept of control volume, simplified governing equations for water transients in pipes can be obtained based on the following assumptions:

1. Slightly compressible fluid
2. Elastic pipe wall
3. One-dimensional flow (radial velocity and velocity distribution is small)
4. Fluid velocity is much smaller than the wave speed

Then the unsteady continuity and momentum equations are

$$\frac{\partial p}{\partial t} + V\frac{\partial p}{\partial x} + \rho a^2 \frac{\partial V}{\partial x} = 0 \tag{7.1}$$

$$\frac{\partial V}{\partial t} + V\frac{\partial V}{\partial x} + \frac{1}{\rho}\frac{\partial p}{\partial x} + g\sin\theta + gJ = 0 \tag{7.2}$$

in which, x = distance along the pipe, t = time, p = pressure, V = velocity, ρ = density, g = gravity acceleration, θ = slope of the pipe with horizontal, D = pipe diameter, f = the Darcy-Weisbach friction factor, a = transient wave speed, and J = friction resistance term during the transient event. The calculation of the friction resistance is normally divided into two parts: a steady friction term and an unsteady friction term as

$$J = J_s + J_u \tag{7.3}$$

where $J_s = \frac{fV|V|}{2gD}$ = quasi-steady friction resistance, and J_u = unsteady friction resistance.

Several models have been developed for the calculation of the unsteady friction, and these models are discussed in the next section.

In most engineering applications, the convection terms are relatively small compared to other terms, and may be neglected. After replacing p and V by piezometric head H and discharge Q, which are common in hydraulic engineering analysis, simplified governing equations for transients in closed pipes are

$$\frac{\partial H}{\partial t} + \frac{a^2}{gA}\frac{\partial Q}{\partial x} = 0 \tag{7.4}$$

$$\frac{\partial H}{\partial x} + \frac{1}{gA}\frac{\partial Q}{\partial t} + J = 0 \tag{7.5}$$

Discharge from a leak is a function of pressure in a pipe and size of a leak and may be expressed by the orifice equation

$$Q_L = C_d A_L \sqrt{2g\Delta H_L} \tag{7.6}$$

where $\Delta H_L = H_L - z_L$ = pressure head at a leak (assuming the pressure outside of the pipe is atmospheric), H_L = piezometric head in the pipeline at the leak, z_L = pipe elevation at the leak, C_d = leak discharge coefficient, and A_L = leak area.

7.4 Unsteady friction models

The quasi-steady transient models, in which the shear stress is approximated by steady-state friction dissipation formulas, fail to predict accurately the transient pressure (head) behaviour beyond the first cycle. The main reason for this failure stems from the inability of the steady-state dissipation formulas to incorporate the two-dimensional, sometimes three-dimensional, dynamic behaviour of the velocity field in a transient event. A number of unsteady friction models have been developed during the past 40 years to account for the effects of the dynamic behaviour of the velocity field on the shear stress, and then on the pipeline transients. In the review of Bergant et al. (2001), unsteady friction models were classified into six groups depending on the relationship between the unsteady friction term and the mean flow velocity. Two different classification methods were

applied in Vítkovský (2001) to the proposed unsteady friction model. In the first classification system, the unsteady friction models were divided into seven groups: instantaneous velocity based models, simple temporal acceleration based models, complex temporal acceleration based models, derivative of acceleration based models, boundary layer based models, velocity profile shell models and turbulence based models. An alternative classification for unsteady friction models is based on their applicability, namely: steady flow, pure accelerating or decelerating flows, oscillating flows, water hammer flows, transition (from laminar to turbulence) flows and generalised flows.

Among these different types of unsteady friction models, three types have been widely used during the past decade because they agree better with experiment. These are:
1. Unsteady friction models based on the derivatives of instantaneous flow velocity. This type of model includes that of Brunone et al. (1995) and several modified Brunone models (Vítkovský et al. 2000, Bughazem and Anderson 2000, Pezzinga 2000).
2. Convolution based unsteady friction models. This group has been used by Zielke (1968) and modified by Trikha (1975) and Suzuki et al. (1991) for laminar flow region and by Vardy and Brown (1996) and Ghidaoui and Mansour (2002) for turbulent flow.
3. Two-dimensional and quasi-two-dimensional models. Most of these approaches are for turbulence flow (Vardy and Huang 1991; Eichinger and Lein 1992; Silva-Araya and Chaudhry 1997; Silva-Araya and Chaudhry 2001; Pezzinga 1999). Prado and Larreteguy (2002) presented a quasi-two-dimensional laminar model to calculate the shear stress in water hammer problems.

Among these three groups of unsteady friction models, the two-dimensional approaches provide a detailed description of the instantaneous velocity profile, shear stress and dissipation fields during a water hammer event. The results of these two-dimensional models generally have been found to be in good agreement with available laboratory data. However, the associated computational expense often makes these models impractical, especially for the purpose of inverse calculation, in which a significant number of transient runs are involved. In the convolution based models, the calculation of the wall shear stress, which is fundamentally a two dimensional problem is reduced to an one dimensional problem by relating the calculation of shear stress to the instantaneous mean velocity and to the weighted past velocity changes. These types of models are physically based models although there are several assumptions in Vardy-Brown model (1996) to

deal with the turbulent pipe flow. Due to the dimensional reduction from two to one, convolution based unsteady friction models are more computational efficient than two-dimensional models. However, the computational costs increase significantly as the time steps increase in these models because the calculation of shear stress is based on weighted past velocity changes. Several numerical algorithms (Kagawa et al. 1983; Suzuki et al. 1991) have been presented with the goal of improving the efficiencies of these models; however, the computational time based on these improved models is still significantly large from inverse transient point of view. Some of these improved models (Trikha 1975; Ghidaoui and Mansour 2002) sacrifice accuracy.

In contrast, unsteady friction models based on the derivatives of instantaneous flow velocity are empirical models, and there is no clear physical meaning for the terms and parameters used in these models. Axworthy et al. (2000) derived instantaneous acceleration-based unsteady friction models from extended irreversible thermodynamics and provide some physical explanations for these types of models, although these explanations are only valid for limited cases (Ghidaoui and Mansour 2002). The major advantage of these types of models over other types of unsteady friction model is their efficiency. The computational time for the unsteady friction models based on instantaneous velocity is hundreds or thousands times less than the convolution-based models and two-dimensional approaches. Because the efficiency of the transient model is important for the application of the inverse transient method, a modified Brunone unsteady friction model called k_A & k_P model (Vítkovský et al. 2000) was chosen for this study for the calculation of unsteady friction in the transient model. Before applying the transient model in ITM for leak detection, the model has been carefully calibrated in experimental tests to determine the values of the parameters.

A general form of the relationship for a modified Brunone unsteady friction model (Vítkovský 2001) is:

$$J_u = \phi_V \frac{k_A}{gA}\left|\frac{\partial Q}{dt}\right| + \frac{k_P}{gA}\frac{\partial Q}{dt} \tag{7.7}$$

in which $\phi_V = 1$ for $V \geq 0$, $\phi_V = -1$ for $V < 0$, and k_A and k_P = undetermined unsteady friction parameters. Parameter k_A influences the damping of a transient event and

parameter k_P influences the phase. For slow transient events $k_P = 0$. The values of these parameters are defined as (Vítkovský 2001)

$$K_A = 3.75\sqrt{\frac{f}{512}} \text{ and } K_P = \frac{5f}{128\kappa^2} + 3.75\sqrt{\frac{f}{512}} \tag{7.7a}$$

where $\kappa = 0.4$ is von Karman constant.

7.5 The method of characteristics (MOC)

The continuity and momentum equations (7.4) and (7.5) are nonlinear, hyperbolic partial differential equations. No closed-form solution exists for these equations. However, they can be solved numerically using the finite difference method (Holloway and Chaudhry 1985; Streeter 1972), the method of characteristics (MOC) (Streeter 1972; Wylie and Streeter 1993), the finite element method (Baker 1983), the spectral method (Gottlieb and Orszag 1977) and the boundary integral equation method (Liggett 1984). Among these methods, the MOC has become quite popular and is extensively used. It has been proven that the MOC is superior to other methods for solving the transient governing equations for pipe flow in several aspects, such as correct simulation of steep wave front, easy programming, conceptual simplicity and efficiency of computation (Wylie and Streeter 1993).

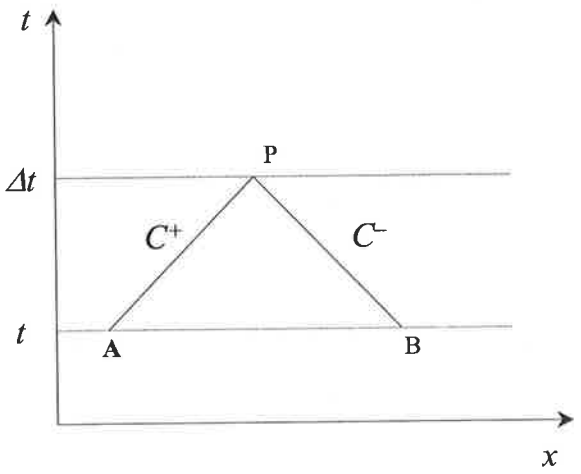

Figure 7.2 Characteristic grids

The characteristic equations are (Wylie and Streeter 1993)

$$\frac{dH}{dt}+\frac{a}{gA}\frac{dQ}{dt}+Ja=0,\quad \text{along } \frac{dx}{dt}=a \tag{7.8}$$

$$-\frac{dH}{dt}+\frac{a}{gA}\frac{dQ}{dt}+Ja=0,\quad \text{along } \frac{dx}{dt}=-a \tag{7.9}$$

The partial derivatives over time and space in equations (7.4) and (7.5) are expressed in ordinary derivatives in equation (7.8) and (7.9). This allows the dependent variables H and Q to be solved directly by integration. However, there are tradeoffs, which limit the solution only along the characteristic lines (Figure 7.2). When Eqs. (7.8) and (7.9) are solved using the finite difference method, the Courant-Friedrich-Lewy (CFL) stability condition requires

$$\Delta t\, a \le \Delta x \tag{7.10}$$

The Courant number C_r is defined as:

$$C_r=\frac{a\Delta t}{\Delta x}. \tag{7.11}$$

When Courant number is less than 1, interpolation schemes (Chen 1995) are necessary in the finite difference scheme to analyse a system. These interpolation schemes introduce numerical dispersion and attenuation. Therefore, the Courant number should be as close to unity as possible to ensure numerical accuracy. In this study, the Courant number is restricted to be equal to 1.0 for all the cases.

Substituting Eqs. (7.3) and (7.7) into Eqs (7.8) and (7.9) gives

$$\frac{dH}{dt}+\frac{a}{gA}\frac{dQ}{dt}+\frac{faQ^2}{2DgA^2}+\left(\phi_V\frac{ak_A}{gA}\left|\frac{dQ}{dt}\right|+\frac{ak_P}{gA}\frac{dQ}{dt}\right)=0,\ \text{along } \frac{dx}{dt}=a \tag{7.12}$$

$$-\frac{dH}{dt}+\frac{a}{gA}\frac{dQ}{dt}+\frac{faQ^2}{2DgA^2}+\left(\phi_V\frac{ak_A}{gA}\left|\frac{dQ}{dt}\right|+\frac{ak_P}{gA}\frac{dQ}{dt}\right)=0,\ \text{along } \frac{dx}{dt}=-a \tag{7.13}$$

in which, terms in the parentheses are the unsteady friction terms. By applying suitable difference schemes, the pressure head (H) and discharge (Q) can be solved along the characteristic lines. Since the time variation of the velocity along the characteristic grid is unknown, a second order implicit approximation of Q, which has been proven to be an accurate and stable scheme, is used in the unsteady friction resistance term. Therefore, the compatibility equations considering the unsteady friction effects by a k_A & k_P model (Vítkovský 2001) may be expressed as

$$(H_P - H_A) + \frac{a}{gA}(Q_P - Q_A) + \frac{f\Delta x}{2gDA^2}\frac{(Q_A + Q_P)^2}{4} + \frac{k_P}{2gA}\left(\frac{dQ_A}{dt} + \frac{dQ_P}{dt}\right)\Delta x + \phi_V^+ \frac{k_A}{2gA}\left|\frac{dQ_A}{dt} + \frac{dQ_P}{dt}\right|\Delta x = 0 \tag{7.14}$$

$$(H_P - H_B) - \frac{a}{gA}(Q_P - Q_B) - \frac{f\Delta x}{2gDA^2}\frac{(Q_B + Q_P)^2}{4} - \frac{k_P}{2gA}\left(\frac{dQ_B}{dt} + \frac{dQ_P}{dt}\right)\Delta x + \phi_V^- \frac{k_A}{2gA}\left|\frac{dQ_B}{dt} + \frac{dQ_P}{dt}\right|\Delta x = 0 \tag{7.15}$$

where the velocity sign operator (ϕ_V) for each compatibility equation is

$$\phi_V^+ = \begin{cases} +1 & \text{if} \quad Q_A + Q_P \geq 0 \\ -1 & \text{if} \quad Q_A + Q_P < 0 \end{cases} \text{ and } \phi_V^- = \begin{cases} +1 & \text{if} \quad Q_B + Q_P \geq 0 \\ -1 & \text{if} \quad Q_B + Q_P < 0 \end{cases} \tag{7.16}$$

In a pipe network, there are four unknown for each pipe section: the upstream flow (Q_u), upstream head (H_u), downstream flow (Q_d) and downstream head (H_d). Besides the above two compatibility equations, Eq. (7.14) and Eq. (7.15), there are two more relationships available: heads of pipe sections at a junction are equal, and a mass is conserved at the junctions. At the boundaries, where these two additional relationships are not available, either head measurement, flow measurement or a relationship between head and flow is needed. By combining all the equations including the boundary conditions, the simultaneous system can be written in a matrix form as

$$[M]\{v^*\} = \{R\} \tag{7.17}$$

where $[M]$ = a matrix of the coefficients of the unknown variables, $\{v^*\}$ = a vector of the unknown heads and flow at present time step and $\{R\}$ = a vector containing other relationships not dependent on the unknown variables.

7.6 Minor losses from elbows and junctions

For a single pipeline system, minor losses, such as the loss though an elbow, are normally neglected compared with the friction loss since the pipelines normally has large pipe length to pipe diameter ratios (commonly called slenderness ratios). However, for a pipeline network, minor losses from non-pipe elements and friction loss in some short pipe sections could be of similar magnitude, making them non-negligible. Wood et al. (1993) studied pipe networks dominated by pipe junctions and showed that steady flows

in a pipe network with small slenderness ratios were significantly different when the minor losses from junctions are considered. There are no accurate theoretical solutions to calculate minor losses from a pipe junction, or an elbow. Formations of minor losses involve complex mixing, flow separation and viscous dissipation mechanisms. Those minor losses are normally calculated by a minor loss coefficient K obtained from experiments (Miller 1978) at steady state flow conditions. Effects of pipeline bends and junctions on transient events were experimentally investigated by Wood and Chao (1971). The first transient peaks were measured. They found a one percent attenuation of the first peak of a transient event by a 90° elbow. For a T type junction, no obvious influence on the first peaks of a transient event was observed compared to the traditional analysis where the minor losses were neglected. In addition to the first peak, the influence of the minor losses from a bend or a junction on a whole transient, which is important for the application the ITM, is not known. In the study detained in this chapter, the minor losses from 90° elbows and T junction are investigated.

7.6.1 Minor losses from elbows

The minor loss from an elbow is normally defined as

$$H_e = K_e \frac{V^2}{2g} \tag{7.18}$$

where H_e = head loss due to an elbow, and K_e = minor losses coefficient for the elbow. For steady state flow, the value of K_e depends on the deflection angle of the elbow, the ratio of radius of curvature of elbow and pipe diameter and Reynolds number of flow. K_e normally has a range of 0.2 to 1.5 (Miller 1978).

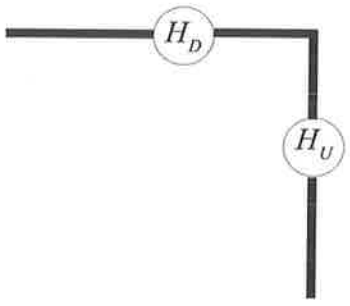

Figure 7.3 An elbow considered in a transient model

To investigate the effects of elbow on a water hammer event, Eq. (7.18) can be incorporated into a transient model by considering an elbow using a pipe section with a negligible length as shown in Figure 7.3. Assuming the minor loss coefficient in the transient state is same as that in the steady state,

$$H_D - H_U = K_e \frac{Q_D^2}{2gA^2} \tag{7.19}$$

Considering mass conservation in the elbow gives

$$Q_U = Q_D \tag{7.20}$$

Although the flow changes direction at an elbow, in a one-dimensional model effect of an elbow on transients is same as a blockage studied in Chapter 6; both are expressed by a minor loss coefficient. Therefore, all the results obtained from Chapter 6 for a blockage can be applied to an elbow. Although no analytical solution is available for transients in a pipe network, the analytical solution in a single pipeline including an elbow can help understand the significance of an elbow on fluid transients in a pipe network.

The relative importance of an elbow on a transient event can be expressed by

$$r_e = \frac{R_{ne}}{R + R_{ne}} \tag{7.21}$$

where r_e = ratio of an elbow-induced damping over total transient damping, R = friction damping coefficients defined in Eq. (6.15), R_{ne} = elbow (blockage)-induced damping on the nth component defined in Eq. (6.33). Substituting Eqs. (6.15) and (6.33) into Eq. (7.21) gives

$$r_e = \frac{2K_e \frac{Q_0^2}{2gA^2}\cos^2(n\pi x_e^*)}{\frac{fL}{D}\frac{Q_0^2}{2gA^2} + 2K_e \frac{Q_0^2}{2gA^2}\cos^2(n\pi x_e^*)} = \frac{S_e \cos^2(n\pi x_e^*)}{1 + S_e \cos^2(n\pi x_e^*)} \tag{7.22}$$

where $S_e = \frac{2DK_e}{fL}$ = sensitivity parameter of an elbow on a transient event, $x_e^* = x_e / L$ = dimensionless location of the elbow and x_e = location of the elbow.

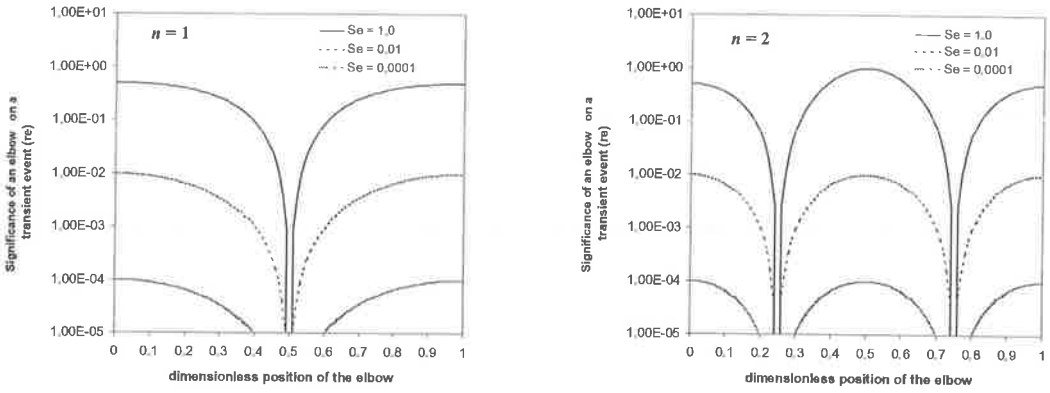

Figure 7.4 Significance of an elbow on transients in a pipeline

Figure 7.4 plots the variation of elbow significance parameter r_e with different values of S_e for the harmonic components $n = 1$ and $n = 2$. The figure shows that the significance of an elbow on a transient event depends on the location of the elbow along the pipeline and the value of sensitivity parameter of S_e, which is a function of elbow loss coefficient (K_e), pipe friction factor (f) and the slenderness ratio (L/D). Since variations of elbow loss coefficient ($K_e = 0.2 \sim 1.5$) and pipe friction factor ($f = 0.01 \sim 0.03$) are relatively small for most of flow conditions, the influence of an elbow on a transient event in a pipeline is more dependent on the geometry of a pipe ($L/D = 1.0 \sim 1.0\times10^5$) and the dimensionless location of the elbow ($x_e^* = 0 \sim 1.0$). For a pipe system with a large slenderness ratio (L/D), the minor losses become less significant.

According to the definition of minor losses in Eq. (7.18), they are proportional to the square of the velocity. For a very small velocity, the minor loss will be close to zero. Therefore, if the flow in a pipe is small, the minor loss, as well as the steady friction loss, is negligible. For such a situation, the dominant loss during a transient event will be the unsteady friction loss, which is more dependent on the speed of the transient event based on the analysis in Section 4.7 of Chapter 4.

Two examples of effects of minor losses at elbows on different transient events illustrate their effects.

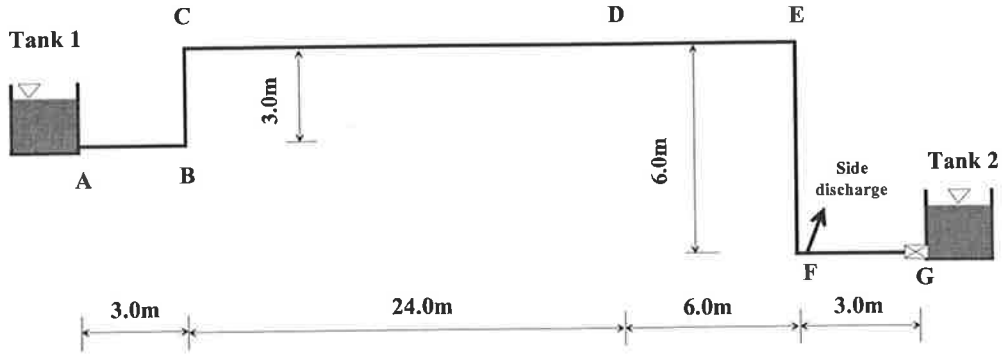

Figure 7.5 A pipe system with elbows

For the pipe system as shown in Figure 7.5, four 90-degree elbows are installed at points B, C, E and F. The minor loss coefficient for each bend is $K_e = 0.6$. The other parameters of the system are

Water level at Tank 1 $H_1 = 3.98$m

Water level at Tank 2 $H_2 = 1.45$m

Wave speed $a = 1030$ m/s

Inside diameter of the pipe $D = 72.94$mm

Relative pipe roughness $\varepsilon/D = 2.0\times10^{-5}$

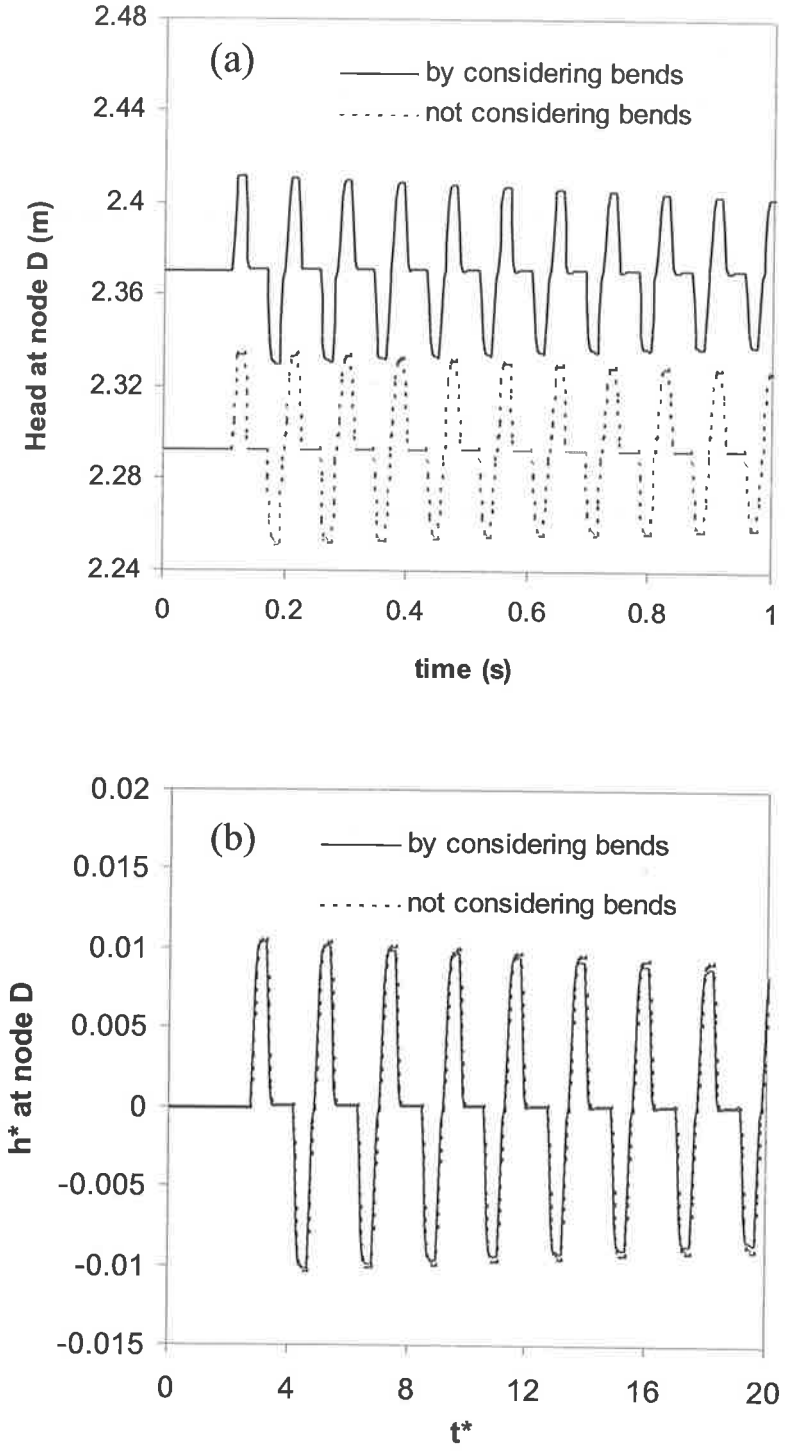

Figure 7.6 Effects of elbows, (a) real-time scale (b) dimensionless scale

For the first example a transient is initiated by closing a small side discharge at point F (see Figure 7.5) at time t = 0.1s from the steady state condition. The size of the side discharge valve is $C_d A_S = 0.2\times10^{-6}\text{m}^2$, and the closing time of the side discharge is 0.02s.

The Darcy-Weisbach friction factor is calculated as f = 0.017, and the sensitivity parameter of elbow S_e (defined in Eq. 7.22) is calculated as 0.114, which is not negligible (see Figure 7.4). The transients at point D (as shown in Figure 7.5) are presented in Figure 7.6 with and without the effects of minor losses. Minor losses at elbows have a significant influence on the steady flow conditions in the pipeline. When the minor losses at elbows are not considered, the steady velocity in the example is V_0 = 2.18 m/s. If the minor losses are considered, the steady velocity is reduced to V_0 = 1.95 m/s. As a result, the heads (H) at point D are different for the two cases as shown in Figure 7.6(a). The damping effect of the elbows on the transient event is shown in Figure 7.6(b) where $h^* = (H-H_0)/H_1$.

In the second example, the transients are generated by closing a partially open valve at point G (in Figure 7.5) from a steady state of Q_0 = 0.1L/s (V_0 = 0.024m/s). The valve is closed within a time period of 0.0s~0.12s. The transients at point D are presented in Figure 7.7. In this example, since the flow in the pipe is so small, the influence of the minor losses on the transient is negligible.

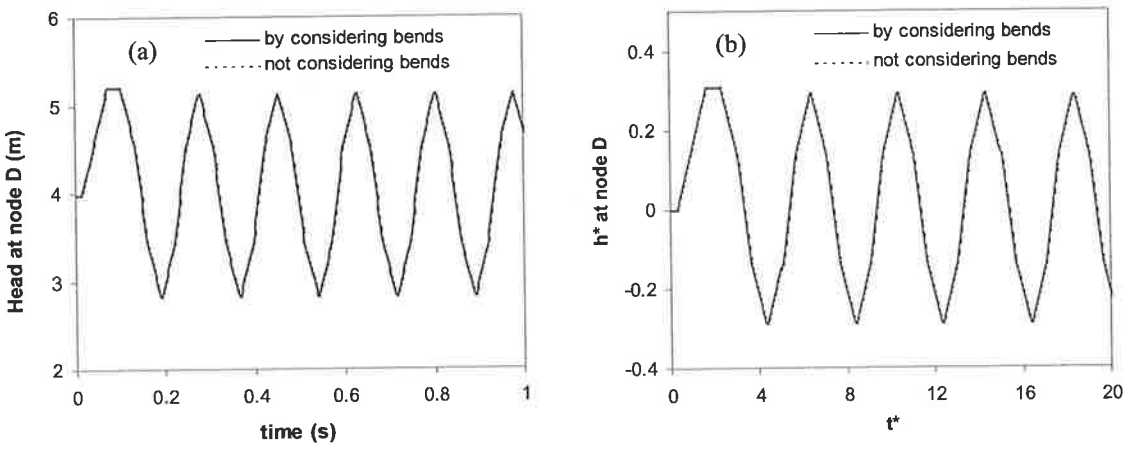

Figure 7.7 Effects of elbows on transients at a small steady state velocity,(a) real-time scale and (b) dimensionless scale

7.6.2 Minor losses from pipe junctions

Compared to an elbow, the minor loss from a pipe junction is more complicated since the minor loss coefficients depend not only on ratios of flow rates in the legs but also on flow directions (Miller 1978). A method to include minor losses from junctions for the simulation of steady states in pipe networks was presented by Wood et al. (1993), in which the calculation of the minor losses from junctions was added in the individual legs. In transient flow, the flow in each leg of a junction changes with time, and the direction of the flow may or may not change depend on the magnitude of the flow changes. Currently, there appears to be no experimental tests available for the loss coefficients under unsteady flow. In this study, the steady state loss coefficients are used in unsteady flow. Based on this assumption, the effects of minor losses from a junction on a transient event are studied numerically. The results in this section are verified experimentally in Chapter 8.

Minor losses from a pipe junction can be simulated using small "head-loss" pipe sections without a length as shown in Figure 7.8. In Figure 7.8, node 0 is a junction connecting three pipes. Nodes 5, 6 and 8 are normal nodes. To simulate the minor losses at such a junction, a "head loss" pipe section (pipes No. 0-1, 0-2, and 0-3) is added at each pipe leg connected to the junction. The minor losses for different legs can be specified by head loss coefficients (K_{ij}) in the corresponding small pipe sections as

$$\Delta H_{10} = K_{10}\frac{(V_1)^2}{2g},\ \Delta H_{20} = K_{20}\frac{(V_2)^2}{2g},\ \Delta H_{03} = K_{30}\frac{(V_3)^2}{2g} \tag{7.23}$$

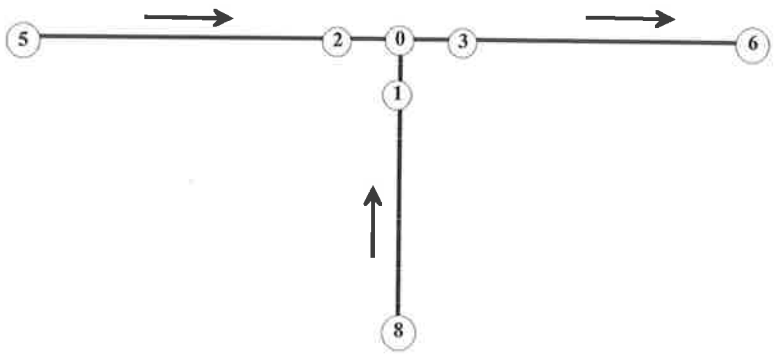

Figure 7.8 Simulation of minor losses at pipe junctions

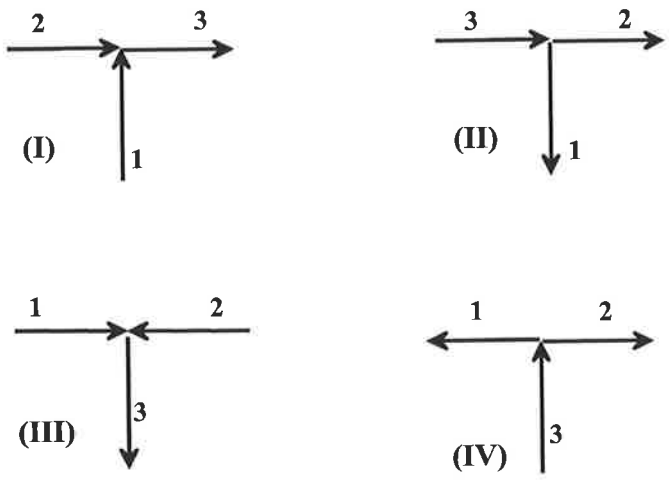

Figure 7.9 Types of pipe junctions

Thus, in principle there is no difference between calculations of minor losses at elbows and minor losses at junctions as outlined here. The main problem in calculating minor losses at a pipe junction is the calculation of the **head loss** coefficients. These coefficients vary with the geometry and flow conditions of junctions. In the pipe network at the University of Adelaide, pipe junctions can be classified into four types as shown in Figure 7.9, where leg 3 is the converging (combining) leg and the cross-section areas for three legs are same. The **minor loss** coefficients for different types can be calculated by the following (Miller 1978; Wood et al. 1993) formulas:

Type (I):

$$K'_{13} = -0.92(1-q^2)+1.2q^2 \text{ and } K'_{23} = -0.41q^2 + 0.94q^2 + 0.03 \tag{7.24}$$

Type (II):

$$K'_{31} = 1.45q^2 - 1.1q + 0.95 \text{ and } K'_{32} = 0.58q^2 - 0.14q + 0.03 \tag{7.25}$$

Type (III):

$$K'_{13} = K'_{23} = 2 + 3(q^2 - q) \tag{7.26}$$

Type (IV):

$$K'_{31} = 1 + 0.3q^2 \text{ and } K'_{32} = 1 + 0.3(1-q)^2 \tag{7.27}$$

where $q = Q_1/Q_3$, and the **minor loss** coefficients K'_{i3} and K'_{3i} ($i = 1$ and 2) are defined by (Miller 1978; Wood et al. 1993)

$$\frac{(V_i)^2}{2g} + H_i - \frac{(V_3)^2}{2g} - H_3 = K'_{i3}\frac{(V_3)^2}{2g} \tag{7.28}$$

$$\frac{(V_3)^2}{2g} + H_3 - \frac{(V_i)^2}{2g} - H_i = K'_{3i}\frac{(V_3)^2}{2g} \tag{7.29}$$

The definition of minor loss coefficients includes the velocity head, while the **head loss** coefficients are defined by

$$H_i - H_3 = K_{i3}\frac{(V_3)^2}{2g} \tag{7.30}$$

$$H_3 - H_i = K_{3i}\frac{(V_3)^2}{2g} \tag{7.31}$$

Substituting Eqs. (7.30) and (7.31) into Eqs. (7.28) and (7.29) gives

$$K_{i3} = K'_{i3} + 1 - q^2 \text{ and } K_{3i} = K'_{3i} - 1 + q^2 \tag{7.32}$$

The head losses calculated from Eq. (7.32) are the total head losses across the junction, which occur at two legs. For example, coefficient K_{13} is for the total head losses occurred at leg 0-1 and leg 0-3. To apply the method described in Eq. (7.23), the total head loss needs to be portioned into each leg. For junctions of types II and IV, most of the total head loss occurs at the downstream of the junction (Miller 1978). Thus

$$K_{01} = K_{31},\ K_{02} = K_{32} \text{ and } K_{30} = 0. \tag{7.33}$$

For junctions of types I and III, the head loss at each leg is calculated by

if $K_{13} > K_{23}$: $K_{20} = 0$, $K_{03} = K_{23}$, and $K_{10} = K_{13} - K_{23}$. (7.34)

if $K_{13} < K_{23}$: $K_{10} = 0$, $K_{03} = K_{13}$, and $K_{20} = K_{23} - K_{13}$. (7.35)

Application using Eqs. (7.23) to (7.35) in simulating minor losses at pipe junctions has been embedded into the program NETTRANS. Because the minor loss coefficients vary with flow rates in each leg, iterative solution procedure is needed. After each iteration in which flow rates are calculated, the loss coefficient at each leg is re-evaluated using the new flow rates. The iterations continue until changes of calculated flow rates are lower than a limit value. More details of this program are introduced in Section 7.9. Similar to minor losses at elbows, the minor losses at junctions are proportional to the square of velocity at junction. Therefore, if the flow at a junction is small, the minor losses at such a junction are negligible.

7.7 Effects of dead ends on transients

When a branch in a network is closed (by a shut valve, for example), a dead end is created. For steady state analysis, that branch can be removed from the network calculation since the flow in it is zero. However, for transient analysis, the dead end may or may not materially influence the solution. A dead end of length approximating other pipe sections in a pipe network can be included in the simulation model as a normal pipe section without difficulty. However, if a control valve in a branch is installed close to a junction, a very short dead end section is created after the valve is closed. If that dead end is considered as a normal computation reach of the MOC, the entire network must be divided into many computational sections of similar length if the Courant number is to be close to unity. Otherwise, accuracy is not guaranteed due to the error induced by interpolation. Therefore, alternative ways must be found in a transient model to consider the effects of dead ends on a transient event. In this section, a lumped parameter model (LP) is developed for this purpose.

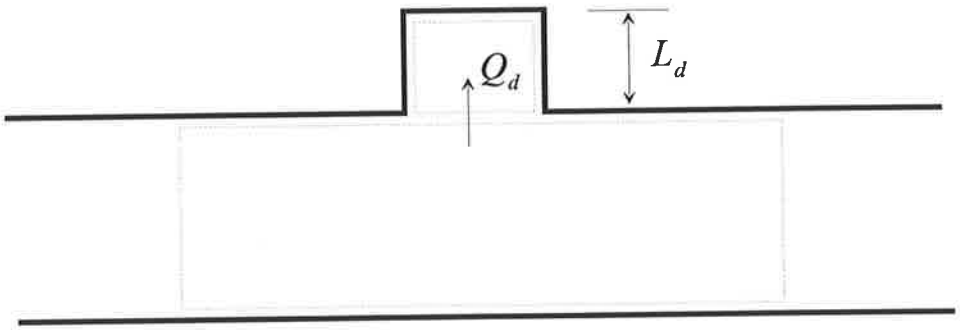

Figure 7.10 A short dead end

7.7.1 A transient model with a lumped parameter dead end

The pressure variation in a short dead is small during a transient event. Therefore, the pressure can be assumed uniform in the dead end (Wylie and Streeter 1993). Integrating the continuity equation (Eq. 7.4) along a dead end gives

$$Q_d = -\frac{\partial H_d}{\partial t}\frac{gW_d}{a_d^2} \tag{7.36}$$

where a_d = wave speed in the dead end section, W_d = volume of the dead end, g = gravitational acceleration, Q_d = flow rate into the dead end and H_d = pressure head in the dead end, which is assumed uniform.

Eq (7.36) can be incorporated in a normal transient program based on the method of characteristics by including Eq (7.36) in the continuity equation at the node where the dead end is connected.

7.7.2 An analytical solution

Using a Dirac delta function (see Chapter 3) gives the continuity equation for the unsteady flow in a pipeline including a dead end as

$$\frac{\partial H}{\partial t}+\frac{Q}{A}\frac{\partial H}{\partial x}+\frac{a^2}{gA}\frac{\partial Q}{\partial x}-\frac{a^2}{gA}Q_d\delta(x-x_d)=0 \tag{7.37}$$

and the conservation of momentum for a pipe with a dead end perpendicular to the pipe axis is

$$\frac{\partial H}{\partial x}+\frac{1}{gA}\frac{\partial Q}{\partial t}+\frac{Q}{gA^2}\frac{\partial Q}{\partial x}+\frac{fQ^2}{2DgA^2}-\frac{QQ_d\delta(x-x_d)}{gA^2}=0 \tag{7.38}$$

Assuming the magnitude of the transient being small (q^*<<1.0), a dimensionless governing equation for the transients in a pipeline with a dead end may be expressed as

$$\frac{\partial^2 h^*}{\partial x^{*2}}=[1+C\delta(x^*-x_d^*)][\frac{\partial^2 h^*}{\partial t^{*2}}+2R\frac{\partial h^*}{\partial t^*}] \tag{7.39}$$

where $x^*=x/L$= dimensionless distance, $t^*=t/(L/a)$= the dimensionless time, L = pipeline length, a = wave speed, $h^*=(H-H_0)/H_1$= the dimensionless head of the transient, H = transient head, H_0 = steady-state head, H_1 = a reference head at a tank, $R=fLQ_0/(2DaA)$= resistance term, Q_0 = steady-state flow rate, f = Darcy-Weisbach friction factor, D = pipe diameter, A = pipe cross section area, $C=\frac{a^2W_d}{a_d^2W}$= dead end parameter, a_d = wave speed in the dead end, W_d = volume of the dead end, $\delta(x^*-x_d^*)$= Dirac delta function, $x_d^*=x_d/L$= dimensionless location of the dead end and x_d = position of the dead end along the pipeline.

For a pipeline connected between two reservoirs with constant heads, the solution to Eq. (7.39) is (details of the derivation of the solution are given in Appendix D)

$$h^*(x^*,t^*) = \sum_{n=1}^{\infty}\left\{e^{-Rt^*}\left[A_n\cos(\lambda t^*) + B_n\sin(\lambda t^*)\right]\sin(n\pi x^*)\right\} \tag{7.40}$$

in which $$\lambda = \frac{n\pi}{\sqrt{1+S_d}} \qquad (n = 1, 2, 3,\ldots) \tag{7.41}$$

and $$S_d = 2C\sin^2(n\pi x_d^*) \tag{7.42}$$

The analytical solution in Eq. (7.40) shows that presence of a dead end in a single pipeline changes the frequencies of the Fourier components. The significance of the effect depends on the parameter S_d defined in Eq. (7.42), which is related to the location of the dead end, relative volume and wave speed of the dead end compare to the pipeline.

7.7.3 Numerical examples

Two numerical examples including a slow and a fast transient event are presented in this section to visualise the effects of a dead end on fluid transients. In addition, the accuracy of the lumped parameter (LP) model discussed in Section 7.7.1 and analytical solution presented in Section 7.7.2 will be verified by comparing to the normal MOC approach in which the dead end is considered as a normal pipe section by dividing the pipeline into a large number of reaches.

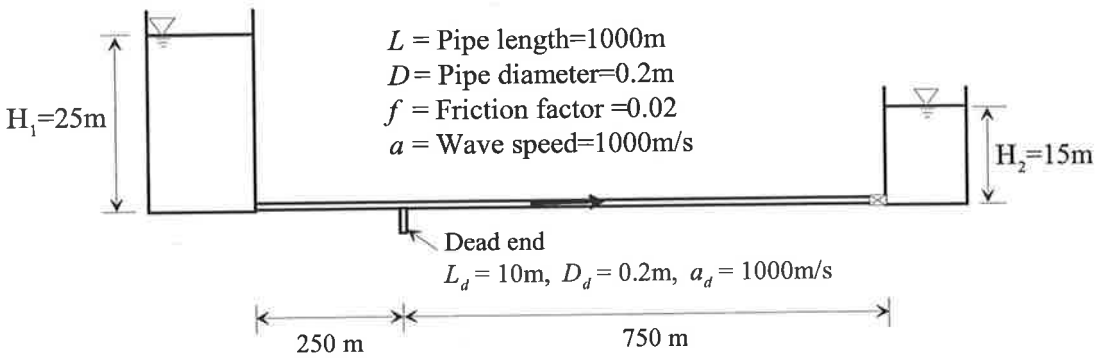

Figure 7.11 A single pipeline with a dead end

For the pipeline connecting two constant-head reservoirs as shown in Figure 7.11, there is a dead end located at the 250m from the upstream reservoir. The length of the dead end is

1% of the pipeline length (L_d = 10m, L = 1000m), and the diameter of the dead end is same as the diameter of the pipeline ($D_d = D$ = 0.2m). The wave speed in the dead end is same as that in the pipeline ($a_d = a$ = 1000m/s). To include such a dead end in a normal MOC simulation and keep the Courant number close to unity, the pipeline reach in the pipeline should be close to the length of the dead end. In this example, the pipeline is divided into 200 reaches and the dead end is divided into 1 reaches giving a Courant number of $C_r = 1.0$.

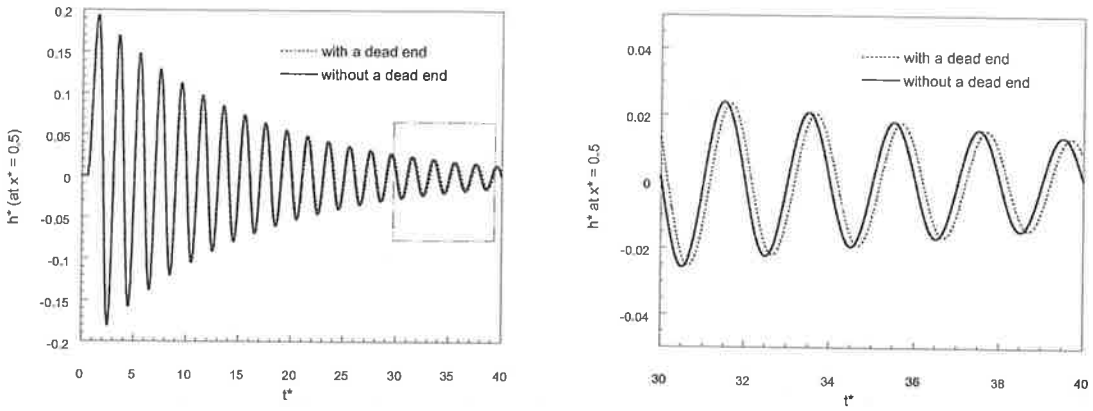

Figure 7.12 Effect of dead end on a slow transient (MOC)

In the first example, a slower transient event is generated by changing the water level at the downstream reservoir in a manner by which a sinusoidal transient is generated in the pipeline. The variation in water level at the downstream reservoir is defined as

$$H_2 = 15 + 5\sin^2(0.5\pi t) \qquad (0 \le t \le 2.0) \qquad (7.43)$$

The mean velocity in the pipeline is V_0 = 1.40 m/s giving the friction damping coefficient $R = (fLV_0)/(2Da) = 0.07$. The dead end parameter C and S_d are calculated as $C = \dfrac{a^2 W_d}{a_d^2 W} =$ 0.01 and $S_d = 2C\sin^2(n\pi x_d^*) = 0.01$ given $n = 1$. The dominant frequency (n = 1.0) of the pipe transient is 1.0π without the dead and 0.995π (Eq. 7.41) with the dead end based on the analytical solution. The transients calculated by the MOC are presented in Figure 7.12 for both cases of with and without a dead end. The effect of the dead end on the transient is not very significant. However, by zooming into details a phase shift between two cases is evident. The total time shift within 40 seconds (20 periods) is 0.2 seconds giving the

frequency difference of 0.005π (= $2\pi/(40/20)-2\pi/(40.2/20)$) for the two events. This frequency difference is in agreement with the analytical solution in Eq. (7.41) for $n = 1$.

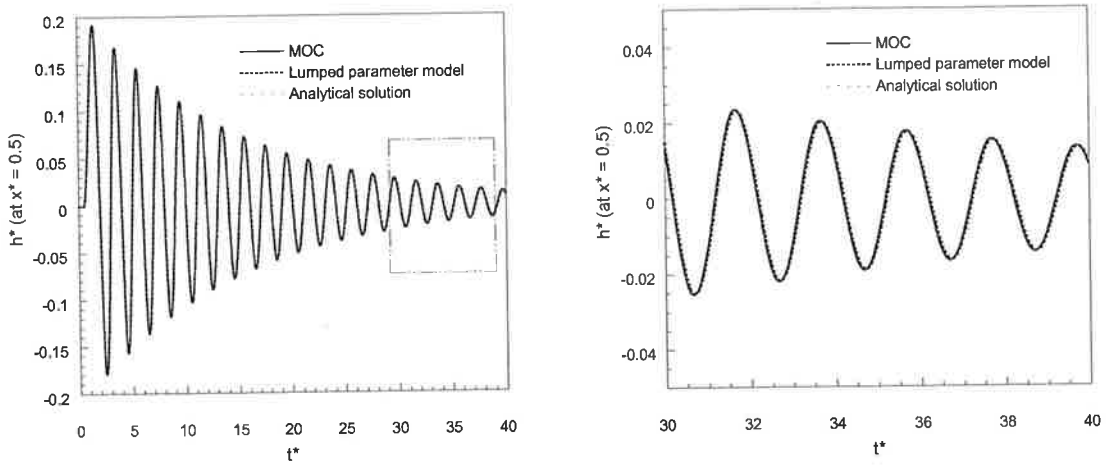

Figure 7.13 Comparison of the lumped parameter (LP) model and analytical solution with the MOC for a slow transient

The effects of the dead end can be considered by a lumped parameter (LP) model, in which a smaller number of reaches can be used for the pipeline. In this example, the pipeline is divided into 16 reaches. The transients calculated using the LP model, the MOC and the analytical solution are given in Figure 7.13. The results based on these three methods are virtually identical, which shows that the effect of a dead end on a slower transient event can be adequately considered by the LP model, and the linearized analytical solution is accurate given $q^* << 1.0$ (in this example $q^* < 0.35$). Because the LP model can use a much smaller number of reaches, the computing time used in LP model is much smaller than that in the normal MOC model. For this example, the computing time used in the normal MOC model (101 reaches and simulation time period of 40.0s) is 163.64s on a PentiumII 500 MHz personal computer, and in LP model (16 reaches and simulation time period of 40.0s) is 0.41s, which is approximately 400 times faster. This improvement is more important when the transient model is used in an inverse calculation in which a great number of transient runs are involved.

In the second example, a faster transient event is initiated by closing the valve at the downstream end of the pipeline as shown in Figure 7.11. The valve is closed

instantaneously from a partially open position that gives the steady flow of Q_0 = 0.005m^3/s. The transients calculated using the MOC are given in Figure 7.14 for both cases with and without a dead end. The effects of the dead end on the fast transient event are more significant than on the slow transient event. A reflection from the dead end is obvious, and the transient form becomes complex after several periods due to the interaction of the reflected and transmitted transients by the dead end.

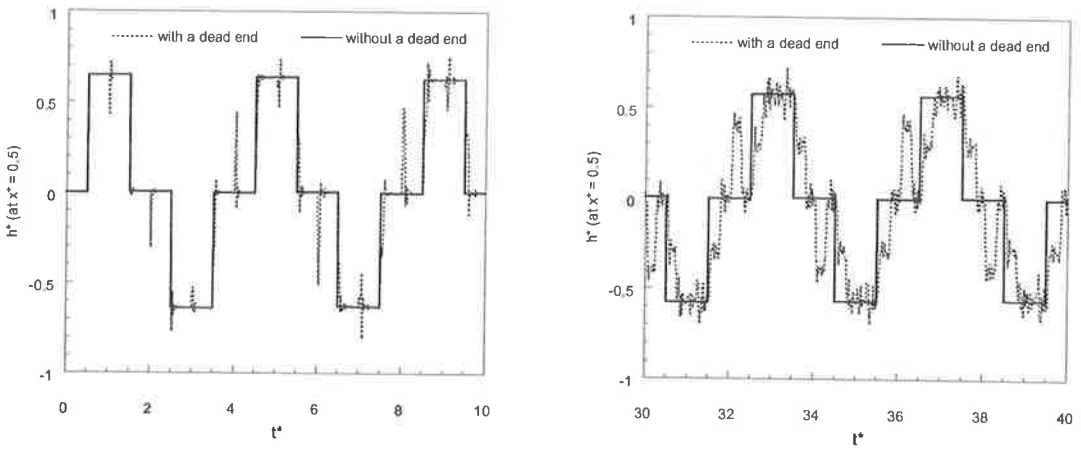

Figure 7.14 Effect of a dead end on a faster transient event (MOC)

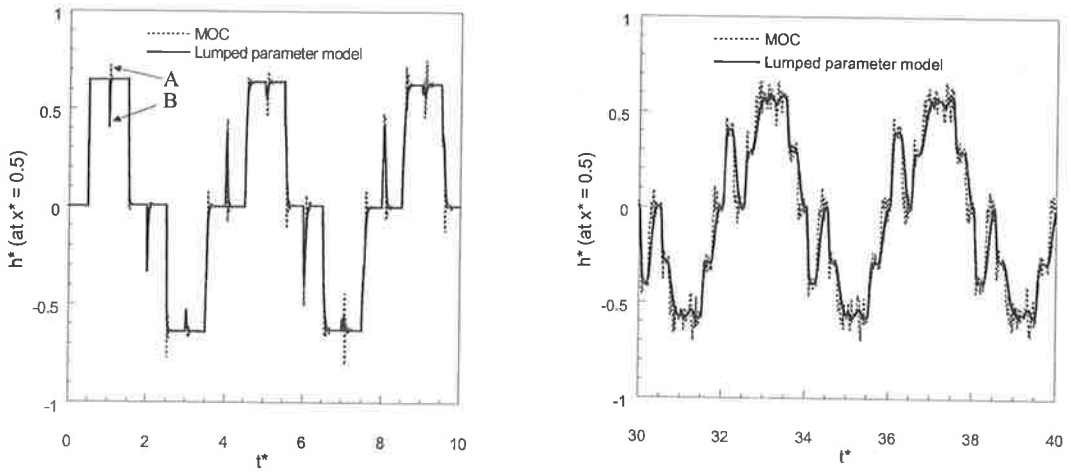

Figure 7.15 Comparison of the LP model with the MOC for a fast transient event

The effects of the dead end on a faster transient event calculated using the MOC and the LP model are presented in Figure 7.15. Due to the large value of q^* (q^* = 1.0 in this

example), which actually invalidates the assumption for the analytical solution, the analytical solution is not suitable for this example, and is not included in Figure 7.15. Generally speaking, the results based on LP model are in good agreement with those based on the normal MOC model. The LP model can successfully simulate the reflection from the dead end (point A in the Figure 7.15). However, the LP model cannot simulate the additional reflections from the end of the dead end (point B) and this is the main reason for the discrepancy between the two models.

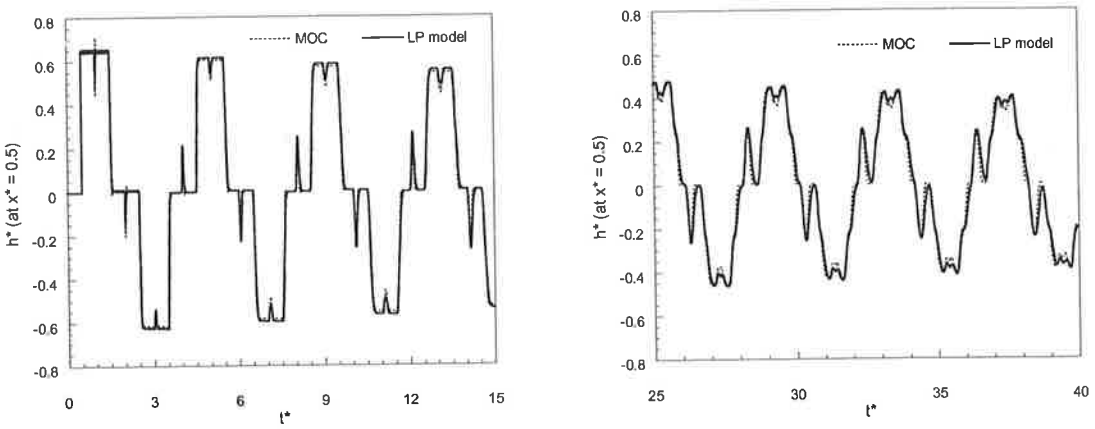

Figure 7.16 Comparison of the lumped parameter (LP) model with the MOC for a faster transient by considering unsteady friction

For a faster transient event, the effects of unsteady friction cause significant damping of higher harmonics and make the transient trace appear smoother. To improve the matter, the modified Brunone unsteady friction model Vítkovský (2001) was applied to the MOC and LP model. Results are presented in Figure 7.16. The results based on LP model are almost identical to those based on the MOC. Therefore, the effects of a dead end on a faster transient event can also be adequately represented by the LP model if the unsteady friction is modelled. The LP model will be used in the inverse transient model to consider the effects of dead ends on the transients in pipe network systems.

7.8 Minimization Techniques

The match between the numerical modelling results and the measurements is measured by an objective function (Chen 1995). A convenient objective function to measure the match between calculated and measured transients is the least-squares function defined as

$$E = \sum_{i=1}^{M} (H_i^m - H_i)^2 \tag{7.44}$$

where $H_i^m = i^{\text{th}}$ measured transient head, $H_i = i^{\text{th}}$ calculated transient head (a function of the parameters of leaks) and M = the number of measurement points. The minimum of the objective function over the entire network at the selected measurement points for the period of transient calculation corresponds to the solution parameters of the leaks. The solution parameters indicate where the actual leaks are and the size of the each leak. If an assumed leak does not correspond to the actual position of the leak, then the leak size should equal to zero, or at least, be orders of magnitude smaller than the size of the actual leak.

Normally the guessed leak parameters will not correspond exactly to actual leak parameters. Thus the calculated transients will not match the measured transients and the objective function value will be large. Improved leak parameters are obtained from minimisation of the objective function. A simple method of minimising the objective function is the steepest descent (S-D) method. The S-D method employs the gradient of the objective function to move to a lower objective function value. The S-D is effective at a distance away from the true minimum; however, when near the minimum it can show slow convergence. This slow convergence problem can be improved by the Levenberg-Marquardt (L-M) algorithm that combines S-D method and the inverse Hessian method, which works better in the neighbourhood of the minimum but performs poorly when far from the minimum for function minimisation. Although the L-M algorithm is more efficient compared to S-D method, overall the L-M algorithm is still a local minimisation algorithm and can suffer when local minima and complex objective function topography are present (Vítkovský 2001, Vítkovský et al. 2002).

A minimisation algorithm that provides a better coverage of the search space is the Shuffled Complex Evolution (SCE) algorithm (Duan et al., 1992, Vítkovský et al. 2002).

The SCE method is based on four main concepts: (i) a combination of deterministic and probabilistic approaches; (ii) the systematic evolution of a "complex" of points spanning the parameter space in the direction of global improvement; (iii) competitive evolution; and (iv) complex shuffling. An initial population of points is randomly sampled from the parameter space. These points are partitioned into a number of complexes that are evolved using competitive evolution techniques in a manner similar to the simplex method. At periodic times during the evolution, the entire set of points is shuffled and reassigned to new complexes, thus enabling information sharing. The competitive evolution ensures that the entire population should move towards the global optimum (given an adequate initial population size). The shuffling allows a more global search and exchange of information from different regions of the search space. The application of ITM based on a single pipeline using the SCE method has produced satisfactory results (Vítkovský et al. 2002).

In this study, applications of ITM for leak detection in pipe networks using the L-M and SCE methods are investigated. Application of these two minimisation methods has been incorporated into a program called NETFIT, which is described in the following section.

7.9 Computer programs: NETTRANS, and NETFIT

The numerical calculations presented in this thesis are conducted using two computer programs the first of which is called NETTRANS, which is a forward transient solver, and the second is NETFIT which combines NETTRANS and a minimisation solver NLFIT and is a inverse transient program. These two programs are introduced in this section.

7.9.1 NETTRANS

NETTRANS is a program that calculates transients in pipe network systems. The structure of this program was originally developed by Prof. James Liggett of Cornell University. The program is coded with a mixture of FORTRAN 77 and FORTRAN 90. The transient algorithm used in this program is the method of characteristics (MOC) based on an implicit scheme. A main feature for this program is that a sparse solver is included in addition to the normal matrix solver. By saving only the non-zero elements in the coefficient matrix described in Eq. (7.17), not only is the computing storage significantly

reduced, the computing speed is also improved greatly compared to the normal matrix solver, especially for a network with a large number of pipes. In NETTRANS, a linear interpolation scheme is available for pipe network systems in which the Courant number for any of pipe reach is not equal to unity.

Since 1999, as part of this Ph.D. research some new features have been added in NETTRANS and some modifications have been made in order to improve the computing efficiency and user convenience. These new features and changes includes:

1. A steady state solver (Subroutine steady.for) was added. A transient calculation should starts from a correct initial condition. The most common and easiest initial condition is the steady state condition. An alternative way of achieving a steady state is by running a transient process for a period of time. The use of a steady solver is more efficient.
2. Valves in a pipe network system can be considered in NETTRANS. Valves are a very important component in pipeline networks. They are widely used in pipeline networks for flow and pressure control. Despite the seemingly endless variety of valve types invented, most of these complex behaviours are built up by combining several valve functions into one unit. From hydraulics point of view, a valve is a head loss component. It can be simulated by the orifice equation. Normally the opening of a valve is described by parameter τ defined as

$$\tau = \frac{C_d A_v}{(C_d A_v)_0} \tag{7.45}$$

where $(C_dA_v)_0$ = open area for reference conditions ΔH_0 and ΔQ_0. The relationship between the discharge and head loss through a valve at an arbitrary position is expressed as:

$$Q_0 = \tau C_V \sqrt{\Delta H} \tag{7.46}$$

in which $C_V = \frac{Q_0}{\sqrt{\Delta H_0}}$ is a constant coefficient for reference conditions.

3. Three different types of unsteady friction model including Zielke's laminar unsteady friction model, Brunone unsteady friction model and a modified Brunone unsteady friction model have been included in the program. These unsteady friction models can be switched on and off in the program by the control parameters in the input data file.
4. The size of a leak is treated as a time-dependent boundary condition, so a sudden break of a leak can be simulated in NETTRANS. More importantly, the transient generating

process by closing a small side discharge can be simulated using this type of boundary condition.

5. A lumped parameter model to consider the effects of short dead ends on transient has been added. The detail of this model has been discussed in Section 7.7.1.

6. Minor losses at pipe junctions can be considered in the program. The minor losses coefficients are based on experimental results presented in Miller (1978).

7. Some of the elements in the coefficient matrix never change during the calculation since they are only related to the topology of the pipe network system. Therefore, in NETTRANS these elements are only computed at the start of the calculations. This improvement can save about 10% computing time.

8. A subroutine to analyze the damping and frequency characteristics of the output pressure (head) or flow rate at specified locations is included.

7.9.2 Validation of NETTRANS

The accuracy and the efficiency of NETTRANS have been verified against freely or commercially available steady state and transient programs and also analytical solutions. The steady state conditions calculated by NETTRANS have been compared with EPANET (version 2), which was developed by the United States Environmental Protection Agency, and also with the experimental measurements from the laboratory network at the University of Adelaide. When the minor losses are not considered for the looped pipe network in Robin Hydraulics Laboratory at the University of Adelaide, velocities calculated by EPANET and NETTRANS are identical and are presented in Figure 7.17. In both NETTRANS and EPANET, the friction is calculated based on the Darcy-Weisbach formula. The lengths of the pipes in this pipe network are given in Table 7.1, and other properties of the pipes and tanks are:

Water level in the providing Tank1	$H_1 = 3.98$ m
Water level in the outflow Tank 2	$H_2 = 1.45$ m
Inside pipe diameter	$D = 72.94$ mm
Thickness of the pipe wall	$e = 1.63$ mm
Pipe roughness	$\varepsilon = 0.0015$ mm
Bulk modulus of the pipe (copper)	$E = 1.20\times10^{11}$ N/m^2

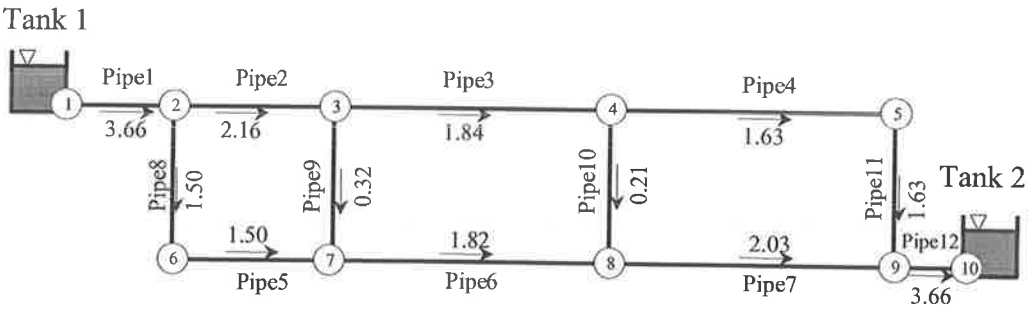

Figure 7. 17 The steady state velocity in a network calculated by NETTRANS and EPANET without considering minor losses (m/s)

When minor losses at elbows and junctions in Figure 7.5 are considered, velocities calculated by NETTRANS are presented in Table 7.2. The calculation of minor losses in NETTRANS is based on the methods described in Section 7.6.2. Velocities at two pipe sections (pipe 1 and pipe 4) measured by two electromagnetic flowmeters are also included in Table 7.2. The details of the measurements and the calibration of the flowmeters are given in Section 8.2.6 in Chapter 8. The velocities calculated by NETTRANS are very close to the experimental measurements.

Table 7.1 Properties of the pipe network in Figure 7.17

Pipe No.	Upstream node	Downstream node	Length (m)
1	1	2	4.575
2	2	3	6.100
3	3	4	12.200
4	4	5	12.200
5	6	7	6.100
6	7	8	12.200
7	8	9	12.200
8	2	6	6.100
9	3	7	6.100
10	4	8	6.100
11	5	9	6.100
12	9	10	3.050

Table 7.2 Steady state velocities in pipe network as shown in Figure 7.17 when the minor losses are considered (m/s)

Pipe No.	Upstream node	Downstream node	NETTRANS	Measurements
1	1	2	2.45	2.45
2	2	3	1.72	
3	3	4	1.36	
4	4	5	1.19	1.18
5	6	7	0.73	
6	7	8	1.09	
7	8	9	1.26	
8	2	6	2.45	
9	3	7	0.73	
10	4	8	0.36	
11	5	9	0.17	
12	9	10	1.19	

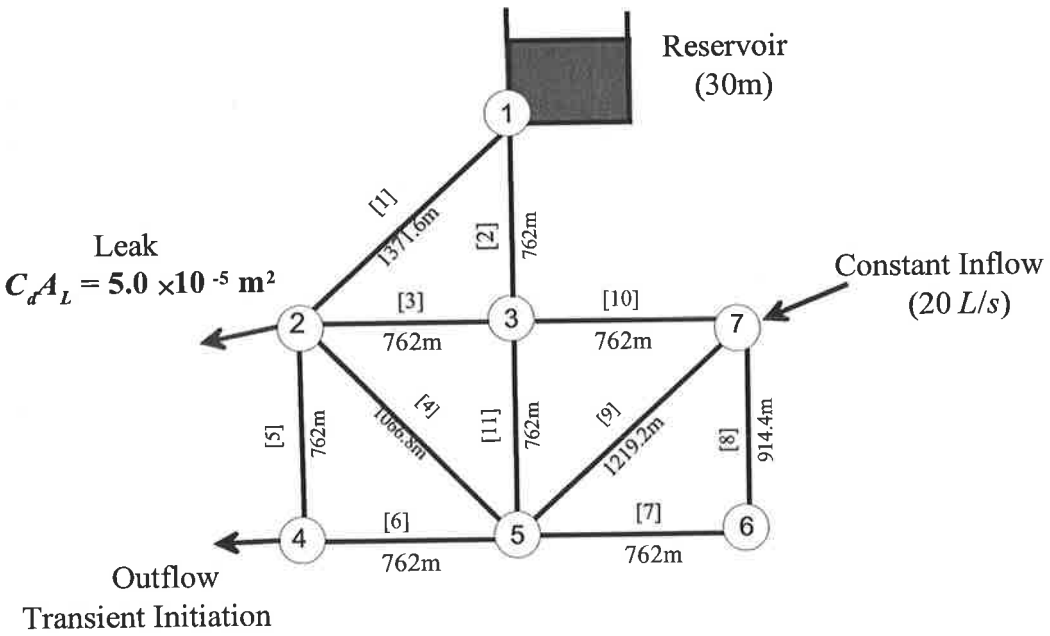

Figure 7.18 Example small network (from Chen 1995)

Applications of NETTRANS in simulating transients have been compared with INVCHAR[1], which was developed by Chen (1995) and further developed and verified by Vítkovský (2001), and also to TRANSAM developed by Professor Bryan Karney at University of Toronto.

A water distribution pipe network as shown in Figure 7.18, which was introduced by Pudar and Liggett (1992) and used in Chen (1995), is considered as the first example. This network consists of 11 pipes and seven nodes. It is supplied from a reservoir and a constant inflow at node 7. The pipe lengths for the network are shown in Figure 7.18 below each pipe. All pipes are 254 mm in diameter with a wall thickness of 1.6 mm and the Darcy-Weisbach friction factor for each pipe is $f = 0.02$. A leak at node 2 has a lumped leak coefficient of $C_d A_0 = 5.0\times10^{-5}$ m^2, corresponding to an approximate leak hole diameter of 13 mm. The inflow at node 7 is constant as 0.02 m^3/s. The transient is initiated by changing the outflow rate from node 4 as shown in Figure 7.19(a). At time $t = 0.0$ the network is at steady state conditions. More details of this network can be found in Chen (1995). The transients at node 6 calculated using NETTRANS and INVCHAR and TRANSAM are plotted in Figure 7.19(b) and the results are almost identical.

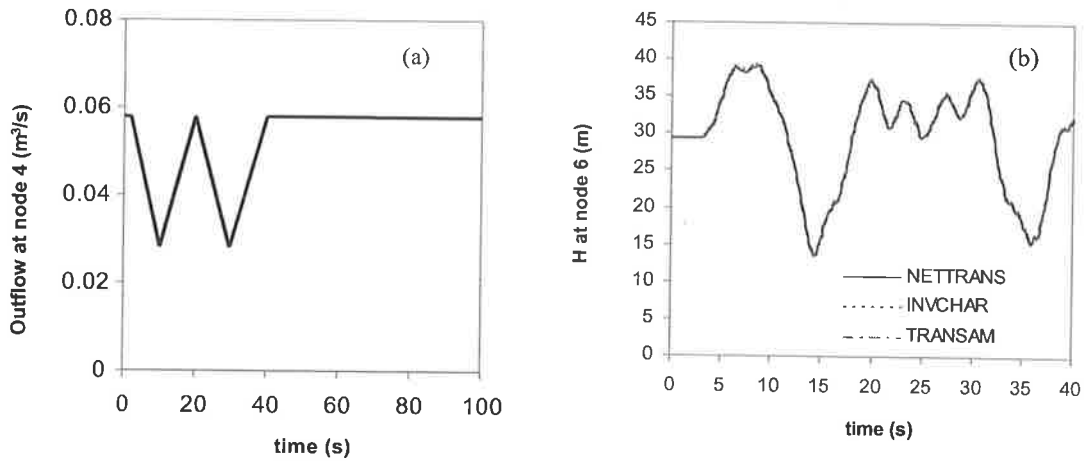

Figure 7.19 Transient in a small network (from Chen 1995) (a) boundary condition at node 4, (b) transients simulated using NETRANS, INVCHAR and TRANSAM

[1] INVCHAR is a program developed by Chen (1995) for leak detection and pipe roughness calibration based the inverse transient method. Because INVCHAR was designed for inverse calculation and includes six different interpolation schemes, this program has a complex structure and is difficult for further developments for transient simulation, for example to include unsteady friction models. When the author of this thesis studied his Ph.D. research at the beginning of 1999, it was decided to develop another more structured transient simulation program - NETTRANS.

Transients measured from a single laboratory pipeline at The University of Adelaide (Bergant et al. 2001) are used to validate the unsteady friction models in NETTRANS. This single pipeline was introduced in Chapter 4 and is repeated here for convenience. The pipeline is 37.2m long and is made of copper pipe with a diameter of 22.1mm. The wave speed in the pipeline was calibrated as a = 1320m/s. The transient was generated by closing a downstream (valve 1) from a steady state of $Q_0 = 1.132 \times 10^{-4}$ m^2/s giving the Reynolds number of **Re** = 5800. Transients measured from two locations, downstream valve and middle of the pipeline, are presented in Figure 7.20. Simulation results calculated using NETTRANS based on the k_A & k_P unsteady friction model (Vítkovský 2001) are compared with corresponding experimental measurements and shows good agreement. In the simulation, unsteady parameters were set as k_A = 0.031 and k_P = 0.0395 which were calculated using Eq. (7.7a).

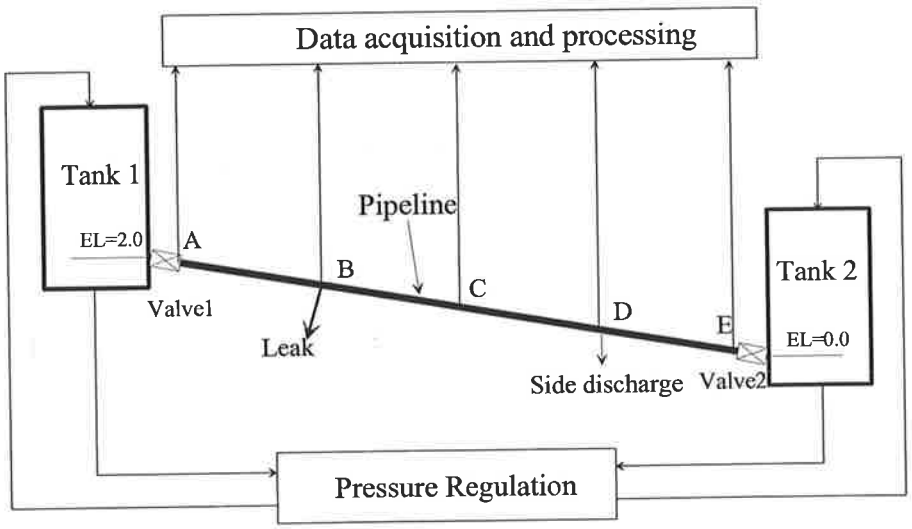

Figure 4.12 (repeated) Laboratory pipeline

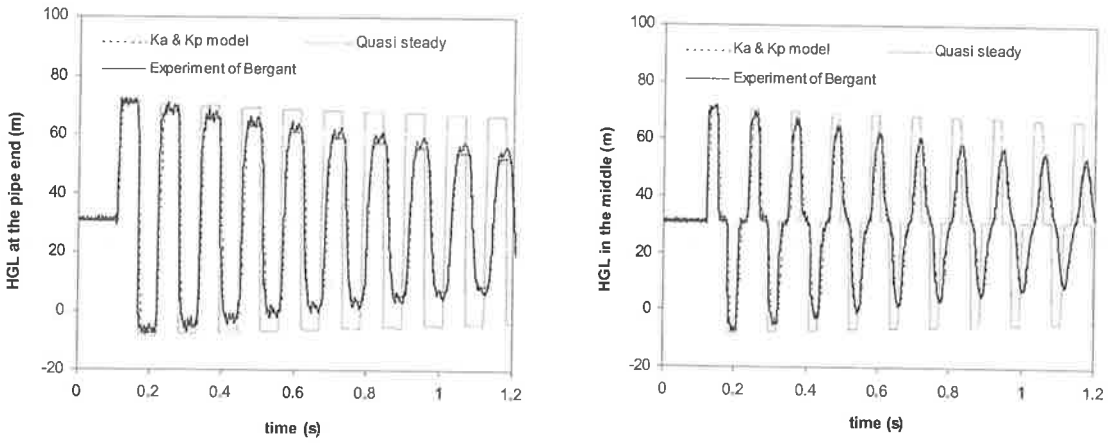

Figure 7.20 Transients in a single laboratory pipeline (**Re** = 5800)

7.9.3 NETFIT

NETFIT is a program that was developed in this Ph.D. research for leak (or blockage) detection and pipe roughness calibration in pipe network systems based on the inverse transient method (ITM). This program is comprised of two parts: NETTRANS, a forward transient solver, and NLFIT, an inverse parameter-fitting program. NLFIT is a Bayesian nonlinear regression program suite developed by Associate Professor George Kuczera at the University of Newcastle. This program suite provides several minimisation methods including the gradient-based Newton-Raphson (N-R) and Levenberg-Marquardt (L-M) methods, and global-based searching methods including the genetic algorithm (GA) and shuffled complex evolution (SCE) methods. NLFIT also provides a series of windows-based interfaces in which the parameters and minimisation schemes can be chosen and the convergence process and fitness of the searched parameter can be monitored. An example window for edit mode is given in Figure 7.21. NETTRANS and NLFIT are connected through two subroutines called **inputt** and **model**. Details of NLFIT can be found in the NLFIT Manual (Kuczera 1994).

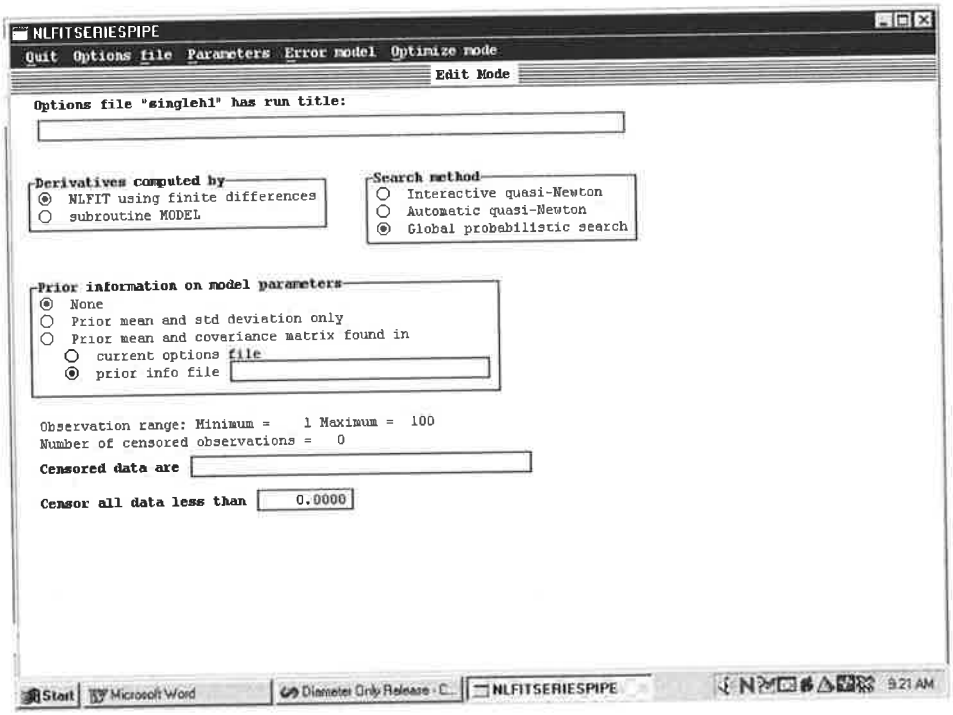

Figure 7.21 A windows interface of NETFIT

7.9.3 Validation of NETFIT based on numerical measurement data

Application of NETFIT to leak detection in a small network as shown in Figure 7.18 is presented in this section using the numerically generated measurement data. The inverse analysis requires the following information:

1. Initial and boundary conditions;
2. Initial guess for the unknown leak parameters; and
3. Measurement data at non-boundary nodes.

In the inverse analysis, the initial and boundary conditions are same as those in the transient analysis. The leaks are assumed at nodes 2, 3, 5 and 6 (node 1 is a constant head boundary condition, and nodes 4 and 7 are constant demand boundary conditions). The guessed sizes of leaks are assumed to be zero at the beginning of the inverse analysis. The transient measured at node 6 within period of 0s to 50s is used in the inverse analysis.

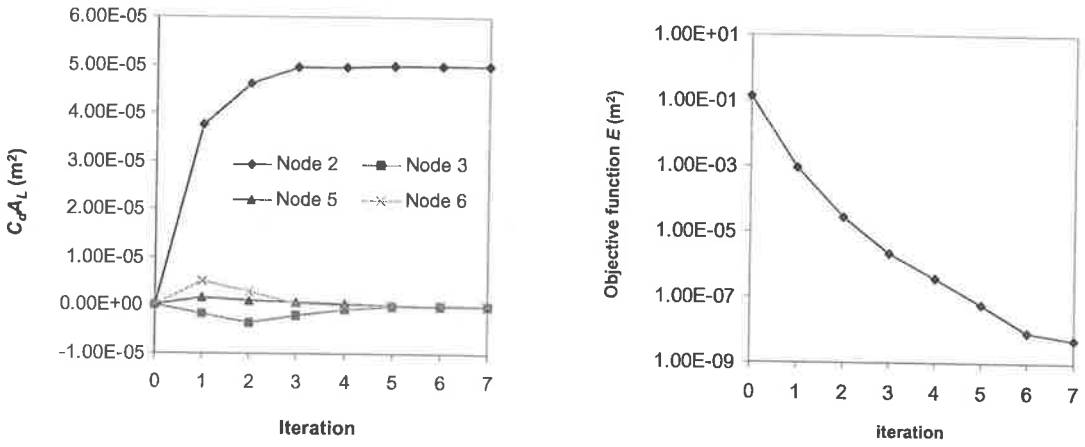

Figure 7.22 Inverse analysis based on L-M method

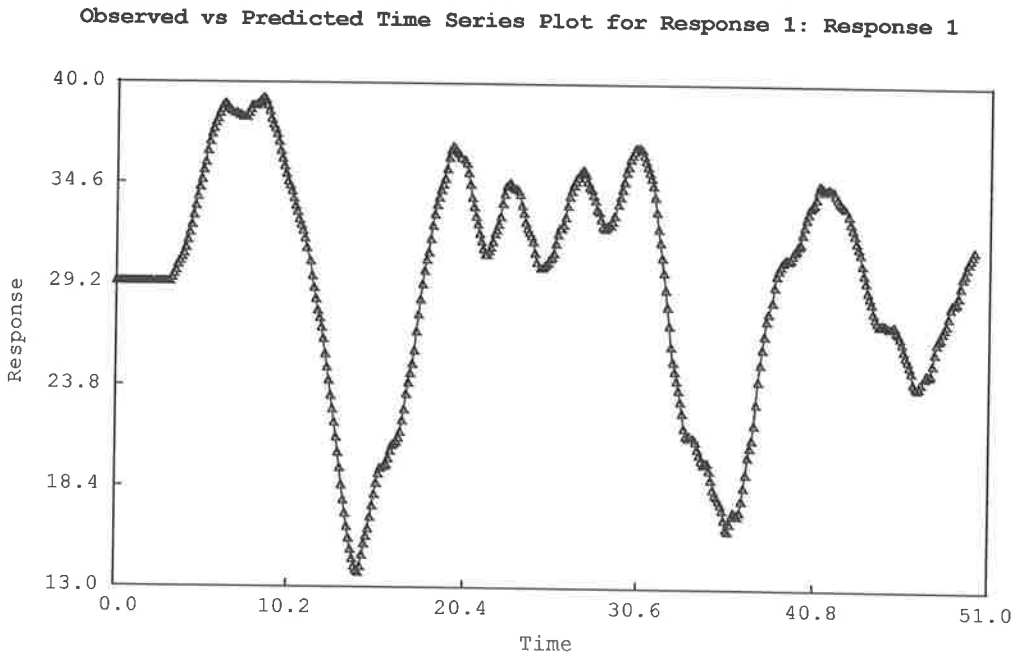

Figure 7.23 Measured and simulated transients (plot from NETFIT, Δ = measurement, —— = simulation)

The results of the inverse analysis using the L-M minimisation method are presented in Figure 7.22. The leak size at node 2, at which a leak is present, converged to the actual value of $C_dA_L = 5.0\times10^{-5}$ m^2 after 5 steps of iteration. Leak sizes at node 3, 5 and 6, where no leak is present, converged to very small magnitudes close to zero. In the L-M method, no limit was put on the leak size. As a result, the size of a leak may be negative (node 3 in table 7.3). However, the negative value is so close to zero that no significant influence on the outcome of analysis. In the transient model, if a negative leak is fed back from the inverse parameter fitting, the leak size is set to zero. The measurement transient and transient calculated using the detected final leak parameters from the inverse analysis are plotted in Figure 7.23, and are visually identical.

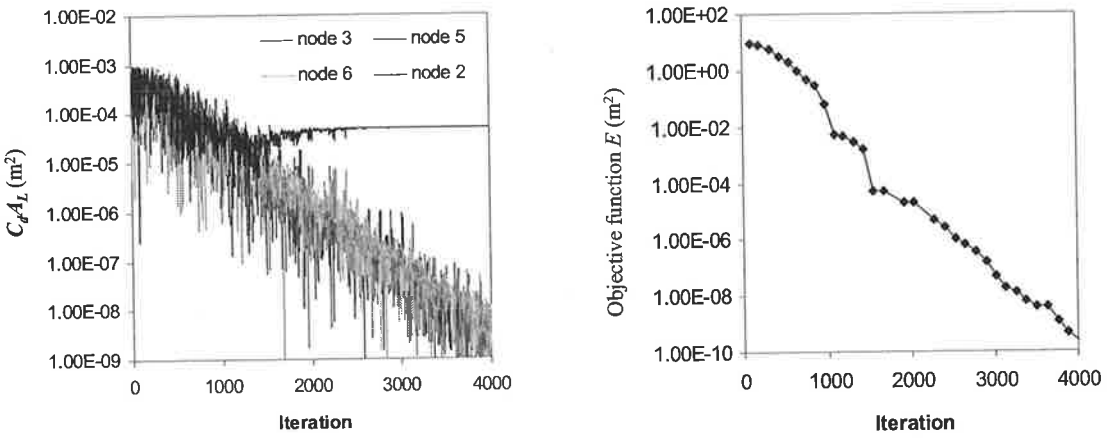

Figure 7.24 Inverse analysis based on SCE method

Table 7.3 Outcome of leak detection using NETFIT

Leak size	Node 2	Node 3	Node 5	Node 6
Real values (m^2)	5.00×10^{-5}	0	0	0
L-M method (m^2)	5.00×10^{-5}	-1.00×10^{-7}	4.66×10^{-8}	3.30×10^{-8}
SCE Method (m^2)	5.00×10^{-5}	8.17×10^{-9}	3.22×10^{-9}	6.16×10^{-9}

The results of the inverse analysis based on SCE method are presented in Figure 7.24. In the SCE method, the leak size can be pre-set within a limit range. In this example sizes of leaks at the assumed locations are set within 0.0~0.001m^2. Because the initial leak parameters are randomly chosen within this range, the sizes of the leaks are further away

from the actual values at the beginning of the inverse analysis compared to L-M method. After about 2000 iteration steps, the size of leak at node 2 converges to the actual value of $C_dA_L = 5.0\times10^{-5}$ m^2 while the leak sizes at nodes 3, 5 and 6 converge to small magnitudes close to zero. The final values of the sizes of the leaks are given in Table 7.3.

7.10 Summary

Compared to a single pipeline, a pipe network not only has more pipes and nodes, but also has some special features including minor losses and dead ends. These features make simulation of transients in a pipe network more challenging. The effects of minor losses at elbows and pipe junctions and dead ends on transient events are investigated in this chapter and methodologies to simulate these effects in a transient model have been developed. A program called NETTRANS for simulating transients in pipe networks has been developed. The accuracy of this program has been verified by comparison with other independent steady state and transient programs and experiment results from a single pipeline.

The minor losses at elbows and pipe junctions are simulated using small "head loss" pipe sections in the transient model. The significance of minor losses on a transient event depends on the flow rates at elbows or pipe junctions and the geometry (ratios of pipe length to pipe diameter) of a pipe system. Minor losses tend to become more important for a pipe system with smaller ratios of pipe length to pipe diameter, and with larger flow rates.

Presence of a short dead end may significantly influence a transient event. An analytical solution expressed in a Fourier series has been developed for transients in a pipeline with a dead end. The analytical solution shows presence of a dead end change the frequencies of the harmonic components. The significance of the effect depends on the parameter S_d defined in Eq. (7.42), which is related to the location of the dead end, relative volume and wave speed of the dead end compare to the pipeline. A lumped parameter model, which can be easily included in the MOC, has been developed to effectively simulate effects of a dead end on a transient event.

An inverse calculation program called NETFIT has been developed to apply the inverse transient method for leak detection in pipe network systems. Applications of NETFIT using numerically generated measurement data has shown that NETFIT can find the leaks including leak location and leak size successfully based on different searching techniques including the Levenberg-Marquardt (L-M) algorithm and the shuffled complex evolution (SCE) method.

Chapter 8

Verification of ITM for Leak Detection in a Laboratory Pipe Network

8.1 Introduction

As part of this Ph.D. research, a three-loop pipe network has been constructed in the Department of Civil & Environmental Engineering at the University of Adelaide to investigate transients and to apply the inverse transient method in network systems. In this chapter the construction, calibration and test results for leak detection observed from this pipe network are described. The unsteady friction models including the k_A & k_P model (Section 7.4) and the Zielke model (Zielke 1971), which have been tested in straight single pipelines (Bergant et al. 2001, Vítkovský 2001), are verified in this chapter against measured transients in the pipe network. The effects of minor losses from pipe junctions and effects of dead ends on the fluid transients, discussed in Chapter 7, are experimentally verified. This chapter presents the experimental verification of the inverse transient method (ITM) for leak detection in pipe networks based on *real*—rather than numerical model generated—measurement data.

8.2 Construction of the experimental apparatus

The design of the experimental pipe network commenced in March 1999 and construction was completed in December 2000. It is located in the Robin Hydraulics Laboratory in the Department of Civil & Environmental Engineering at the University

of Adelaide. A diagram of the pipe network is given in Figure 8.1. The network is made of copper pipe with a diameter of 75mm (3 inches) and is connected to three tanks, Tank 1, Tank 2 and Tank 3 of Figure 8.1(b). The main body of the network is horizontal with two vertical pipes connecting the tanks as shown in Figure 8.1(a). Flanged, one-quarter-turn ball valves are installed in this network for flow control in order to simulate different network configurations, including single pipelines, branched networks, pipelines with dead ends and looped networks. Transients can be initiated in three ways: by adjusting the opening of a valve, by closing a side-discharge valve, or by injecting flow into network using a piston or membrane. Pressure transducers used for acquisition of measurement data—for use in the inverse transient method — can be placed at different nodes (T1, T2, T3, T4, T5 T6 and T7 in Figure 8.1b) in the network.

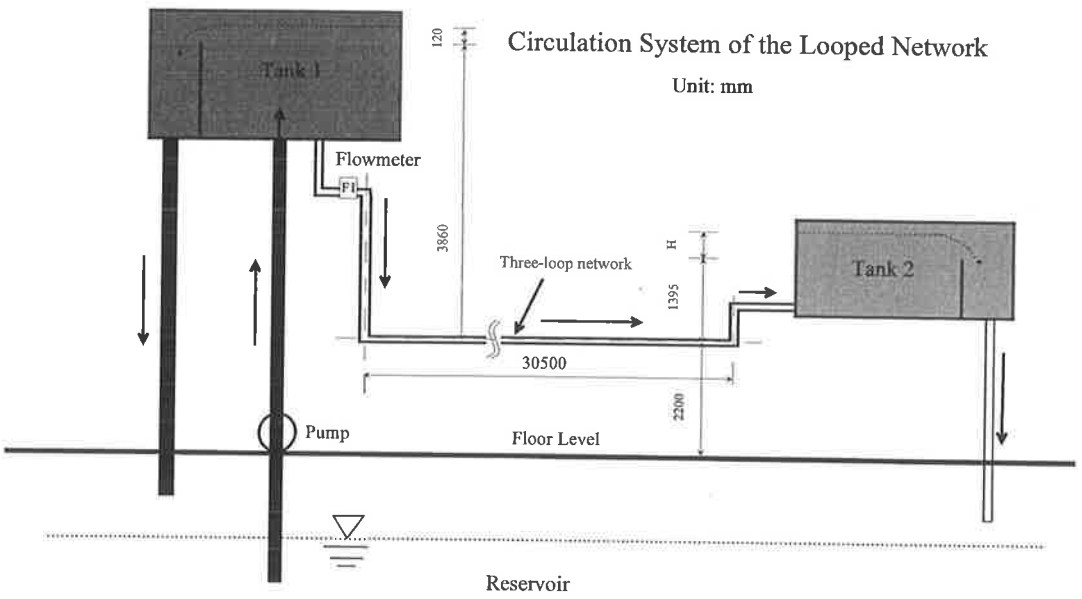

(a) Circulation of flow in the pipe network (Units: mm)

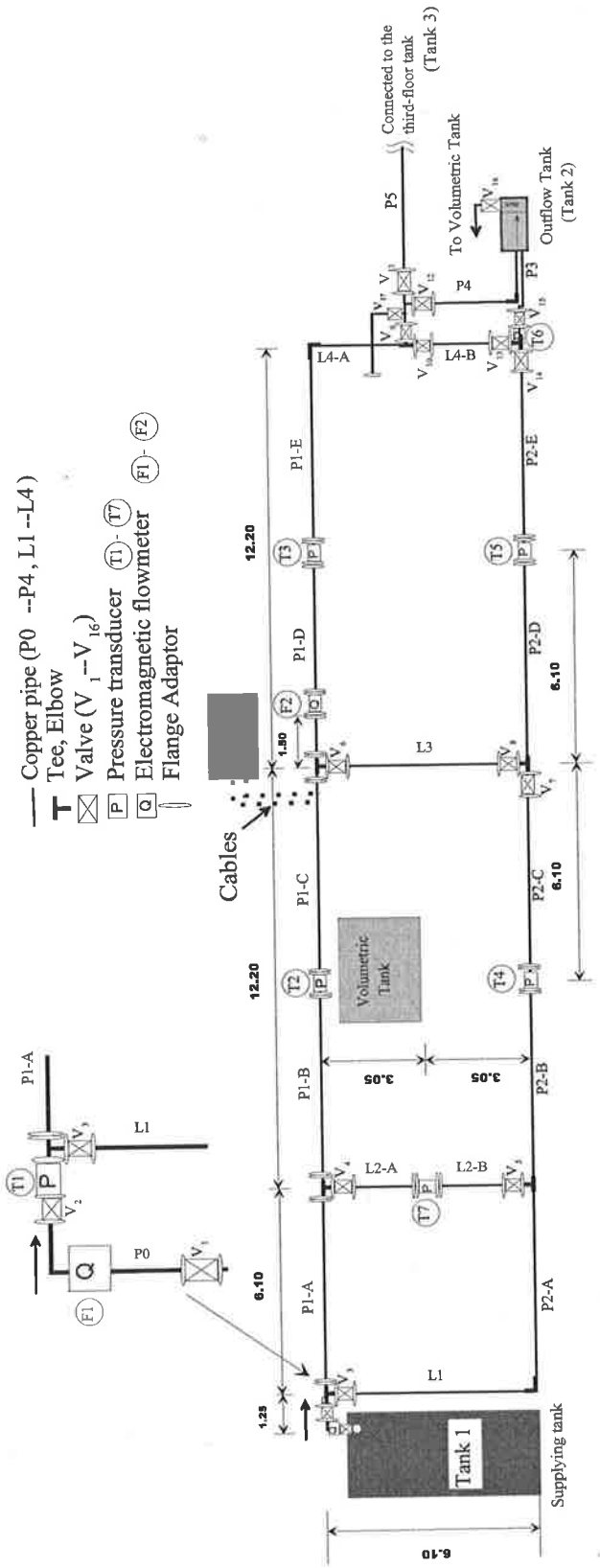

(b) Plan view of the looped network (Units: m)

Figure 8.1 Laboratory pipe network at The University of Adelaide

8.2.1 Pipes

The pipe network is made of DN80 copper pipes of length 6.0m. Details of the pipe characteristics and pipe material properties are given in Table 8.1. During the design of the experimental apparatus, pipes made of steel, stainless steel and copper were considered. Copper pipes were chosen because of the corrosion problems associated with steel pipes and difficulty in machining of stainless steel pipes and fittings. In the network, pipes (also valve and pipe, transducer block and pipe, pipe and tank) are connected using flanges (copper adapters) as shown in Figure 8.2. Flange connections rather than fixed welded connections were chosen so that some of the sections could be replaced with pipes of different roughnesses or diameters; thus, the network can be used for pipe roughness calibration and pipe blockage detection investigations. The estimated roughness of the pipe inner wall (ε) for all the pipes used in this study is 0.0015mm, giving a relative roughness of 2.0×10^{-5}.

Table 8.1 Properties of the copper pipe (AS 1432-1990)

Characteristics or property	Value
Pipe length (L)	6.0 ± 0.01m
Pipe internal diameter (D)	72.94 ± 0.1mm
Wall thickness (e)	1.63 ± 0.05m
Poisson's ratio (μ)	0.34
Young' modulus of elasticity (E)	120 ± 5 Gpa
Design pressure (p_d)	1,620 kPa

During the design of the network, the length of each of the pipe sections was selected carefully to make the Courant number of each section equal to unity. In this network, the smallest computational unit is 1.525m. The main part of the pipe network (see Figure 8.3) is located under the steel beam. The pipes are anchored with supports at an interval of 1.0m in the axial direction. Extra restraints are included at the elbows and junctions, where the flow changes directions.

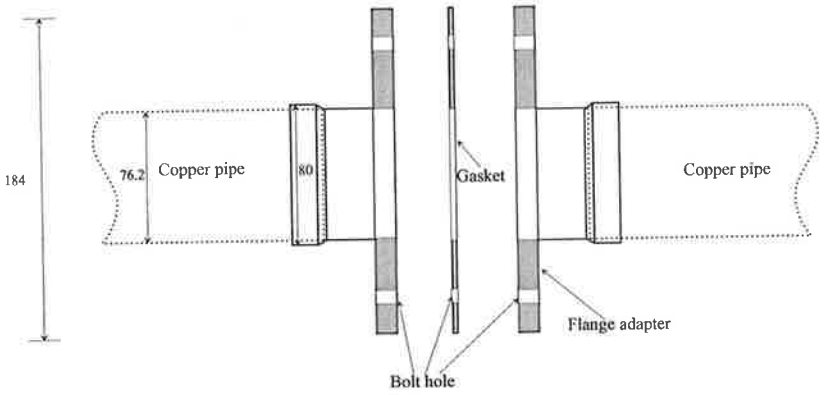

Figure 8.2 Copper pipe flange adapter (units: mm)

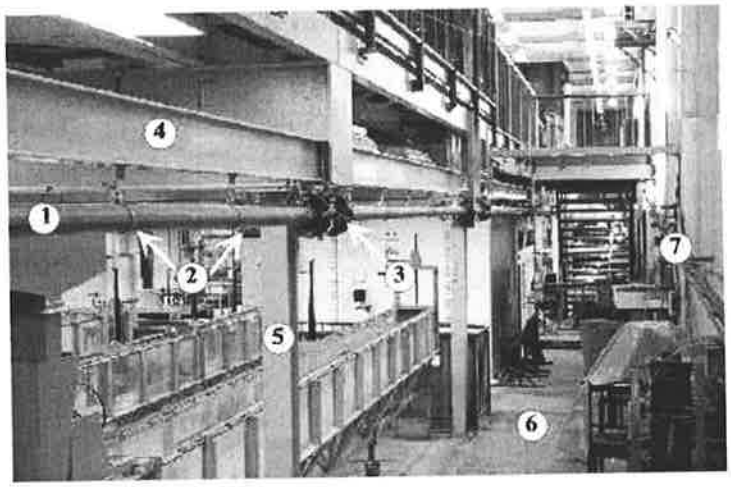

Figure 8.3 The pipe network (1-copper pipe, 2-pipe restrain, 3-flange adapter, 4-steel beam, 5-steel column, 6-concrete floor, 7-a 22mm single pipeline rig)

The strength of the pipes and brackets and the clearance of the pipe network above the floor level and the deflections of the pipes were checked against Australian Standards.

8.2.2 Tanks

Three tanks are connected to the pipe network. Depending on the relative water levels in the different tanks, these tanks can provide different flow conditions. As shown in Figure 8.1(a), a pump is connected to Tank 1, which is located at the western side of the laboratory. Tank 1 is made of steel plate with a size of 6.20m × 1.53m × 1.35m (length × width × height). When the pump is working at capacity with no other users (some other facilities are connected with Tank 1) the water surface in Tank 1 is 3.98m

above the level of the looped network as shown in Figure 8.1(a). When the pump is shutdown, the highest water surface is 3.86m above the level of the network.

Tank 2 is located at the eastern side of the laboratory and is made of PVC. The size of tank is shown in Figure 8.4. Two pipe legs from the looped network are connected with Tank 2. A baffle with holes is placed near the bottom of the tank to diffuse the water flow in order to make the water surface stable. The water flows over a square-edged weir and then flows to a volumetric tank. In addition to achieving a stable water surface, the square-edged weir is used as a flow measurement device in case that the electromagnetic flow meters installed in the pipe network fail to work. The height from the square-edged weir to the level of the looped network is 1.395m. The water surface in Tank 2 above the level of the looped network ranges from 1.395m to 1.45m depending on the flow rates at the weir.

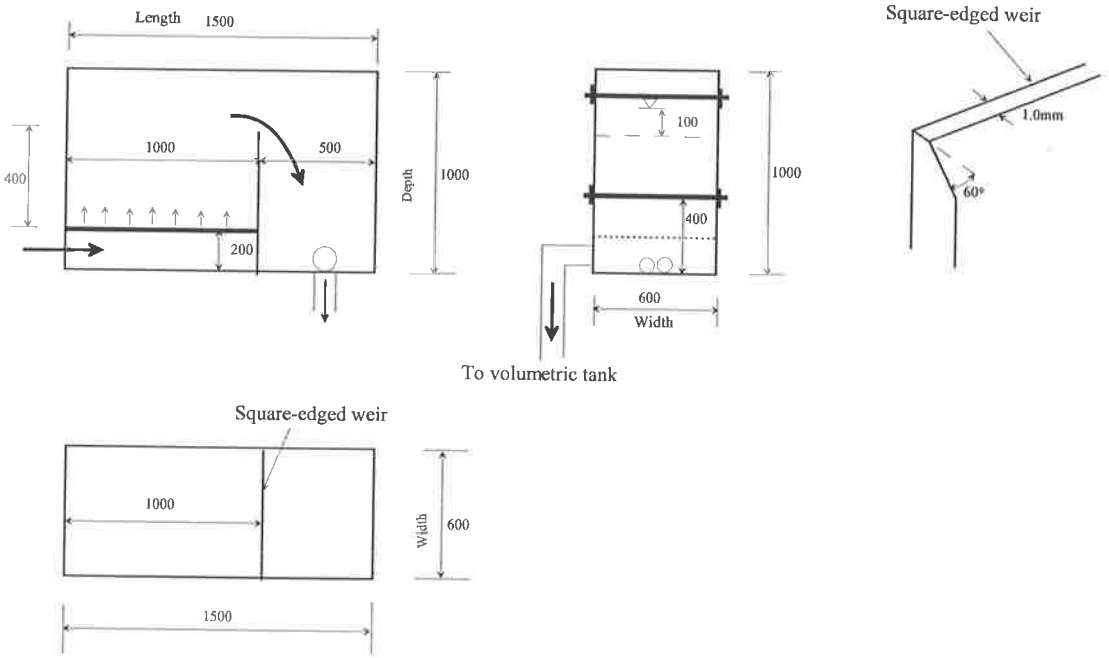

Figure 8.4 Tank 2 and the square edged weir (units: mm)

Tank 3 is located vertically above the Robin Hydraulics Laboratory in the third floor of the Engineering North Building at the University of Adelaide. The water level in Tank 3 is about 14.5m above the network. Tank 3 is connected to the network using two different types of pipes, 75mm copper pipes and 150mm (6 inches) steel pipes. In

this study, Tank 3 has not been used, and is isolated from the pipe network by closing the valve V11 (see Figure 8.1b) for all the experimental tests presented.

8.2.3 Control valves

An important feature of this pipe network is that 16 control valves have been installed within the pipe network in order to obtain the flexibility of simulating different network configurations and for other applications including pipe roughness calibration and blockage detection. To minimise the disturbance on the flow in the network, one-quarter flange ball valves, which have very smooth core profile and an inner diameter equal to that of the copper pipe, were chosen. Two pictures of the flanged ball valves are shown in Figure 8.5. The valve is made of stainless steel with a flange compatible with the copper pipe flange adapter. The location and serial number (ranging from V1 to V16) of each valve is shown in Figure 8.1b.

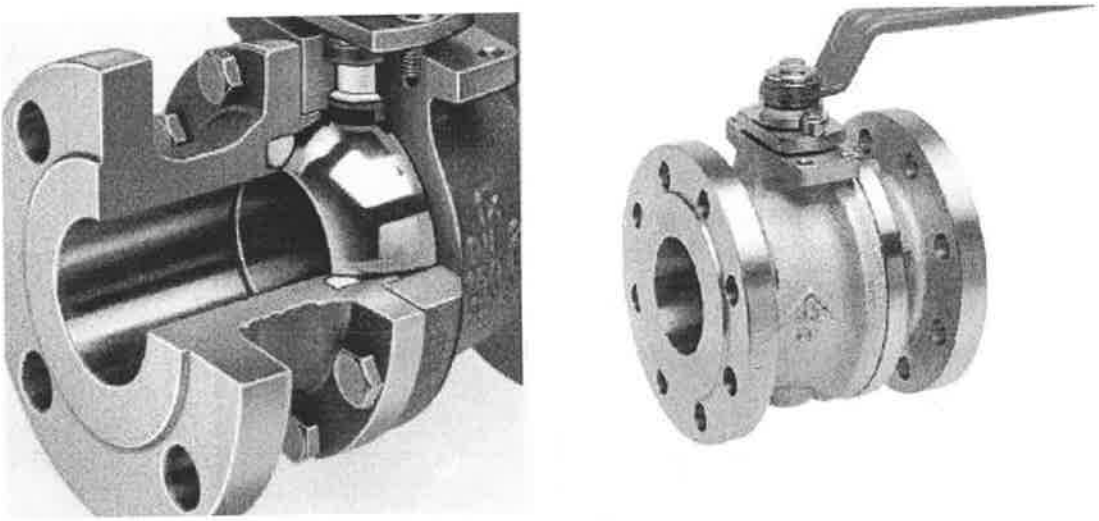

Figure 8.5 The flanged one-quarter turn ball valve

8.2.4 Leak orifices

A primary purpose of the pipe network is to verify the inverse transient method for leak detection. Therefore, leaks can be simulated at different locations in the pipe network. A number of brass blocks as shown in Figure 8.6 were machined and installed in the network for installation of leak orifices and pressure transducers. The

diameter of the leak orifice may be changed based on test requirements. In the present network, leaks with diameters of D_L = 5mm are installed at T3, T4, T5 and T6 and a smaller leak with diameter of D_L = 3mm is installed at T2, which is the one used in this study. The orifice can be switched on and off using a small ball valve that is connected with each orifice as shown in Figure 8.7. In this network, there are 7 brass blocks (leak orifices) installed. Locations of these leaks and their serial number are shown in Figure 8.1b.

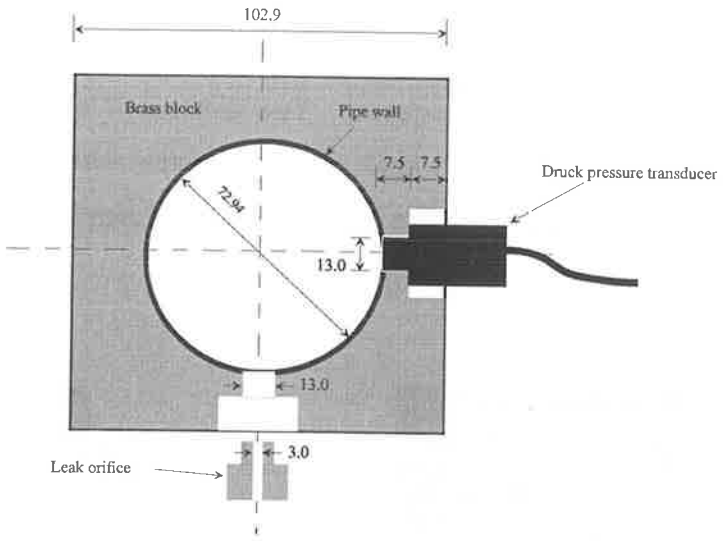

Figure 8.6 Brass block for installation of leak orifice and pressure transducer (units: mm)

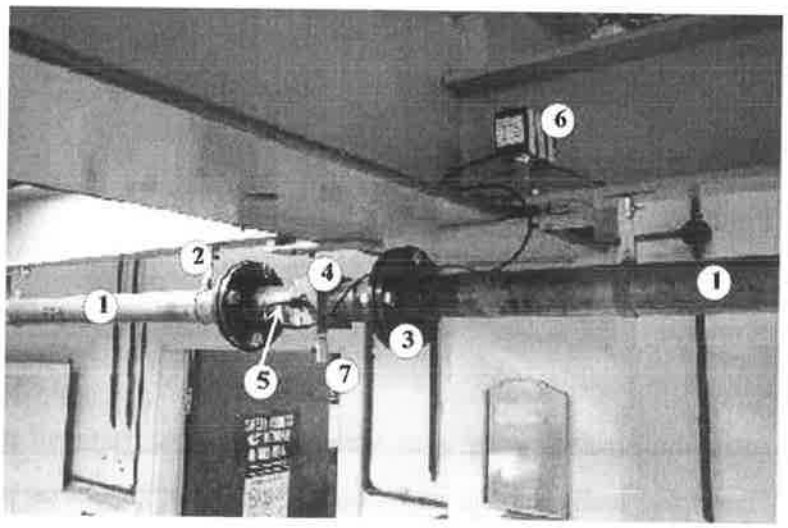

Figure 8.7 The brass block in the network (1-copper pipe, 2-pipe restriction, 3-flange adapter, 4-brass block, 5-pressure transducer, 6-transducer amplifier, 7-leak orifice)

8.2.5 Pressure transducers

Pressure measurements are performed by Druck high-speed pressure transducers. A brass block (as shown in Figure 8.6) was designed and machined for installation of a pressure transducer to ensure that the pipe diameter does not change and the transducer is flush with the inside of the pipe. The characteristics of the Druck pressure transducer are given in Table 8.2. In present network, seven brass blocks are installed as shown in Figure 8.1b. In this study, five Druck transducers at T1, T3, T5, T6 and T7 are installed, and their locations and serial number are shown in Figure 8.1b. The calibration results of the transducers are given in Section 8.3.2.

Table 8.2 Characteristics of the Druck pressure transducers (PDCR-810)

Characteristics	Values
Pressure range	0 to 2bar
Supply voltage	0 to 10V
Output voltage	0 to 100mV
Accuracy	0.06% of pressure range
Temperature range	0°C to 50°C

8.2.6 Flow meters

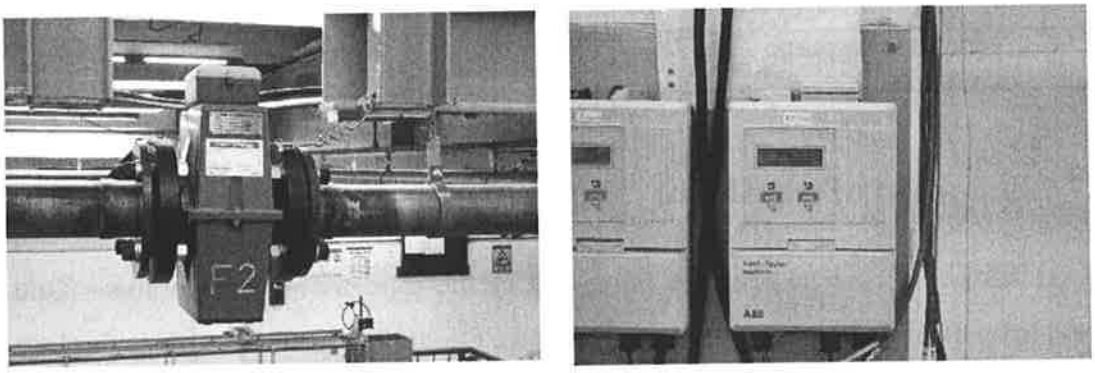

Flow meter sensor LCD output

Figure 8.8 The ABB flow meter

Flow rates in the pipe network are measured by two electromagnetic flow meters. Their positions are shown in Figure 8.1b. The flow meters were provided by ABB International, and the characteristics of the flow meters are given in Table 8.3. The flow meter has the same inner diameter as the copper pipe, which is important in this study to avoid disturbance of the flow. During the design of the experimental apparatus, different types of flow meters that use pressure differences, turbines, and ultrasound were considered. The present ABB Master electromagnetic flow meters were chosen due to their high accuracy, less flow disturbance and reasonable costs. Because they have a low frequency response, less than 3.0Hz, compared to the water hammer frequencies (larger than 6.0Hz depending on the network configuration), the flow meter is only suitable for measuring steady state discharge. There are two output channels for each flow meter as shown in Figure 8.8. One LCD output indicates velocity and flow rate. The other channel is connected to the computer to measure and record voltage signals. The LCD output can be programmed to requirement of the user.

Table 8.3 Characteristics of the electromagnetic flow meter (ABB MegMaster®)

Characteristics	**Values**
Flow rate range	0-15 (L/s)
Meter bore	75mm
Accuracy	0.5% of full range
Temperature range	0-50°C

8.2.7 Generation of transients

Two methods are used to generate transients in the pipe network apparatus. One method is by closing an inline valve. This is a traditional method. Another is to close a side discharge orifice. The side discharge orifice is connected to a fast-acting solenoid valve. A photo of a solenoid valve installed in the pipe network in shown in Figure 8.9. The diameter of the side discharge orifice is 5.0mm. The diameter of the solenoid valve is 1.6mm. For the second method, a transient is generated with a smaller disturbance of the steady flow in the pipe network.

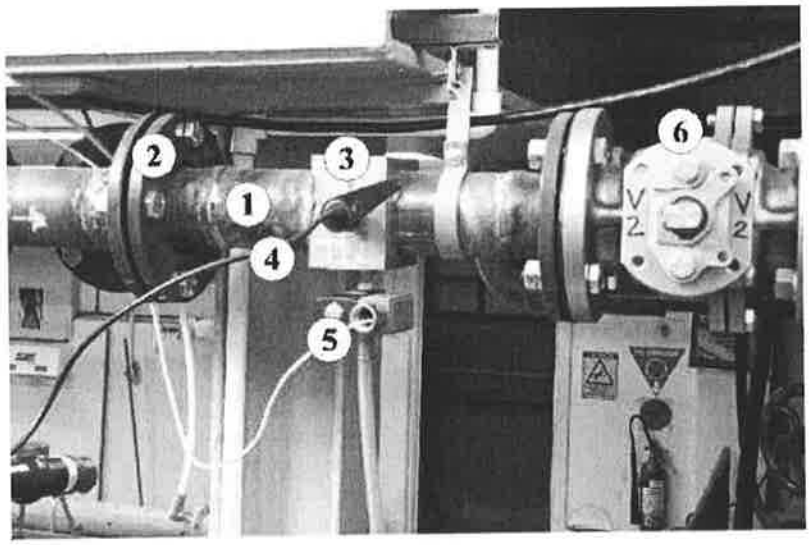

Figure 8.9 A side discharge connected with a solenoid valve for transient generation (1-copper pipe, 2-flange adapter, 3-brass block, 4-pressure transducer, 5-solenoid valve and 6-ball valve)

8.2.8 Computer data acquisition and processing system

Data acquisition is performed on a 166 MHz Pentium personal computer using an Intelligent Instrumentation data acquisition card and Visual Designer software. The data acquisition card is of Type PCI-20428W-3, which can accept 16 single-ended analogue input channels. The conversion of these analogue signals to digital signals is performed with 12-bit resolution. The possible voltage ranges are ±5V, ±10V, 0-5V and 0-10V, of which the range 0-10V was used in the tests. The card has a maximum sampling range of 100,000 Hz for one channel; however, depending on how many channels are used, the maximum sampling rate is lower. The Visual Designer software provides an easy-to-use graphical representation of the data acquisition process. A graphical example for a transient test is given in Figure 8.10. Control over the number of input channels, sampling rates, processing of data and storage of the data in a file are controlled via the software.

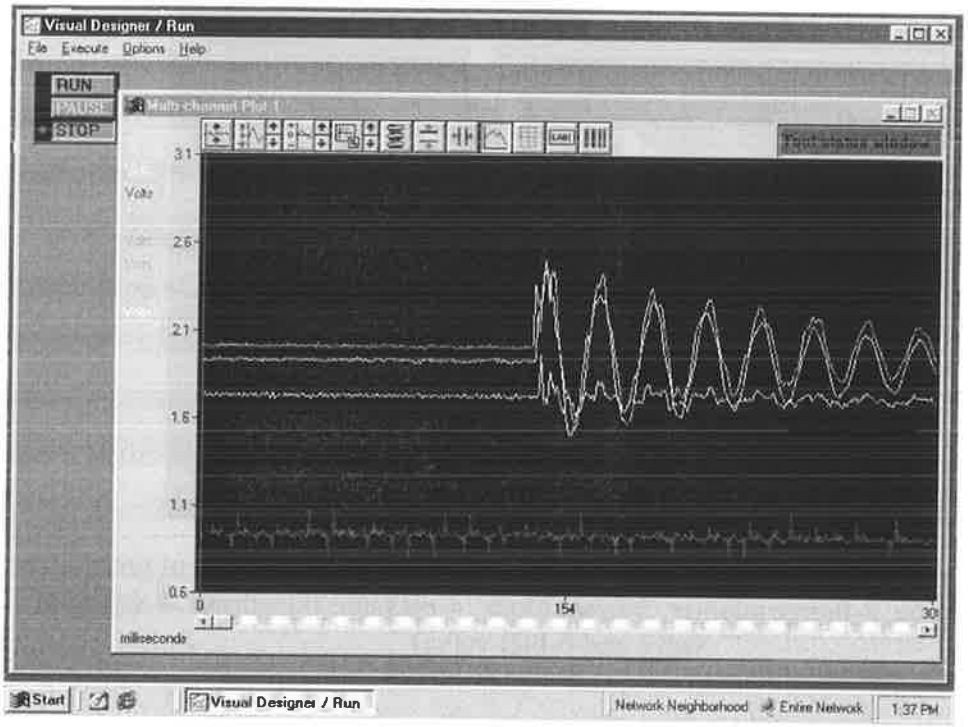

Figure 8.10 A graphical plot window in the Visual Designer Software for a transient test

8.3 Calibration of the network apparatus

Various properties of the experimental apparatus are needed for accurate measurements. Calibration results, including the friction factors of the pipes, properties of the pressure transducers, properties of leak orifices and the wave speed are presented in this section. Calibration results related to the flow meters, square-edged weir, and the ball valve are included in the Appendix E.

8.3.1 Pipe friction

The estimated roughness of the copper pipe is ε = 0.0015mm, giving a relative roughness of $\varepsilon/D = 2.0\times10^{-5}$. The Darcy-Weisbach friction factor, as calculated from the Colebrook-White formula, is presented in Figure 8.11 for different Reynolds numbers. The friction factor of the pipes in the pipe network at steady state were verified using the pressure difference measured between T2 and T3 (Figure 8.1b) and

the measured flow. Experimental results for steady state conditions below a Reynolds number of 20,000 could not be plotted because the pressure difference was smaller than the measurement resolution. A minor head loss coefficient of 0.15 (at valve V6) was applied in calculating head losses between T2 and T3 in the experimental verifications.

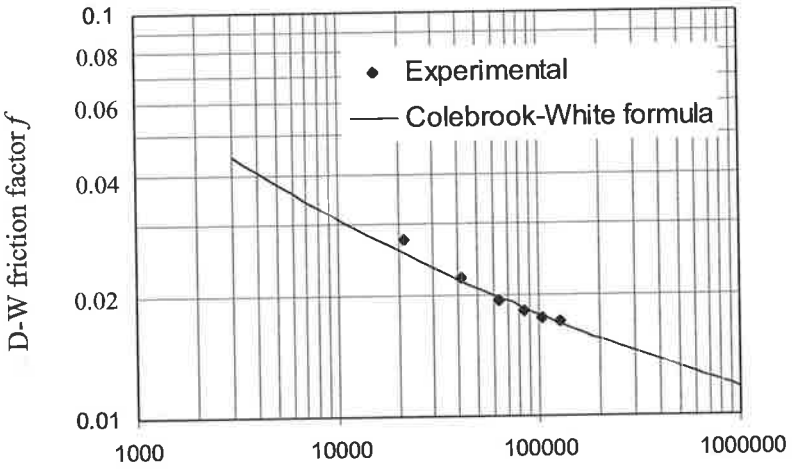

Figure 8.11 Steady-state friction factor

Minor losses at elbows and junctions in the pipe network are calculated based on the formula of Miller (1993) as given in Section 7.6.2. The validation of these formula for estimating the minor losses in the pipe network is presented in the Appendix E where steady states at different configurations are calculated using the numerical model discussed in Section 7.6.2.

8.3.2 Calibration of pressure transducers

Calibration was performed for each of the five pressure transducers using a hand pressure tester, the result of which for transducer B at T6 is in Figure 8.12, which shows a linear relationship between the voltage and pressure. From a linear regression the R^2 term in each case is close to 1 ($R > 0.99$), indicating a good fit. Calibration results for the other transducers are included in Appendix E.

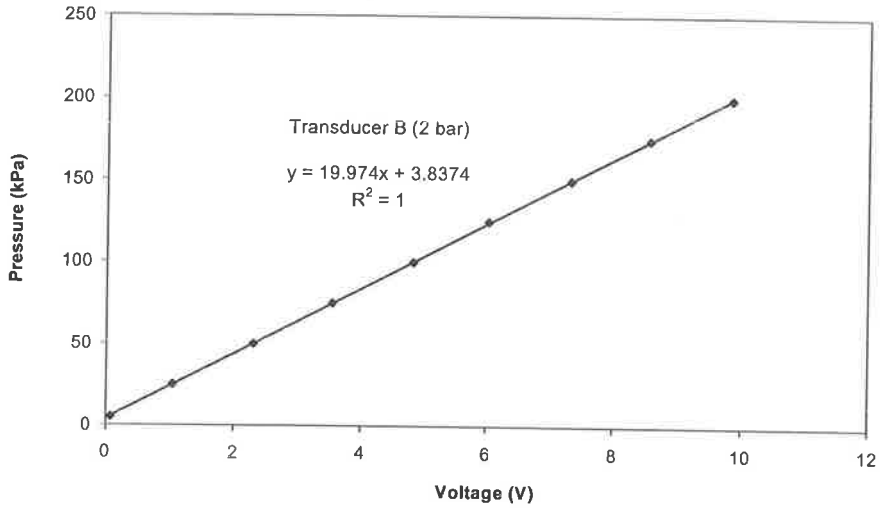

Figure 8.12 Calibration of the pressure transducer (at T6)

An important property of the pressure measurement is the error associated with each transducer. Random error is caused by electromagnetic interference (EMI) from environmental electromagnetic radiation. The error is visualised by observing the scatter from the each pressure transducer. Figure 8.13 shows the scatter for the pressure transducer at T3 (see Figure 8.1b).

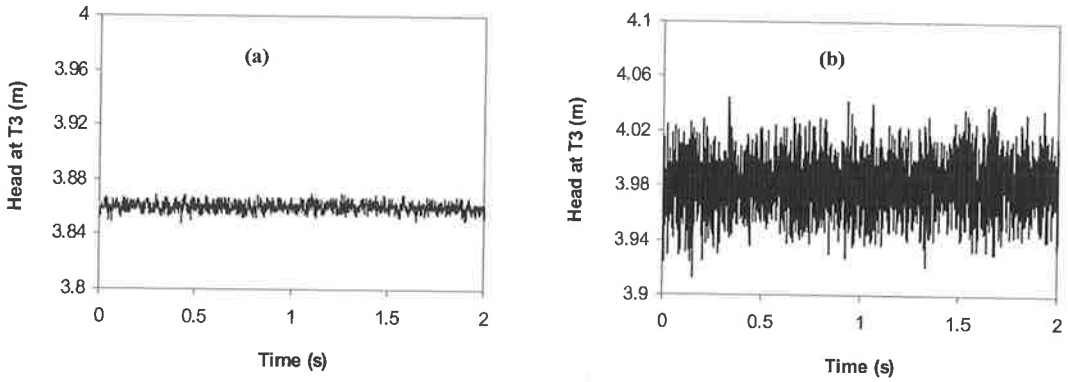

Figure 8.13 Random error in the pressure transducer: (a) Pump is shut down and (b) Pump is operating

Assuming that the error has a normal distribution, the standard deviation of the random error in the signal of Figure 8.13(a) is 3.1mm when the pump is shutdown. When the pump is on, the standard deviation is 18.5mm, indicating that random error in the signals is significantly larger when the pump is operating. This large random error is caused by the vibration of the pipe network due to the pump operation. The standard

deviations of the measured pressure at different locations are given in Table 8.4. Tests conducted when the pump is shut down improve the accuracy of the leak detection.

Table 8.4 Standard deviation at pressure transducers

Transducers	T1 (m)	T3 (m)	T5 (m)	T6 (m)	T7 (m)
Pump off	0.0049	0.0031	0.0034	0.0052	0.0038
Pump on	0.0243	0.0185	0.0242	0.0291	0.0151

8.3.5 Calibration of leak orifices

The calibration result for the D_L = 3mm leak orifice at T2 (see Figure 8.1) is given in Figure 8.14. The orifice equation is fitted to the data using a standard least square fit, which yields

$$Q_L = 7.0\times10^{-6}(2gH_L)^{0.489} \tag{8.2}$$

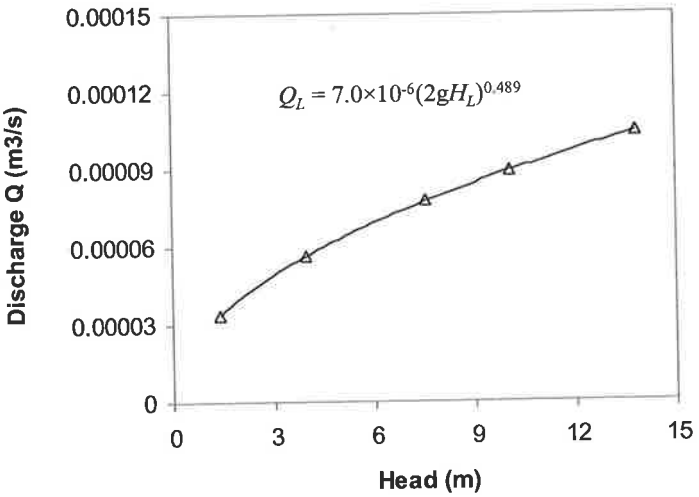

Figure 8.14 Calibration of the leak orifice at T2 (D_L = 3mm)

From the previous analysis in Chapter 3, a leak with a non-theoretical relationship ($b \neq 0.5$) can be expressed by an equivalent theoretical leak ($b = 0.5$). The calibrated non-theoretical relationship given in Eq. (8.2) can be expressed as a theoretical leak given the steady head of H_{L0} = 3.86m at the leak (see Eq. 3.35c)

$$Q_L = 6.5\times10^{-6}(2gH_L)^{0.5} \tag{8.3}$$

Since the discharge relationship of a leak is normally not known in advance, an equivalent theoretical leak size $C_dA_L = 6.5 \times 10^{-6}\text{m}^2$ is used in the following sections for the leak detection analysis.

8.3.6 Calibration of wave speed

The theoretical wave speed for water in the thin-walled (D/e = 44.7 > 25) elastic copper pipe is calculated as (Wylie and Streeter 1993)

$$a = \sqrt{\frac{\frac{K}{\rho}}{1+\frac{KD}{Ee}c_1}} = \sqrt{\frac{\frac{2.19\times10^9}{998}}{1+\frac{2.19\times10^9\times0.07294}{120\times10^9\times0.00163}1.00}} = 1099\text{m/s} \qquad (8.4)$$

in which the dimensionless parameter c_1, describing the effect of pipe constraint conditions on the wave speed (Wylie and Streeter 1993), is chosen as c_1 = 1.0 for a pipe anchored with expansion joints throughout.

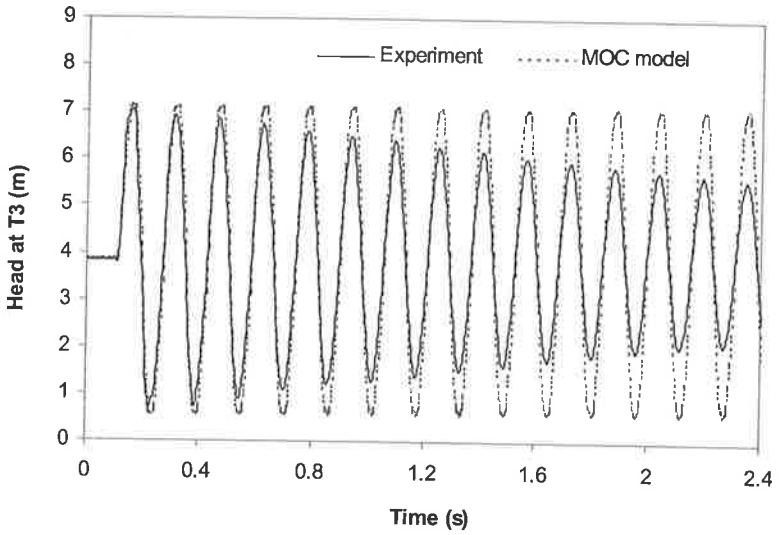

Figure 8.15 Calibration of wave speed

The wave speed is calibrated in a single pipeline case within the pipe network as shown in Figure 8.16 (achieved by closed valves V3, V4, V6, V9 and V14). The transient was generated by closing V13 from a steady state. In the pipeline as shown in Figure 8.16, there are four short dead ends (consisting of the same pipe and with length L_D = 0.23m) located at nodes of 4, 8, 16 and 26. Previous analysis in Section 7.7 has shown that presence of dead ends decreases the harmonic frequencies of a

transient event. In this study, the wave speed was calculated based on an inverse fitting using the MOC (Figure 8.15), in which the wave speed was determined by a trial and error to give the best match on the frequency of the measured transients. The wave speed was determined as a = 1065m/s, which is used in the further analysis of the experimental tests. If the wave speed is directly calculated from the dominant frequency of the measurement using a Fourier frequency analysis, the wave speed is 1055m/s, which has been influenced by the dead ends. There are clear differences between the theoretical and the calibrated wave speed. This may be due to the uncertainties in the water and pipe properties (i.e. the elasticity of the copper pipe and bulk modulus of the water).

8.4 Simulation of transients

Two groups of transient tests conducted in the pipe network are presented in this section. The first group of tests was conducted based on a single pipeline configuration as shown in Figure 8.16. The second group of tests was conducted based on a three-loop configuration, a more complex case, as shown in Figure 8.20. Within each group, two types of tests, with and without a 3mm leak at T2, were conducted. Tests without leaks were conducted to calibrate the unsteady friction parameters in the numerical model. Each type of test was repeated three times. The sampling frequency for all tests presented in this chapter is 2000Hz at each transducer.

8.4.1 Experimental tests in a single pipeline layout

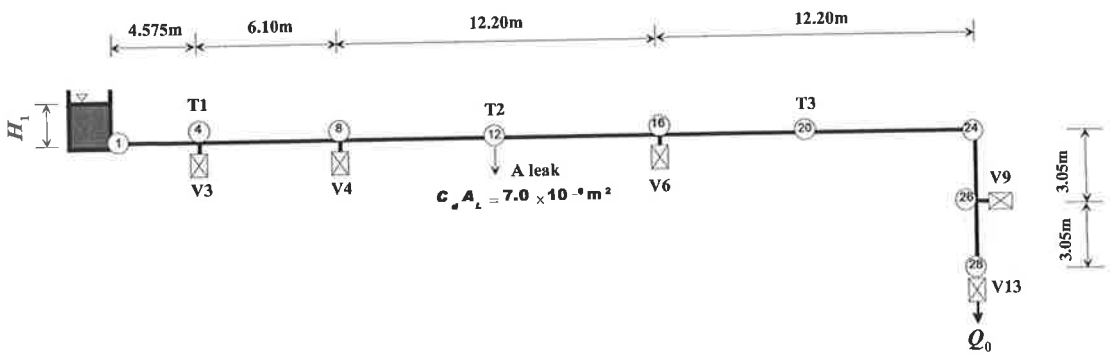

Figure 8.16 Layout of a single pipeline configuration

(H_1 = 3.86m, Q_0 = 0.125L/s)

For the pipe system shown in Figure 8.16 (test1, leak at T2 closed), a transient was generated by closing valve V13 from a steady state of Q_0 = 0.125L/s, giving a Reynolds number of **Re** = 1914 (in the laminar range). The transient measured at T3 and simulation results –using unsteady friction models including k_A & k_P model (Vítkovský 2001) and Zielke unsteady friction model (Zielke 1968)— are presented in Figure 8.17. In the simulation model, the pipeline is divided into 27 reaches and 28 nodes. Each of the calculation units is equal to 1.525m giving the Courant number of C_r = 1.0. The boundary condition at the downstream (node 28) is treated as a flow boundary condition. The flow rate at node 28 is linearly decreased from 0.125L/s to 0.0 within the period of 0.1s~0.135s. The unsteady parameters in k_A & k_P model are determined by a trial and error process as k_A = 0.02 and k_P = 0.0. If calculated using Eq. (7.7a) k_A = 0.03.

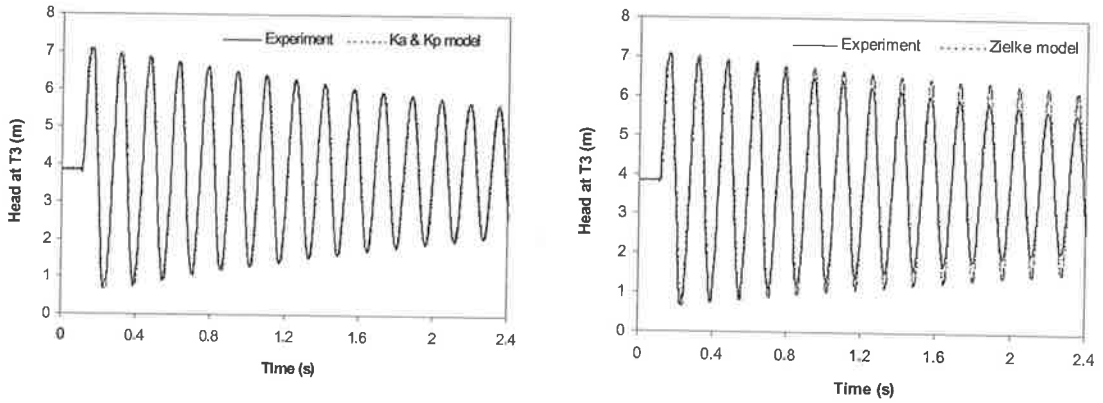

Figure 8.17 Comparison of transients measured from a single pipeline without a leak and simulation results using different models (test1)

Since the Zielke model is physically based and was developed for laminar flow, no calibration is needed to simulate transients in a straight pipeline for laminar flow. However, Figure 8.17 shows that Zielke model under-estimates the damping of the transient event compared to the experimental measurement. Since unsteady-friction effects of a transient event can be reasonably estimated by the Zielke's model, the discrepancy between the simulation and experimental tests suggests that there are additional damping factors in the experiment. These damping factors may include the dissipation at the flange connections, unsteady mixing at the junctions of dead ends and pipe and viscous-elastic effects of the pipe material and water. Therefore, given the good agreement between the k_A & k_P model and experimental results, the

parameters used in k_A & k_P model actually include these additional effects although the model is called an unsteady friction model. In the author's view, if parameters k_A and k_P are fitted as described above it is more accurate to call the parameters **unsteady calibration parameters** rather than unsteady friction parameters since unsteady friction only accounts for part of damping and phase changes in a transient event.

As mentioned earlier, there are four short dead ends (L_d = 230mm, D_d = 72.94mm, a_d = 1065m/s) as shown in Figure 8.16. The effects of these dead ends on transients have been considered numerically using a lumped parameter model presented in Section 7.7. Neither the experimental tests nor the numerical simulation results show reflection from dead ends. This indicates a slow transient event. If the dead ends are not considered in the simulation, a phase difference is observed as shown in Figure 8.18. Although good agreement between the experimental tests and simulation on the phase of a transient can be achieved by adjusting the wave speed for this type of slow transient event, that is not the case for fast transients in which case the inclusion of dead ends is necessary as discussed in Chapter 7 (section7.7).

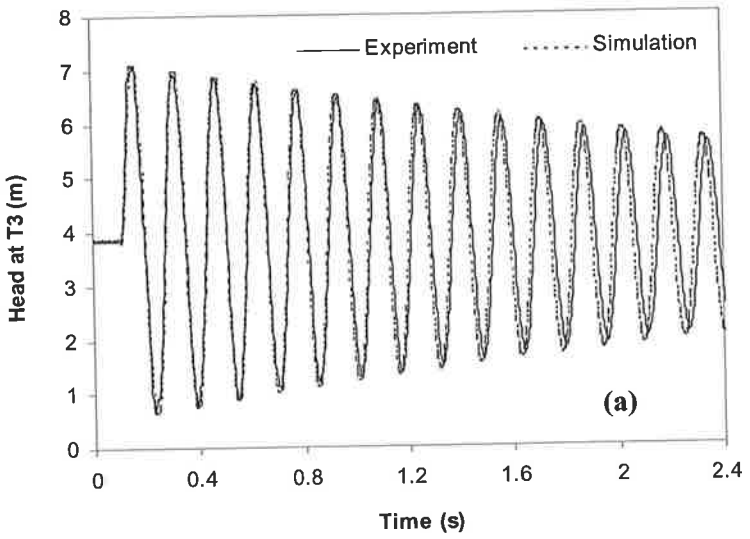

Figure 8.18 Effects of dead ends on pipeline transients

By leaving the leak orifice at T2 open and sharply closing V13 from a steady state of Q_0 = 0.125L/s (at the downstream pipe of the leak), a transient event was generated. The transient measured at T3 and the simulation results are presented in Figure 8.19. In the simulation, two types of calibration parameters are considered, k_A = 0.03 and k_P = 0.0, which are theoretically calculated using Eq. (7.7a), and k_A = 0.02 and k_P = 0.0

which were determined in the previous calibration test. Both simulations agree well with the experimental results suggesting an insignificant dependence on the unsteady friction parameters.

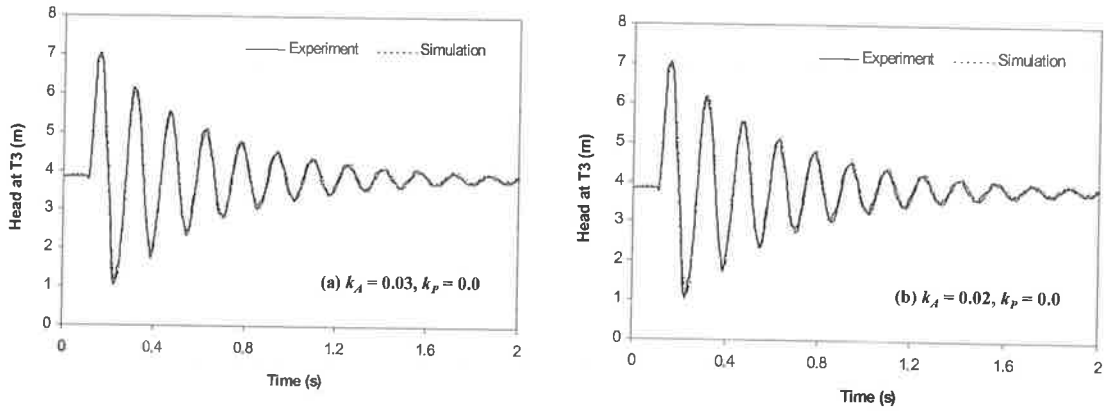

Figure 8.19 Comparison of transient measured from a single pipeline with a leak and simulation result (test1L)

8.4.2 Experimental tests in the looped network

Two types of tests, with and without a 3mm leak at T2 (Figure 8.20), were conducted. The transients were generated by closing valve V15 from a steady state of Q_0 = 0.25L/s for the no-leak case and Q_0 = 0.31L/s for the leak case (measured at flow meter F1). The Reynolds number of the flow in the network ranges from **Re** = 119 to **Re** = 3518 for the no-leak case and ranges from **Re** = 19 to **Re** = 4383 for the case of with a leak at T2.

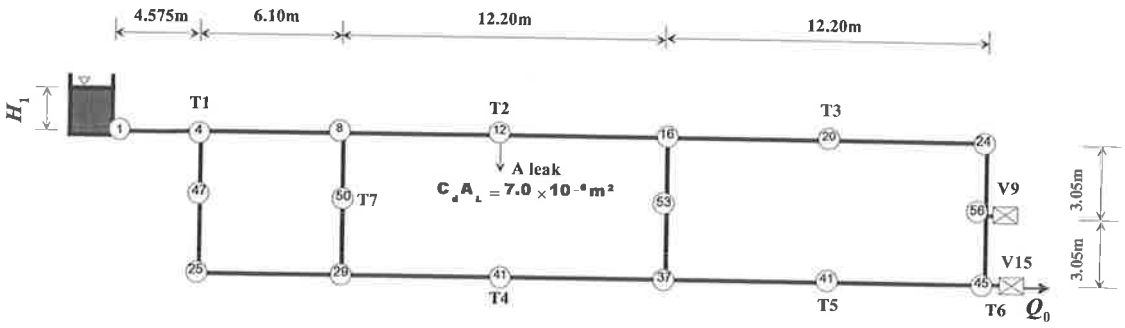

Figure 8.20 Layout of a three-loop network configuration

(H_1 = 3.86m, Q_0 = 0.25L/s)

Transients measured at T3 and T7 for cases of with (test2L) and without a leak (test2) and the corresponding simulation results using the k_A & k_P model (Section 7.3) and

Zielke model (Zielke 1968) are presented in Figure 8.21 and Figure 8.22. In the numerical simulation, the network is divided into 59 pipe units with equal length of 1.525m with 57 nodes giving the Courant number of $C_r = 1.0$. The parameters in the k_A & k_P model are calculated using Eq 7.7(a). Because of the different Reynolds numbers at different pipes, parameter k_A ranges from 0.033 to 0.1215 and k_P ranges from 0.041 to 0.2515. Parameters k_A and k_P at pipe P0 are the lowest since the flow rate at pipe P0 is the largest while parameters at pipe L3 are the largest because of the smallest flow rate in the pipe (see Eq. 7.7a). Compared to the measurements, both the k_A & k_P model and Zielke model can simulate the first peaks of the transient correctly. However, both models under-simulate the damping of the transient and there is an obvious phase difference between the simulation and the measurement results.

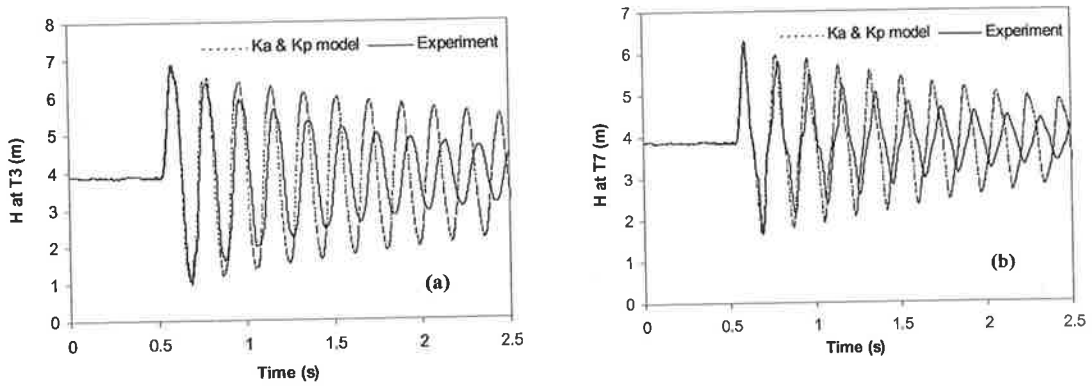

Figure 8.21 Transients from a three-loop network for the case of without a leak using the k_A & k_P model based on the theoretical parameters: (a) at T3 and (b) at T7

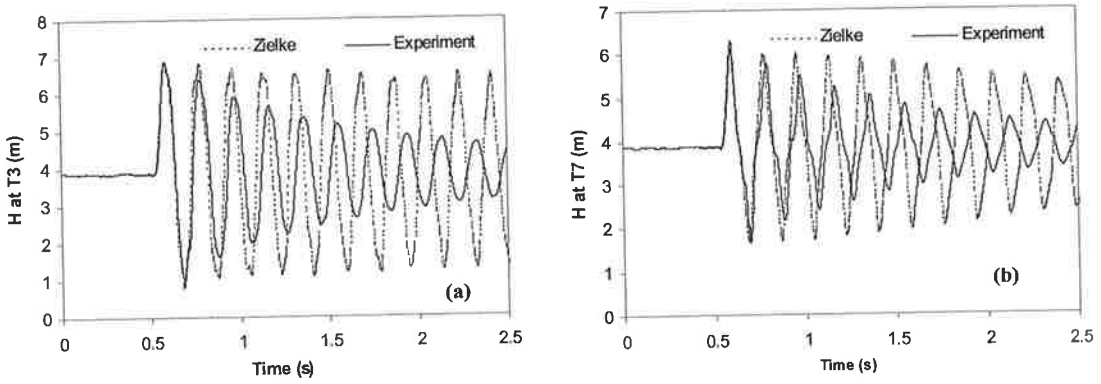

Figure 8.22 Transients from a three-loop network for the case of without a leak using the Zielke model: (a) at T3, and (b) at T7

There are several possible reasons for the discrepancy between the simulation and measurement results. Firstly, dissipation at the flange connections and the unsteady mixing at pipe junctions may contribute additional damping on a transient event. Secondly, air that dissolved in the water may be realised during the transient event, and as a result, this should influence both the damping and phase of the transient. The influences of dissolved and realised air in a pipe network system on the fluid transients are discussed in Section 8.4.3.

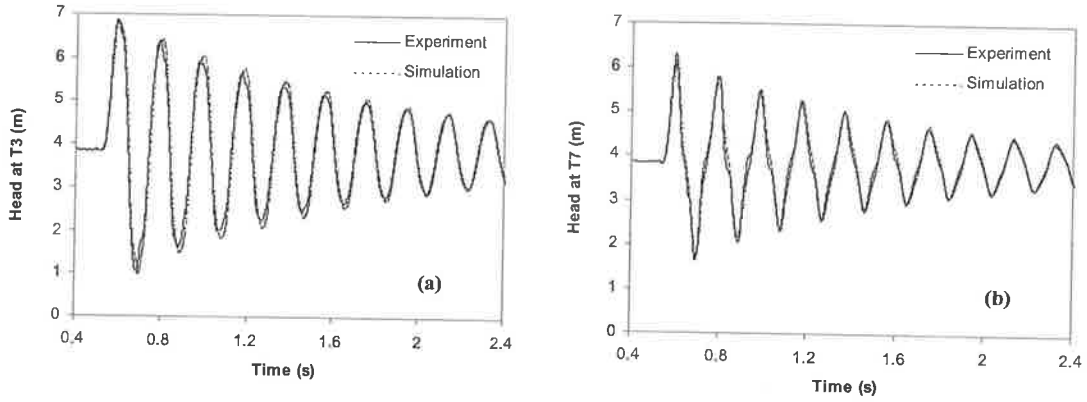

Figure 8.23 Transients from a three-loop network at case of without a leak (test2): (a) at T3, and (b) at T7

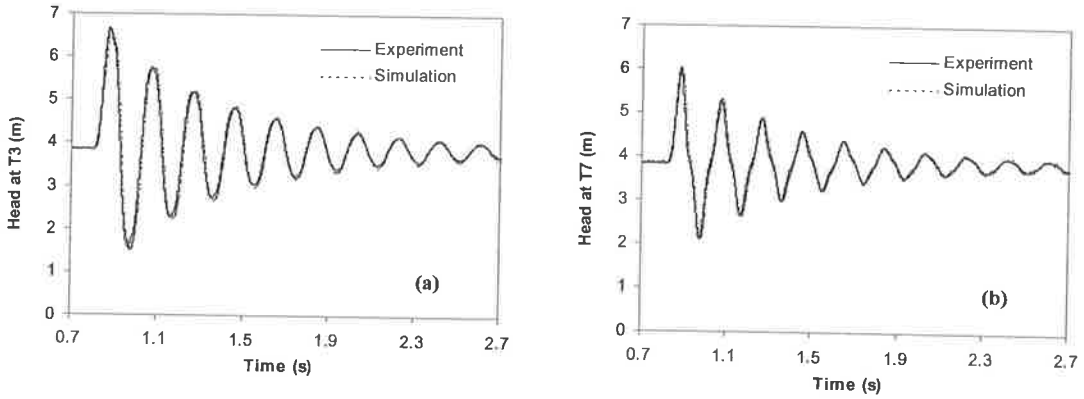

Figure 8.24 Transients from a three-loop network at case of with a leak of $C_dA_L = 6.5\times10^{-6}m^2$ at T2 (test2L): (a) at T3, and (b) at T7

In order to match the measurement, parameters in the k_A & k_P model are adjusted using a trial and error procedure. For the case of no leak (test2), the calibration parameters in the numerical model were determined as $k_A = 0.0875$ and $k_P = 0.123$. Simulation results using the k_A & k_P model based on these adjusted parameter are given in Figure 8.23. Based on these parameters ($k_A = 0.0875$ and $k_P = 0.123$), the simulation results

for the case of with a leak at T2 are given in Figure 8.24. Simulated transients agree well with the measurements for both cases with and without a leak. In the numerical simulation, the minor losses at elbow and junction are not considered because the flow rates in the network are so small that the steady minor losses effects are negligible based on the analysis presented in Chapter 7. Cases in which the minor losses cannot be neglected are discussed in Section 8.4.4.

Given the capability of k_A & k_P model in simulating transients in a pipe system, this model is applied in this study for leak detection analysis.

8.4.3 Air in pipe systems

During the commissioning stage of experimental tests, air dissolved in the water and entrapped in the network caused severe problems on transient measurements. Figure 8.24a gives a transient test that was significantly influenced by entrapped air in the system. The test was conducted in the three-loop network (without a leak) as described in Figure 8.20, and the transient was generated by closing valve V15 from a steady state of Q_0 = 0.30L/s (measured at flow meter F1). Compared to the results in Figure 8.23 which were measured from the same network and the transients were generated in the same way, the transients presented in Figure 8.24a decays much faster. The period of the transient in Figure 8.24a is about 0.22s while that in Figure 8.23 is about 0.19s.

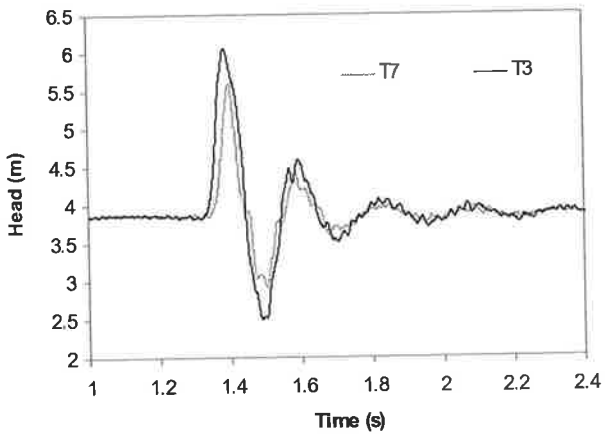

Figure 8.24a A transient test that is influenced by entrapped air (H_1 = 3.86m, Q_0 = 0.30L/s)

Because the network was horizontal, air entrapped in the system was difficult to expel for the network. As a remedial measure, air release valves were installed in the network in order to get rid of the entrapped air in the pipe network before a transient test. Before each test the system was flushed thoroughly. In addition, air that was dissolved in the water may be liberated during a valve operation. For example, when an upstream valve is closed, dissolved air tends to be released. Therefore, a procedure for the valve operating order was designed in order to avoid release of the dissolved air. In order to reduce the volume of dissolved air in the water during a transient test, all the transient tests were conducted after the pump was shut down for at least half a day; thus the air that was dissolved in the water during pump operation could be released in the tank. Despite above measures, however, there is no guarantee that air can be completely avoided during a transient event. Although two-phase transient flow is not the main subject of this study, the influence of air on the transient simulation and leak detection in a pipe network system is discussed in this section.

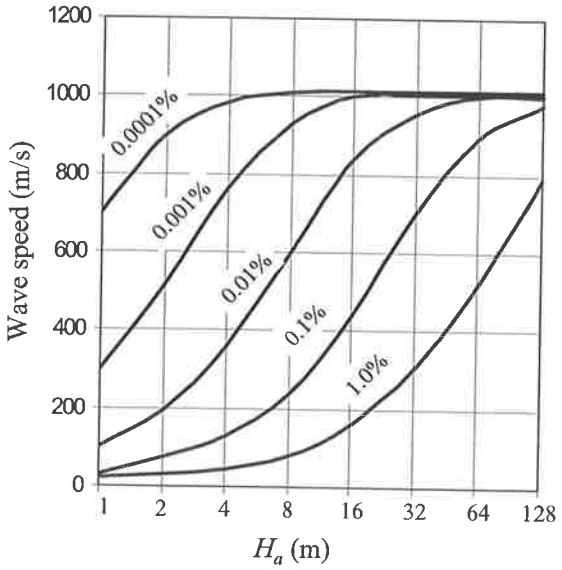

Wavespeed for air water-mixtures. Percent represents the percentage of air by volume at standard pressure. $(K_l/E)(D/e) = 1$

Figure 8.25 Figure 8.2 in Wylie and Streeter (1993)

A comprehensive study of two-component and single-component two-phase transient flows is given in Chapter 8 of Wylie and Streeter (1993). For dissolved air in water, a significant effect on a transient event is the decrease of wave speed because the air in water reduces the bulk modulus of water. Figure 8.2 in Wylie and Streeter (1993) is

reproduced in Figure 8.25. Figure 8.25 shows that influence of air volume is more significant for a lower pressure system such as the present network system because the influence of air volume on the bulk modulus of water is more pronounced at a lower pressure than at a higher pressure. Given the maximum water surface of H_1 = 3.98m in Tank 1, an air volume of 0.001% in the network can reduce the wave speed to less than 800m/s from the maximum value of 1010m/s. Dissolved air in water may be the main reason for the discrepancy between the theoretical and calibrated wave speed in Section 8.3.6. The influence of the wave speed on the transients is investigated in the pipeline as shown in Figure 8.16. Transients calculated using the MOC (based on two wave speeds, a = 1065m/s and a = 800 m/s are given in Figure 8.25a. In the MOC, the unsteady parameters of k_A & k_P model and the boundary conditions are same as those used in Section 8.4.1. The decrease of wave speed from 1065m/s to 800 m/s increases the transient period and reduces the magnitude of the transient.

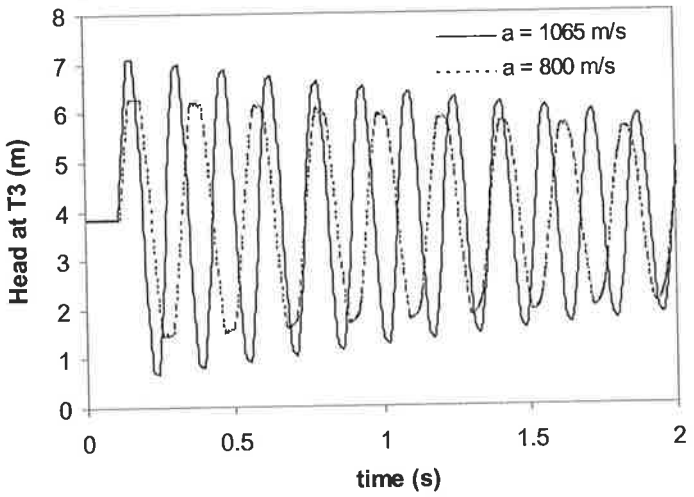

Figure 8.25a Influence of wave speed on the transients in the pipeline as shown in Figure 8.16 (H_1 = 3.86m, Q_0 = 0.125L/s)

In addition to reducing the wave speed, dissolved air may be released during a transient event and then the released air is trapped in the pipe network system. Previous research has been conducted regarding the influence of the entrapped air on fluid transients (Martin 1976; Wylie and Streeter 1993;. Zhou et al. 2002). Compared to a water hammer event in a pipe system without air, entrapped air tends to cause extra damping and to reduce the frequency of a transient event due to the cushion effects of the air (Lee and Martin 1999; Chaiko and Brinchman 2002). Previous

analysis in Chapter 3 indicated that a leak in a pipe system also causes damping of a transient event. Therefore, a method is necessary to distinguish leak damping from damping caused by entrapped air, otherwise, a leak may be perceived as entrapped air.

Previous analysis in Chapter 3 indicated that a leak causes damping of a transient event; however, the leak (small size) has no influence on the wave speed (frequency) of the transient. In contrast, entrapped air in a pipe system increases both damping and period of a transient event. Therefore, the presence of a leak in a pipe system can be recognised by an increased damping, while presence of entrapped air is characterised by an increased transient period compared to a normal situation.

8.4.4 Steady-state calibration and transient calibration

In the previous experimental tests, the flow rates in the pipe system are so small that the hydraulic head losses in the pipe system are negligible. Heads at different locations in the pipe system are same as the head (H) of the Tank1 (H = 3.86m). As a result, no steady-state calibration is needed. In this section, cases of with larger flow rates are discussed.

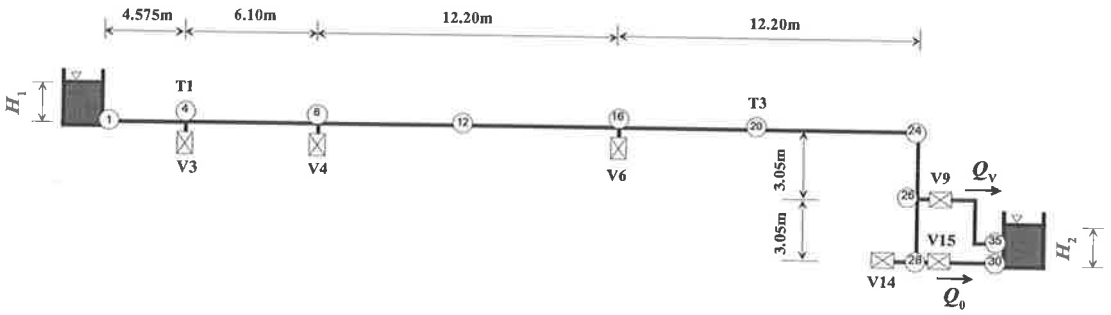

Figure 8.26 Layout of a single pipeline (V15 is fully open)

(H_1 = 3.86m, H_2 = 1.43m, Q_0 = 7.23L/s, Q_V = 0.63L/s)

For the pipeline as shown in Figure 8.26, valve V15 is fully open and valve V9 is partially open. The water levels at two tanks are H_1 = 3.86m and H_2 = 1.43m (distance between the water level and the horizontal network). The steady flow at V15 is Q_0 = 7.23L/s and discharge at V9 is Q_V = 0.63L/s. A transient event is generated by closing V9. The transients, measured at T1 and T3, are plotted in Figure 8.27.

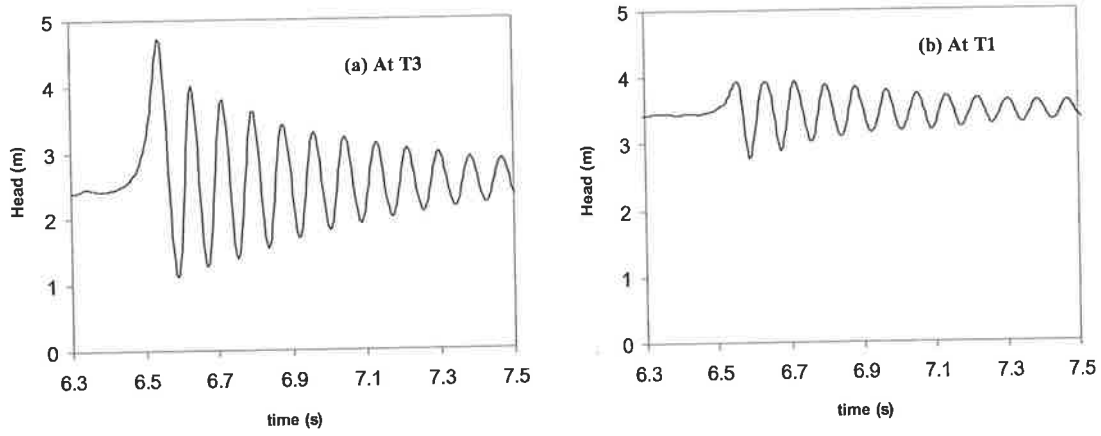

Figure 8.27 Transients from the single pipeline as shown in Figure 8.26

In this case, the flow rates in the pipeline segment within the network are not negligible both before and after valve V9 is closed. As a result, the minor losses at elbows and junctions (dead end junctions) are not negligible. As shown in Table 8.5, if the minor losses are not considered, both the simulated steady flow rate (Q_0 at V15) and the heads (at T1 and T3) are significantly different from the measured values. The effects of minor losses on steady state can be considered by either adjusting the friction factors in different pipe sections or using head loss elements **(steady state calibration)** to make the simulation results, including flow rate and pressures, equal to the corresponding measurements. Based on the adjusted friction factors, which give the correct steady state conditions, the transient event is then simulated using suitable calibration parameters k_A and k_P **(transient calibration)**. Therefore, the calibration process before a leak detection calculation includes the steady state calibration, in which the steady-state friction factors and minor losses coefficients are determined, and the transient calibration, in which the unsteady calibration parameters k_A and k_P are determined.

Table 8.5 Influence of minor losses on the steady state flow rates and heads

Cases	Flow rate (L/s)	Head at T1 (m)	Head atT7 (m)
Measurement	7.26	3.57	2.56
Simulation (without minor losses)	8.97	3.71	2.29
Simulation (with minor losses)	7.26	3.57	2.56

When the flow rates in a pipe system are so small that the influence on the pressure distribution in the system is negligible, steady state calibration is not necessary. The head along the pipe may be assumed to be fairly constant at the value of the upstream supply tank. In addition, previous analyses conducted in Chapter 6 and Chapter 7 have shown that the damping effect of minor losses (head loss elements) on a transient event is proportional to the steady-state flow rates. Therefore, it is simpler and more accurate to conduct a leak detection operation under condition of negligible flow rates in a pipe system.

8.5 Application of ITM for leak detection

The Application of the inverse transient method (ITM) for leak detection using real measurement data from the looped pipe network is presented in this section. Two cases, a single pipeline layout and a three-loop network are discussed in Section 8.5.1 and Section 8.5.2. All transient tests were conducted under a condition of a small flow rate, high enough for transient generation but small enough so that minor losses (and steady friction losses) are negligible.

8.5.1 A single pipeline case

For the single pipeline layout as shown in Figure 8.19 (leak at T2 open), the transient measured at T3, as shown in Figure 8.19, is used in the ITM for leak detection. Six possible leak candidates were assumed at nodes 4, 8, 12, 16, 20 and 24. The minimisation results using the Levenberg-Marquardt (L-M) method and Shuffled Complex Evolution (SCE) algorithm are shown in Table 8.6. The convergence of the minimisation and the response of detected leaks (SCE method) in comparison of measured transients are given in Figure 8.28. These results show that leak is incorrectly found at node 4 by both methods with a larger leak size than the actual value. The main reason for the failure to find the location of the leak is due to small sensitivity of a smooth transient event, which lacks high harmonics, to the leak location. This phenomenon was also observed in the experimental tests for the straight single pipeline (Vítkovský 2001).

Table 8.6 Application of ITM for leak detection in a single pipeline

Node	Real size (m^2)	L-M method (m^2)	SCE (m^2)
4	0	**2.17E-05**	**9.90E-06**
8	0	-1.22E-06	1.67E-06
12	6.50E-06	-0.302E-07	4.09E-08
16	0	8.25E-07	3.07E-09
20	0	7.32E-07	9.60E-07
24	0	9.98E-07	1.07E-06

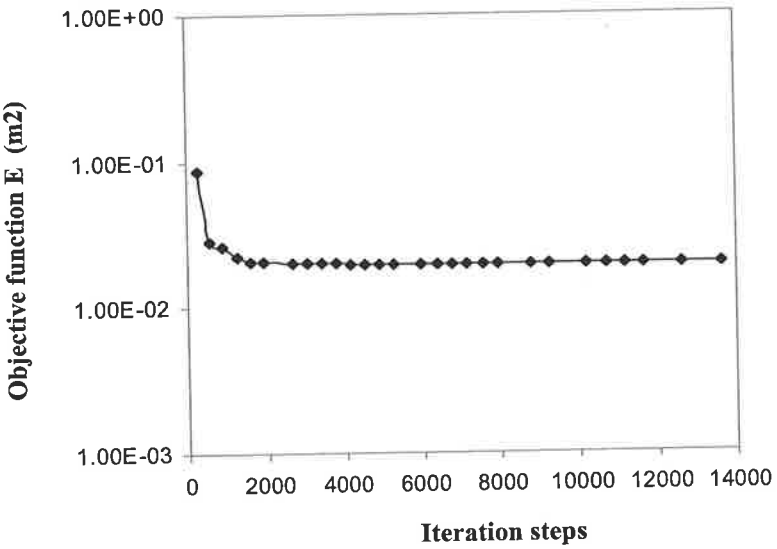

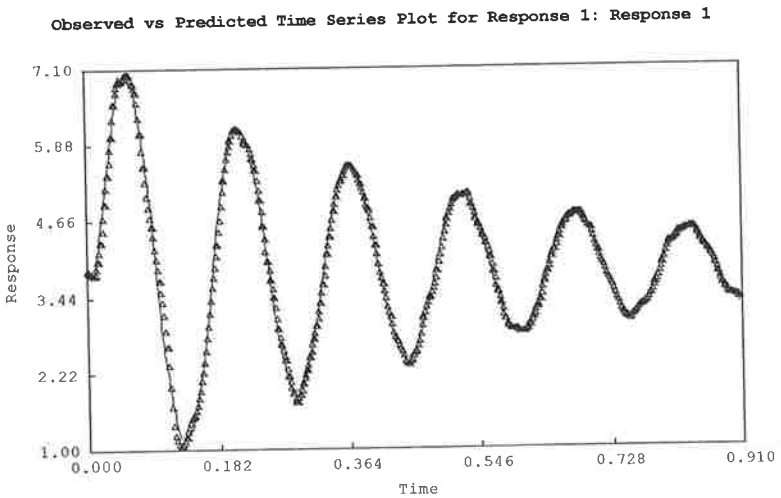

Figure 8.28 Leak detection in the single pipeline by SCE method (a) Objective function, (b). Response based on detected leak parameters

As discussed in Chapter 3, a transient in a pipeline can be expressed in a Fourier series. For an individual frequency n, leaks at different locations with different sizes can have same response as long as these leaks have a same leak damping parameter R_{nL} ($R_{nL} = \frac{C_d A_L}{A} \frac{a}{\sqrt{2gH_{L0}}} \sin^2(n\pi x_L^*)$). For a transient with enough harmonics, leaks at different locations along the pipeline cannot have the same damping parameter for all harmonics except a symmetrical leak in a reservoir-pipeline-reservoir system. However, for a smooth transient event that lacks high harmonics and is close to a sinusoidal signal, theoretically two leaks with different sizes at any location along the pipeline can have the same damping parameter R_{nL}. This results in an ill-posed leak detection problem with an infinite number of solutions. Figure 8.29 shows that the transients response based on the detected (incorrect) leak parameters given in Table 8.6 is almost identical to that based on the actual situation, a leak of $C_dA_L = 6.5\times10^{-6}$ m^2 at node 12.

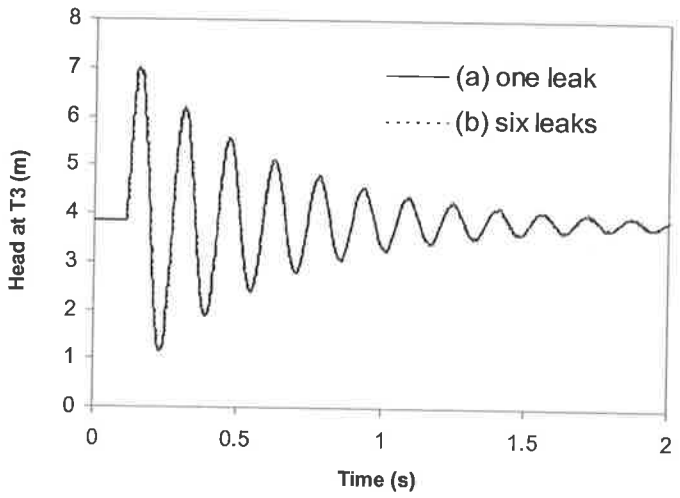

Figure 8.29 Response of different leak solutions: (a) a leak of $C_dA_L = 6.5\times10^{-6}$ m^2 at node 12, and (b) six detected leaks given in Table 8.6 (SCE method)

The objective function based on the detected leak parameters is $E = 7.2$ m^2 while based on actual leak parameter is $E = 9.3$ m^2 indicating a successful minimisation. Therefore, if the size of a leak is not known, it is impossible to locate the leak using a sinusoidally smooth transient event. To better apply a transient for leak detection, the transient event should have as many harmonics as possible. Progress on generating fast (but not large) transient event is under taken in this pipe network using

controllable injections and vibrating membrane method (Lee 2002). A faster transient event initiated by closing a solenoid valve is discussed in Section 8.5.3.

In additional to a smooth transient event, the simulation of boundary condition at the valve V13 (node 28) influences the performance of ITM for leak detection. In the simulation, node 28 is treated as a flow boundary condition of Q_0 = 0.125L/s, and is linearly reduced to zero within 0.035 second. The actual process of flow change is not known and difficult to measure in the experiment.

8.5.2 A three-loop network

Application of the ITM for leak detection in a three-loop network, as shown in Figure 8.20, is presented in this section. A transient event was initiated by closing valve V15 from a steady state flow of Q_0 = 0.31L/s (measured at flow meter F1) with a 3mm leak located at T2. The transient was measured at five locations T1, T3, T5, T6 and T7. Measurements at T3 and T7, shown in Figure 8.24, are used in the ITM for leak detection. In the transient model used in the ITM, the network is divided into 59 calculation units and 57 nodes, and the unsteady parameters k_A and k_P are from the transient calibration test that has been discussed in Section 8.4.2.

Table 8.7 Application of the ITM for leak detection in a three-loop network

Node	Real size (m^2)	L-M method (m^2)	SCE (m^2)
4	0	**4.17E-06**	1.63E-06
8	0	-5.93E-07	2.31E-07
12	6.50E-06	1.97E-06	1.50E-07
16	0	2.59E-06	3.12E-07
20	0	1.45E-06	9.61E-07
24	0	-1.27E-06	9.83E-07
25	0	-1.82E-06	**3.58E-06**
29	0	-1.67E-06	8.45E-07
33	0	-1.23E-07	3.90E-07
37	0	1.17E-06	2.38E-07
41	0	9.63E-07	3.63E-07

Twelve possible leak candidates were assumed at nodes 4, 8, 12, 16, 20, 24, 25, 29, 33, 37 and 41 (see Figure 8.20). The minimisation results using the L-M method and the SCE algorithm are given in Table 8.7. These results show that the leak is incorrectly found at several different locations by the L-M method and the SCE method. The convergence process using SCE method and the response based on detected leaks are presented in Figure 8.30. Figure 8.30 shows that response (measured at T7) based on the detected *incorrect* leaks agree well with the measurement.

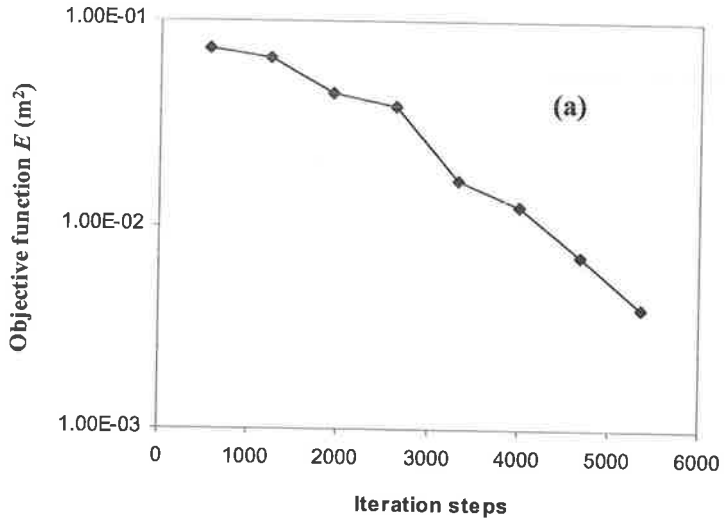

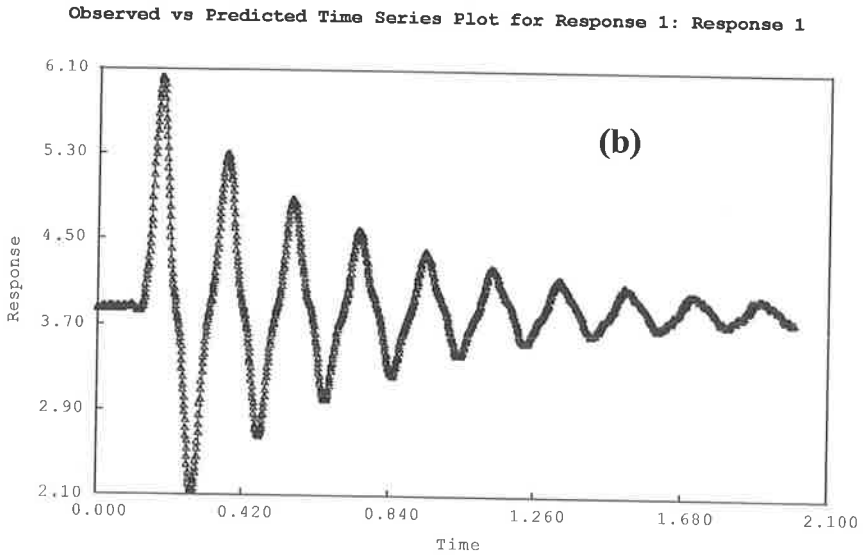

Figure 8.30 Leak detection in the three-loop network by SCE method (a) Objective function, (b). Response based on detected leak parameters

Similar to the situation in a single pipeline discussed in Section 8.5.1, the main reason for the failure of leak location is because of the smooth transient event. For a smooth transient event, which lacks high frequencies, leaks at different locations with different sizes may generate the same or similar response. Figure 8.31 plots the responses (measured at T3 and T7) for two different leak cases, a leak of $C_dA_L = 6.5\times10^{-6}m^2$ at T2 and a leak of $C_dA_L = 3.88\times10^{-6}m^2$ at T3. The responses by these two different leak situations are almost identical. Due to this low sensitivity to leak location, in order to apply the ITM for leak detection, a fast transient event is necessary.

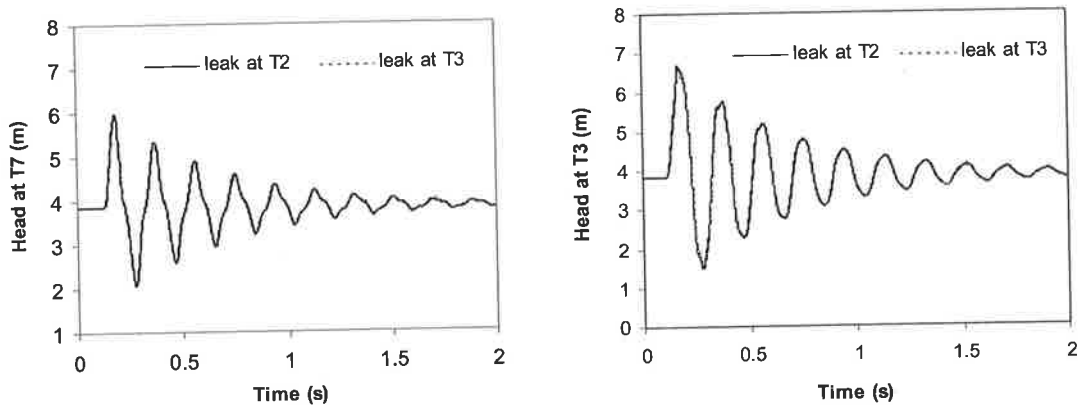

Figure 8.31 Transients for two different leak situations (a leak of $C_dA_L = 6.5\times10^{-6}\,m^2$ at T2 and a leak of $C_dA_L = 3.88\times10^{-6}m^2$ at T3)

8.5.3 Transients initiated by closing a solenoid valve

To generate a faster transient event aiming to improve the performance of the inverse transient method for leak detection, two solenoid valve were installed in the network at T3 and T6 (see Figure 8.20). The closing time of the solenoid valve was less than 6 milliseconds. For a single pipeline layout as shown in Figure 8.16, where valve V13 is closed, transients generated by closing the solenoid valve at T3 are presented in Figure 8.32. The water level in Tank1 was $H_1 = 3.86$m and discharge through the solenoid valve was $Q_0 = 0.044$L/s.

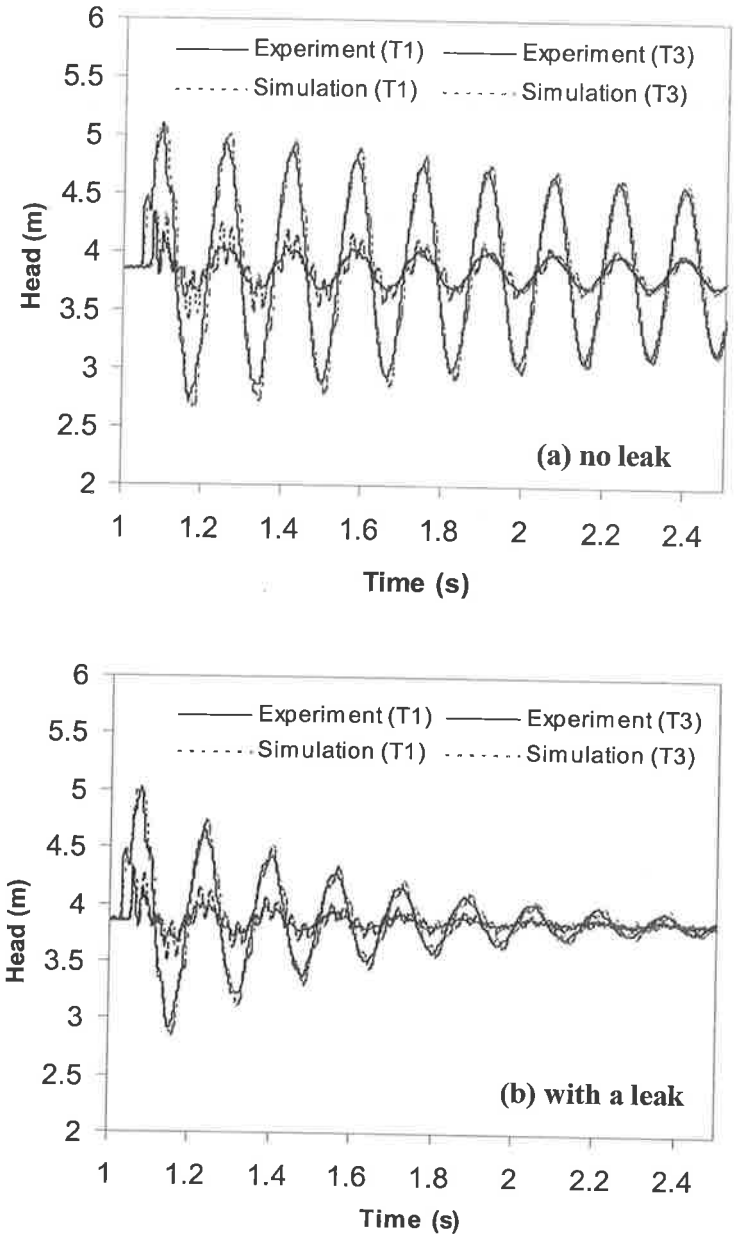

Figure 8.32 Transients generated by closing a solenoid valve at T3 (Figure 8.16)

The transients simulated using the k_A & k_P model are given in Figure 8.32. The step characteristic of the fast transient event in the first cycle of the transient can be simulated by the model. However, after the first cycle, the transient quickly becomes smooth, which means that higher frequencies decay quickly. In addition to unsteady friction, dissipation at flange connections, mixing at the pipe junctions may contribute to quick damping of higher frequencies. This rapid decay of high frequencies can only be partially simulated in the k_A & k_P model. Discrepancy between the simulation and measurement at T1 is more significant compared to that at T3.

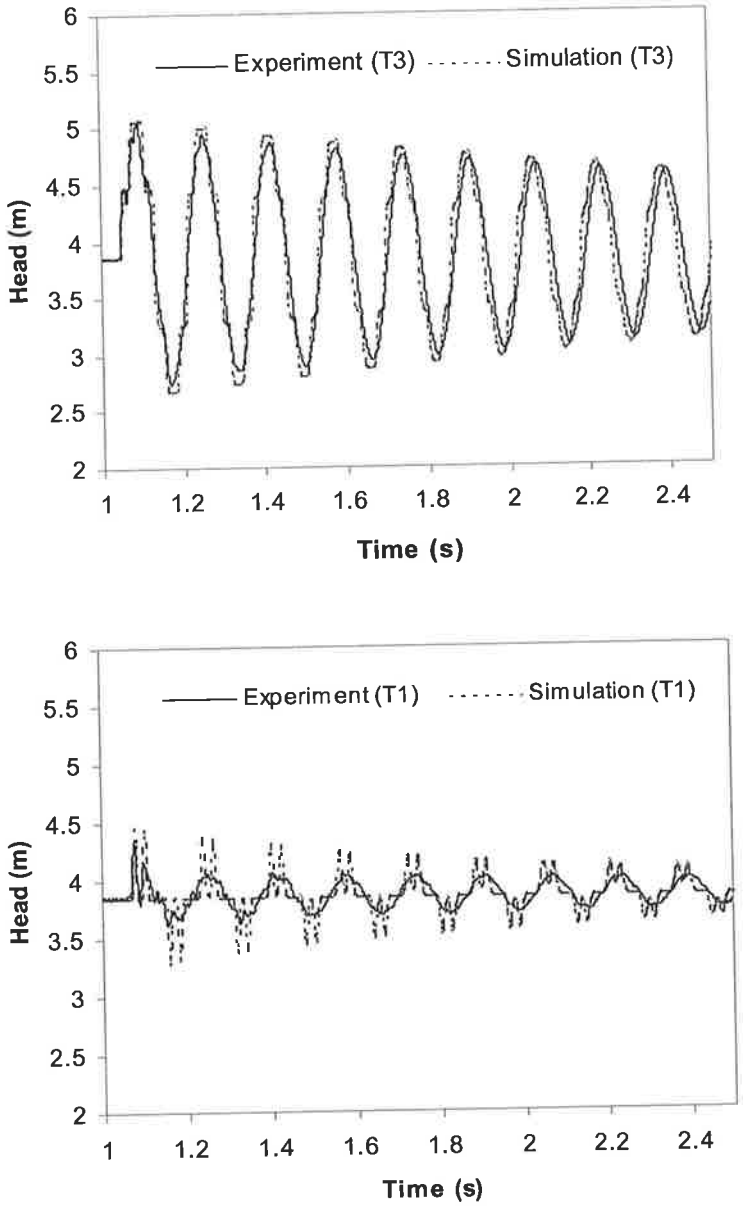

Figure 8.33 Transients when the dead ends are not considered in simulation (no leak case)

In addition to unsteady friction, the fast decay of the high frequencies observed in Figure 8.32 may be caused by mixing at dead ends and dissipation at flange connections. In the simulation presented in Figure 8.32, four dead ends at nodes 4, 8, 16, and 26 were considered. By neglecting these dead ends, the transients calculated using the k_A and k_P model are given in Figure 8.33. In addition to a phase shift, the shape discrepancy between the measurement and the simulation becomes more obvious, which indicates the important effects of dead ends on a fast transient event.

8.6 Summary

A three-loop pipe network has been constructed at The University of Adelaide for pipe flow studies and development of advanced leak and blockage detection techniques. The network is made of copper pipe with an internal diameter of 75mm, and is connected to three tanks with constant water surface. This network is able to simulate single pipelines, pipelines with dead ends, and branched and looped pipe network systems. The pipe network is fully operational for tests.

Transients measured from a single pipeline and a three-loop network are simulated using program NETTRANS for both cases of a leak and no leak. Due to the dissipation and mixing effects caused by pipe connections, in addition to unsteady friction, the instantaneous acceleration-based k_A & k_P model is more suitable than Zielke model to simulate transients from this network system. The effects of dead ends are not negligible for both slow and fast transient events, and can be considered by a lumped parameter model.

The application of the inverse transient method for leak detection is able to indicate presence of a leak; however, it may or may not be able to locate the leak, depending on the guessed leak location, due to insensitivity of leak for a slow transient event. Use of a fast transient event may improve the performance of ITM for leak detection. Improvements to the transient model for simulating a fast transient event from present pipe network are needed.

Extra measures should be taken during transient tests to eliminate air in the pipe system since air reduces the wave speed significantly. Air can be distinguished from a leak during the calibration process since a leak causes damping on a transient event while air also causes phase shift. Before applying a leak detection operation, the model needs calibrations based on both steady state and unsteady state conduction. It is simpler and more accurate to conduct a leak detection operation under the condition of negligible flow rate in a pipe system.

Chapter 9

Conclusions

9.1 Conclusions

The work presented in this thesis can be classified into four parts: (i) the development of analytical solutions for transients in a pipeline including leaks, blockages and dead ends; (ii) the development of new leak and blockage detection methods; (iii) the development of computer programs for transient simulation and application of the inverse transient method for leak detection; and (iv) construction of a looped experimental network and application of the inverse transient method in this pipe network system. Conclusions for each of these parts are presented in each of the following sections.

9.1.1 Analytical solutions for transients in a pipeline

In this Ph.D. research, several analytical solutions for transients in a pipeline system have been developed. These solutions include analytical solutions for transients in a pipeline including leaks under constant boundary conditions (in Chapter 3) and variable boundary conditions (in Chapter 5), an analytical solution for transients in a pipeline including blockages (in Chapter 6), and an analytical solution for transients in a pipeline including dead ends (in Chapter 7). These analytical solutions that are expressed in terms of a Fourier series, have provided significant insight into, and a better understanding of, pipeline transient problems that are influenced by pipe friction, and non-pipe elements including leaks, blockages and short dead ends.

The governing equations for transients in a pipeline for different cases of a non-pipe (local) element including a leak, a blockage and a dead end have been derived. These non-pipe element are considered in the governing equations by using a delta function, an innovative way that enables the influence of leaks (or blockages and dead ends) on the transients to be explicitly expressed in the governing equations. Dimensionless governing equations, Eqs. (3.17) and (3.18) for the leak problem, Eqs. (6.13) and (6.14) for the blockage problem, and Eqs. (7.37) and (7.38) for the dead end problem, have been derived. Dimensionless parameters describing the effects of pipe friction (parameter R), a leak (parameter F_L), a blockage (parameter G), and a dead end (parameter C) on fluid transients have been obtained. The definitions of these parameters reveal the factors that influence the transients in terms of pipe friction and non-pipe elements. For example, the influence of a blockage on fluid transients depends on the flow rate in the pipeline and the wave speed, which is similar to the pipe friction, while the influence of a leak on fluid transients doesn't depend on flow rate but rather depends on the pressure in the pipeline. The effects of a dead end on a transient event in a pipeline depend on the volume ratio of the dead end with respect to the pipeline.

The analytical solution (Eq. 3.33) for transients in a pipeline including a leak shows that transients in a pipeline under constant boundary conditions are damped by both pipe friction and leaks. The steady friction damping is exactly exponential (if R is assumed to be constant), and leak damping is exactly exponential for each of the individual harmonic components of the Fourier series solution. Leak-induced damping of the total transient event is approximately exponential. Since the total damping depends on the form of a transient in addition to the size and location of the leak, leaks cannot be detected effectively by only measuring the overall damping of a transient event. For an individual harmonic component, the leak-induced damping is proportional to the wave speed in the pipeline and the ratio of leak size with respective to the pipe cross-sectional area, and is also proportional to the square root of the pressure in the pipeline. The leak-induced damping on of individual harmonic component is influenced by the location of the leak location in a form of sine square (Eq. 3.32). The accuracy of the analytical solution has been verified by a sensitivity analysis and comparisons with the non-linear numerical results from the method of characteristics under the condition of transients of small magnitude.

The analytical solution developed in Chapter 5 shows that a steady oscillation forms in a pipeline under a continually varying boundary perturbation. The formation time and the amplitude of the steady oscillation depend on the pipe friction, the leaks in the pipeline and input signals. Under a variable boundary condition, the presence of a leak in a pipeline reduces the amplitude of resonance frequencies of a transient, and almost has no influence on the amplitude of non-resonant frequencies. The influence of the leak on the resonant amplitude is frequency dependent, and depends on the leak location and size (Eq. 5.18).

The analytical solution for transients in a pipeline including a blockage (Eq. 6.27) shows that a blockage also contributes damping of fluid transients in a pipeline. Like leak damping, the blockage-induced damping is exactly exponential for each of the individual harmonic components. However, the blockage-induced damping on an individual harmonic component is influenced by the location of the blockage in a form of cosine square (Eq. 6.33) compared to a sine-square relationship for leak damping (Eq. 3.32). The analytical solution is valid under conditions of small magnitude transients based on the sensitivity analyses. The accuracy of the analytical solution has been verified by comparison with the non-linear numerical results from the method of characteristics. Although the analytical solution, Eq. (6.27), was developed for the blockage problem, this solution is valid for effects of any local head-loss element on fluid transients in a pipeline.

Another analytical solution developed in this thesis is for transients in a pipeline including a short dead end. The condition for this analytical solution is that the dead end is short so that the pressure in the dead end can be assumed uniform (neglecting the wave propagation within the dead end). The analytical solution, Eq. (7.40), shows that presence of a dead end in a single pipeline changes the frequencies of the Fourier components. The significance of the effects of the dead end depends on the parameter S_d, defined in Eq. (7.42), which is related to the location of the dead end, relative volume and wave speed of the dead end compared to the pipeline. Comparisons with the numerical results based on MOC show that the analytical solution is accurate for slower transient events and less accurate for the faster transient events.

9.1.2 New leak and blockage detection methods

Two new leak detection methods and one blockage detection method have been developed in this thesis based on the analytical solutions. These new methods are (1) leak detection using leak-induced damping of fluid transients; (2) leak detection using leak-induced resonant frequency response; and (3) blockage detection using blockage-induced damping of fluid transients.

Based on the analytical solution developed in Chapter 3, a new leak detection method that is able to detect, locate and quantify a leak in a pipeline using leak-induced damping of fluid transients has been developed in Chapter 4. Based on the developed leak detection method, the damping rate of an individual Fourier component is useful for finding the magnitude of a leak while the ratio of damping rates between different harmonic components is useful for finding the leak location. Leaks of 0.1% of a pipeline's cross-sectional area or smaller can be detected and located based on numerical analysis and experimental results. This method does not require rigorous determination and modelling of boundary conditions and transient behavior in the pipeline. Due to the symmetrical properties of the leak damping, the leak locations obtained using this technique may or may not be unique depending on the leak location itself and the transient event used. Sensitivity analysis shows that linearization generates an insignificant error in both leak location and quantification. Inaccurate steady-state friction determination (if it is used to find the leak damping by subtraction from the total damping), on the other hand, may or may not be significant, depending on the parameters of the pipeline, and flow and the location of a leak. Also, if subtraction is used to find leak damping, the added damping caused by unsteady friction may become important. Because of larger relative uncertainties in estimating pipe friction, the friction factor has a greater influence on the leak detection compared to transient magnitude if the friction damping is obtained from the definition based on the steady state conditions.

For transients in a pipeline under variable conditions, a new technique that is able to detect the presence, location and magnitude of a leak, has been developed by examining the magnitudes of the resonant amplitudes of different frequencies. In addition, since leak-induced reduction of resonant amplitudes depends on the

relationship of the Fourier component and leak location (Eq. 5.18), a leak can be located by examining the leak-induced frequency response diagram. These techniques have been verified to be successful based on numerical applications.

A new blockage detection technique by using the blockage-induced damping on fluid transients has been developed in Chapter 6 based on the analytical solution. The technique is similar to the leak detection technique developed in Chapter 4. The damping rate of an individual Fourier component is useful for finding the magnitude of a blockage while the ratio of damping rates between different harmonic components is useful for finding blockage location. Because the blockage-induced damping of fluid transients depends on the flow rate in the pipeline, the blockage detection should be conducted at a reasonable flow rate, which is the opposite situation to that of leak detection. As a result, the magnitude of the blockage may not be accurately found based on the sensitivity analyses that have been conducted. The sensitivity analyses show that the error in friction damping, which is difficult to estimate, has a significant influence on the calculation of the blockage magnitude and a less significant influence on the blockage location.

The new leak and blockage detection techniques presented in this thesis do not need rigorous determination and modelling of boundary conditions and transient behaviour required in the inverse transient method and are simple to use and apply. However, these methods don't have the generality of the inverse transient method, and are not generally applicable to complex systems such as pipe networks. Difficulties in complicated geometries include the complex waveforms created by branches and loops and demands, which may be difficult to distinguish from leaks and blockages.

9.1.3 Computer programs NETTRANS and NETFIT

In addition to the theoretical developments, two computer program, NETTRANS for simulating transients in pipelines and pipe network systems by using the method of characteristics (MOC) and NETFIT for leak detection using the inverse transient method (ITM), have been developed in this Ph.D. research.

Inclusion of a sparse matrix solver has significantly improved the calculation efficiency of NETTRANS compared to the normal matrix solvers. A lumped parameter model that can adequately consider the effects of short dead ends on fluid transients in a pipe network without dividing the network into a significant large number of computational units has been included in this program. Three unsteady friction models including the Zielke unsteady friction model, the Brunone unsteady friction model and a modified Brunone unsteady friction model the called k_A & k_P model have been included in NETTRANS. Compared to the experimental tests for single pipelines and looped networks, the k_A & k_P model gives the best agreement; however, the empirical parameters in this model have to be determined from experimental tests for a non-leaking case.

Program NETFIT is composed of two parts, NETTRANS for transient simulation and NLFIT developed by George Kuczera at the University of Newcastle for parameter fitting based on Bayesian nonlinear regression. Several minimisation methods are available in NETFIT for parameter fitting. These methods include gradient-based Newton-Raphson (N-R) method and Levenberg-Marquardt (L-M) method, and global-based searching methods including genetic algorithm (GA) and shuffled complex evolution (SCE) method. NETFIT also provides a series of windows-based interfaces in which the parameters and minimisation schemes can be chosen and the convergence process and fitness of the searched parameter can be monitored. Applications of NETFIT by using numerically generated measurement data has shown that NETFIT can find the leaks including leak location and leak size successfully based on different searching techniques including Levenberg-Marquardt (L-M) algorithm and shuffled complex evolution (SCE) method.

9.1.4 Construction of a looped pipe network and experimental application of the inverse transient method

A three-loop pipe network has been constructed in The University of Adelaide for pipe flow studies and development of advanced leak and blockage detection techniques. The network is made of copper pipe with a diameter of 75mm, and is connected to three tanks with constant water surfaces. This network is able to simulate single pipelines, pipelines with dead ends, branched and looped pipe network systems. The

apparatuses in pipe network have been fully calibrated, and the network is operational for both steady state and unsteady state tests.

Transients measured from a single pipeline and a three-loop network were simulated using program NETTRANS for both cases of with a leak and no leak. Due to the dissipation and mixing effects caused by pipe connections in addition to unsteady friction, the instantaneous acceleration-based k_A & k_P unsteady friction model is more suitable than the Zielke unsteady friction model to simulate transients from this network system. Effects of dead ends are not negligible for both slow and fast transient events, and can be considered by a lumped parameter model.

Applications of the inverse transient method for leak detection can indicate presence of a leak; however, it may or may not be able to locate the leak, depending on the guessed leak location, due to insensitivity of leak on a slow transient event. Use of a fast transient event improves the performance of ITM for leak detection. However, improvements on the transient model simulating a fast transient event are needed.

9.2 Recommendations for future work

In the derivation of analytical solutions for the transients in a pipeline, the unsteady friction damping on a harmonics is assumed to be exponential. Although this has been experimentally verified to be an accurate assumption (Section 4.8), it is expected that an analytical solution may be available to describe the exponential characteristics of the unsteady friction damping for laminar flow. Some effort has already been made in this direction. By decomposing a transient event simulated by using the Zielke's unsteady friction model into a Fourier series, it has been shown that damping of each component is exponential, and the damping coefficient of each component depends on the initial transient condition in the pipeline. This may give some indication of future work on unsteady friction studies. If a theoretical relationship of the unsteady friction damping can be obtained, the friction damping then can be theoretically estimated rather than from a leak-free test.

In addition to the theoretical investigation of unsteady friction effects on pipeline transients, the modelling of unsteady frictional effects and other dissipation effects that directly influences the performance of the inverse transient method for leak detection is also a largely unsolved problem. The k_A & k_P unsteady friction model has shown reasonable agreement with the experimental results from the straight 22mm single pipeline in the laboratory based on the parameters which are determined from theoretical analysis. However, to simulate transients from the looped network in which there are additional disturbances at pipe connections, the parameter used in the k_A & k_P model need to be experimentally determined in order to give the best match between the numerical and experiment results. This discrepancy may be caused by the disturbances at the pipe connections, which apparently influence the boundary developments during a transient event. These connections are not uncommon in a real pipe network system. To fully understand the effects of these connections on the shear stress during a transient event, a three-dimensional model or at least two-dimensional model is needed.

Bibliography

1. Abramowitz, M., and Stegun, I. A. (1972). *Handbook of Mathematical Functions with Formulas, Graphs, and Mathematical Tables*, National Bureau of Standards, Washington, USA.

2. Adewumi, M. A., Eltohami, E. S., and Ahmed, W. H. (2000). "Pressure transients across constrictions." *Journal of Energy Resources Technology,* ASME, 122, 34-41.

3. Allievi, L. (1925). *Theory of Waterhammer* (Translated by E. E. Halmos). Riccardo Garoni, Rome.

4. Almeida, A. B. d. (1992). *Fluid transients in pipe networks*, Computational Mechanics Publication, Southampton, Boston.

5. American Water Works Association. (1987). *Leaks in water distribution systems: a technical/economic overview*, American Water Works Association, Denver, U.S.

6. Axworthy, D. H., Ghidaoui, M. S., and McInnis, D. A. (2000). "Extended thermodynamics derivation of energy dissipation in unsteady pipe flow." *Journal of Hydraulic Engineering,* ASCE, 126(4), 276-287.

7. Baghdadi, A. H. A., and Mansy, H. A. (1988). "A mathematical model for leak location in pipelines." *Applied Mathematical Modelling*, 12, 25-30.

8. Baker, A. J. (1983). *Finite Element in Computational Fluid Mechanics*, McGraw-Hill, New-York.

9. Belsito, S., Lombardi, P., Andreussi, P., and Banerjee, S. (1998). "Leak detection in liquefied gas pipelines by artificial neural networks." AIChE *Journal*, 44(12), 2675-2688.

10. Bergant, A., Simpson, A. R., and Vitkovsky, J. (2001). "Developments in unsteady pipe flow friction modelling." *Journal of Hydraulic Research*, IAHR, 39(3), 249-257.

11. Billmann, L., and Isermann, R. (1987). "Leak detection method for pipelines." *Automatica*, 23(3), 381-385.

12. Black, P. (1992). "A review of pipeline leak detection technology." *Pipeline Systems*, B. Coulbeck and E. Evans, eds., Kluwer Academic Publishers, 287-297.

13. Bray, D. E. (1992). *Nondestructive Testing Techniques*, Wiley, New York, U.S.

14. British Gas. (1994). "British gas uses ultrasonic vehicle for assessing pipeline integrity." *Pipeline & Gas Journal*, 221(12), 40-42.

15. Brunone, B. (1999). "Transient test-based technique for leak detection in outfall pipes." *Journal of Water Resources Planning and Management,* ASCE, 125(5), 302-306.

16. Brunone, B., Golia, U. M., and Greco, M. (1991). "Modelling of fast transients by numerical methods." *International Meeting on Hydraulic Transients with Column Separation,* IAHR, Valencia, Spain, 201-209.

17. Brunone, B., Golia, U. M., and Greco, M. (1995). "Effects of two-dimensionality on pipe transients modeling." *Journal of Hydraulic Engineering,* ASCE, 121(12), 906-912.

18. Brunone, B., Karney, B. M., Mecarelli, M., and Ferrante, M. (2000). "Velocity profiles and unsteady pipe friction in transient flow." *Journal of Water Resources Planning and Management*, ASCE, 126(4), 236-244.

19. Brunone, B., Karney, B. M., Mecarelli, M., and Ferrante, M. (2002). "Closure: Velocity profiles and unsteady pipe friction in transient flow." *Journal of Water Resources Planning and Management*, ASCE, 128(2), 86.

20. Bughazem, M. B., and Anderson, A. (2000). "Investigation of an unsteady friction model for waterhammer and column separation." *8th International Conference on Pressure Surges*, The Hague, Netherlands, 483-498.

21. Chaiko, M. A., and Brinckman, K. W. (2002). "Models for analysis of water hammer in piping with entrapped air." *Journal of Fluids Engineering,* ASME, 124, 194-204.

22. Chaudhry, M. H. (1986). *Applied Hydraulic Transients*, Van Nostrand Reinhold Company, New York.

23. Chen, L.-C. (1995). "Pipe network transient analysis-the forward and inverse problems," Ph.D. Thesis, Dept. of Civil and Environmental Engineering, Cornell University, Ithaca, New York.

24. Covas, D., Ramos, H., and Almeida, A. B. D. (2000). "Leak location in pipe systems using pressure surges." *8th International Conference on Pressure Surges, "Safe Design and Operation of Industrial Pipe Systems,"* BHR Group, The Hague, The Netherlands, 169-179.

25. Covas, D., and Ramos, H. (1999). "Leakage detection in single pipeline using pressure wave behaviour." *Water Industry System: modelling and optimization application*, Baldock, Hertfordshire, England, 287-299.

26. Davis, P. A. (1998). "Remote sensing of cooling water discharges." Encyclopedia of Environmental Control Technology, Geotechnology applications, Leak detection, treatment options, P. N. Cheremisinoff, ed.

27. Dinis, J. M., Wojtanowicz, A. K., and Scott, S. L. (1999). "Leak detection in liquid subsea flowlines with no recorded feed rate." *Journal of Energy Resources Technology,* ASME, 121, 161-166.

28. Duan, Q., Sorooshian, S., and Gupta, V. (1992). "Effective and efficient global optimization for conceptual rainfall-runoff models." *Water Resources Research,* 28(4), 1015-1031.

29. Duffy, D. G. (1994). *Transform Methods for Solving Partial Differential Equations*, CRC Press, Inc.

30. Eckert, E. G., Maresca, J. W. J., Hillger, R. W., and Yezzi, J. J. (1993). "Location of leaks in pressurized petroleum pipelines by means of passive-acoustic sensing methods." *ASTM Special Technical Publication,* (1161), 53-69.

31. Eichinger, P., and Lein, G. (1992). "The influence of friction on unsteady pipe flow." *Conference on Unsteady Flow and Fluid Transients*, Durham, UK, 41-50.

32. Farmer, E., Kohlrust, R., Myers, G., and Verduzco, G. (1988). "Leak detection tool undergoes field tests." *Oil and Gas Journal*, 86(51), 48-53.

33. Fuchs, H. V., and Riehle, R. (1991a). "Acoustic analysis detects leaks." *Water Engineering and Management*, 138(1), 11-13.

34. Fuchs, H. V., and Riehle, R. (1991b). "Ten years of experience with leak detection by acoustic signal analysis." *Applied Acoustics*, 33(1), 1-19.

35. Fukushima, K., Maeshima, R., Kinoshita, A., and Shiraishi, H. (2000). "Gas pipeline leak detection system using the online simulation method." *Computers and Chemical Engineering*, 24, 453-456.

36. Furness, R. A., and Reet, J. D. (1998). "Pipe line leak detection techniques." *Pipe Line Rules of Thumb Handbook*, E. W. McAllister, ed., Gulf Publishing Company, Houston, Texas, 476-484.

37. Ghafurian, R., Dominguez, J., Santini, A., and Sobel, C. (1999). "New advances in mitigating environmental impact of pipe-type cables." IEEE *Transactions on Power Delivery*, 14(2), 314-318.

38. Ghidaoui, M. S., and Mansour, S. (2002). "Efficient treatment of the Vardy-Brown unsteady shear in pipe transients." *Journal of Hydraulic Engineering,* ASCE, 128(1), 102-112.

39. Gottlieb, D. and Orszag, S. A. (1977). "Theory of spectral methods for mixed initial-boundary value problems." Part I and Part II, ICASE, NASA Langley Research Center, Hampton, VA.

40. Griebenow, G., and Mears, M. (1989). "Leak detection implementation: modeling and tuning methods." *Journal of Energy Resources Technology,* ASME, 111, 66-71.

41. Holloway, M. B., and Chaudhry, M. H. (1985). "Stability and accuracy of water hammer analysis." *Advances in Water Resources*, 8, 121-128.

42. Hough, J. E. (1988). "Leak testing of pipeline uses pressure and acoustic velocity." *Oil and Gas Journal*, 86(47), 35-41.

43. Hovey, D. J., and Farmer, E. J. (1999). "DOT states indicate need to refocus pipeline accident prevention." *Oil & Gas Journal*, 97(11), 52-53.

44. Hsiung, J. T., and Himmelblau, D. M. (1996). "Detection of leaks in a liquid-liquid heat exchanger using passive acoustic noise." *Computers & Chemical Engineering*, 20(9), 1101-1111.

45. Hunaidi, O., and Chu, W. T. (1999). "Acoustical characteristics of leak signals in plastic water distribution pipes." *Applied Acoustics*, 58(3), 235-254.

46. Hunt, A. (1996). "Fluid properties determine flow line blockage potential." *Oil & Gas Journal*, 94(29, July 15), 62-66.

47. Jiang, Y., Chen, H., and Li, J. (1996). "Leakage and Blockage detection in water network of district heating system." ASHRAE *Transactions*, 102(1), 291-196.

48. Jönsson, L. (1995). "Computer and laboratory studies of leak detection using hydraulic transients." *Water Resources Management under Drought or Water Shortage Conditions*, Balkema, Rotterdam, 119-126.

49. Jönsson, L., and Larson, M. (1992). "Leak detection through hydraulic transient analysis." Pipeline Systems, B. Coulbeck and E. Evans, eds., Kluwer Academic Publishers, 273-286.

50. Joukowsky, N. (1898). "Über den dydraulischen stoss in Wasserleitungsröhren (On the hydraulic hammer in water supply pipes). Mémories de l'Académie Impériale des Sciences de St.–Pétersbourg, 1900, Series 8, 9, No. 5 (in German).

51. Kagawa, T., I. Lee, et al. (1983). "High Speed and Accurate Computing Method of Frequency-Dependent Friction in Laminar Pipe Flow for Characteristics Method." *Transactions of the Japanese Society of Mechanical Engineers*, 49(447): 2638-2644.

52. Kiuchi, T. (1993). "A leak localization method of pipeline by means of fluid transient model." *Journal of Energy Resources Technology,* ASME, 115, 162-167.

53. Kreyszig, E. (1999). *Advanced Engineering Mathematics*, John Willy & Sons, Inc.

54. Kuczera, G. (1994). NLFIT *a Bayesian Nonlinear Regression Program Suite*, University of Newcastle, Australia.

55. Leauber, C. E. (1997). "Leak detection cost-effective and beneficial." *Journal of American Water Works Association*, 89(7), 10-10.

56. Lee, N. H., and Martin, C. S. (1999). "Experimental and analytical investigation of entrapped air in a horizontal pipe." 3rd ASME/JSME *Joint Fluids Engineering Conference,* San Francisco, CA, USA, FEDSM 99-6881.

57. Lee, P.J., Tang, V.M., Kuo, Y.L., and Huang J.Y. (2000). "Analysis of Leaks in Pipeline Systems Using Coded Transients," Final Year Student Project Report, Dept. of Civil & Environmental Engineering, The University of Adelaide, Australia.

58. Lee, P. J., Vítkovský, J., Lambert, M. F., Simpson, A. R., and Liggett, J. A. (2002). "Leak detection in pipelines using an inverse resonant method." EWRI *Conference*, Roanoke, Virginia, USA.

59. Levine, H. (1997). *Partial Differential Equations*, American Mathematical Society, International Press.

60. Liggett, J. A. (1984). "The boundary element method-some fluid applications." *Multi-dimensional Fluid Transients*, M. H. Chaudhry and C. S. Martin, eds., 1-8.

61. Liggett, J. A., and Chen, L.-C. (1994). "Inverse transient analysis in pipe network." *Journal of Hydraulic Engineering,* ASCE, 120(8), 934-955.

62. Liou, C. P. (1991). "Maximum pressure head due to linear valve closure." *Journal of Fluids Engineering,* ASME, 113, 643-647.

63. Liou, C. P. (1994). "Mass imbalance error of waterhammer equations and leak detection." *Journal of Fluids Engineering,* ASME, 116, 103-109.

64. Liou, C. P. (1998). "Pipeline leak detection by impulse response extraction." *Journal of Fluids Engineering,* ASME, 120, 833-838.

65. Liou, C. P., and Tian, J. (1995). "Leak detection-transient flow simulation approaches." *Journal of Energy Resources Technology,* ASME, 117, 243-248.

66. Lippitt, T. (1987). "Williams system signals advance in leak detection." *Oil & Gas Journal*, July, 43-47.

67. Liston, D. A., Brown, T. G., Brainard, F. S., Britt, D. E., Corless, J. P., Craft, R. G., Finger, W. A., Hock, J. G., Kleinert, C. J., Luta, W. E., Nelson, K. J., Phipps, G. C., Wadsworth, K., Wheadon, D. A., Wicklund, L. H., and Zelch, G. N. (1996). "Committee report: Water accountability." *Journal American Water Works Association*, 88(7), 108-111.

68. Makar, J., and Chagnon, N. (1999). "Inspecting systems for leaks, pits, and corrosion." *Journal American Water Works Association*, 91(7), 36-46.

69. Maresca, J. W. J., and Fierro, M. R. (1996). "Demonstration of an innovative technology for the detection of small leaks from the underground pipelines in airport hydrant fuel distribution systems." *First International Pipeline Conference,* ASME, Calgary, Alberta, Canada, 1155-1166.

70. Martin, C. S. (1976). "Entrapped air in pipelines". Proceedings of 2nd International Conference on Pressure Surges, NHRA, 15-28.

71. McInnis, D., and Karney, B. (1995). "Field tests and demand models." *Journal of Hydraulic Engineering,* ASCE, 121(3), 218-231.

72. Mears, M. N. (1988). "Major pipeline installs system to pinpoint leak size, location." *Oil & Gas Journal*, Apr, 37-43.

73. Megyesy, E. F. (1998). *Pressure vessel handbook*, Tulsa, UK: Pressure Vessel Pub.

74. Miller, D. S. (1978). *Internal flow systems*, BHRA Fluid Engineering.

75. Mpesha, W., Chaudhry, M. H., and Gassman, S. L. (2002). "Leak detection in pipes by frequency response method using a step excitation." *Journal of Hydraulic Research,* IAHR, 40(1), 55-62.

76. Mpesha, W., Gassman, S. L., and Chaudhry, M. H. (2001). "Leak detection in pipes by frequency response method." *Journal of Hydraulic Engineering,* ASCE, 127(2), 134-147.

77. Mukherjee, J., and Narasimhan, S. (1996). "Leak detection in networks of pipelines by the generalized likelihood ratio method." *Industrial & Engineering Chemistry Research*, 35(6), 1886-1893.

78. Nash, G. A., and Karney, B. W. (1999). "Efficient inverse transient analysis in series pipe systems." *Journal of Hydraulic Engineering,* ASCE, 125(7), 761-764.

79. Nigol, O. (1970a). "Hydraulic method for locating oil leaks in underground cables." IEEE *Transactions on Power Apparatus and Systems*, PAS-89(7), 1434-1439.

80. Nigol, O. (1970b). "Location of leaks in gas-filled underground cables." IEEE *Transactions on Power Apparatus and Systems*, PAS-89(7), 1440-1443.

81. Paquin, F., Babineau, D., Brissette, F., and Leconte, R. (2000). "Development of a methodology for locating leaks in water lines." *Canadian Journal of Civil Engineering*, 27(1), 151-159.

82. Pezzinga, G. (1999). "Quasi-2D model for unsteady flow in pipe networks." *Journal of Hydraulic Engineering,* ASCE, 125(7), 676-685.

83. Pezzinga, G. (2000). "Evaluation of unsteady flow resistances by quasi-2D or 1D models." *Journal of Hydraulic Engineering,* ASCE, 126(10), 778-785.

84. Pezzinga, G. (2002a). "Discussion: Velocity profiles and unsteady pipe friction in transient flow." *Journal of Water Resources Planning and management,* ASCE, 27(1), 85-86.

85. Prado, R. A., and Larreteguy, A. E. (2002). "A transient shear stress model for the analysis of laminar water-hammer problems." *Journal of Hydraulic Research,* IAHR, 40(1), 45-53.

86. Press, W.H., Teukolsky, S.A., Vetterling, W.T., and Flannery, B.P. (1992). *Numerical Recipes*: *The Art of Scientific Computing*. Cambridge University Press, Cambridge, U.K.

87. Pudar, R. S., and Liggett, J. A. (1992). "Leaks in pipe networks." *Journal of Hydraulic Engineering,* ASCE, 118(7), 1031-1046.

88. Rajtar, J. M., and Muthiah, R. (1997). " Pipeline leak detection system for oil and gas flowlines." *Journal of Manufacturing Science and Engineering, Transactions of the* ASME, 119(1), 105-109.

89. Rao, P. V., and Sridharan, K. (1996). "Discussion: Inverse transient analysis in pipe networks." *Journal of Hydraulic Engineering,* ASCE, 122(5), 287-289.

90. Rich, G. R. (1945). "Water-hammer analysis by the Laplace-Mellin transformation." *Transaction of* ASME, 67, 361-376.

91. Rogers, L. M. (1995). "Pipeline blockage location by strain measurement using an ROV." *Proceedings of the 1995 Offshore Technology Conference*, Houston, TX, USA, 521-528.

92. Schwendeman, T. (1987). "Detecting underground piping leaks." *Civil Engineering*, 8, 56-58.

93. Scott, D. (1999). "DOT mandates API document for leak detection." *Oil & Gas Journal*, 97(2), 51-54.

94. Scott, S. L., and Satterwhite, L. A. (1998). "Evaluation of the back pressure technique for blockage detection in gas flowlines." *Journal of Energy Resources Technology,* ASME, 120, 27-31.

95. Scott, S. L., and Yi, J. (1999). "Flow testing methods to detect and characterize partial blockages in looped subsea flowlines." *Journal of Energy Resources Technology,* ASME, 121, 154-160.

96. Seaford, H. (1994). "Acoustic leak detection through advanced signal-processing technology." *Noise and Vibration Worldwide*, 25(5), 17-18.

97. Silva, R. A., Buiatti, C. M., Cruz, S. L., and Pereira, J. A. F. R. (1996). "Pressure wave behaviour and leak detection in pipelines." *Computers & Chemical Engineering*, 20(Suppl), S491-S496.

98. Silva-Araya, W. F., and Chaudhry, H. M. (1997). "Computation of energy dissipation in transient flow." *Journal of Hydraulic Engineering,* ASCE, 123(2), 108-115.

99. Silva-Araya, W. F., and Chaudhry, M. H. (2001). "Unsteady friction in rough pipes." *Journal of Hydraulic Engineering,* ASCE, 127(7), 607-618.

100. Smith, L. A., Fields, K. A., Chen, A. S. C., and Tafuri, A. N. (2000). *Options for Leak and Break Detection and Repair for Drinking Water Systems*, Battelle Press, Columbus, Ohio, US.

101. Stephens, M. L., Simpson, A. R., Lambert, M. F., Vitkovsky, J. P., and Nixon, J. B. (2002). "The detection of pipeline blockages using transients in the field." *Australian Water Association SA Brach Regional Conference*, Adelaide, No. 4.

102. Streeter, V. L., and Lai, C. (1962). "Water-hammer analysis including fluid friction." *Journal of Hydraulics Division,* ASCE, 88(3), 79-112.

103. Streeter, V. L. and E. B. Wylie (1983). *Fluid Mechanics*. Singapore, McGraw-Hill Book Company.

104. Suzuki, K., Taketomi, T., and Sato, S. (1991). "Improving Zielke's method of simulating frequency-dependent friction in laminar liquid pipe flow." *Journal of Fluids Engineering*, 113, 569-573.

105. Trikha, A. K. (1975) "An efficient method for simulating frequency-dependent friction in transient liquid flow." *Journal of Fluids Engineering*, ASME, 97, 97-105.

106. Tubb, M. (2001). "International pipeline construction outlook." *Pipeline & Gas Journal*, August, 16-32.

107. Vardy, A. E., and Brown, J. (1996). "On turbulent, unsteady, smooth-pipe friction." *Conference on Pressure Surges and Fluid Transients*, Durham, UK, 289-311.

108. Vardy, A. E., and Hwang, K.-L. (1991). "A characteristics model of transient friction in pipes." *Journal of Hydraulic Research,* IAHR, 29(5), 669-684.

109. Vista Research Inc. (2001). Leak detection and Location Equipment: HT-100 and SPAL system, http://www.vistaleakdetection.com., 31 May 2001.

110. Vítkovský, J. (2001). "Inverse Analysis and Modelling of Unsteady Pipe Flow: Theory, Applications and Experimental Verification," Ph.D. Thesis, Dept. of Civil & Environmental Engineering, The University of Adelaide, Adelaide, Australia.

111. Vítkovský, J., Simpson, A. R., and Lambert, M. F. (2000). "Leak detection and calibration using transients and genetic algorithms." *Journal of Water Resources Planning and Management,* ASCE, 126(4), 262-265.

112. Vítkovský, J., Simpson, A. R., and Lambert, M. F. (2002). "Minimization algorithms and experimental inverse transient leak detection." EWRI *Conference*, ASCE, Roanoki, Virginia, USA.

113. Vítkovský, J., Simpson, A. R., Lambert, M. F., and Wang, X.-J. (2001). "An experimental verification of inverse transient technique for leak detection." *6th Conference on Hydraulics in Civil Engineering,* IEAust, Hobart, Australia.

114. Waller, R. O. (1969). "Locating leaks in mains and services." *Journal of the American Water Works Association*, 62(7), 403-406.

115. Wang, G. Z., Fang, C. Z., and Wang, K. F. (1991). "State Estimation and Leak Detection and Location in Pipeline." *International Conference on Industrial Electronics*, Kobe, Japan, 155-160.

116. Wang, X.-J., Lambert, M. F., Simpson, A., R., Liggett, J. A., and Vítkovský, J. P. (2002). "Leak detection in pipelines using the damping of fluid transients." *Journal of Hydraulic Engineering,* ASCE, 128(7), 697-711.

117. Wang, X.-J., Lambert, M. F., and Simpson, A. R. (2001a). "Analysis of a transient in a pipeline with a leak using Laplace transforms." *14th Australasian Fluid Mechanics Conference*, Adelaide, Australia. CD-ROM.

118. Watanabe, K., and Himmelblau, D. M. (1986). "Detection and location of a leak in a gas-transport pipeline by a new acoustic method." AIChE *Journal*, 32(10), 1690-1701.

119. Watanabe, K., and Koyama, H. (1990). " Location and estimation of a pipeline leak." *Electrical Engineering in Japan*, 110(7), 92-101.

120. Weil, G. J., Graf, R. J., and Forister, L. M. (1994). "Remote sensing pipeline rehabilitation methodologies based upon the utilization of infrared thermography." *Urban Drainage Rehabilitation Programs and Techniques*, 173-181.

121. Wiggert, D. C. (1968). "Unsteady flows in lines with distributed leakage." *Journal of Hydraulics Division,* ASCE, 94, 143-162.

122. Williams, J. A., Kozak, S., and Rodenbaugh, T. J. (1983). "Leak location methods for HV underground cables." IEEE *Transactions on Power Apparatus and Systems*, PAS-102(7), 2029-2036.

123. Wolfgang, S. H. (1982). *Transportation and Traffic Engineering Handbook*, Englewood Cliffs, N.J : Prentice-Hall.

124. Wood, D. J., and Chao, S. P. (1971). "Effect of pipeline junctions on water hammer surges." *Transportation Engineering Journal, Proceedings of* ASCE, 97(3), 441-457.

125. Wood, D. J., Reddy, L. S., and Funk, J. E. (1993). "Modeling pipe networks dominated by junctions." *Journal of Hydraulics Engineering,* ASCE, 119(8), 949-958.

126. Wood, F. M. (1937). "Application of Heaviside's operational calculus to the solution of problems in water hammer." *Transaction of* ASME, 59, 707-713.

127. Wu, Q. (1994). "Reconstruction of blockage in a duct from single spectrum." *Applied Acoustics*, 41(3), 229-236.

128. Wylie, E. B. (1996). "Unsteady internal flows-dimensionless numbers and time constants." *7th International Conference on Pressure Surges & Fluid Transients in Pipelines and Open Channels*, Harrogate, UK, 313-322.

129. Wylie, E. B., and Streeter, S. L. (1993). *Fluid Transients in Systems*, Prentice-Hall Inc., Englewood Cliffs, New Jersey, USA.

130. Zhang, J. (2001). "Statistical pipeline leak detection for all operating conditions." *Pipeline & Gas Journal*, 228(2), 42-45.

131. Zhang, J. (1996). "Designing a cost effective and reliable leak detection system." *Pipeline Reliability Conference*, Houston, USA.

132. Zhou, F., Hicks, F. E., and Steffler, A. M. (2002). "Transient flow in a rapidly filling horizontal pipe containing trapped air." *Journal of Hydraulic Engineering,* ASCE, 128(6), 625-634.

133. Zielke, W. (1968). "Frequency-dependent friction in transient pipe flow." *Journal of Basic Engineering,* ASME, 90, 109-115.

Appendix A: Derivation of the analytical solution for the transients in a pipeline (with a leak) under constant boundary conditions (Eq. 3.33)

The governing equation for transients in a pipeline with a leak is

$$\frac{\partial^2 h^*}{\partial x^{*2}} = \frac{\partial^2 h^*}{\partial t^{*2}} + [2R + F_L \delta(x^* - x_L^*)]\frac{\partial h^*}{\partial t^*} + 2RF_L \delta(x^* - x_L^*)h^* \qquad \text{(A1, repeated 3.27)}$$

Consider a pipeline connecting constant upstream and downstream reservoirs so that the boundary conditions for the dimensionless hydraulic line are

$$h^*(0, t^*) = 0 \text{ and } h^*(1, t^*) = 0 \qquad \text{(A2, repeated 3.29)}$$

Supposing a transient is initiated in the pipeline, the initial conditions are

$$h^*(x^*,0) = f(x^*), \text{ and } \frac{\partial h^*(x^*,0)}{\partial t^*} = g(x^*) \qquad \text{(A3, repeated 3.30)}$$

For a pipeline with a leak, the pipeline can be considered as two portions divided by the leak with a small neighborhood 2ε as shown in Figure A1.

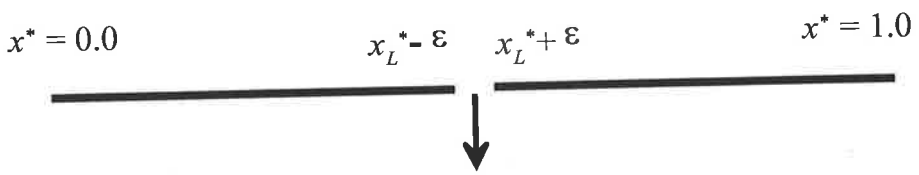

Figure A1 A pipeline with a leak (repeated)

For all points in the pipe except the position of the leak, the linearized equation becomes the wave equation,

$$\frac{\partial^2 h^*}{\partial x^{*2}} = \frac{\partial^2 h^*}{\partial t^{*2}} + 2R\frac{\partial h^*}{\partial t^*} \qquad (0 < x^* < x_L^* - \varepsilon), (x_L^* + \varepsilon < x^* < 1) \qquad \text{(A4)}$$

The continuity of the pressure at a small leak (Wylie and Streeter 1993) gives

$$h^*(x_L^* - \varepsilon, t^*) = h^*(x_L^* + \varepsilon, t^*) \qquad \text{(A4}^+\text{)}$$

Noticing the boundary conditions in Eq. (A2), transient in the pipeline can be expressed as (Levine 1997)

$$h^*(x^*,t^*) = \sum_{n=1}^{\infty} T_n(t^*)\sin(n\pi x^*) \qquad (0 \le x^* < x_L^* - \varepsilon), (x_L^* + \varepsilon < x^* \le 1) \qquad \text{(A5)}$$

A common set of coefficients $T_n(t^*)$ are necessary in order to ensure the overall continuity of pressure at the leak (Levine 1997). Because of the continuous behaviour of the pressure at the leak, Eq. (A5) is valid for the whole pipeline domain ($0 \le x^* \le 1$). The main purpose next is to find coefficients, $T_n(t^*)$, that satisfy Eq. (A1).

Integrating Eq. (A1) over a small neighborhood on either side of the leak gives

$$\begin{aligned}\int_{x_L^*-\varepsilon}^{x_L^*+\varepsilon} \frac{\partial^2 h^*}{\partial x^{*2}} dx^* &= \int_{x_L^*-\varepsilon}^{x_L^*+\varepsilon} \left(\frac{\partial^2 h^*}{\partial t^{*2}} + 2R\frac{\partial h^*}{\partial t^*}\right) dx^* \\ &+ \int_{x_L^*-\varepsilon}^{x_L^*+\varepsilon} \left(F_L \frac{\partial h^*}{\partial t^*} - 2RF_L h^*\right)\delta(x^* - x_L^*) dx^*\end{aligned} \tag{A6}$$

Letting ε approach zero, the first integral on the right hand side of Eq. (A6) is zero. Thus Eq. (A6) becomes

$$\left.\frac{\partial h^*}{\partial x^*}\right|_{x_L^*-\varepsilon}^{x_L^*+\varepsilon} = \left(F_L \frac{\partial h^*}{\partial t^*} - 2RF_L h^*\right)\Big|_{x_L^*} \int_{x_L^*-\varepsilon}^{x_L^*+\varepsilon} \delta(x^* - x_L^*) dx^* \tag{A7}$$

Given the definition of Dirac delta function of $\int_{x_L^*-\varepsilon}^{x_L^*+\varepsilon} \delta(x^* - x_L^*) dx^* = 1$, substituting Eq. (A5) into the right-hand side of Eq. (A7) gives

$$\left.\frac{\partial h^*}{\partial x^*}\right|_{x_L^*+\varepsilon} - \left.\frac{\partial h^*}{\partial x^*}\right|_{x_L^*-\varepsilon} = \sum_{n=1}^{\infty}\left[\left(F_L \frac{dT_n}{dt^*} - 2RF_L T_n\right)\sin(n\pi x_L^*)\right] \tag{A8}$$

Expressing the coefficient functions T_n in Eq. (A5) by integrals in the two regions at each side of the leak (Levine 1997) gives

$$T_n(t^*) = \frac{2}{x_L^*}\int_0^{x_L^*-\varepsilon} h_l^*(x^*, t^*)\sin(n\pi x^*) dx^* \tag{A9}$$

$$T_n(t^*) = \frac{2}{1-x_L^*}\int_{x_L^*+\varepsilon}^{1} h_r^*(x^*, t^*)\sin(n\pi x^*) dx^* \tag{A10}$$

where the subscript l on the $h^*(x^*, t^*)$ refers to the region to the left of the leak, and subscript r refers to the region to the right of the leak.

Differentiating Eq. (A9) twice leads to

$$\frac{d^2 T_n}{dt^{*2}} = \frac{2}{x_L^*}\int_0^{x_L^*-\varepsilon} \frac{\partial^2 h_l^*(x^*, t^*)}{\partial t^{*2}}\sin(n\pi x^*) dx^* \tag{A11}$$

Differentiating Eq. (A9) and multiplying $2R$ leads to

$$2R\frac{dT_n}{dt^*} = \frac{2}{x_L^*}\int_0^{x_L^*-\varepsilon} 2R\frac{\partial h_l^*(x^*,t^*)}{\partial t^*}\sin(n\pi x^*)dx^* \tag{A12}$$

Adding Eq. (A11) and (A12), and substituting Eq. (A4) gives

$$\frac{d^2T_n}{dt^{*2}} + 2R\frac{dT_n}{dt^*} = \frac{2}{x_L^*}\int_0^{x_L^*-\varepsilon}\frac{\partial^2 h_l^*(x^*,t^*)}{\partial x^{*2}}\sin(n\pi x^*)dx^* \tag{A13}$$

Applying integration by parts twice to Eq. (A13) gives

$$\frac{d^2T_n}{dt^{*2}} + 2R\frac{dT_n}{dt^*} = \frac{2}{x_L^*}\left[\frac{\partial h_l^*(x^*,t^*)}{\partial x^*}\sin(n\pi x^*)\Big|_0^{x_L^*-\varepsilon} - (n\pi)h_l^*(x^*,t^*)\cos(n\pi x^*)\Big|_0^{x_L^*-\varepsilon} - (n\pi)^2\int_0^{x_L^*-\varepsilon} h_l^*(x^*,t^*)\sin(n\pi x^*)dx^*\right] \tag{A14}$$

in which

$$\frac{\partial h_l^*(x^*,t^*)}{\partial x^*}\sin(n\pi x^*)\Big|_0^{x_L^*-\varepsilon} = \frac{\partial h_l^*(x^*,t^*)}{\partial x^*}\Big|_{x_L^*-\varepsilon}\sin(n\pi x_L^*) - 0 \tag{A15}$$

$$(n\pi)h_l^*(x^*,t^*)\cos(n\pi x^*)\Big|_0^{x_L^*-\varepsilon} = (n\pi)h_l^*(x_L^*,t^*)\cos(n\pi x_L^*) - 0 \tag{A16}$$

due to $h^*(0, t^*) = 0$ according to the boundary conditions in Eq. (A2)

and $$(n\pi)^2\int_0^{x_L^*-\varepsilon} h_l^*(x^*,t^*)\sin(n\pi x^*)dx^* = (n\pi)^2\frac{x_L^*}{2}T_n(t^*) \tag{A17}$$

Substituting Eqs. (A15), (A16) and (A17) into Eq. (A14) gives

$$\frac{d^2T_n}{dt^{*2}} + 2R\frac{dT_n}{dt^*} = \frac{2}{x_L^*}\left[\frac{\partial h_l^*(x^*,t^*)}{\partial x^*}\Big|_{x_L^*-\varepsilon}\sin(n\pi x_L^*) - (n\pi)h_l^*(x_L^*,t^*)\cos(n\pi x_L^*)\right] - (n\pi)^2T_n \tag{A18}$$

Similarly for Eq. (A10) that applies on the right side of the leak,

$$\frac{d^2T_n}{dt^{*2}} + 2R\frac{dT_n}{dt^*} = \frac{2}{1-x_L^*}\left[-\frac{\partial h_r^*(x^*,t^*)}{\partial x^*}\Big|_{x_L^*+\varepsilon}\sin(n\pi x_L^*) + n\pi h_r^*(x_L^*,t^*)\cos(n\pi x_L^*)\right] - (n\pi)^2T_n \tag{A19}$$

Multiplying Eq. (A18) by x_L^* and Eq. (A19) by $(1-x_L^*)$, and adding gives

$$\frac{d^2T_n}{dt^{*2}} + 2R\frac{dT_n}{dt^*} = -2\left[\frac{\partial h_l^*(x^*,t^*)}{\partial x^*}\Big|_{x_L^*+\varepsilon} - \frac{\partial h_r^*(x^*,t^*)}{\partial x^*}\Big|_{x_L^*-\varepsilon}\right]\sin(n\pi x_L^*) - (n\pi)^2T_n \tag{A20}$$

Substituting for the term in square brackets on the right hand side of Eq. (A20) from Eq. (A5)

$$\frac{d^2T_n}{dt^{*2}} + 2R\frac{dT_n}{dt^*} = -2\sum_{k=1}^{\infty}\left[(F_L\frac{dT_k}{dt^*} - 2RF_LT_k)\sin(k\pi x_L^*)\right]\sin(n\pi x_L^*) - (n\pi)^2T_n \tag{A21}$$

Taking the n^{th} term out of the summation and rearranging

$$\frac{d^2T_n}{dt^{*2}} + [2R + 2F_L\sin^2(n\pi x_L^*)]\frac{dT_n}{dt^*} + [(n\pi)^2 - 4RF_L\sin^2(n\pi x_L^*)]T_n = -2\sin(n\pi x_L^*)\sum_{\substack{k=1\\k\neq n}}^{\infty}\left[(F_L\frac{dT_k}{dt^*} - 2RF_LT_k)\sin(k\pi x_L^*)\right] \tag{A22}$$

The general solution of Eq. (A22) is (Kreyszig 1999, p104)

$$T_n(t^*) = e^{-(R+R_{nL})t^*}[A_n\cos\sqrt{(n\pi)^2 - 4RR_{nL} - (R+R_{nL})^2}\,t^* + B_n\sin\sqrt{(n\pi)^2 - 4RR_{nL} - (R+R_{nL})^2}\,t^*] + T_{ns}(t^*) \tag{A23}$$

in which

$$R_{nL} = F_L\sin^2(n\pi x_L^*) \tag{A24}$$

is the leak parameter, and $T_{ns}(t^*)$ is a particular solution to Eq. (A22). Since normally the values of R and R_{nL} are much smaller than unity, Eq. (A23) can be simplified as

$$T_n(t^*) = e^{-(R+R_{nL})t^*}(A_n\cos n\pi t^* + B_n\sin n\pi t^*) + T_{ns}(t^*) \tag{A25}$$

Substituting Eq. (A25) into Eq. (A5) gives the general solution

$$h^*(x^*,t^*) = \sum_{n=1}^{\infty}\left\{e^{-(R+R_{nL})t^*}\left[(A_n\cos(n\pi t^*) + B_n\sin(n\pi t^*)\right]\sin(n\pi x^*)\right\} + \sum_{n=1}^{\infty}\left\{T_{ns}(t^*)\sin(n\pi x^*)\right\} \tag{A26}$$

Using the method of undetermined coefficients (Kreyszig 1999), a particular solution for Eq. (A22) can be expressed in form of

$$T_{ns}(t^*) = \sum_{\substack{k=1\\k\neq n}}^{\infty}[C_{k1}\frac{dT_k(t^*)}{dt} + C_{k2}T_k(t^*)] = \sum_{\substack{k=1\\k\neq n}}^{\infty}2C_{k1}\int_0^1\frac{\partial}{\partial t^*}h^*(x^*,t^*)\sin(k\pi x^*)dx^* + 2C_{k2}\int_0^1 h^*(x^*,t^*)\sin(k\pi x^*)dx^* \tag{A27}$$

where C_{k1} and C_{k2} are the undetermined coefficient. Substituting Eq. (A27) to Eq. (A26) and noticing the orthogonality, the second summation term in Eq. (A26) is equal to zero. Therefore, the general solution to Eq. (A1) subject to the initial and boundary conditions in Eqs. (A2) and (A3) is

$$h^*(x^*,t^*) = \sum_{n=1}^{\infty}\left\{e^{-(R+R_{nL})t^*}\left[(A_n\cos(n\pi t^*) + B_n\sin(n\pi t^*)\right]\sin(n\pi x^*)\right\} \quad \text{(A28, repeated 3.33)}$$

The values of Fourier coefficients in Eq. (A28) are calculated using the initial conditions as

$$A_n = 2\int_0^1 f(x^*)\sin(n\pi x^*)dx^* \qquad (n = 1, 2, 3,.....) \qquad \text{(A29, repeated 3.34)}$$

$$B_n = \frac{1}{n\pi}[\int_0^1 2g(x^*)\sin(n\pi x^*)dx^* + A_n R] \qquad (n = 1, 2, 3,.....) \qquad \text{(A30, repeated 3.35)}$$

Appendix B: Fourier transform of a transient period by period

When a time-domain transient (measured at a particular location x^*) is divided into sections period by period as shown in Figure B1, each transient period can be expressed as a Fourier series based on Eq. (3.33).

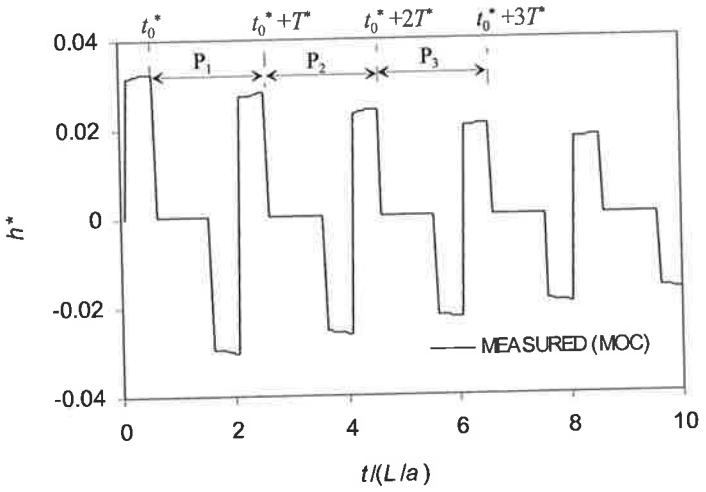

Figure B1. A time-domain pipeline transient (generated by MOC)

For the first period P_1:

$$h^*(x^*,t^*)=\sum_{n=1}^{\infty}\left\{e^{-(R+R_{nL})t^*}\left[A_n\cos(n\pi t^*)+B_n\sin(n\pi t^*)\right]\sin(n\pi x^*)\right\}(t_0^*<t^*<t_0^*+T^*) \quad \text{(B1)}$$

where t_0^* = starting time of analysis, and T^* = dimensionless period defined as $T^* = T/(L/a)$, in which T = natural period of pipeline. For the case in Figure B1, $T^* = 2.0$.

For the second period P_2:

$$h^*(x^*,t_2^*)=\sum_{n=1}^{\infty}\left\{e^{-(R+R_{nL})t_2^*}\left[A_n\cos(n\pi t_2^*)+B_n\sin(n\pi t_2^*)\right]\sin(n\pi x^*)\right\} \quad \text{for} \quad (t_0^*+T^*<t_2^*<t_0^*+2T^*) \quad \text{(B2)}$$

Setting $t_2^*=t^*+T^*$ and noticing the periodic property of the sinusoid functions give

$$h^*(x^*,t^*+T^*)=\sum_{n=1}^{\infty}e^{-(R+R_{nL})T^*}\left\{e^{-(R+R_{nL})t^*}\left[A_n\cos(n\pi t^*)+B_n\sin(n\pi t^*)\right]\sin(n\pi x^*)\right\} \quad \text{for} \quad (t_0^*<t^*<t_0^*+T^*) \quad \text{(B3)}$$

For the i^{th} period P_i

$$h^*(x^*,t_i^*)=\sum_{n=1}^{\infty}\left\{e^{-(R+R_{nL})t_i^*}\left[A_n\cos(n\pi t_i^*)+B_n\sin(n\pi t_i^*)\right]\sin(n\pi x^*)\right\} \quad \text{for} \quad (t_0^*+(i-1)T^*<t_i^*<t_0^*+iT^*) \tag{B4}$$

Setting $t_i^*=t^*+(i-1)T^*$ gives

$$h^*(x^*,t^*+(i-1)T^*)=\sum_{n=1}^{\infty}e^{-(R+R_{nL})(i-1)T^*}\left\{e^{-(R+R_{nL})t^*}\left[A_n\cos(n\pi t^*)+B_n\sin(n\pi t^*)\right]\sin(n\pi x^*)\right\} \quad (t_0^*<t^*<t_0^*+T^*) \tag{B5}$$

A similar Fourier series is now fitted period by period to the "measured" transient data given in Fig. B1 (created by MOC). For the i^{th} period transient the fitted Fourier series is

$$h^*(x^*,t^*+(i-1)T^*)=C_0^{(i)}+\sum_{m=1}^{\infty}\left[C_m^{(i)}\cos(m\pi t^*)+D_m^{(i)}\sin(m\pi t^*)\right] \quad \text{for} \quad (t_0^*+<t^*<t_0^*+T^*) \tag{B6}$$

The Fourier coefficients $C_0^{(i)}$, $C_m^{(i)}$ and $D_m^{(i)}$ are defined as

$$C_0^{(i)}=\frac{1}{T^*}\int_{t_0^*}^{t_0^*+T^*}h^*(x^*,t^*+(i-1)T^*)dt^* \tag{B7}$$

$$C_m^{(i)}=\frac{2}{T^*}\int_{t_0^*}^{t_0^*+T^*}h^*(x^*,t^*+(i-1)T^*)\cos(m\pi t^*)dt^* \tag{B8}$$

$$D_m^{(i)}=\frac{2}{T^*}\int_{t_0^*}^{t_0^*+T^*}h^*(x^*,t^*+(i-1)T^*)\sin(m\pi t^*)dt^* \tag{B9}$$

Substituting the theoretical solution of $h^*(x^*, t^*+(i\text{-}1)T^*)$ from (B5) into (B7) gives

$$C_0^{(i)}=\frac{1}{T^*}\int_{t_0^*}^{t_0^*+T^*}\sum_{n=1}^{\infty}e^{-(R+R_{nL})(i-1)T^*}\left\{e^{-(R+R_{nL})t^*}\left[A_n\cos(n\pi t^*)+B_n\sin(n\pi t^*)\right]\sin(n\pi x^*)\right\}dt^* \tag{B10}$$

Thus

$$C_0^{(i)}=\frac{1}{T^*}\sum_{n=1}^{\infty}\sin(n\pi x^*)e^{-(R+R_{nL})(i-1)T^*}\int_{t_0^*}^{t_0^*+T^*}\left\{e^{-(R+R_{nL})t^*}\left[A_n\cos(n\pi t^*)+B_n\sin(n\pi t^*)\right]\right\}dt^* \tag{B11}$$

The integral term in (B11) is zero (Abramowitz and Stegun 1972). Therefore,

$$C_0^{(i)}=0 \tag{B12}$$

Substituting the theoretical solution of $h^*(x^*, t^*)$ from (B5) into (B8) gives

$$C_m^{(i)} = \frac{2}{T^*}\int_{t_0^*}^{t_0^*+T^*}\sum_{n=1}^{\infty} e^{-(R+R_{nL})(i-1)T^*}\left\{e^{-(R+R_{nL})t^*}\left[A_n\cos(n\pi t^*) + B_n\sin(n\pi t^*)\right]\sin(n\pi x^*)\right\}\cos(m\pi t^*)dt^* \quad \text{(B13)}$$

Thus

$$C_m^{(i)} = \frac{2}{T^*}\sum_{n=1}^{\infty}\sin(n\pi x^*)e^{-(R+R_{nL})(i-1)T^*}\int_{t_0^*}^{t_0^*+T^*}\left\{e^{-(R+R_{nL})t^*}\left[A_n\cos(n\pi t^*) + B_n\sin(n\pi t^*)\right]\right\}\cos(m\pi t^*)dt^* \quad \text{(B14)}$$

The integral term in (B14) is zero except when $n = m$ (Abramowitz and Stegun 1972). Then (B14) is expressed as

$$C_n^{(i)} = -\frac{e^{-(R+R_{nL})(t_0^*+T^*)} - e^{-(R+R_{nL})t_0^*}}{(R+R_{nL})T^*}\sin(n\pi x^*)A_n e^{-(R+R_{nL})(i-1)T^*} \quad \text{(B15)}$$

Similarly by substituting (B5) into (B9) the Fourier coefficient $D_m^{(i)}$ is expressed as

$$D_n^{(i)} = -\frac{e^{-(R+R_{nL})(t_0^*+T^*)} - e^{-(R+R_{nL})t_0^*}}{(R+R_{nL})T^*}\sin(n\pi x^*)B_n e^{-(R+R_{nL})(i-1)T^*} \quad \text{(B16)}$$

The amplitude $E_n^{(i)}$ for a component n at the i^{th} period P_i is

$$E_n^{(i)} = -\frac{e^{-(R+R_{nL})(t_0^*+T^*)} - e^{-(R+R_{nL})t_0^*}}{(R+R_{nL})T^*}\sin(n\pi x^*)\sqrt{A_n^2+B_n^2}\,e^{-(R+R_{nL})(i-1)T^*} \quad \text{(B17)}$$

or $$E_n^{(i)} = E_n^{(1)}e^{-(R+R_{nL})(i-1)T^*} \quad \text{(B18)}$$

where $E_n^{(1)} = -\frac{e^{-(R+R_{nL})(t_0^*+T^*)} - e^{-(R+R_{nL})t_0^*}}{(R+R_{nL})T^*}\sin(n\pi x^*)\sqrt{A_n^2+B_n^2}$ is the amplitude of the component n at the first period.

Each Fourier component is exponentially damped in time. The damping rate of component n is $(R + R_{nL})$, which is the parameter to be determined.

Appendix C: Derivation of the analytical solution for the transients in a pipeline (with a leak) under variable boundary conditions (Eq. 5.7)

The partial differential equation (P.D.E.), boundary conditions (B.C.) and initial conditions (I.C.) for $v(x^*,t^*)$ derived in Chapter 5 are repeated here

P.D.E
$$\frac{\partial^2 v^*}{\partial x^{*2}} = \frac{\partial^2 v^*}{\partial t^{*2}} + [2R + F_L\delta(x^* - x_L^*)]\frac{\partial v^*}{\partial t^*} - x^*[2R + F_L\delta(x^* - x_L^*)]E^*\omega\cos(\omega\, t^*) + x^*E^*\omega^2\sin(\omega\, t^*) \quad \text{(C1, repeated 5.4)}$$

B.C.
$$v^*(0,\ t^*) = 0, \text{ and } v^*(1,\ t^*) = 0 \quad \text{(C2, repeated 5.5)}$$

I.C.
$$v^*(x^*,\ 0) = 0 \quad \frac{\partial v^*(x^*,\ 0)}{\partial t^*} = x^*E^*\omega \quad \text{(C3, repeated 5.6)}$$

To solve Eq. (C1) subject to Eq. (C2) and Eq. (C3), the variable $v(x^*,t^*)$ can be expressed as

$$v^*(x^*,t^*) = \sum_{n=1}^{\infty} V_n(t^*)\sin(n\pi x^*) \quad \text{(C4)}$$

For all points in the pipe except the position of the leak, the Eq. (C1) becomes

$$\frac{\partial^2 v^*}{\partial x^{*2}} = \frac{\partial^2 v^*}{\partial t^{*2}} + 2R\frac{\partial v^*}{\partial t^*} + x^*[2Rf'(t^*) + f''(t^*)] \quad \text{(C5)}$$

Integrating Eq. (C1) over a small neighborhood on either side of the leak gives

$$\int_{x_L^*-\varepsilon}^{x_L^*+\varepsilon}\frac{\partial^2 v^*}{\partial x^{*2}}dx^* = \int_{x_L^*-\varepsilon}^{x_L^*+\varepsilon}\{\frac{\partial^2 v^*}{\partial t^{*2}} + 2R\frac{\partial v^*}{\partial t^*} + x^*[2Rf'(t^*) + f''(t^*)]\}dx^* + \int_{x_L^*-\varepsilon}^{x_L^*+\varepsilon}[\frac{\partial v^*}{\partial t^*} + x^*f'(t^*)]F_L\delta(x^* - x_L^*)dx^* \quad \text{(C6)}$$

Letting ε approach zero, the first integral on the right hand side of Eq. (C6) is zero. Thus Eq. (C6) becomes

$$\frac{\partial v^*}{\partial x^*}\Big|_{x_L^*-\varepsilon}^{x_L^*+\varepsilon} = F_L\frac{\partial v^*}{\partial t^*}\Big|_{x_L^*} \int_{x_L^*-\varepsilon}^{x_L^*+\varepsilon}\delta(x^* - x_L^*)dx^* + F_Lf'(t^*)\int_{x_L^*-\varepsilon}^{x_L^*+\varepsilon}x^*\delta(x^* - x_L^*)dx^* \quad \text{(C7)}$$

Given $\int_{x_L^*-\varepsilon}^{x_L^*+\varepsilon}\delta(x^* - x_L^*)dx^* = 1$, and $\int_{x_L^*-\varepsilon}^{x_L^*+\varepsilon}x^*\delta(x^* - x_L^*)dx^* = x_L^*$, substituting Eq. (C4) into the right-hand side of Eq. (C7) gives

$$\left.\frac{\partial v^*}{\partial x^*}\right|_{x_L^*+\varepsilon} - \left.\frac{\partial v^*}{\partial x^*}\right|_{x_L^*-\varepsilon} = \sum_{n=1}^{\infty}\left[F_L \frac{dV_n}{dt^*}\sin(n\pi x_L^*)\right] + F_L x_L^* f'(t^*) \tag{C8}$$

Because the independent sets of eigenfunctions are separately orthogonal, the coefficient functions V_n in Eq. (C4) can be expressed by integrals in the two regions at each side of the leak. To the left of the leak

$$V_n(t^*) = \frac{2}{x_L^*}\int_0^{x_L^*-\varepsilon} v_l^*(x^*,t^*)\sin(n\pi x^*)dx^* \tag{C9}$$

and to the right of the leak

$$V_n(t^*) = \frac{2}{1-x_L^*}\int_{x_L^*+\varepsilon}^{1} v_r^*(x^*,t^*)\sin(n\pi x^*)dx^* \tag{C10}$$

where the subscript l on the $v^*(x^*, t^*)$ refers to the region to the left of the leak, and subscript r refers to the region to the right of the leak.

Differentiating Eq. (C9) twice leads to

$$\frac{d^2V_n}{dt^{*2}} = \frac{2}{x_L^*}\int_0^{x_L^*-\varepsilon}\frac{\partial^2 v_l^*(x^*,t^*)}{\partial t^{*2}}\sin(n\pi x^*)dx^* \tag{C11}$$

Differentiating Eq. (C9) and multiplying $2R$ leads to

$$2R\frac{dV_n}{dt^*} = \frac{2}{x_L^*}\int_0^{x_L^*-\varepsilon} 2R\frac{\partial v_l^*(x^*,t^*)}{\partial t^*}\sin(n\pi x^*)dx^* \tag{C12}$$

Adding Eq. (C11) and (C12), and substituting Eq. (C5) gives

$$\begin{aligned}\frac{d^2V_n}{dt^{*2}} + 2R\frac{dV_n}{dt^*} = {} & \frac{2}{x_L^*}\int_0^{x_L^*-\varepsilon}\frac{\partial^2 v_l^*(x^*,t^*)}{\partial x^{*2}}\sin(n\pi x^*)dx^* \\ & -\frac{2}{x_L^*}\int_0^{x_L^*-\varepsilon} x^*[2Rf'(t^*)+f''(t^*)]\sin(n\pi x^*)dx^*\end{aligned} \tag{C13}$$

where

$$\begin{aligned}-\frac{2}{x_L^*}\int_0^{x_L^*-\varepsilon} x^*[2Rf'(t^*)+f''(t^*)]\sin(n\pi x^*)dx^* = {} & \\ -\frac{2[2Rf'(t^*)+f''(t^*)]}{x_L^*}\left[\frac{\sin(n\pi x_L^*)}{(n\pi)^2} - \frac{x_L^*\cos(n\pi x_L^*)}{n\pi}\right] & \end{aligned} \tag{C14}$$

Applying integration by parts twice to the first term of the right-hand side of Eq. (C13) gives

$$\frac{2}{x_L^*}\int_0^{x_L^*-\varepsilon}\frac{\partial^2 v_l^*(x^*,t^*)}{\partial x^{*2}}\sin(n\pi x^*)dx=\frac{2}{x_L^*}\Bigg[\left.\frac{\partial v_l^*(x^*,t^*)}{\partial x^*}\sin(n\pi x^*)\right|_0^{x_L^*-\varepsilon}- \left.(n\pi)v_l^*(x^*,t^*)\cos(n\pi x^*)\right|_0^{x_L^*-\varepsilon}-(n\pi)^2\int_0^{x_L^*-\varepsilon}v_l^*(x^*,t^*)\sin(n\pi x^*)dx^*\Bigg] \tag{C15}$$

in which

$$\left.\frac{\partial v_l^*(x^*,t^*)}{\partial x^*}\sin(n\pi x^*)\right|_0^{x_L^*-\varepsilon}=\left.\frac{\partial v_l^*(x^*,t^*)}{\partial x^*}\right|_{x_L^*-\varepsilon}\sin(n\pi x_L^*)-0 \tag{C16}$$

$$\left.(n\pi)v_l^*(x^*,t^*)\cos(n\pi x^*)\right|_0^{x_L^*-\varepsilon}=(n\pi)v_l^*(x_L^*,t^*)\cos(n\pi x_L^*)-0 \tag{C17}$$

due to $v^*(0, t^*) = 0$ according to the boundary conditions

and $$(n\pi)^2\int_0^{x_L^*-\varepsilon}v_l^*(x^*,t^*)\sin(n\pi x^*)dx^*=(n\pi)^2\frac{x_L^*}{2}V_n(t^*) \tag{C18}$$

Substituting Eqs. (C16), (C17) and (C18) into Eq. (C15) and then into Eq. (C13) gives

$$\frac{d^2V_n}{dt^{*2}}+2R\frac{dV_n}{dt^*}=\frac{2}{x_L^*}\left[\left.\frac{\partial v_l^*(x^*,t^*)}{\partial x^*}\right|_{x_L^*-\varepsilon}\sin(n\pi x_L^*)-(n\pi)v_l^*(x_L^*,t^*)\cos(n\pi x_L^*)\right] \tag{C19}$$
$$-\frac{2[2Rf'(t^*)+f''(t^*)]}{x_L^*}\left[\frac{\sin(n\pi x_L^*)}{(n\pi)^2}-\frac{x_L^*\cos(n\pi x_L^*)}{n\pi}\right]-(n\pi)^2V_n$$

Similarly for Eq. (C10) that applies on the right side of the leak,

$$\frac{d^2V_n}{dt^{*2}}+2R\frac{dV_n}{dt^*}=\frac{2}{1-x_L^*}\left[-\left.\frac{\partial v_r^*(x^*,t^*)}{\partial x^*}\right|_{x_L^*+\varepsilon}\sin(n\pi x_L^*)+n\pi v_r^*(x_L^*,t^*)\cos(n\pi x_L^*)\right] \tag{C20}$$
$$-\frac{2[2Rf'(t^*)+f''(t^*)]}{1-x_L^*}\left[-\frac{\cos(n\pi)}{n\pi}-\frac{\sin(n\pi x_L^*)}{(n\pi)^2}+\frac{x_L^*\cos(n\pi x_L^*)}{n\pi}\right]-(n\pi)^2T_n$$

Multiplying Eq. (C19) by x_L^* and Eq. (C20) by $(1-x_L^*)$, and adding gives

$$\frac{d^2V_n}{dt^{*2}}+2R\frac{dV_n}{dt^*}=-2\left[\left.\frac{\partial v_l^*(x^*,t^*)}{\partial t^*}\right|_{x_L^*+\varepsilon}-\left.\frac{\partial v_r^*(x^*,t^*)}{\partial t^*}\right|_{x_L^*-\varepsilon}\right]\sin(n\pi x_L^*) \tag{C21}$$
$$+\frac{2\cos(n\pi)[2Rf'(t^*)+f''(t^*)]}{n\pi}-(n\pi)^2V_n$$

Substituting for the term in square brackets on the right hand side of Eq. (C21) from Eq. (C8)

$$\frac{d^2V_n}{dt^{*2}}+2R\frac{dV_n}{dt^*}=-2\left\{\sum_{k=1}^{\infty}\left[F_L\frac{dV_k}{dt^*}\sin(k\pi x_L^*)\right]+F_Lx_L^*f'(t^*)\right\}\sin(n\pi x_L^*) \tag{C22}$$
$$+\frac{2\cos(n\pi)[2Rf'(t^*)+f''(t^*)]}{n\pi}-(n\pi)^2T_n$$

Taking the n^{th} term of V_n out of the summation and rearranging

$$\frac{d^2V_n(t^*)}{dt^{*2}}+[2R+2F_L\sin^2(n\pi x_L^*)]\frac{dV_n(t^*)}{dt^*}+(n\pi)^2V_n(t^*)$$
$$=\left\{\frac{2\cos(n\pi)[2Rf'(t^*)+f''(t^*)]}{n\pi}-2F_Lx_L^*f'(t^*)\sin(n\pi x_L^*)\right\}\qquad(k\neq n)\qquad\text{(C23)}$$
$$-2\sin(n\pi x_L^*)\sum_{k=1}^{\infty}\left[F_L\frac{dV_k(t^*)}{dt^*}\sin(k\pi x_L^*)\right]$$

The general solution of Eq. (C23) is (Kreyszig 1999, p89 and p104)

$$V_n(t^*)=e^{-(R+R_{nL})t^*}[A_n\cos\sqrt{(n\pi)^2-(R+R_{nL})^2}\,t^*+$$
$$B_n\sin\sqrt{(n\pi)^2-(R+R_{nL})^2}\,t^*]+V_{s1}(t^*)+V_{s2}(t^*)\qquad\text{(C24)}$$

in which

$$R_{nL}=F_L\sin^2(n\pi x_L^*)\qquad\text{(C25)}$$

is the leak parameter. A special solution to Eq. (C23) can be given as $V_{s1}(t^*)+V_{s2}(t^*)$ with each part accounting for each of two right-hand-side terms of Eq. (C23) respectively. Actually the second term on the right-hand side does not influence the solution due to the orthogonality property. Therefore, Eq. (C23) is simplified to

$$\frac{d^2V_n(t^*)}{dt^{*2}}+2[R+R_{nL}]\frac{dV_n(t^*)}{dt^*}+(n\pi)^2V_n(t^*)$$
$$=\left\{\frac{2\cos(n\pi)[2Rf'(t^*)+f''(t^*)]}{n\pi}-2P_{nL}f'(t^*)\right\}\qquad\text{(C26)}$$

in which $P_{nL}=F_Lx_L^*\sin(n\pi x_L^*)\qquad\text{(C27)}$

Substituting $f(t^*)=E\sin(\omega\,t^*)$ into Eq. (C26), the right hand side of Eq. (C26) is

$$\frac{2\cos(n\pi)[2RE\omega\cos(\omega\,t^*)-E\omega^2\sin(\omega\,t^*)]}{n\pi}-2P_{nL}E\omega\cos(\omega\,t^*)\qquad\text{(C28)}$$

Assuming $n\pi\neq\varpi$ (this presumption is only needed if there is no damping in the pipeline system where a resonance will occur at $n\pi=\varpi$) a particular solution of Eq. (C26) can be determined by the method of undetermined coefficients, accordingly as

$$V_p(t^*)=[A_{np}\cos(\omega\,t^*)+B_{np}\sin(\omega\,t^*)]\qquad\text{(C29)}$$

Substituting Eqs (C28) and (C29) into Eq. (C26) and equating the coefficients obtain

$$A_{np}=\frac{a[(n\pi)^2-\omega^2]-2b(R+R_{nL})\omega}{[(n\pi)^2-\omega^2]^2+[2(R+R_{nL})\omega]^2}\qquad\text{(C30)}$$

$$B_{np}=\frac{2a(R+R_{nL})\omega+b[(n\pi)^2-\omega^2]}{[(n\pi)^2-\omega^2]^2+[2(R+R_{nL})\omega]^2}\qquad\text{(C31)}$$

where $a = \dfrac{4RE\omega\cos(n\pi)}{n\pi} - 2P_{nL}E\omega$, $\qquad b = \dfrac{-2E\omega^2\cos(n\pi)}{n\pi}$ (C32)

Therefore, the general solution for Eq. (C26) is

$$V(t^*) = e^{-(R+R_{nL})t^*}[A_n\cos(n\pi t^*) + B_n\sin(n\pi t^*)] + A_{np}\cos(\omega\, t^*) + B_{np}\sin(\omega\, t^*) \tag{C33}$$

The coefficients A_n and B_n in Eq. (C33) can be determined from the initial condition Eq. (C3) as

$$A_n = -A_{np} \text{ and } B_n = \frac{2E\omega\cos(n\pi)}{(n\pi)^2} + \frac{(R+R_{nL})A_{np} - \omega B_{np}}{n\pi} \tag{C34}$$

Substituting Eq3. (C33) and (C34) into Eq. (C4) gives the general solution

$$v(x^*,t^*) = \sum_{n=1}^{\infty} e^{-(R+R_{nL})t^*}[A_n\cos(n\pi t^*) + B_n\sin(n\pi t^*)]\sin(n\pi x^*) + \sum_{n=1}^{\infty}\{A_{np}\cos(\omega\, t^*) + B_{np}\sin(\omega\, t^*)\}\sin(n\pi x^*) \tag{C35}$$

which is Eq. (5.7) presented in Chapter 5, and the Fourier coefficients in Eq. (C35) are defined as

$$A_{np} = \frac{a[(n\pi)^2 - \omega^2] - 2b(R+R_{nL})\omega}{[(n\pi)^2 - \omega^2]^2 + [2(R+R_{nL})\omega]^2}, B_{np} = \frac{2a(R+R_{nL})\omega + b[(n\pi)^2 - \omega^2]}{[(n\pi)^2 - \omega^2]^2 + [2(R+R_{nL})\omega]^2}$$

$$A_n = -A_{np}, \qquad B_n = \frac{2E^*\omega\cos(n\pi)}{(n\pi)^2} + \frac{(R+R_{nL})A_{np} - \omega B_{np}}{n\pi}$$

$$a = \frac{4RE^*\omega\cos(n\pi)}{n\pi} - 2F_L x_L^*\sin(n\pi x_L^*)E^*\omega, \text{ and } b = \frac{-2E^*\omega^2\cos(n\pi)}{n\pi}$$

Appendix D: Derivation of the analytical solution for the transients in a pipeline with a short dead end (Eq. 7.40)

The partial differential equation (P.D.E.), boundary conditions (B.C.) and initial conditions (I.C.) for the transients in a pipeline (with a short dead end) under constant boundary conditions are repeated here

P.D.E $$\frac{\partial^2 h^*}{\partial x^{*2}} = [1 + C\delta(x^* - x_d^*)][\frac{\partial^2 h^*}{\partial t^{*2}} + 2R\frac{\partial h^*}{\partial t^*}] \quad \text{(D1)}$$

B.C. $$h^*(0,\ t^*) = 0, \text{ and } h^*(1,\ t^*) = 0 \quad \text{(D2)}$$

I.C. $$h^*(x^*,\ 0) = f(x^*) \qquad \frac{\partial h^*(x^*,\ 0)}{\partial t^*} = g(x^*) \quad \text{(D3)}$$

For a pipeline with a dead end, the pipeline can be considered as two portions divided by the dead end with a small neighbourhood 2ε as shown in Figure D1.

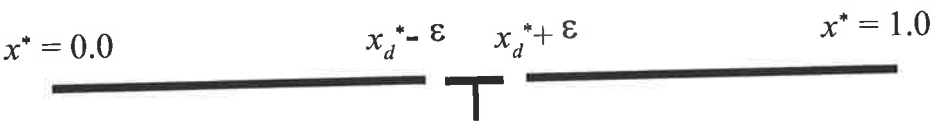

Figure D1 A pipeline with a dead end

For all points in the pipe except the position of the dead end, the linearized equation (D1) becomes a wave equation,

$$\frac{\partial^2 h^*}{\partial x^{*2}} = \frac{\partial^2 h^*}{\partial t^{*2}} + 2R\frac{\partial h^*}{\partial t^*} \quad \text{(D4)}$$

Noticing the boundary condition as those in Eq. (D2) and the continuity of pressure at the lumped dead end (Wylie and Streeter 1993), the transients in the pipeline can be expressed as (Levine 1997)

$$h^*(x^*, t^*) = \sum_{n=1}^{\infty} T_n(t^*)\sin(n\pi x^*) \qquad (0 \le x^* \le 1) \quad \text{(D5)}$$

Integrating Eq. (D1) over a small neighborhood on either side of the dead end gives

$$\int_{x_d^*-\varepsilon}^{x_d^*+\varepsilon} \frac{\partial^2 h^*}{\partial x^{*2}} dx^* = \int_{x_d^*-\varepsilon}^{x_d^*+\varepsilon} (\frac{\partial^2 h^*}{\partial t^{*2}} + 2R\frac{\partial h^*}{\partial t^*})dx^* + \int_{x_d^*-\varepsilon}^{x_d^*+\varepsilon} C(\frac{\partial^2 h^*}{\partial t^{*2}} + 2R\frac{\partial h^*}{\partial t^*})\delta(x^* - x_d^*)dx^* \quad \text{(D6)}$$

Letting ε approach zero, the first integral on the right hand side of Eq. (D6) is zero. Thus Eq. (D6) becomes

$$\left.\frac{\partial h^*}{\partial x^*}\right|_{x_d^*-\varepsilon}^{x_d^*+\varepsilon} = \left.\left(C\frac{\partial^2 h^*}{\partial t^{*2}} + 2RC\frac{\partial h^*}{\partial t^*}\right)\right|_{x_d^*} \int_{x_d^*-\varepsilon}^{x_d^*+\varepsilon} \delta(x^* - x_d^*)dx^* \tag{D7}$$

Given the definition of Dirac delta function of $\int_{x_d^*-\varepsilon}^{x_d^*+\varepsilon} \delta(x^* - x_d^*)dx^* = 1$, substituting Eq. (D5) into the right-hand side of Eq. (D7) gives

$$\left.\frac{\partial h^*}{\partial x^*}\right|_{x_d^*+\varepsilon} - \left.\frac{\partial h^*}{\partial x^*}\right|_{x_d^*-\varepsilon} = \sum_{n=1}^{\infty}\left[\left(C\frac{d^2T_n}{dt^{*2}} + 2RC\frac{dT_n}{dt^*}\right)\sin(n\pi x_d^*)\right] \tag{D8}$$

Because the independent sets of eigenfunctions are separately orthogonal, the coefficient functions T_n in Eq. (D5) can be expressed by integrals in the two regions at each side of the dead end. First, to the left of the dead end

$$T_n(t^*) = \frac{2}{x_d^*}\int_0^{x_d^*-\varepsilon} h_l^*(x^*,t^*)\sin(n\pi x^*)dx^* \tag{D9}$$

and to the right of the dead end

$$T_n(t^*) = \frac{2}{1-x_d^*}\int_{x_d^*+\varepsilon}^{1} h_r^*(x^*,t^*)\sin(n\pi x^*)dx^* \tag{D10}$$

where the subscript l on the $h^*(x^*, t^*)$ refers to the region to the left of the dead end, and subscript r refers to the region to the right of the dead end.

Differentiating Eq. (D9) twice leads to

$$\frac{d^2T_n}{dt^{*2}} = \frac{2}{x_d^*}\int_0^{x_d^*-\varepsilon}\frac{\partial^2 h_l^*(x^*,t^*)}{\partial t^{*2}}\sin(n\pi x^*)dx^* \tag{D11}$$

Differentiating Eq. (D9) and multiplying $2R$ leads to

$$2R\frac{dT_n}{dt^*} = \frac{2}{x_d^*}\int_0^{x_d^*-\varepsilon} 2R\frac{\partial h_l^*(x^*,t^*)}{\partial t^*}\sin(n\pi x^*)dx^* \tag{D12}$$

Adding Eq. (D11) and (D12), and substituting Eq. (D4) gives

$$\frac{d^2T_n}{dt^{*2}} + 2R\frac{dT_n}{dt^*} = \frac{2}{x_d^*}\int_0^{x_d^*-\varepsilon}\frac{\partial^2 h_l^*(x^*,t^*)}{\partial x^{*2}}\sin(n\pi x^*)dx^* \tag{D13}$$

Applying integration by parts twice to Eq. (D13) gives

$$\frac{d^2T_n}{dt^{*2}} + 2R\frac{dT_n}{dt^*} = \frac{2}{x_d^*}\left[\left.\frac{\partial h_l^*(x^*,t^*)}{\partial x^*}\sin(n\pi x^*)\right|_0^{x_d^*-\varepsilon} - \left.(n\pi)h_l^*(x^*,t^*)\cos(n\pi x^*)\right|_0^{x_d^*-\varepsilon} - (n\pi)^2\int_0^{x_d^*-\varepsilon} h_l^*(x^*,t^*)\sin(n\pi x^*)dx^*\right] \tag{D14}$$

in which

$$\frac{\partial h_l^*(x^*,t^*)}{\partial x^*}\sin(n\pi x^*)\Big|_0^{x_d^*-\varepsilon} = \frac{\partial h_l^*(x^*,t^*)}{\partial x^*}\Big|_{x_d^*-\varepsilon}\sin(n\pi x_d^*) - 0 \tag{D15}$$

$$(n\pi)h_l^*(x^*,t^*)\cos(n\pi x^*)\Big|_0^{x_d^*-\varepsilon} = (n\pi)h_l^*(x_d^*,t^*)\cos(n\pi x_d^*) - 0 \tag{D16}$$

due to $h^*(0, t^*) = 0$ according to the boundary conditions in Eq. (D2)

and $$(n\pi)^2\int_0^{x_d^*-\varepsilon} h_l^*(x^*,t^*)\sin(n\pi x^*)dx^* = (n\pi)^2\frac{x_d^*}{2}T_n(t^*) \tag{D17}$$

Substituting Eqs. (D15), (D16) and (D17) into Eq. (D14) gives

$$\frac{d^2T_n}{dt^{*2}} + 2R\frac{dT_n}{dt^*} = \frac{2}{x_d^*}\left[\frac{\partial h_l^*(x^*,t^*)}{\partial x^*}\Big|_{x_d^*-\varepsilon}\sin(n\pi x_d^*) - (n\pi)h_l^*(x_L^*,t^*)\cos(n\pi x_d^*)\right] - (n\pi)^2T_n \tag{D18}$$

Similarly for Eq. (D10) that applies on the right side of the dead end,

$$\frac{d^2T_n}{dt^{*2}} + 2R\frac{dT_n}{dt^*} = \frac{2}{1-x_d^*}\left[-\frac{\partial h_r^*(x^*,t^*)}{\partial x^*}\Big|_{x_d^*+\varepsilon}\sin(n\pi x_d^*) + n\pi h_r^*(x_d^*,t^*)\cos(n\pi x_d^*)\right] - (n\pi)^2T_n \tag{D19}$$

Multiplying Eq. (D18) by x_d^* and Eq. (D19) by $(1-x_d^*)$, and adding gives

$$\frac{d^2T_n}{dt^{*2}} + 2R\frac{dT_n}{dt^*} = -2\left[\frac{\partial h_l^*(x^*,t^*)}{\partial t^*}\Big|_{x_d^*+\varepsilon} - \frac{\partial h_r^*(x^*,t^*)}{\partial t^*}\Big|_{x_d^*-\varepsilon}\right]\sin(n\pi x_d^*) - (n\pi)^2T_n \tag{D20}$$

Substituting for the term in square brackets on the right hand side of Eq. (D20) from Eq. (D8)

$$\frac{d^2T_n}{dt^{*2}} + 2R\frac{dT_n}{dt^*} = -2\sum_{k=1}^{\infty}\left[\left(C\frac{d^2T_k}{dt^{*2}} + 2RC\frac{dT_k}{dt^*}\right)\sin(k\pi x_d^*)\right]\sin(n\pi x_d^*) - (n\pi)^2T_n \tag{D21}$$

Taking the n^{th} term out of the summation and rearranging

$$[1+2C\sin^2(n\pi x_d^*)]\frac{d^2T_n}{dt^{*2}} + 2R[1+2C\sin^2(n\pi x_d^*)]\frac{dT_n}{dt^*} + (n\pi)^2T_n = -2\sin(n\pi x_d^*)\sum_{\substack{k=1\\k\neq n}}^{\infty}\left[\left(C\frac{d^2T_k}{dt^{*2}} + 2RC\frac{dT_k}{dt^*}\right)\sin(k\pi x_d^*)\right] \tag{D22}$$

The general solution of Eq. (D22) is (Kreyszig 1999, p104)

$$T_n(t^*) = e^{-Rt^*}[A_n \cos\sqrt{\frac{(n\pi)^2}{1+S_d} - R^2}\,t^* + B_n \sin\sqrt{\frac{(n\pi)^2}{1+S_d} - R^2}\,t^*] + T_{ns}(t^*) \tag{D23}$$

in which

$$S_d = 2C\sin^2(n\pi x_d^*) \tag{D24}$$

is the dead end parameter, and $T_{ns}(t^*)$ is a particular solution to Eq. (D22) and has no influence on the solution of $h^*(x^*,t^*)$ due to orthogonality (Appendix A). Since normally the value of R is much smaller than unity, Eq. (D23) can be simplified as

$$T_n(t^*) = e^{-Rt^*}(A_n \cos\lambda t^* + B_n \sin\lambda t^*) + T_{ns}(t^*) \tag{D25}$$

in which $$\lambda = \frac{n\pi}{\sqrt{1+S_d}} \tag{D26}$$

Substituting Eq. (D25) without $T_{ns}(t^*)$ into Eq. (D5) gives the general solution

$$h^*(x^*,t^*) = \sum_{n=1}^{\infty}\left\{e^{-Rt^*}\left[(A_n \cos(\lambda t^*) + B_n \sin(\lambda t^*)\right]\sin(n\pi x^*)\right\} \tag{D27}$$

which is the Eq. (7.40) presented in Chapter 7.

Appendix E: Additional calibration results of the pipe network

E1. Calibration results of pressure transducers

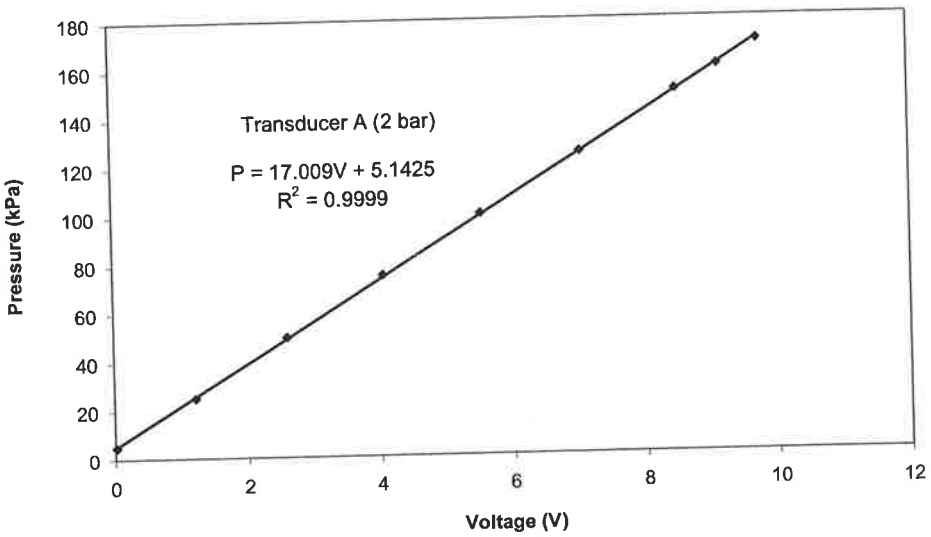

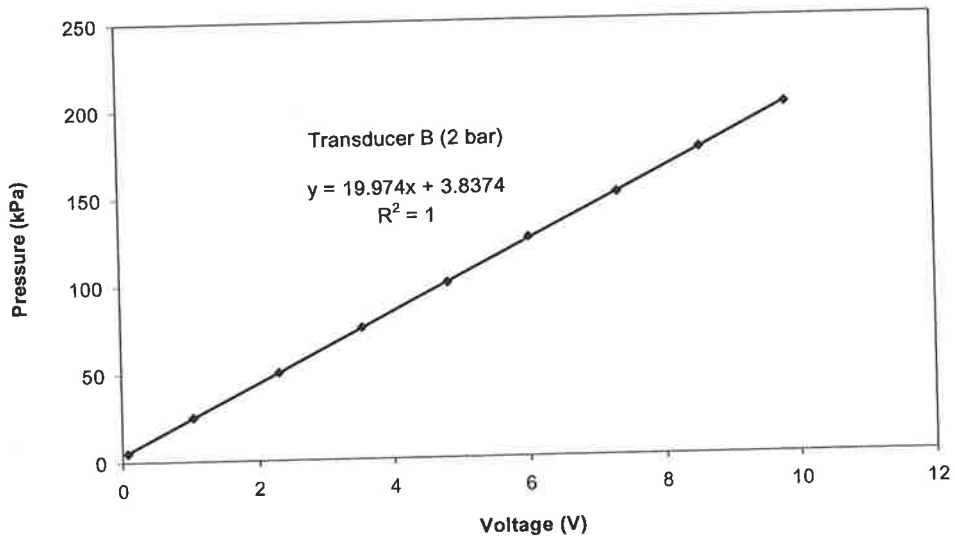

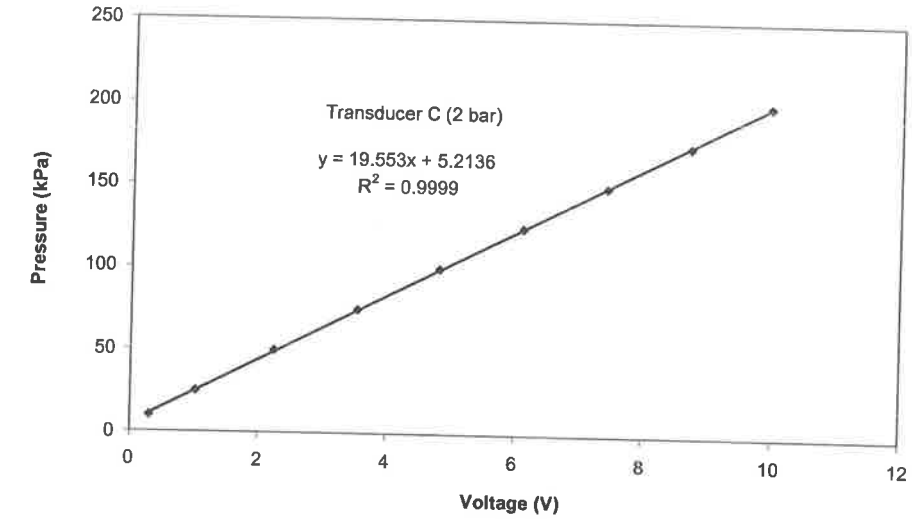

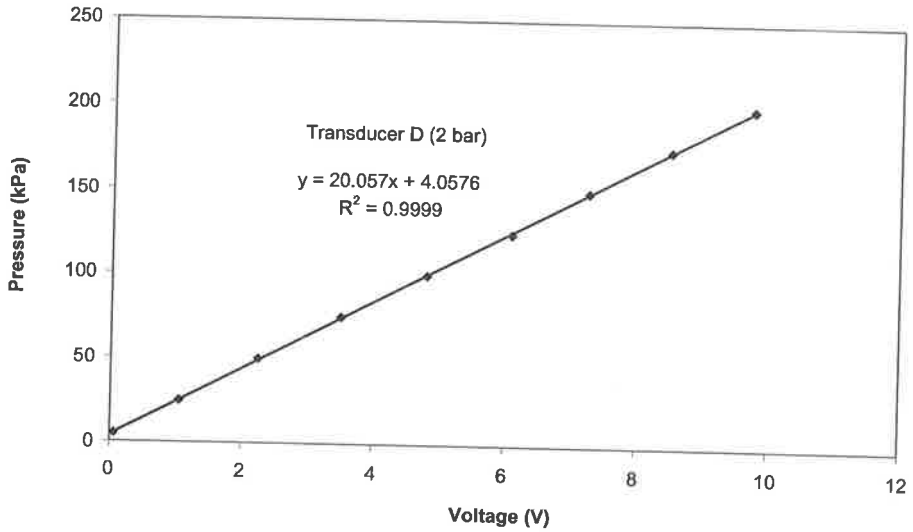

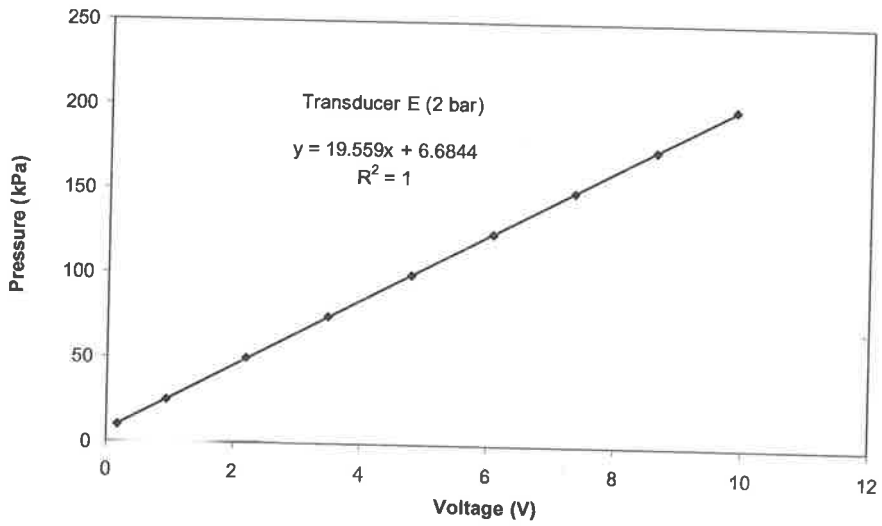

Figure E1 Calibration results of pressure transducers (A at T3, B at T6, C at T7, D at T5 and E at T1)

E2 Calibration of flowmeter and square-edged weir

Two flowmeters were calibrated using the volumetric tank at the eastern end of the laboratory. The calibration results, including LCD output and voltage signal output connected with the data acquisition computer, are given in Figure E2. Since the LCD outputs have been calibrated by the manufacturer, they are almost identical to the flow rates measured by the volumetric tank.

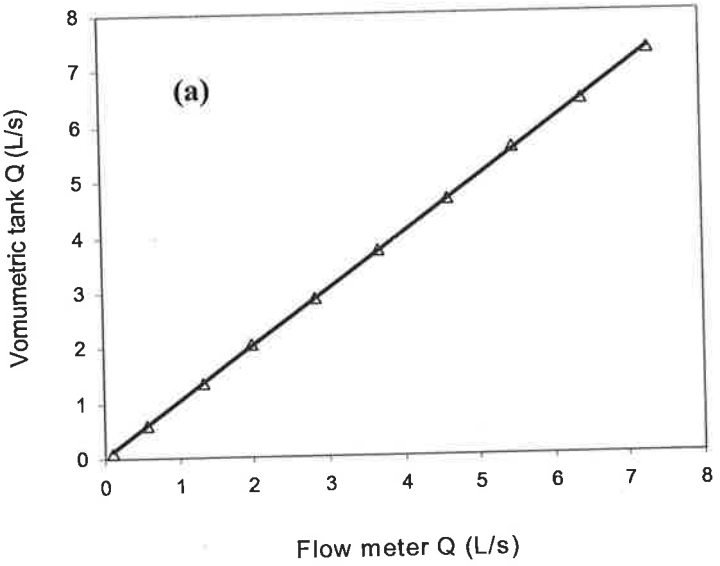

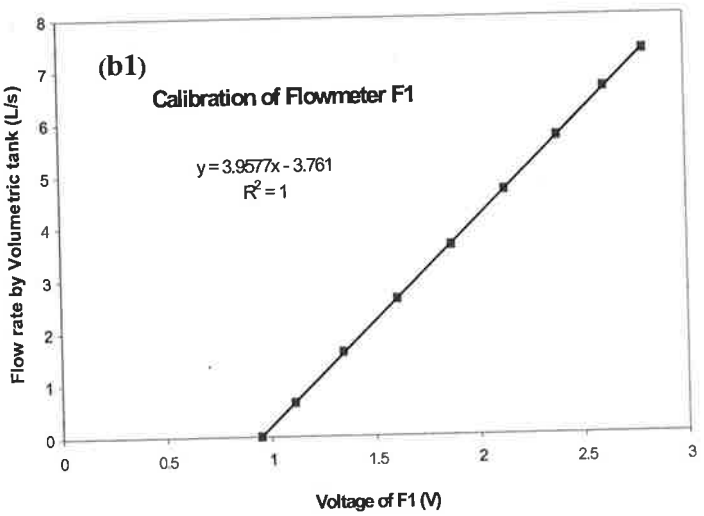

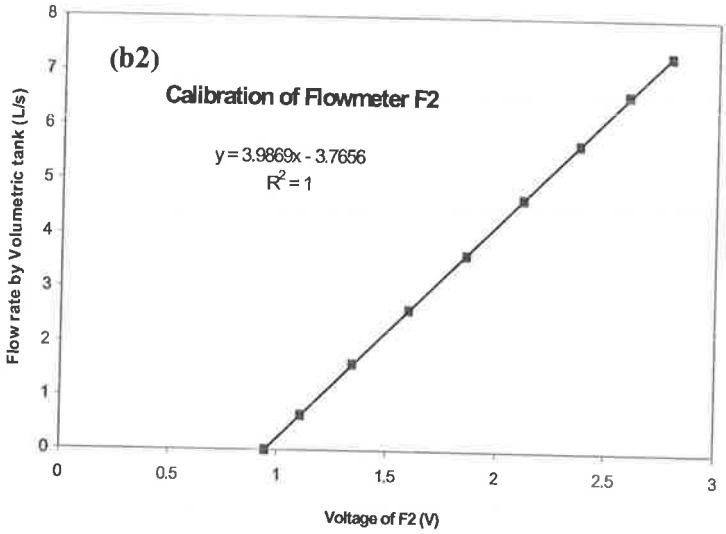

Figure E2 Calibration result of the flowmeter (a) LCD output, (b) digital voltage output

The discharge over the rectangular square-edged weir is calculated by (Rehbock equation)

$$Q_W = \frac{2}{3}\sqrt{2g}C_W b h_w^{1.5} \qquad \text{(E1)}$$

where b = width of the weir (= 0.6m), h = water level head above the weir, C_W = weir coefficient (= 0.652 based on the calibration as shown in Figure E2), and P = weir height (= 0.4m). The square-edged weir was calibrated using the volumetric tank with results in Figure E3. The surface of the weir is 1.395m above the level of the looped network. The head of the water surface (h) in Tank 2 ranges from 20mm to 50 mm depending on the flow in the pipe network. The accuracy of the weir for flow measurement is within 0.05L/s.

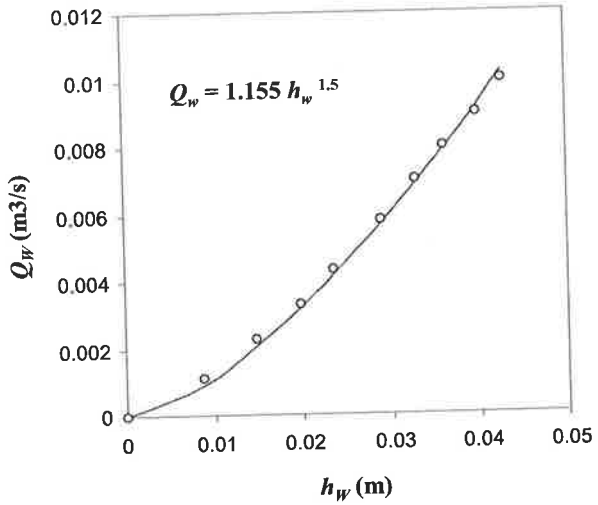

Figure E3 Calibration of outflow weir against the volumetric tank

E3 Calibration of ball valves

Calibration result of the control valve is given in Figure E4. The characteristics of the control valves are calibrated in steady state by measuring the head loss and discharge through a valve at different opening positions. At a full opening position, which corresponds $\tau = 1.0$, the valve parameter defined in Eq. (7.46) is $C_V = 0.0028$.

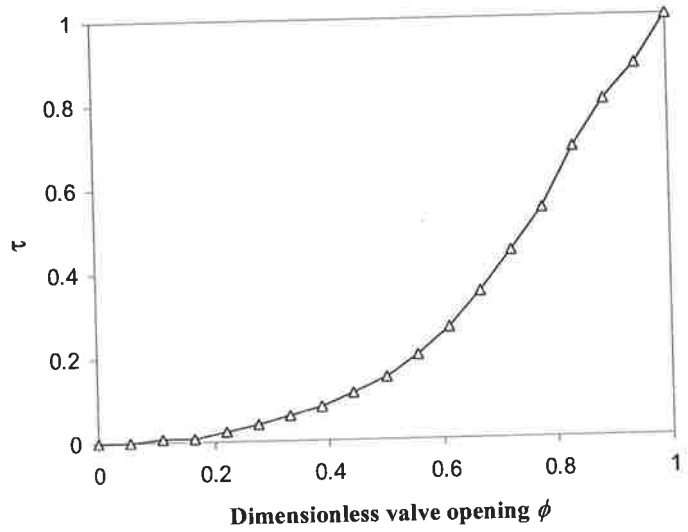

Figure E4 Calibration of the flanged ball valve

E4 Simulation of steady flow in the pipeline

The steady state conditions at different flow configurations were simulated and compared to the experimental results. The purpose of the simulations was to verify the minor losses induced by the elbows and pipe junctions. Previous analyses in Chapter 6 and Chapter 7 have shown that minor losses are important when the flow rate in the pipe network is not small enough. In present pipe network, when the flow rate is less than 1.0L/s, given a minor loss coefficient of (K_{ij}) 1.5 at a junction, the minor head loss ($K_{ij}Q^2/2gA^2$) caused by such a pipe junction is less than 0.005m. Such a small head loss is lower than the resolution (0.01m) of the pressure transducers. As a result, the minor losses caused by elbows and junctions are only important, and are considered when the maximum flow rate is larger than 1.0L/s. Actually, when the flow rate is smaller than 1.0L/s, both friction loss and minor losses are negligible. The heads at different locations in the pipe network are equal to the head in the provide Tank.

Table E1 Configurations of steady-state tests (c--valve closed; o--valve opened)

Valves	A	B	C	D	E
V1	o	o	o	o	o
V2	o	o	o	o	o
V3	c	o	o	c	o
V4	c	o	c	o	o
V5	c	o	c	o	o
V6	c	c	c	c	c
V7	c	c	o	o	o
V8	c	c	c	c	c
V9	c	c	c	c	c
V10	o	o	o	o	o
V11	c	c	c	c	c
V12	c	c	c	c	c
V13	o	o	o	o	o
V14	c	c	o	o	o
V15	o	o	o	o	o

Results presented in Table E2 shows that the minor losses from the elbows and junctions are important in calculating the steady states when the network is fully operating (maximum flow rate) at different configurations. If the minor losses are not considered, simulated steady state conditions (flow rates and heads) are significantly different from the measurement results. Inclusion of these minor losses is important in a transient simulation. Analyses in Chapter 6 and Chapter 7 have shown that minor losses (head losses elements) cause frequency-dependent damping of a transient event.

Table E2 Comparisons of simulation and experimental results
(Num. I: without minor losses, Num. II: with minor losses)

Cases		F1 (L/s)	F2 (L/s)	T1 (m)	T3 (m)	T6 (m)	T7 (m)
A	Exp.	7.26	7.27	3.57	2.56	1.62	N/A
	Num. I	9.26	9.26	3.72	2.31	1.61	N/A
	Num. II	7.25	7.25	3.57	2.56	1.62	N/A
B	Exp.	7.47	7.47	3.69	2.86	1.59	4.07
	Num. I	9.67	9.67	3.69	2.38	1.62	3.55
	Num. II	7.47	7.46	3.69	2.86	1.59	4.05
C	Exp.	10.16	5.44	3.27	3.04	1.83	N/A
	Num. I	14.42	7.21	3.39	2.32	1.82	N/A
	Num. II	10.15	5.44	3.27	3.04	1.83	1.83
D	Exp.	9.41	5.26	3.41	2.93	1.75	3.37
	Num. I	13.44	6.72	3.46	2.18	1.79	2.67
	Num. II	9.41	5.26	3.41	2.93	1.75	3.37
E	Exp.	10.20	5.17	3.23	2.95	1.85	3.63
	Num. I	15.28	7.20	3.33	2.78	1.88	2.98
	Num. II	10.21	5.17	3.23	2.95	1.85	3.63